BT-2727 Investigation of Dynamic Behavior of Tethered Balloon Systems

Access Number
BT-2727

Title
Investigation of Dynamic Behavior of Tethered Balloon Systems

Author
Jerome J. Vorachek, James W. Burbick, George R. Doyle

Responsible Organization
Goodyear Aerospace Corp.

Funding Organization
Air Force Cambridge Research Labs.

Date
31 Jan 1972

Report Number
AFCRL-72-0113, GER-15497

Repository Number

Contract Number
F19628-71-C-0091

Description
Scientific Report, 164 p, 4 refs

Notes
Project 6665

Key Words
Tethered balloons, aerodynamics, stability, tether cables

Content
An analytical investigation of the dynamic behavior of tethered balloons was conducted. This report covers definition of tethered balloon systems and a study of stability characteristics and their dynamic

response to wind gusts. Balloon systems which are investigated use the British BJ Barrage Balloon, the Vee Balloon and a Goodyear Aerospace Single-Hull Balloon. The major tether construction is NOLARO using prestretched polyester filaments. Three design altitudes, 5,000, 10,000 and 20,000 feet, are considered. The model for the tethered balloon system consists of the streamlined balloon and a tether made up of three discrete links. The derivation of non-linear equations of motion for this system in three dimensions is presented.

Available From
WFF/BTL

Goddard Library

BT-2727

Investigation of Dynamic Behavior of Tethered Balloon Systems

Goodyear Aerospace Corp.

Jerome J. Vorachek, James W. Burbick, George R. Doyle

ca Feb 1972

AFCRL - 72 -0113

INVESTIGATION OF DYNAMIC BEHAVIOR OF TETHERED BALLOON SYSTEMS

Jerome J. Vorachek
James W. Burbick
George R. Doyle, Jr.

Goodyear Aerospace Corporation
Akron, Ohio 44315

Contract No. F19628-71-C-0091

Project No. 7659

Task No. 765906

Work Unit No. 76590601

Final Report

1 January 1971 through 31 January 1972

Contract Monitor: Don E. Jackson, Capt., USAF
Aerospace Instrumentation Laboratory

Approved for public release; distribution unlimited

Prepared for

AIR FORCE CAMBRIDGE RESEARCH LABORATORIES
AIR FORCE SYSTEMS COMMAND
UNITED STATES AIR FORCE
BEDFORD, MASSACHUSETTS 01730

ABSTRACT

An analytical investigation of the dynamic behavior of tethered balloons was conducted. This report covers definition of tethered balloon systems and a study of stability characteristics and dynamic response to wind gusts of tethered balloon systems. Balloon systems which are investigated use the British BJ Barrage Balloon, the Vee Balloon and a Goodyear Aerospace Model No. 1649 Single-Hull Balloon. The major tether construction is Columbian Rope Company's NOLARO utilizing prestretched polyester filaments. Three design altitudes, 5,000, 10,000 and 20,000 feet, are considered.

The model for the tethered balloon system consists of the streamlined balloon and a tether made up of three discrete links. The derivation of nonlinear equations of motion for this system in three dimensions is presented. The equations are linearized for stability analysis and treated as uncoupled in the longitudinal and lateral degrees of freedom. Characteristic equations which incorporate the physical, aerodynamic, and mass characteristics of the system are developed and solved for the roots which represent the frequency and damping qualities. The nonlinear equations of motion are programmed for solution on a digital computer.

An exploratory investigation to establish the trends of dynamic characteristics for various design parameters is reported. Design parameters considered include balloon shape and altitude, trim angle of attack, vertical location of the bridle confluence point, net static lift, tail size, reduced wind profiles, varying altitude as encountered in launch and retrieval, payload location, and wind location above mean sea level.

FOREWORD

This research was supported by the Air Force Systems Command, USAF, DOD, and was under the technical cognizance of the Air Force Cambridge Research Laboratories under Contract No. F 19628-71-C-0091.

The project is being carried out under the direction of Captain Don Jackson as Contract Monitor for the Air Force Cambridge Research Laboratories. Mr. Jerome Vorachek is the Goodyear Aerospace Corporation Project Engineer. Technical effort has been provided by Mr. George Doyle for derivation of the equations of motion and characteristic equations of the tethered balloon systems, programming of equations for solution of stability and dynamic response. Mr. James Burbick generated dynamic response data and evaluation of dynamic response results with the IBM 360 computer. Mr. William Ebert developed the aerodynamic characteristics for the balloon system, and mass characteristics were generated by Mr. Walt Stricker. Technical assistance was also provided by Mr. Philip Myers and Mr. Louis Handler.

The contractor's number for this report is GER-15497.

TABLE OF CONTENTS

Section		Page
I	INTRODUCTION	1
II	BALLOON DESCRIPTION	3
III	TECHNIQUES FOR STUDY OF DYNAMIC BEHAVIOR OF TETHERED BALLOONS	7
	1. Mathematical Models	7
	2. General Stability Theory	9
	3. Stability Analysis	11
	4. Dynamic Response Analysis	12
IV	DYNAMIC RESPONSE OF TETHERED BALLOONS	15
	1. Design Conditions Investigated	15
	2. General Discussion of Dynamic Response of Tethered Balloon Systems	17
	3. Effects of Design Parameters on Tethered Balloon Design	29
V	CONCLUSIONS AND RECOMMENDATIONS ON TETHERED BALLOON DYNAMIC BEHAVIOR	44
	1. Gust Effects on Nominal BJ Balloon	44
	2. Comparison of Balloon Types	45
	3. Influence of Trim Angle on Longitudinal and Lateral Dynamic Behavior	45
	4. Effect of Tail Size on Longitudinal and Lateral Dynamic Behavior	46
	5. Effect of Altitudes Intermediate to the Design Altitude on Behavior of the BJ Tethered Balloon System	46
	6. Effects of Reduced Wind on the Behavior of the BJ Tethered Balloon System	47
	7. Nolaro vs Amgal Tethers	47
	8. Effect of Payload Location	47
	9. Effect of Winch Altitude Location	47
	10. BJ Tethered Balloon Systems Designed for Various Altitudes	48
REFERENCES		49
APPENDICES		
A	Equations of Motion for Dynamic Simulation	A-1
B	Dynamic Response Input and Output Data	B-1

LIST OF FIGURES

Figure		Page
1	BJ Configuration.	4
2	Vee-Balloon Configuration	4
3	GAC No. 1649 Balloon Configuration.	6
4	Balloon Tether Model in Longitudinal Plane.	7
5	Balloon Tether Model in Lateral Plane	8
6	Balloon Geometry and Applied Forces	9
7	Longitudinal Dynamics of Tethered Balloon - BJ Nominal	13
8	Longitudinal Dynamics of Tethered Balloon - BJ Nominal	13
9	Lateral Wind Gusts.	17
10	Lateral Stability Characteristics of Nominal BJ Tethered Balloon at 10,000 Feet Altitude.	20
11	Lateral Case 28, Coordinates Response	21
12	Lateral Case 28, Power Spectral Density	22
13	Longitudinal Stability Characteristics of Nominal BJ Tethered Balloon at 10,000 Feet Altitude.	25
14	Lateral Case 4, Coordinates Response.	26
15	Lateral Case 4, Power Spectral Density.	27

LIST OF TABLES

Table		Page
I	Summary of Balloon/Cable Systems.	5
II	Summary of Cable Solutions.	6
III	A. Comparison of Longitudinal Dynamic Cases	16
	B. Comparison of Lateral Dynamic Cases.	16
IV	Summary of Lateral Stability Case 1	19
V	Peak Amplitudes for Lateral Dynamics Case 28.	23
VI	Summary of Longitudinal Stability Case 1 (Reference 2)	24
VII	Wind Gust Duration Effects on BJ Nominal Balloon in Longitudinal Plane.	29
VIII	Wind Gust Ramp Rise Time Effects on BJ Nominal Balloon in Laterial Plane	30
IX	Effect of Increase in Gust Velocity on BJ Nominal Balloon in Lateral Plane.	31
X	Effect of Trim Angle of Attack on Longitudinal Response of Three Balloon Types	32
XI	Effect of Lateral Wind Gusts on the Lateral Response of the Three Balloon Types.	32
XII	Longitudinal Response of BJ Balloon with Tail Size Variation	34
XIII	Lateral Response of BJ and Vee Balloons with Tail Size Variation.	34
XIV	Effect of Intermediate Altitudes on Longitudinal Response of the BJ Balloon.	35
XV	Effect of Intermediate Altitudes on Lateral Response of the BJ Balloon	35
XVI	Effect of Reducing Winds on Longitudinal and Lateral Response.	37
XVII	Effect of Nolaro and Amgal Tethers on Longitudinal Response.	38

Table		Page
XVIII	Effect of Nolaro and Amgal Tethers on Lateral Response	38
XIX	Effect of Payload Location on Longitudinal Response .	39
XX	Effect of Winch Altitude Location on Longitudinal Response.	39
XXI	Effect of Various Design Operational Altitudes. . . .	40
XXII	Structural Design Parameters.	41
XXIII	Instrumentation Design Parameters	41
XXIV	Maximum Variations of Structural and Instrumentation Design Performance Parameters - Longitudinal Cases. .	42
XXV	Maximum Variations of Structural and Instrumentation Design Performance Parameters - Lateral Cases	43

SECTION I

INTRODUCTION

The objective of this program is to investigate the dynamic behavior of tethered balloons and in so doing to establish design criteria for tethered balloons, tethers and payloads. The program is organized into three steps:

(1) Definition of balloon systems for dynamic analysis

(2) A study of stability characteristics of tethered ballon systems

(3) A study of dynamic response of tethered balloon systems to wind gusts

Reference 1 presents a definition of tethered balloon systems to be used for dynamic studies. These systems are summarized in this report. Reference 2 presents a development of the study of stability characteristics of the tethered balloon systems. This report presents further development of the equations of motion and solutions for the dynamic response of the tethered balloon system. Recommendations for the design of tethered balloon systems are presented in this report.

The system is defined as a balloon tethered at the end of a cable which is fixed to a stationary winch. The tether is represented by 3 straight links, each of the same length. The links are considered rigid and connected to each other by frictionless hinges. Goodyear Aerospace Corporation has employed this method of representation of the tethered system for other studies such as that described in Reference 3.

For design purposes in the subject investigation the following design parameters were specified by AFCRL.

Payload and Design Altitude

Payload (lb) P	Float Altitude (ft above MSL) h
1500	5,000
1000	10,000
600	20,000

Tethers

Two specific tether constructions are to be considered, NOLARO by Columbian Rope Company, and Amgal-Monitor AA wire rope by United States Steel.

A safety factor of 2.0 will be used with NOLARO; 1.5 for Amgal-Monitor. Tether design load will be based on a survival wind of 1.3 times the operational wind at balloon altitude.

Wind Profile

The wind profile as specified is tabulated below:

Altitude (ft above MSL)	Operational Wind Speed (knots)	Survival Wind Speed (knots)
Sea Level	10	13.
5,000	31	40.3
10,000	40	52.
20,000	54	70.2

SECTION II

BALLOON DESCRIPTION

The balloon systems evaluated in this stability investigation have been described in Reference 1. The three balloon types in these systems are the British BJ Balloon, the Vee-Balloon* and the GAC No. 1649 Single Hull Balloon as depicted in Figures 1, 2, and 3. The nominal tethered systems characteristics defined in Reference 1 are summarized in Tables I and II.

Static and dynamic aerodynamic characteristics for the balloons have been determined from experimental data where available and by analytical techniques otherwise. The aerodynamic characteristics are presented and discussed in Reference 2 along with additional mass and suspension system geometries which were not included in Reference 1.

Design parameters varied in the stability investigation include the trim angle of attack, vertical location of the suspension system confluence point below the balloons, the free-static lift, and the tail size.

The trim angle of attack can be controlled by locating the confluence point of the suspension system. The location of this point is established by the two coordinates as shown in Figure 1. The fuselage station from the nose and the waterline below the centerline of the balloon defines this point. The trim angle of attack change as a function of bridle apex point location has been calculated and is given in Reference 2.

The free-static lift as used in this report is the excess buoyant lift provided by the balloon after the balloon physical weight and the weight of the tether in no wind is supported.

Nominal tail sizes for each balloon are depicted in Figures 1, 2, and 3. For the British BJ Balloon, tail size is increased and decreased about the nominal by changing the linear dimensions of each of the three tails and maintaining similar proportions. The intersection of the trailing edge of the tails and the hull is maintained at the same point for all tail sizes. For the Vee-Balloon the horizontal tail geometry is maintained. The vertical tails are increased in size in two steps for tails below the hulls. Also investigated are the conditions where vertical tails are located symmetrically above and below the hulls. In addition to establishing aerodynamic characteristics for these tail configurations as noted in Reference 2, the increase in physical mass and additional mass was computed and used in the determination of stability characteristics.

Ascent and descent studies for a specific balloon also incorporate the change in mass characteristics due to air density changes with altitude.

---

* Trademark, Goodyear Aerospace Corporation, Akron, Ohio 44315

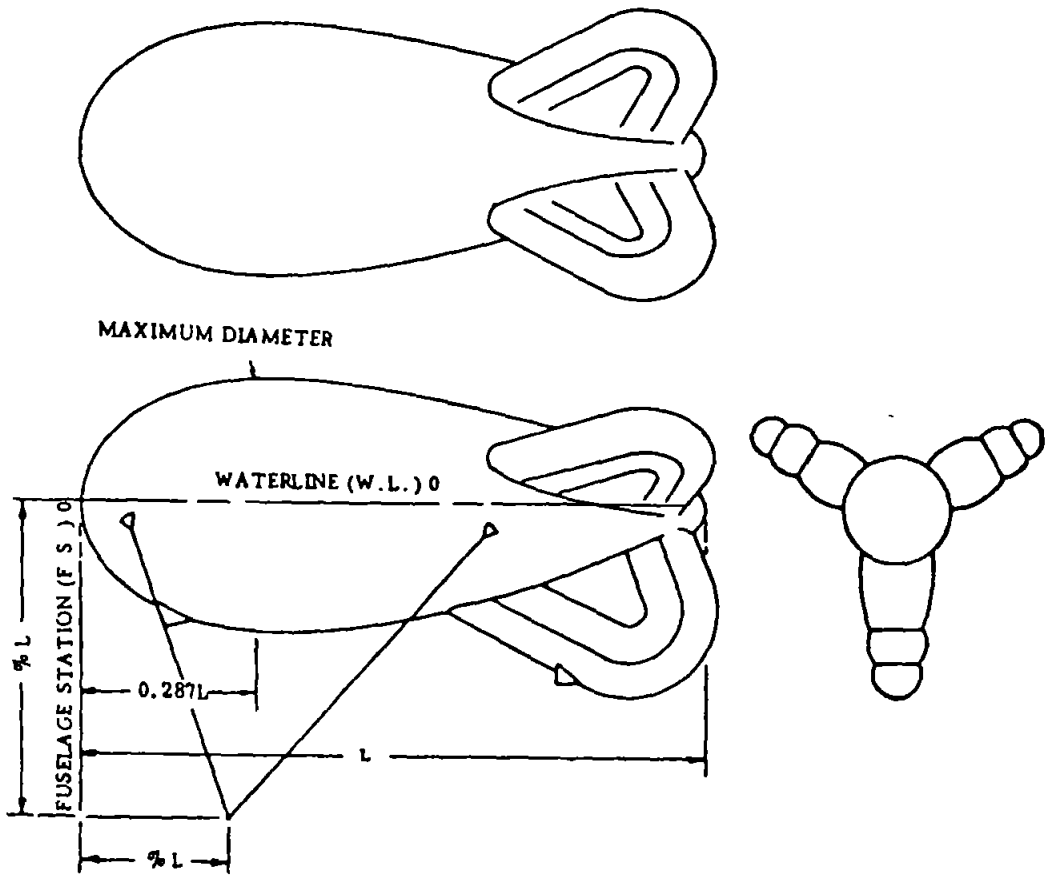

Figure 1. BJ Configuration

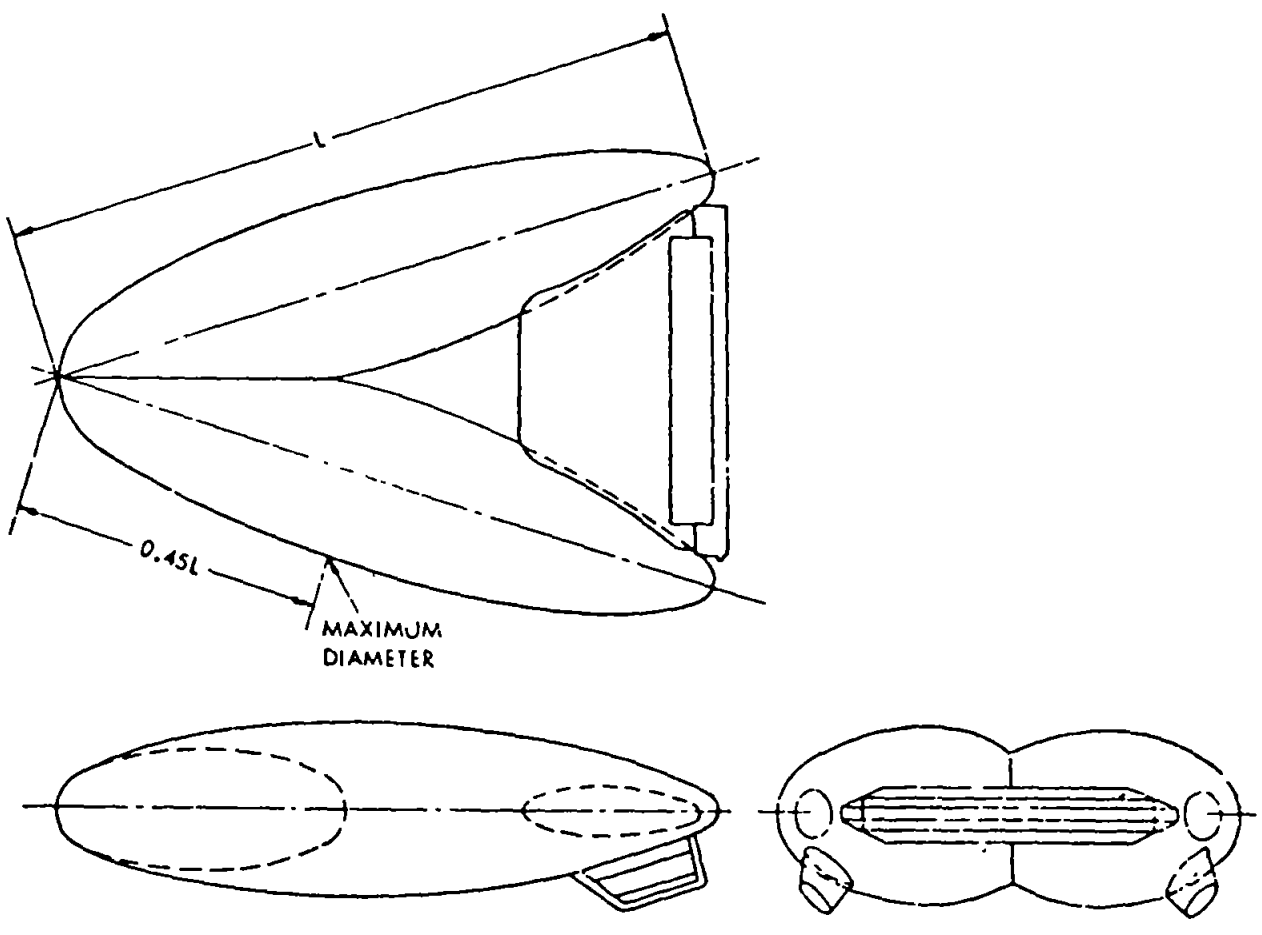

Figure 2. Vee-Balloon Configuration

Table I. Summary of Balloon/Cable Systems

Balloon Type	h	Hull Volume (ft^3)	Gross Static Lift (lb)	W_{B_1} (lb)	P (lb)	L_{S_1} (lb)	Survival					Operational					Tether *		
							α_{Trim} **	L_a (lb)	D (lb)	L_N (lb)	T (lb)	α_{Trim} **	L_a (lb)	D (lb)	L_N (lb)	T (lb)	Type	O.D. (in)	B.S. (lb)
BJ	5,000	46,000	2,534	635	1,500	399	8.7	1,391	656	1,790	1,906	7.0	659	351	1,058	1,115	NOLARO	0.321	3,813
Vee-Balloon	10,000	80,000 (85,363)[1]	4,029	1,541	1,000	1,488	5.7	6,427	2,422	7,916	8,278	6.9	4,437	1,514	5,925	6,116	NOLARO	0.585	16,600
		144,000 (153,654)[1]	7,253	2,712	1,000	3,541	5.7	9,509	3,583	13,050	13,533	6.9	6,564	2,239	10,105	10,350	AMGAL	7/16	20,000
BJ		60,000	2,832	1,031	1,000	801	10.2	2,706	1,219	3,507	3,713	8.2	1,391	651	2,192	2,287	NOLARO	0.410	7,540
		75,000	3,540	1,276	1,000	1,264	10.2	3,140	1,414	4,405	4,626	8.2	1,614	755	2,878	2,975	AMGAL	1/4	6,750
#1649 w/ Thin Fins		80,000	3,776	1,548	1,000	1,228	10.2	4,963	1,346	6,191	6,336	8.2	2,508	757	3,736	3,812	NOLARO	0.520	12,700
		133,000	6,278	2,511	1,000	2,767	10.2	6,965	1,887	9,732	9,913	8.2	3,519	1,061	6,286	6,376	AMGAL	3/8	14,800
BJ	20,000	500,000	17,037	8,933	600	7,504	8.7	15,420	6,785	22,924	23,907	7.0	7,571	3,577	15,075	15,494	NOLARO	0.993	47,814

W_{B_1} Total balloon and suspension weight (no gas, payload or tether)

L_{S_1} Net static lift (Gross static lift - W_{B_1} - P)

*See Table II for detail cable description

**Trim angle of attack α_{TRIM} is as defined by Table VI of Reference 1

Table II. Summary of Cable Solutions

Balloon Type	Altitude (ft)	Hull Volume (ft^3)	Tether Type	B.S. (lb)	O.D. (ft)	Wt/Ft (lb/ft)	X (ft)	Ø (deg)	T (lb)	Length (ft)	Total Tether Weight (lb)
BJ	5,000	46,000	NOLARO	3,813	0.02679	0.03211	0	161.6	1,115	0	--
h = 5,000 ft P = 1,500 lb	S.L.						2,672	144.2	956	5,692	183
Vee-Balloon	10,000	80,000	NOLARO	16,600	0.04875	0.11400	0	165.7	6,115	0	--
	5,000						1,775	154.7	5,552	5,314	606
h = 10,000 ft P = 1,000 lb	S.L.						4,594	146.6	4,991	11,060	1,260
	10,000	144,000	AMGAL	20,000	0.03642	0.30400	0	167.5	10,350	0	--
	5,000						1,389	160.8	8,836	5,193	1,580
	S.L.						3,452	153.9	7,300	10,605	3,230
BJ	10,000	60,000	NOLARO	7,540	0.03420	0.05600	0	163.4	2,287	0	--
	5,000						2,456	143.6	2,036	5,600	314
h = 10,000 ft P = 1,000 lb	S.L.						7,377	127.7	1,761	12,639	708
	10,000	75,000	AMGAL	6,750	0.02083	0.09970	0	165.3	2,975	0	--
	5,000						1,843	153.2	2,482	5,340	532
	S.L.						5,072	140.3	1,989	11,305	1,128
#1649 w/Thin Fins	10,000	80,000	NOLARO	12,700	0.04330	0.0900	0	168.5	3,812	0	--
	5,000						1,702	153.0	3,374	5,298	476
h = 10,000 ft P = 1,000 lb	S.L.						4,950	141.1	2,930	11,274	1,015
	10,000	133,000	AMGAL	14,800	0.03125	0.22000	0	170.4	6,375	0	--
	5,000						1,193	161.8	5,281	5,145	1,132
	S.L.						3,253	152.7	4,187	10,559	2,325
BJ	20,000	500,000	NOLARO	47,814	0.08281	0.32427	0	166.7	15,494	0	--
	15,000						1,646	155.9	13,897	5,272	1,710
h = 20,000 ft P = 600 lb	10,000						4,495	143.7	12,171	11,039	3,580
	5,000						9,106	130.2	10,702	17,856	5,790
	S.L.						17,231	112.0	9,107	27,436	8,900

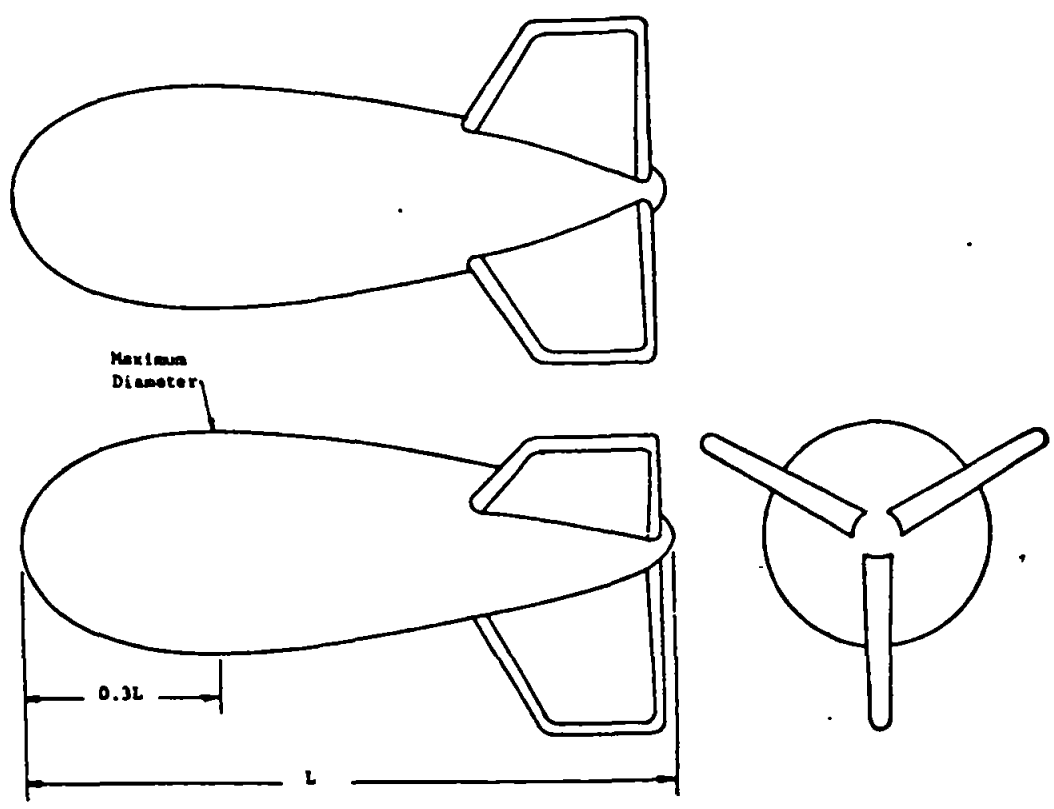

Figure 3. GAC No. 1649 Balloon Configuration

SECTION III

TECHNIQUES FOR STUDY OF DYNAMIC BEHAVIOR OF TETHERED BALLOONS

1. MATHEMATICAL MODELS

A system of differential equations was developed (Reference 2 and Appendix A of this report) that describes the motion of the tethered balloon in three dimensions. The degrees of freedom associated with the motion are yaw, pitch and roll of the balloon about its dynamic mass center, and pitch and yaw (lateral rotation) of the tether. There are a total of 3 + 2N degrees of freedom where N is the number of links used to simulate the tether.

First consider the longitudinal degrees of freedom. The dependent variables shown in Figure 4 are θ (pitch of the balloon) and ζ_r (pitch of the "r"th link), where r is a particular link. All angles are shown positive.

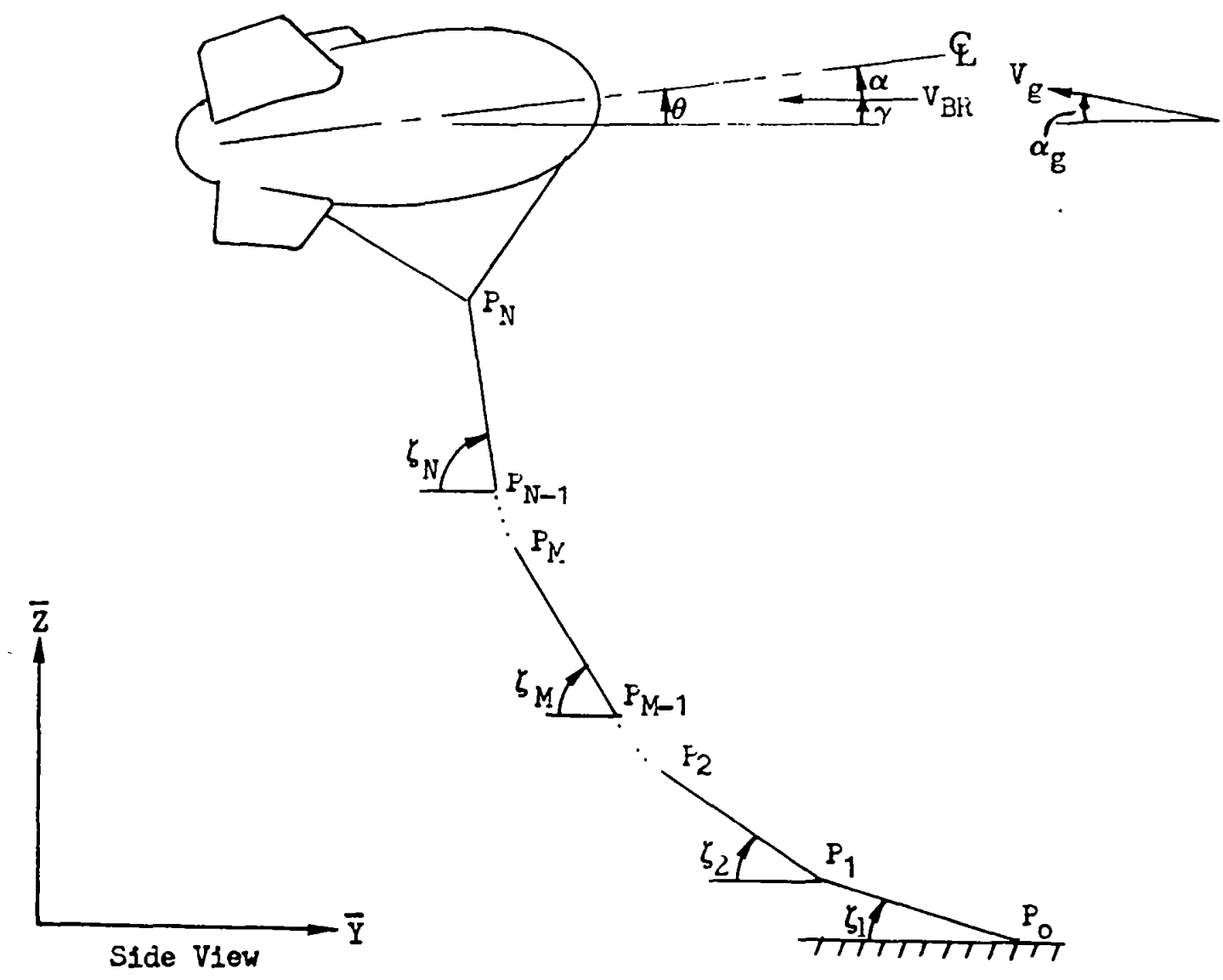

Figure 4 . Balloon Tether Model in Longitudinal Plane

In Figure 4 V_{BR} is the relative velocity of the balloon's center of gravity with respect to the air and is the resultant of the steady wind, the wind gust, the balloon translational motion and the velocity due to rotation of the balloon about its center of mass. The angle of attack (α) is the angle that the relative wind forms with the longitudinal axis of the balloon.

The lateral degrees of freedom are displayed in Figure 5 which gives the front and top views of the tethered balloon. The lateral degrees of freedom are: Ψ(yaw of balloon), ϕ (roll of balloon), and σ_r (yaw of "r"th link). All angles are shown positive.

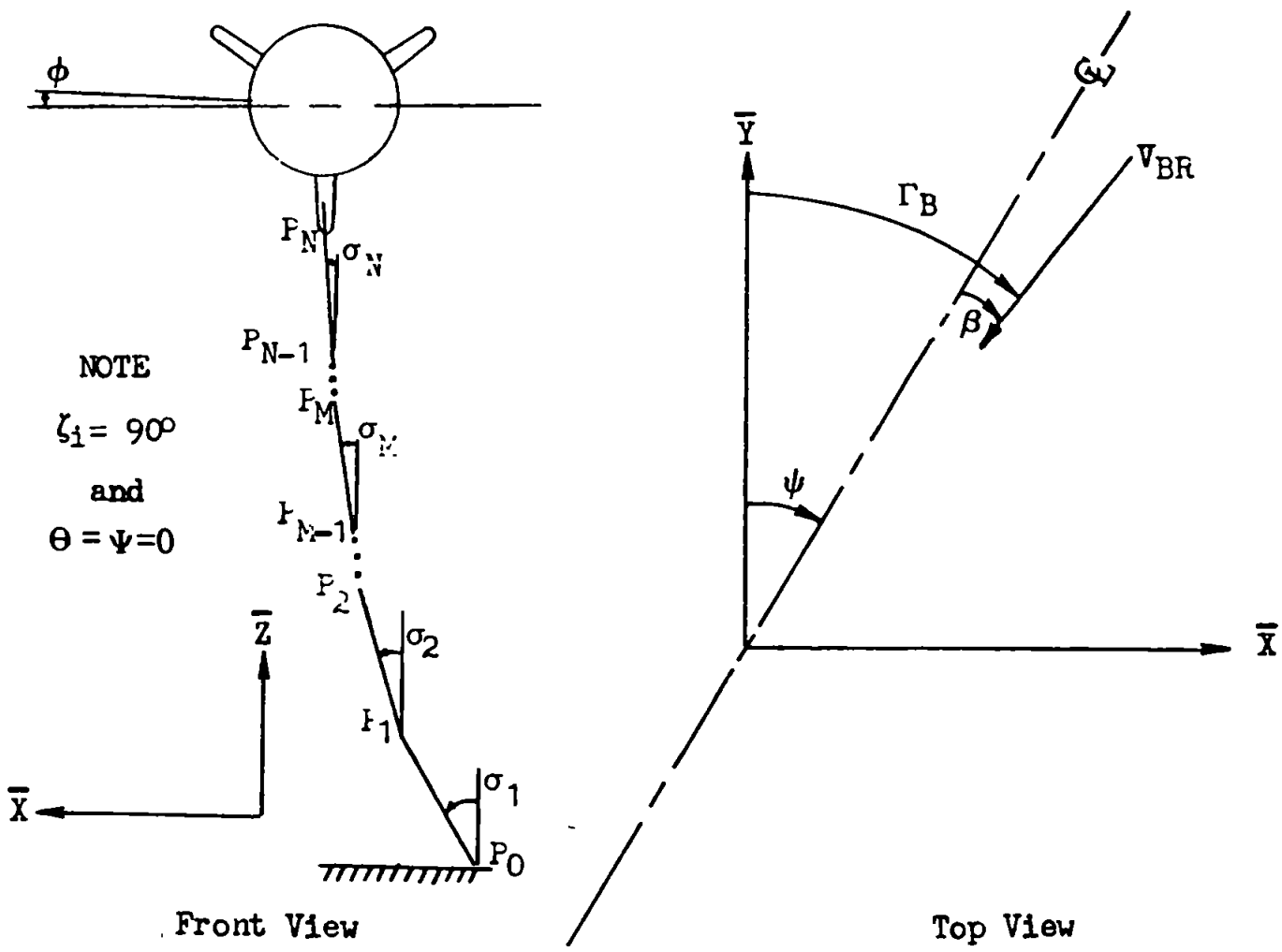

Figure 5. Balloon Tether Model in Lateral Plane

Pertinent geometry of the tethered balloon and applied forces are identified in Figure 6.

In order to separate the equations of motion into a longitudinal response and a lateral response, it was further assumed that the system was near equilibrium. This resulted in a set of equations describing the longitudinal motion which is coupled only in the pitching variables of the balloon and the pitching variables of the tether. However, the second set of equations for the lateral motion does not completely uncouple from the

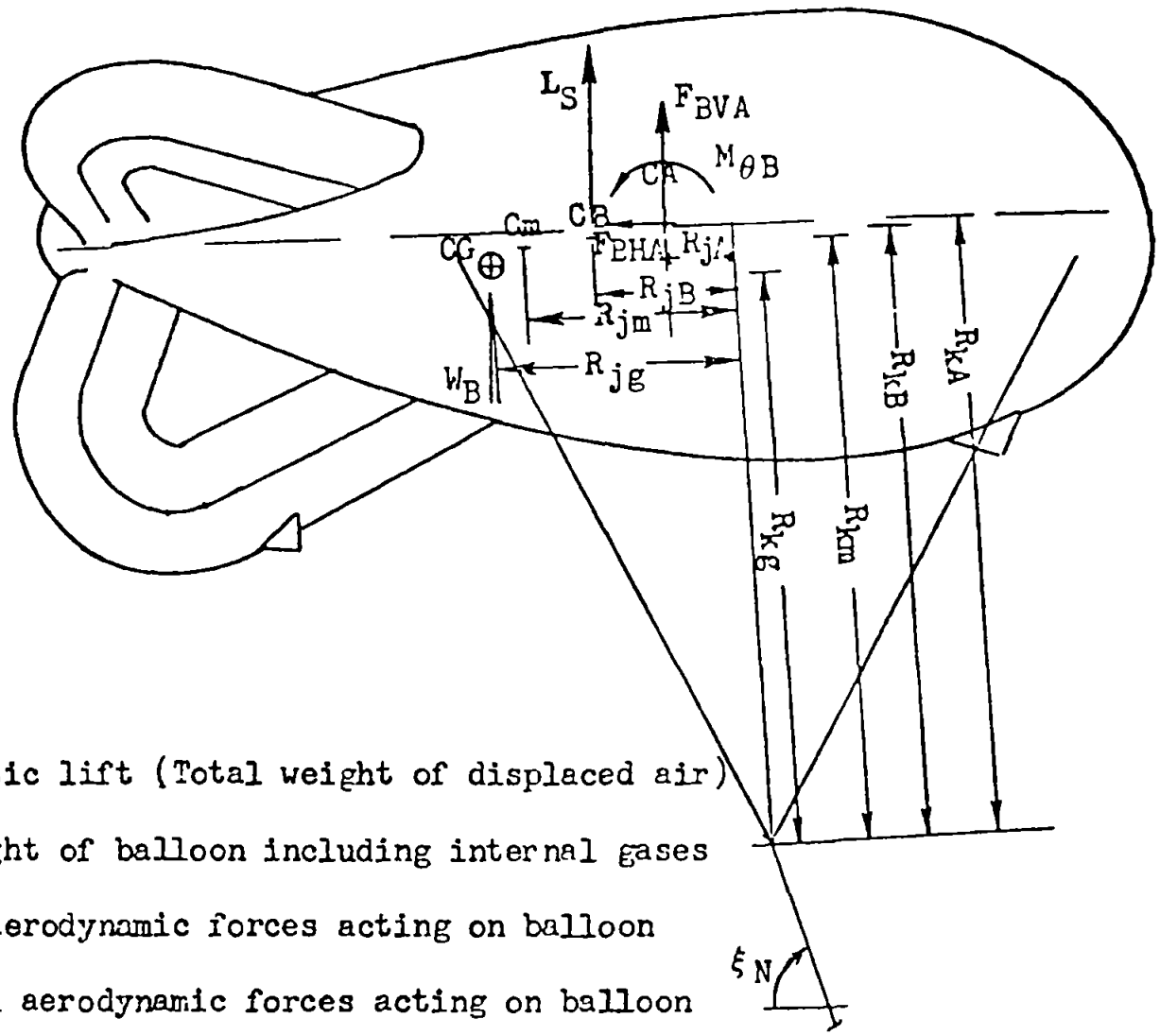

L_S - Gross static lift (Total weight of displaced air)

W_B - Total weight of balloon including internal gases

F_{BVA} - Vertical aerodynamic forces acting on balloon

F_{BHA} - Horizontal aerodynamic forces acting on balloon

$M_{\theta B}$ - Aerodynamic pitching moment acting on balloon

CA - Aerodynamic reference center (at center of hull volume)

CB - Center of buoyancy of total displaced volume

Cm - Apparent mass center and dynamic center in pitch (and yaw)

CG - Center of gravity of total weight of balloon

Figure 6. Balloon Geometry and Applied Forces

longitudinal degrees of freedom because the equilibrium angles in the longitudinal plane are not zero. Therefore, when solving the lateral degrees of freedom, it must be assumed that the longitudinal variables remain constant and equal to their equilibrium values. In both the longitudinal and lateral cases, the tether is simulated by three rigid links. The number of uncoupled dynamic equations is four for the longitudinal response and five for the lateral response.

2. GENERAL STABILITY THEORY

The equilibrium configuration of a tethered ballon can be defined as that position which demands that the summation of all applied moments equals zero. The equilibrium is said to be stable if, for any small disturbance,

the system ultimately returns to its equilibrium conditions. Two types of stability are of interest. In the first (statically stable), a small displacement of the system will create forces which tend to return the system to its equilibrium position. The second (dynamically stable) produces a motion which eventually restores equilibrium. If the motion is periodic, it is characterized by a damped frequency and a damping ratio. Similar definitions apply for statically and dynamically unstable motions. A third possibility is for the system to be neutrally stable during which the motion neither diverges nor converges.

It was necessary during this study to develop techniques to investigate and understand the stability of the system. To this end, characteristic equations are derived. The general approach is as follows:

(1) Derive the nonlinear equations of motion in three dimensions for each degree-of-freedom

(2) Assume the motion is near equilibrium so that the equations can be linearized and separated into a longitudinal motion and a lateral motion

(3) Laplace transform the linear equations from the time domain to the "S" domain assuming that the initial conditions are zero. This establishes a matrix equation of the following form:

$$\left[A\right] \left\{X\ (S)\right\} = \left\{0\right\} \tag{1}$$

where $\{X\ (S)\}$ is the eigenvector and $[A]$ is a square matrix whose elements are quadratics in S containing the physical properties of the system.

(4) Expand the determinant of $[A]$ such that the characteristics polynominal is obtained.

Each root of the characteristic equation represents a term in the general solution of the form, $A_i e\ S_i t$, where S_i is the "i"th root and A_i is an amplitude, dependent on the initial conditions of the system. Both real and complex roots may appear where the complex roots occur in conjugate pairs. In general for "n" degrees of freedom, the characteristic equation will yield "2n" roots. Each pair of complex conjugate roots represents one oscillatory motion, while each real root represents one aperiodic motion.

First consider an oscillatory system. This motion is characterized by two roots of the form $S_i = X \pm i\ Y$, where X and Y are real numbers and $i = \sqrt{-1}$. Several important quantities can be found from the root. The natural frequency associated with this motion is $\omega_n = \sqrt{X^2 + Y^2}$. The damping ratio is $\zeta = \frac{-X}{\omega_n}$. The damping frequency is $\omega_d = \omega_n \sqrt{1 - \zeta^2} = Y$. It is also of interest to know the time to half amplitude for a stable root or the time to double amplitude for an unstable root. This quantity can easily be found by considering one oscillatory motion. The general solution for free vibration is

$$Z = Ce^{-\zeta \omega_n t} \sin(\omega_d t + \emptyset) \tag{2}$$

where $\emptyset$ is the phase angle dependent upon initial conditions

C is a constant dependent upon initial conditions

The second possibility is an aperiodic motion given by the expression

$$Z = Ce^{Xt} \tag{3}$$

where X is the real part of one root and the imaginary part (Y) is zero

If X is negative, Z approaches zero as time increases indefinitely and the motion is said to be overdamped. Like the oscillatory motion, roots which give overdamped motions will also occur in pairs. However, unlike the complex conjugate roots which result in one oscillatory motion, each real root is a dinstinct motion. Therefore, it is possible for an "n" degree-of-freedom system to have "2n" distinct motions if the system is so heavily damped that all the roots to the characteristic equation are real.

There is a third possible motion which is a borderline case. If two roots are real and equal, the system is said to be critically damped. The motion will be aperiodic and both roots will give the same motion.

The general solution to the motion of the system is a linear combination of all the motions defined by the roots to the characteristic equation. Associated with each root is a mode shape which gives the relative amplitudes of each degree of freedom when the system is responding to one particular root. It is of interest to establish these mode shapes so that each stability curve can be associated with a definite motion of the whole system. For example, one mode shape may show that the pitching motion of the balloon is very large compared to the motion of the tether.

3. STABILITY ANALYSIS

Derivations of the equations of motion of the tethered balloon system and development of the characteristic equations for a tethered balloon system approximated with a three-link tether are given in Reference 2.

The four linearized longitudinal equations are Laplace transformed, and an eighth order characteristic equation generated which specifies stability characteristics of the system. In like manner, the five linearized lateral equations can be reduced to a tenth order equation which gives stability information in the lateral degrees-of-freedom. The roots of these characteristic equations identify the natural frequencies, damped frequencies and damping ratios.

Results of characteristic equations analysis can be displayed in the form of plots in a complex plane typically as shown in Figure 10 of this report. In these plots, the abscissa is the real part of the roots to the characteristic equation, the ordinate is the imaginary part. A negative real part means that mode of oscillation is converging or stable; a positive real part is a diverging mode. Only the first and second quadrants are displayed because the roots are complex conjugates which are symmetric to the real axes, except in the case of overdamped roots which lie on the real axes. In general, the following information is easily available for each root directly from the plots. The natural frequency is measured in rad/sec as the distance from the origin to the root; the damped frequency (rad/sec) is the value of the imaginary part of the root; the damping ratio is equal to the absolute value of the real part of the root divided by the natural frequency.

4. DYNAMIC RESPONSE ANALYSIS

The calculation of the balloon system response to specific disturbances is the subject of the dynamic response analysis. The most general motion the system can have is a linear superposition of the normal modes.

Each aperiodic or nonoscillatory normal mode has one arbitrary constant (the initial value of any one of the variables) associated with it; and each periodic or oscillatory normal mode has two arbitrary constants (the amplitude and phase angle of any one of the variables) associated with it. The total number of arbitrary constants is then equal to the number of aperiodic modes plus twice the number of periodic modes; i.e. to the degree of the characteristic equation, or the order of the system. A specific disturbance will excite the normal modes in varying degrees and establish the values of the arbitrary constants.

The dynamic response of tethered balloon systems to various wind disturbances is obtained by integrating numerically the longitudinal and lateral equations of motion to produce a time history of the dynamics. The start conditions, or equilibrium conditions for the dynamic response computer programs are obtained from the linearized stability computer programs (Reference 2). This approach to analysis has the advantage that wind gusts can be produced and the actual motion of the system can be observed. The major disadvantage is that a greater amount of computer time is required when compared to evaluation of stability by investigating the roots of the characteristic equations.

The equations of motion for the longitudinal dynamics of a tethered balloon system were initially derived in two forms (see Appendix A):
1) inertia terms which contain products of angular velocities are neglected,
2) inertia terms which contain products of angular velocities are included.
The concept of neglecting products of angular velocities is associated with the assumption that angular velocities are small; and therefore, products of angular velocities are negligible.

Numerical integrations were made with the computer to determine the effect of neglecting the inertia terms containing products of angular velocities. Although the effect is obviously present (Figures 7 and 8), the overall differences between the results of the two sets of equations is small.

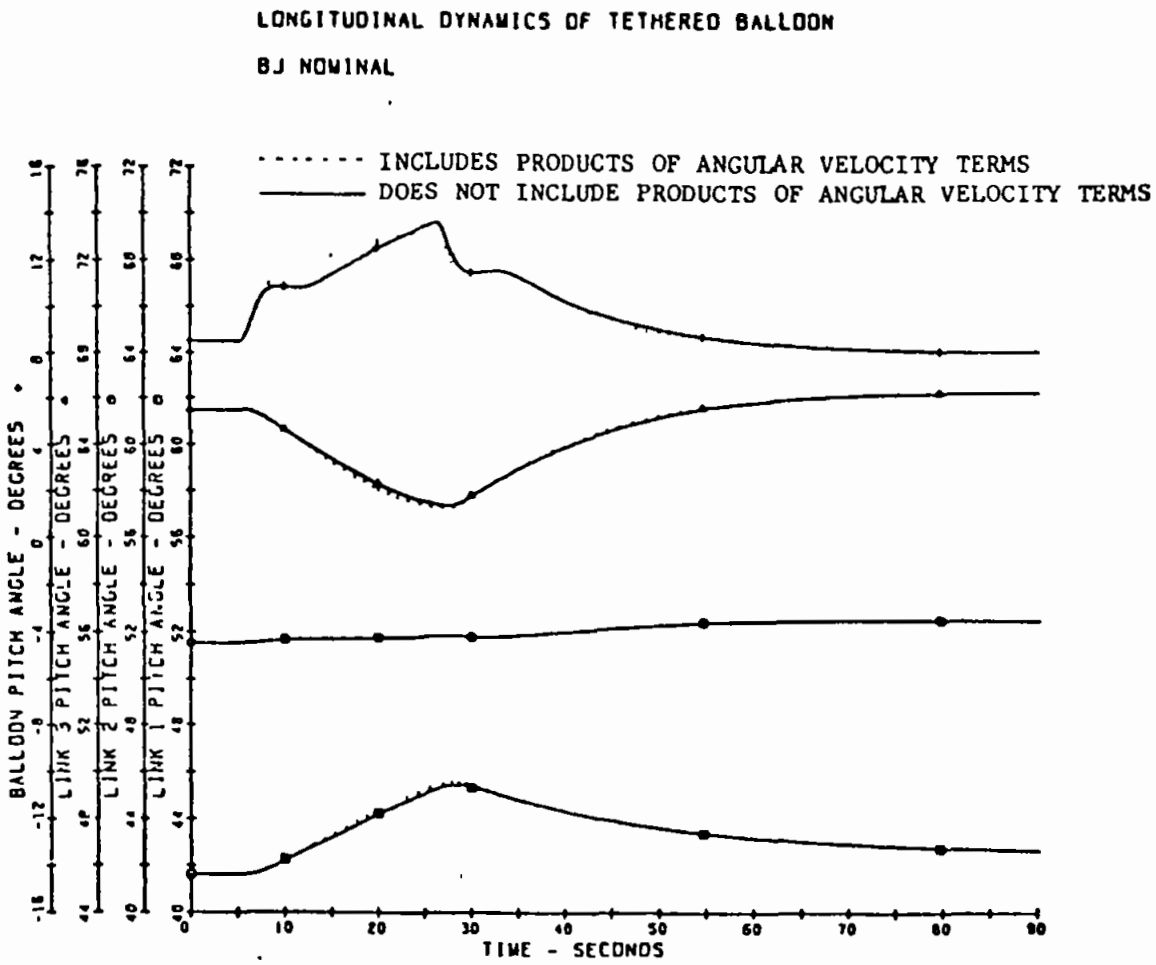

Figure 7

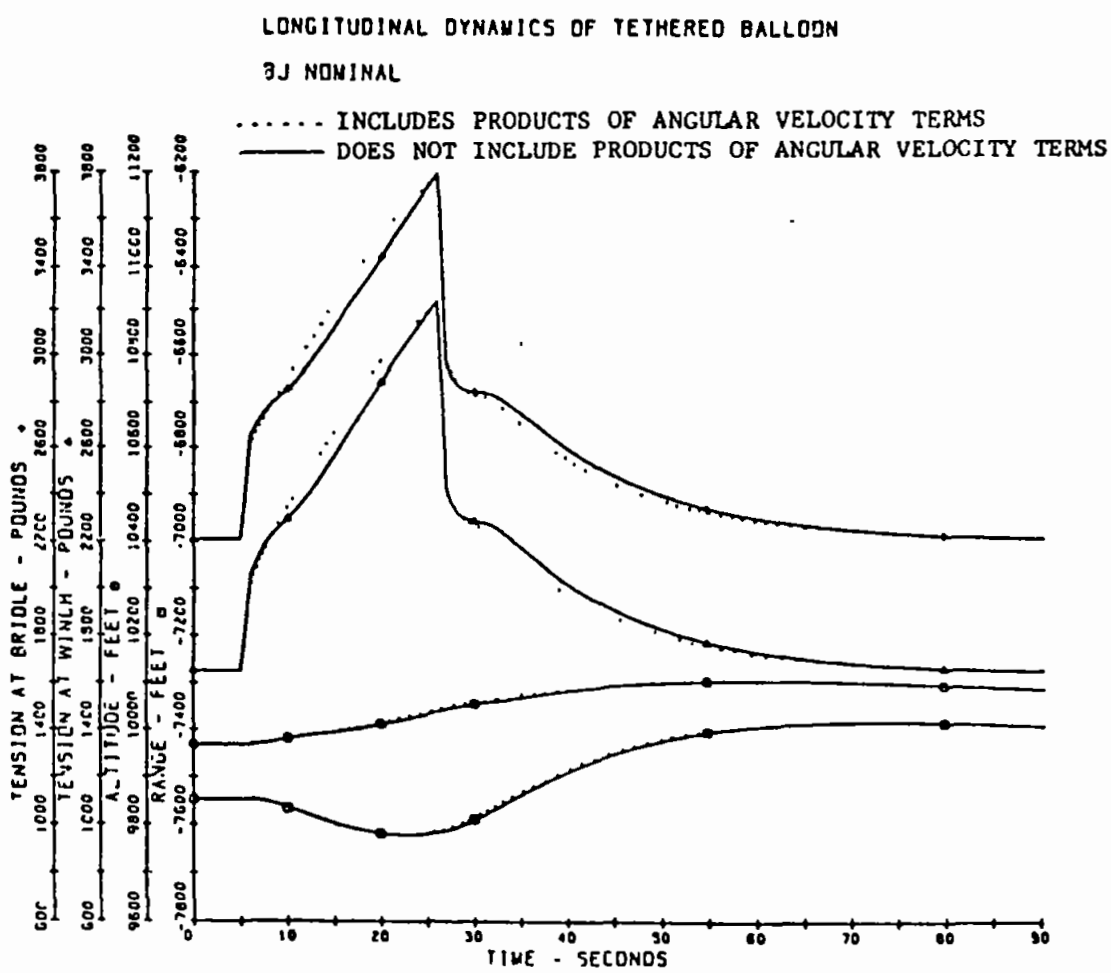

Figure 8

Figure 7 shows the time history of the four generalized coordinates ζ_1, ζ_2, ζ_3, and θ. A horizontal gust of 20 feet per second with a duration of 20 seconds was applied. The dotted lines represent the angular displacement when the products of angular velocities are included in the inertia terms. Figure 8 presents the range and altitude of the balloon as a function of time and also the variation in tether tension at the winch and at the bridle confluence point. Since this gust velocity is considered to be high, it is concluded that the difference between the solid lines and the dotted lines is maximum.

It was decided that dynamic simulation studies would be conducted with a model which neglects products of angular velocities for three reasons. First, the equations containing products of angular velocities are shown to give only slightly different results. Second, it is desirable to keep the dynamic equations compatible to the equations used in the stability study (the stability study used linearized equations). Third, it is desirable to keep the longitudinal equations compatible to the lateral equations (to derive the lateral equations of motion containing products of angular velocities in the inertia terms would be a very difficult task because of the number of terms involved.)

SECTION IV

DYNAMIC RESPONSE OF TETHERED BALLOONS

1. DESIGN CONDITIONS INVESTIGATED

The parametric study conditions found in Appendix B, Tables B-I and B-II and Reference 2 are the source of information for the results and recommendations of this report. Each parametric dynamic response study condition has a computer drawn plot of various balloon parameters versus time. These plots are found in Appendix B.

The parameters chosen for investigation during this study are placed in three major categories:

(1) "Balloon on Station" performance parameters

(2) "Structural Design" performance parameters

(3) "On Board Instrumentation" Design parameters

The "Balloon on Station" performance parameters are defined as balloon displacements from equilibrium and, specifically, are changes in balloon range, altitude, pitch angle, roll angle, yaw angle, and lateral displacement induced by a parameter variation, such as a change in trim angle.

The "Structural Design" performance parameters of interest are the cable tension at winch and bridle, and the balloon translational and rotational accelerations.

The "On Board Instrumentation" design parameters are defined as the balloon angular displacements and rates.

The effects of gusts, trim angle, altitude, tail size, and other parameters on balloon performance parameters are reviewed in detail later in this section of the report. Table III lists the cases compared and the reason for comparison for the longitudinal and lateral cases.

The operational winds used for the investigation, as a function of altitude, are listed in the Introduction to this report. Gusts used for dynamic response are added to the operational winds and are applied to the balloon. The gusts used in analysis are discussed next.

Consider the nominal altitude condition of 10,000 feet where the operational design wind was 67.5 feet per second. Longitudinal gusts were applied where the horizontal wind increased by 30 percent, for a discrete time, to a value of 1.3 x 67.5 = 87.6 fps. Gusts of 2, 10, and 20 seconds and infinite time durations were investigated with various rise times. A case was also investigated where the 30 percent gust increment was applied vertically upward.

Table III

A. Comparison of Longitudinal Dynamic Cases

Cases Compared	Balloon Type	Reason for Comparison
1,2,3,4,5	BJ Nominal	Gusts and Wind Effects
3,21,18	All	Comparison of Balloon Types
3,6,7	BJ Nominal	Trim Angle Effects *
18,19,20	VEE Balloon	Trim Angle Effects *
21,22,23	GAC Balloon	Trim Angle Effects *
11,3,12	BJ Nominal	Tail Size Effect
3,14,15	BJ Nominal	Winching Effects
13,3	BJ Nominal	Reduced Wind (40%) Effect
10,3	BJ Nominal	Amgal vs NOLARO
16,3	BJ Nominal	Effect of Payload on Underside of Balloon
17,3	BJ Nominal	Winch at 5000 Ft, and 0.0 Ft.
8,3,9	BJ	Operational Altitude Effects

* Trim angle changed by varying fore and aft location of bridle confluence poin

B. Comparison of Lateral Dynamic Cases

Cases Compared	Balloon Type	Reason for Comparison
24,25,26	BJ Nominal	Effects of Gust Ramp Time
27,26	BJ Nominal	Effects of 50% Increase in Gust Velocity
40,37,25	BJ, VEE,GAC	Comparison of Balloon Types
32,25,33	BJ	Tail Size Effect
37,38,39	VEE Balloon	Tail Size Effect
35,36	BJ Nominal	Winch Effects
34,25	BJ Nominal	Reduced Wind Effect (100%→40%)
31,25	BJ Nominal	Effects of Amgal vs NOLARO
29,25,30	BJ	Operational Altitude Effects

The lateral gusts applied to the tethered balloon systems to investigate dynamic response may be generally interpreted in two ways as shown in Figure 9 which depicts the wind in a horizontal plane.

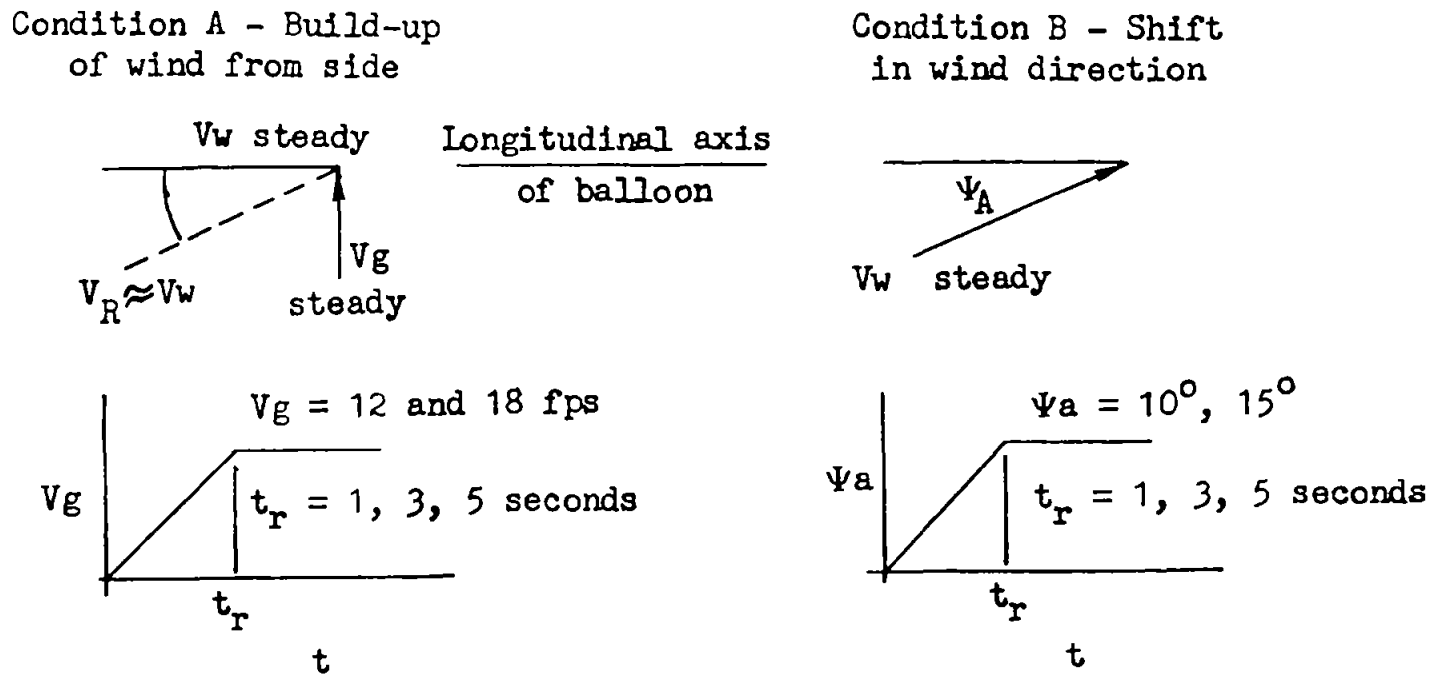

Figure 9 . Lateral Wind Gusts

In Condition A the wind gust from the side builds up with time. This is approximately equivalent to the Condition B where the wind remains constant in magnitude and changes heading direction with time.

2. GENERAL DISCUSSION OF DYNAMIC RESPONSE OF TETHERED BALLOON SYSTEMS

The non-linear differential equations defining the motion of a tethered balloon system and the linearized equations used in studying the stability characteristics of the balloon system are given in Reference 2 together with the results of the stability analysis of various balloon systems. Appendix A of this report expands the equations of motion of Reference 2 to include wind gusts. The response of the non-linear balloon system when subjected to wind gusts has been programmed for computer solution using numerical integration methods. Various balloon systems, subjected to different types of gusts, have been studied using this computer program and the results are found in Appendix B.

The response plots shown in Appendix B reveal that the balloon systems are highly damped. This agrees with the stability analyses of the balloon systems given in Reference 2. In fact, the motion is so highly damped that the lower frequency response modes are, in general, damped out within two cycles or less of motion. Thus, the high aerodynamic damping involved in the balloon systems, makes it very difficult to evaluate the response plots with regard to phase relationships between coordinates, damping characteristics, and the frequencies involved in the motion. It becomes evident after looking at the

response plots that only the amplitude and direction of the response can be obtained. A mathematical tool will be required to obtain information regarding phase relationships, natural frequencies, and damping characteristics of the modal motions involved. Such a tool would be very valuable for evaluating flight data from tethered balloons.

What then, is this mathematical tool? The response of a highly damped multidegree of freedom system to a known disturbance can be represented mathematically as the sum of the system's modal responses. Assuming the system follows the response of a viscously damped system, a modal response definition is given by the following equation.

$$Z_i = \left(C_i e^{-\zeta_i \omega_{n_i} t}\right) \sin(\omega_{d_i} t + \phi_i)$$

The total response Z_T of a particular coordinate is then given by

$$Z_T = \sum_{i=1}^{i=N} \left(C_i e^{-\zeta_i \omega_{n_i} t}\right) \sin(\omega_{d_i} t + \phi_i) \qquad (1)$$

N represents the number of frequencies involved in the response

ζ represents the damping ratio

ω_n represents the natural frequency

ω_d represents the damped frequency

ϕ_i represents the phase angle

C represents an amplitude constant

Each modal response Z_i has 4 unknowns, since ω_d is related to ω_n by $\omega_d = \omega_n \sqrt{1 - \zeta^2}$.

Thus any response curve which is defined by a sufficient number of points can be mathematically represented by Equation (1) and solved for the unknown constants using numerical curve fitting methods. No curve fitting program is presently available to the project for use with Equation (1); however, there is a curve fitting program available which uses a Fourier Transform and performs a power spectral density (P.S.D.) analysis of the Fourier Transformation. This program is only valid for analyzing systems with no damping. The program still gives a general overall view of the frequencies involved in the motion and it is thought worthwhile to analyze the response of two dynamic cases and to compare the frequencies found with the frequencies obtained from the stability analysis of the same balloon configurations given in Reference 2. The dynamic cases chosen for frequency comparison are lateral dynamic response Case 28 and longitudinal dynamic response Case 4. The cases represent a nominal BJ balloon at 10,000 feet. Lateral response is for a 10 second duration step side gust and longitudinal response is for a 20 second duration step horizontal gust.

a. COMPARISON OF THE NON-LINEAR LATERAL DYNAMICS CASE 28, WITH THE LINEARIZED STABILITY CASE 1

The small displacement motion of a forced non-linear system, in the time era after the forcing function is removed, should result in system motions similar to the sum of the mode shape times participation factor for each mode found in the linearized stability analysis of the system. To verify this, Lateral Dynamics Case 28 and Lateral Stability Case 1 (Reference 2) were chosen for comparison. A complete description of Lateral Dynamics Case 28 is found in Appendix B, and the Lateral Stability Case 1 description is found in Reference 2. For convenience the results of Lateral Stability Case 1 are summarized in Table IV and Figure 10 of this report. In order to analyze the coordinate motions of Case 28, a power spectral density analysis with Fourier Transform was performed on each of the lateral coordinate degrees of freedom; ψ, ϕ, σ_1, σ_2, σ_3. The input coordinate waveforms and PSD plots for each degree of freedom are given in Figures 11 and 12.

The PSD plots reveal that there are two predominate modes involved in the system motion. These are underdamped oscillatory modes 1 and 2 with natural frequencies and damping ratios of $f_{n_1} = 0.0051$ Hz and $\zeta_1 = 0.511$ for mode 1 and $f_{n_2} = 0.136$ Hz and $\zeta_2 = 0.207$ for mode 2. Mode one (0.0051 Hz) is the predominate mode with mode 2 (0.136 Hz) of smaller amplitude superimposed on mode 1. The lateral wind gust disturbance in Case 28 is removed after T = 11 seconds, therefore all comparisons should be made after the first peak is reached beyond 11 seconds. It should be noted that mode 2 is predominately a ϕ or roll mode, and this is evident from the plots of the coordinates, since only the ϕ coordinate plot has evidence of a 0.136 Hz mode. On the ϕ plot mode 2 appears damped out of the ϕ motion by the time T = 37 sec.

Table IV. Summary of Lateral Stability Case 1

Normalized Modes

Mode Number	Frequency Hz	Damping Ratio	ψ		ϕ		σ_1		σ_2		σ_3	
			Ampl.	$\measuredangle^{o}$	Ampl.	$\measuredangle^{o}$	Ampl.	$\measuredangle^{o}$	Ampl.	$\measuredangle^{o}$	Ampl.	$\measuredangle^{o}$
1	0.0051	0.511	1.0	0.0	0.195	301	0.342	83.3	0.429	222	0.483	275
2	0.1363	0.207	1.0	0.0	9.12	252	0.016	17.7	0.051	215	0.102	58.9
3	0.000215	1.0	1.0	0.0	0.0082	0	8.86	180	2.51	180	0.487	180
4	0.0252	1.0	1.0	0.0	0.927	0	1.22	360	2.27	180	0.957	360
5	0.0578	1.0	1.0	0.0	1.58	0	2.02	360	3.59	180	1.54	360
6	0.1295	1.0	1.0	0.0	23.1	180	0.345	180	0.147	360	0.513	360
7	0.1608	1.0	1.0	0.0	60.7	360	7.34	180	6.09	180	12.7	360
8	0.4320	1.0	1.0	0.0	0.988	360	0.00007	180	0.0006	360	0.0051	180

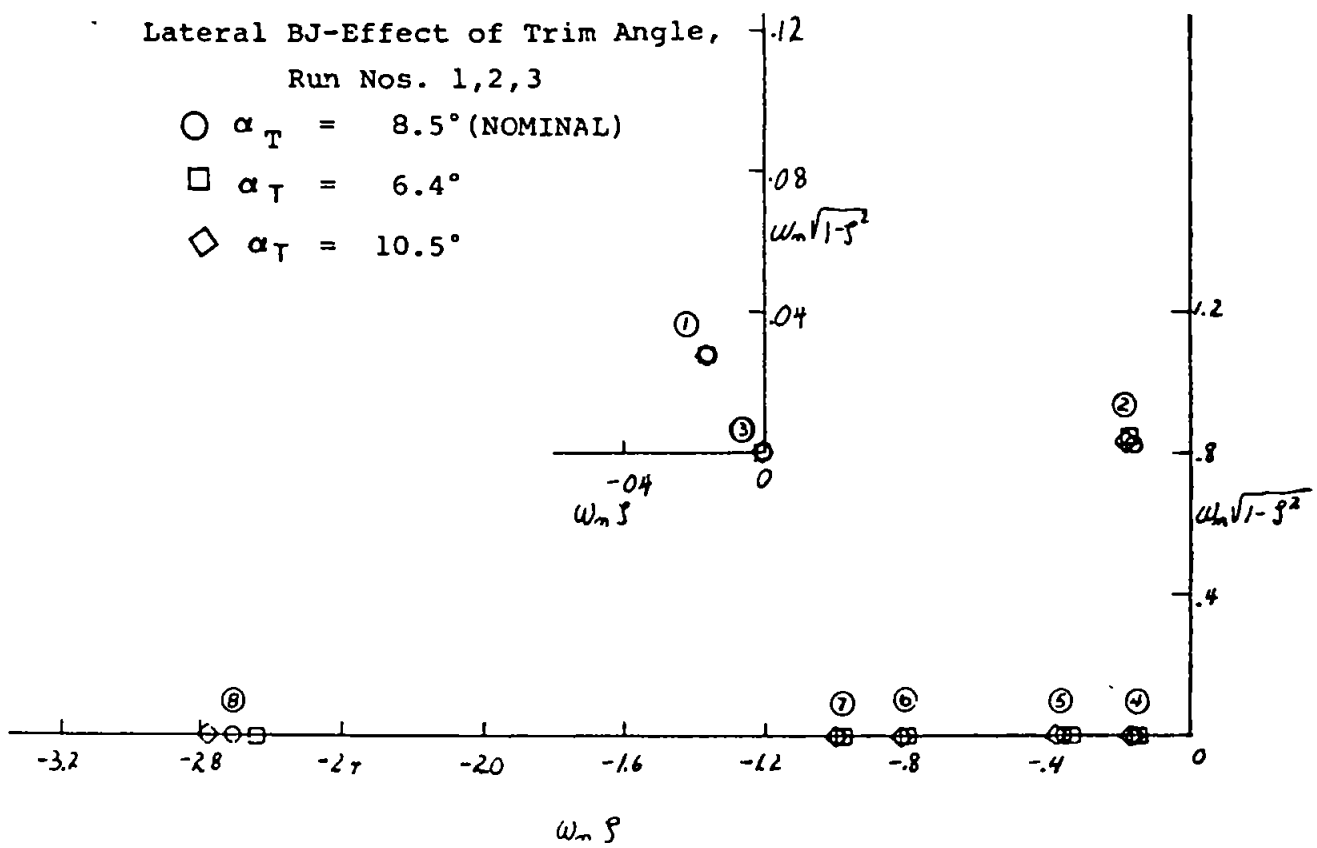

Lateral BJ-Nominal, Run No. 1

Mode Shapes

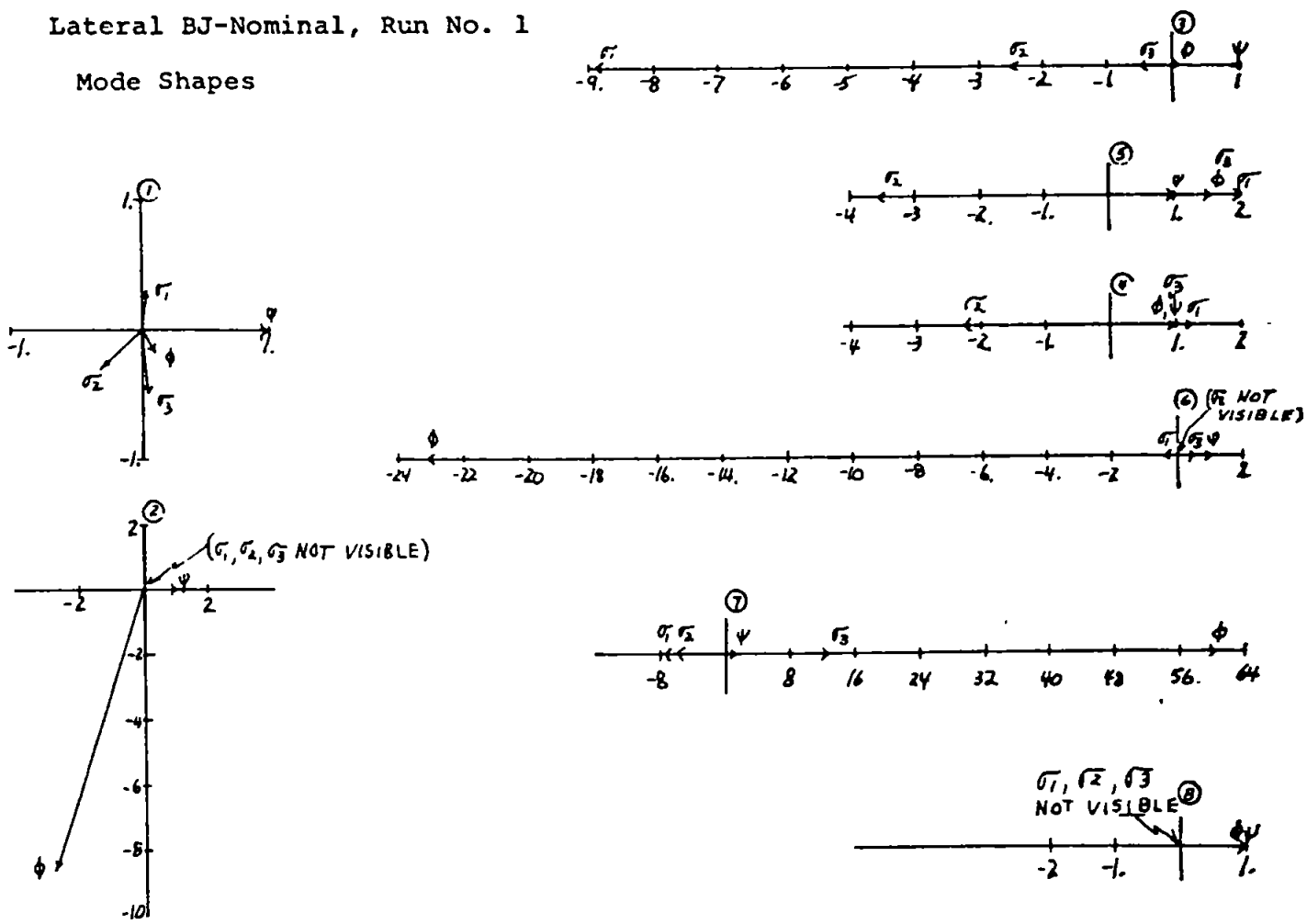

Figure 10. Lateral Stability Characteristics of Nominal BJ Tethered Balloon at 10,000 Feet Altitude

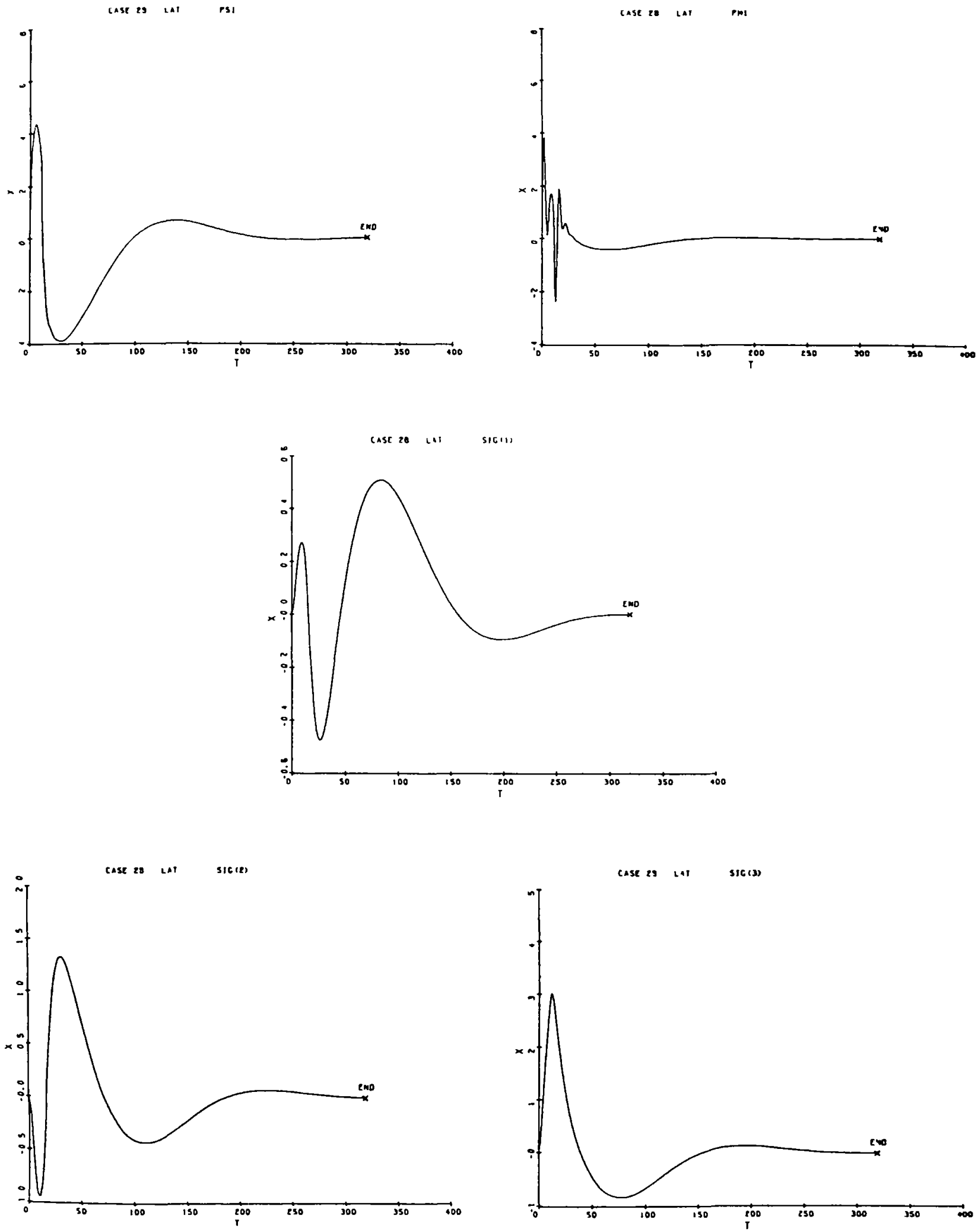

Figure 11. Lateral Case 28, Coordinates Response

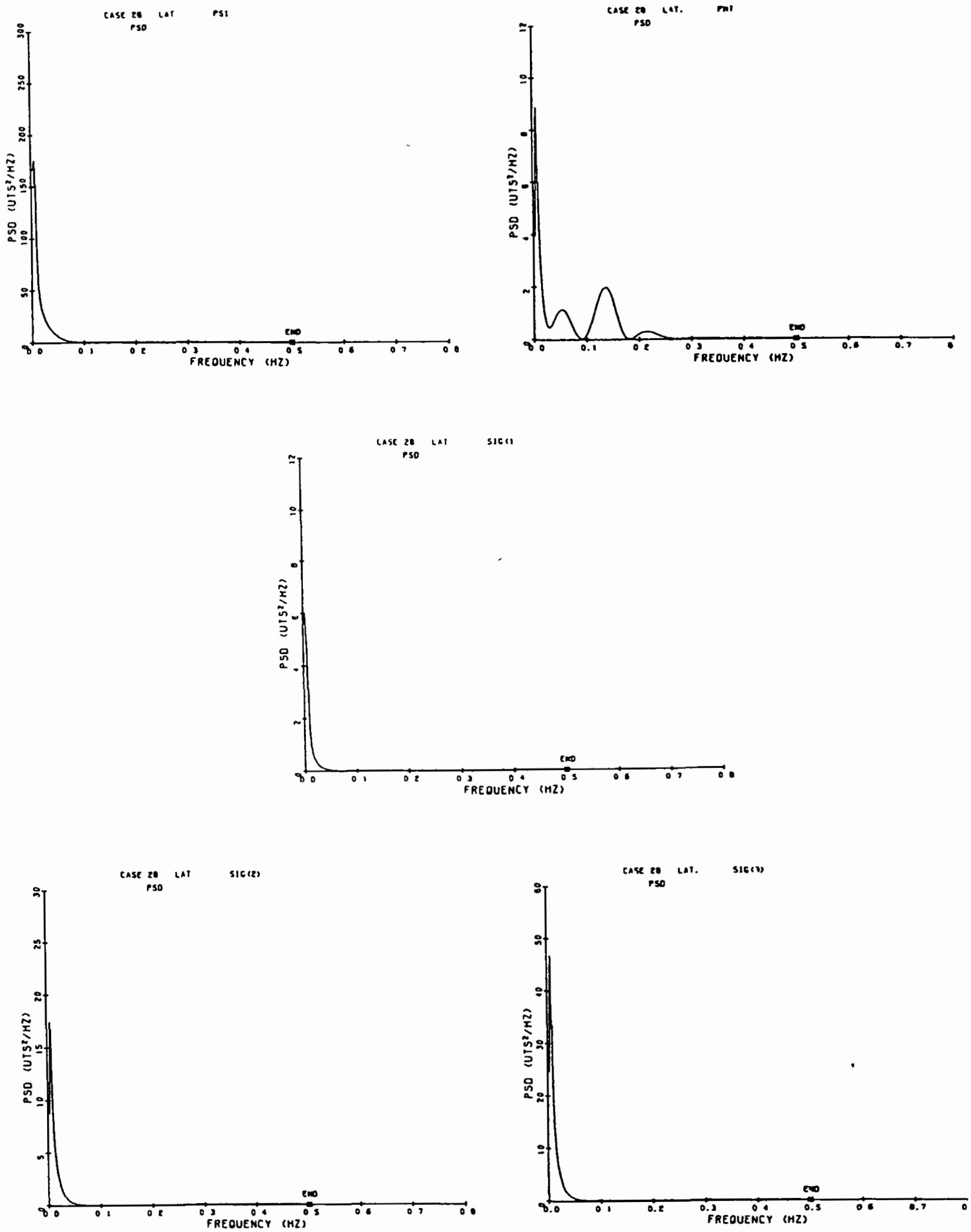

Figure 12. Lateral Case 28, Power Spectral Density

The aerodynamic damping characteristics of the system appear viscous in nature for the 0.0051 Hz mode.

Table V lists, for Case 28, the time and amplitude of the various coordinates for the first and second peaks after the gust is removed. Included in Table V is the period, amplitude ratio, and frequency as calculated from the coordinate data of Case 28.

The period and amplitude ratio for the coordinates ψ, ϕ, and σ_3 show very good agreement with a 0.0051 Hz viscously damped (ζ = 0.51) system. The period between peaks of a 0.0051 Hz viscously damped system with $\zeta = 0.51$ is given by

$$T = \frac{1}{f\sqrt{1 - \zeta^2}} = \frac{1}{0.0051\sqrt{1 - 0.51^2}} = 228 \text{ sec.}$$

The amplitude ratio between successive peaks is given by

$$\frac{X_{n+1}}{X_n} = e^{\left[\frac{-2\pi\zeta}{\sqrt{1-\zeta^2}}\right]} = e^{\left[\frac{-2\pi\ (0.51)}{\sqrt{1-0.51^2}}\right]} = 0.025$$

Table V. Peak Amplitudes for Lateral Dynamics Case 28

Coordinate	First Peak After Gust		Second Peak After Gust		Period T Sec.	Frequency $\frac{1}{T}$	Ampl. Ratio $\frac{X_{n+1}}{X_n}$
	Time	Ampl.	Time	Ampl.			
ψ	29	-3.905	250	-0.099	221	0.0045	0.0253
ϕ	61	-0.404	289	-0.00973	228	0.0044	0.0241
σ_1	26	-0.475	197	0.0943	171	0.0059	0.199
σ_2	31	1.33	224	0.0630	193	0.0052	0.0474
σ_3	76	-0.834	304	-0.0207	228	0.0044	0.0248

b. COMPARISON OF NON LINEAR LONGITUDINAL DYNAMICS, CASE 4, WITH LINEARIZED LONGITUDINAL STABILITY, CASE 1

A description of Longitudinal Dynamics, Case 4, is found in Appendix B and Linearized Longitudinal Stability, Case 1, is defined in Reference 2. A summary of the Longitudinal Stability, Case 1, is given in Table VI and Figure 13 of this report.

A Fourier and PSD analysis is performed on each of the Longitudinal Dynamics, Case 4, coordinate degrees of freedom θ, ξ_1, ξ_2, and ξ_3. The input coordinate waveform and PSD plot for each degree of freedom is given in Figures 14 and 15 respectively.

The need of a mathematical tool for analyzing a highly damped response is very evident in Longitudinal Dynamics, Case 4. The response of every coordinate is damped out, or nearly so, in less than one cycle. The Fourier and PSD non-damped harmonic analyis of this motion is not too meaningful. However, it does indicate that the motion is comprised of frequencies below 0.05 Hz with the most power below 0.01 Hz.

Table VI. Summary of Longitudinal Stability Case 1
(Reference 2)

Normalized Modes

Mode Number	Frequency Hz	Damping Ratio	θ		ξ_1		ξ_2		ξ_3	
			Ampl.	∠°	Ampl.	∠°	Ampl.	∠°	Ampl.	∠°
1	0.00554	-0.037	1.0	0.0	2.14	281.	1.27	238.	1.28	194.0
2	0.0728	0.653	1.0	0.0	0.131	197.	0.080	353.	0.058	39.7
3	0.0986	0.51	1.0	0.0	0.0747	9.6	0.214	188.	0.145	7.4
4	0.0156	1.0	1.0	0.0	0.888	0.0	0.800	0.0	0.363	180.
5	0.1715	1.0	1.0	0.0	0.00033	0.0	0.0123	0.0	0.0066	180.

c. YAW-ROLL COUPLING IN LATERAL DYNAMIC CASES

Yaw-roll coupling for BJ and GAC single hull balloons subjected to lateral wind is evident when the ψ response plots are reviewed. The Vee balloon appears to have negligible coupling. As an example, observe the motion of coordinate ψ (Reference Appendix B) for Lateral Case 28. One would think that, when a balloon is in equilibrium with a steady head wind and then is subjected to a side gust from the left, the balloon would yaw into the resultant wind. This would be a negative yaw angle, however, Lateral Case 28 shows the balloons first yaw motion is positive or away from the resultant wind for a time of approximately 7 seconds and to $\psi = +4°$ before the balloon starts yawing toward the resultant wind.

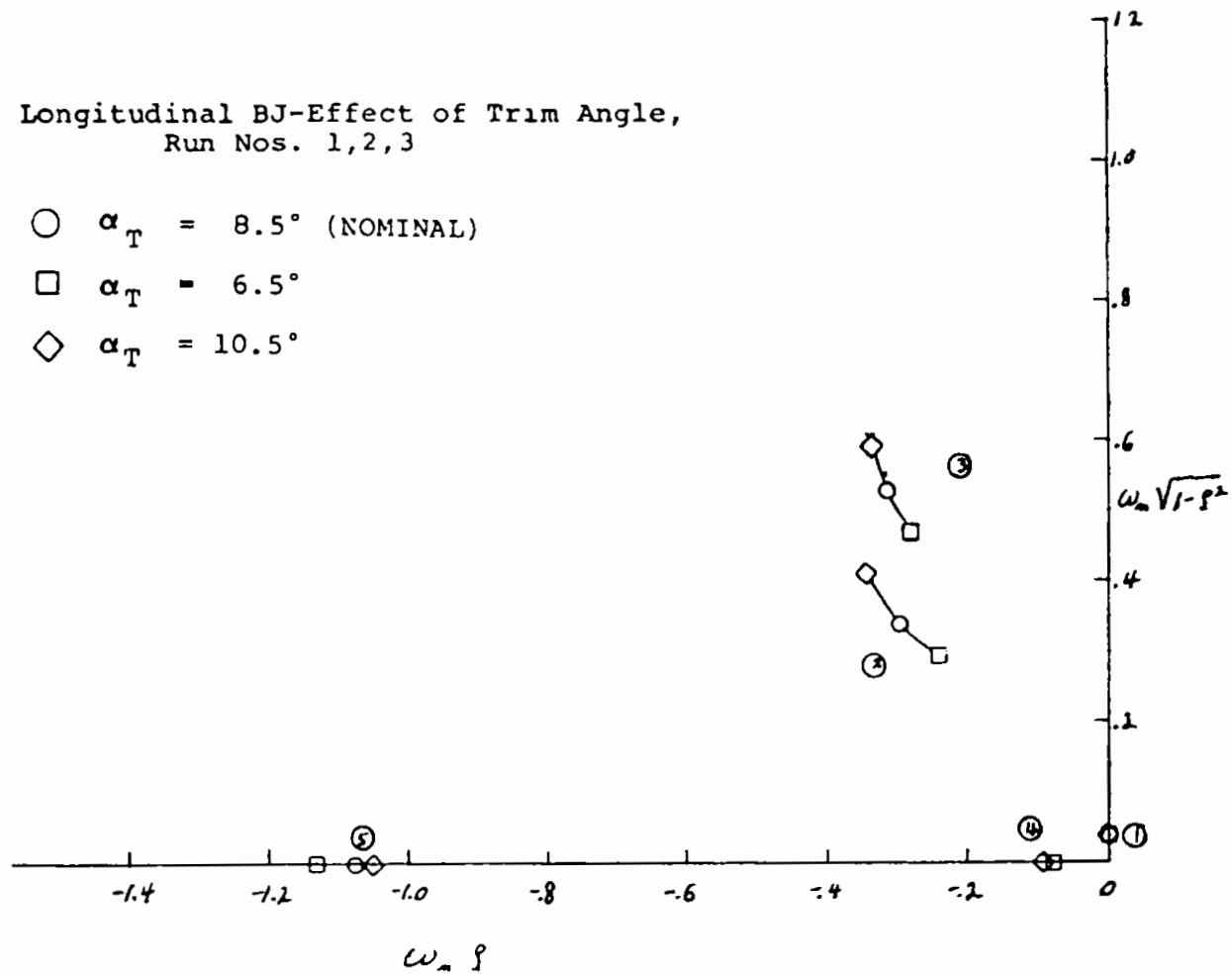

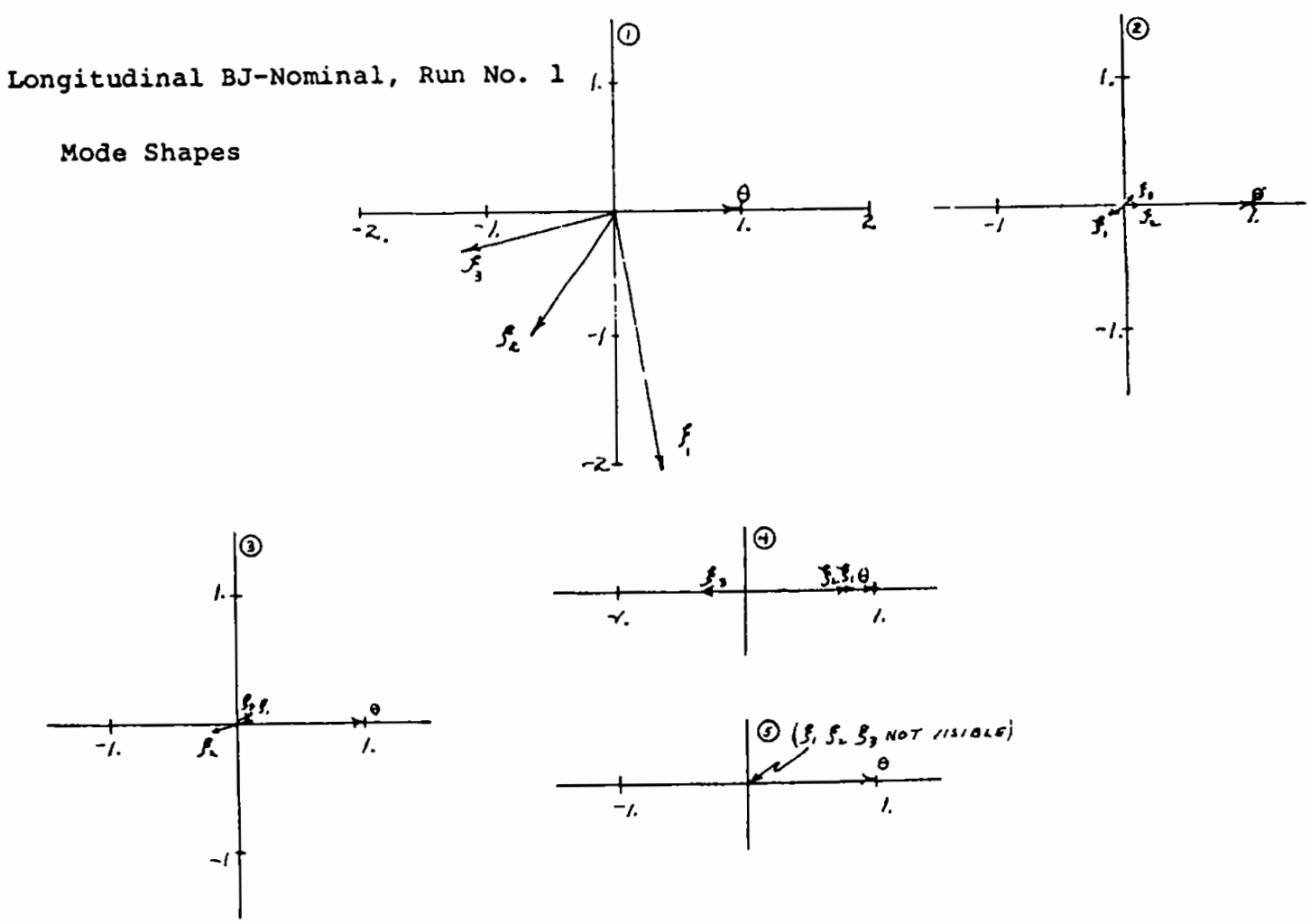

Figure 13. Longitudinal Stability Characteristics of Nominal BJ Tethered Balloon at 10,000 Feet Altitude

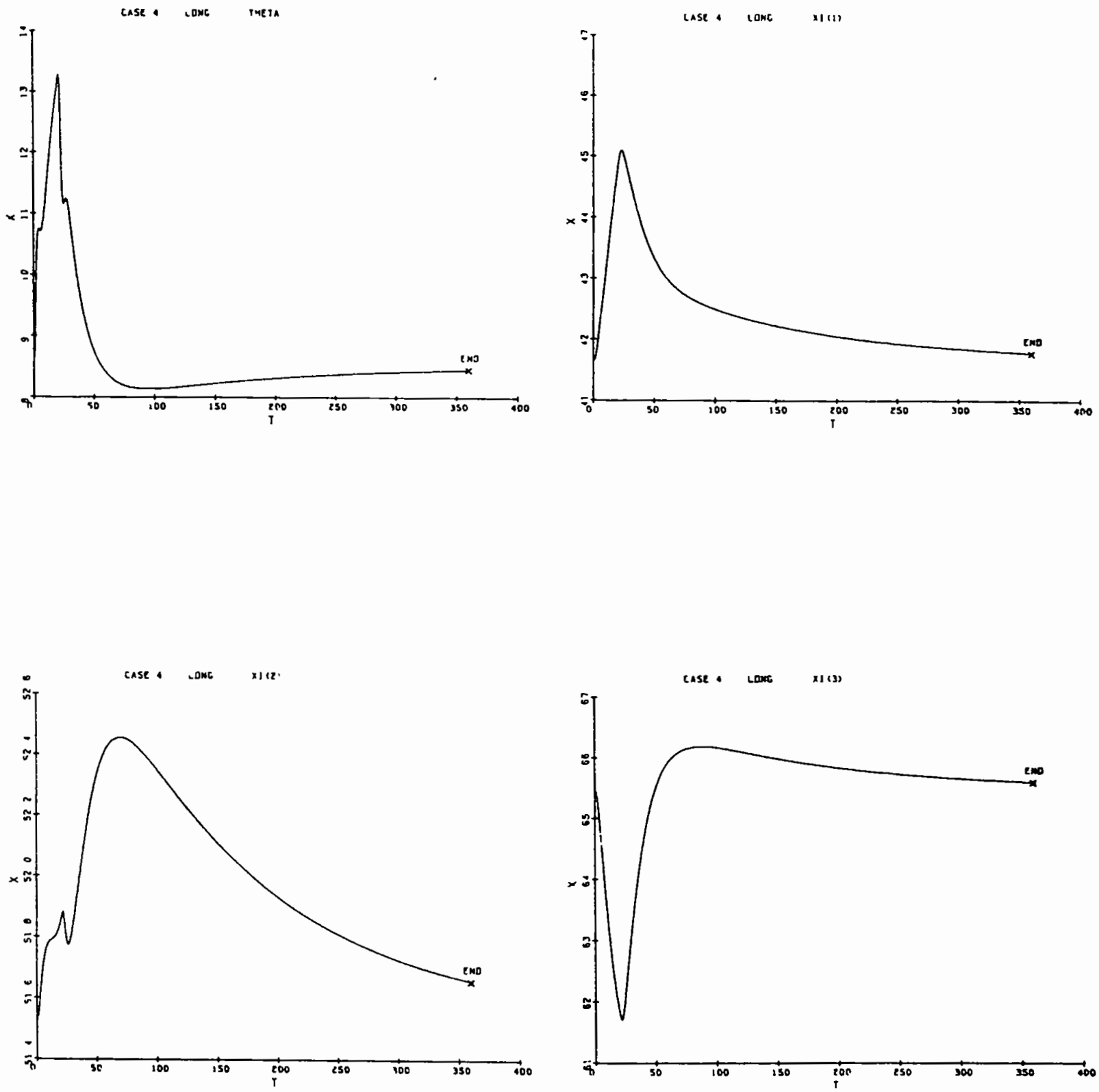

Figure 14. Lateral Case 4, Coordinates Response

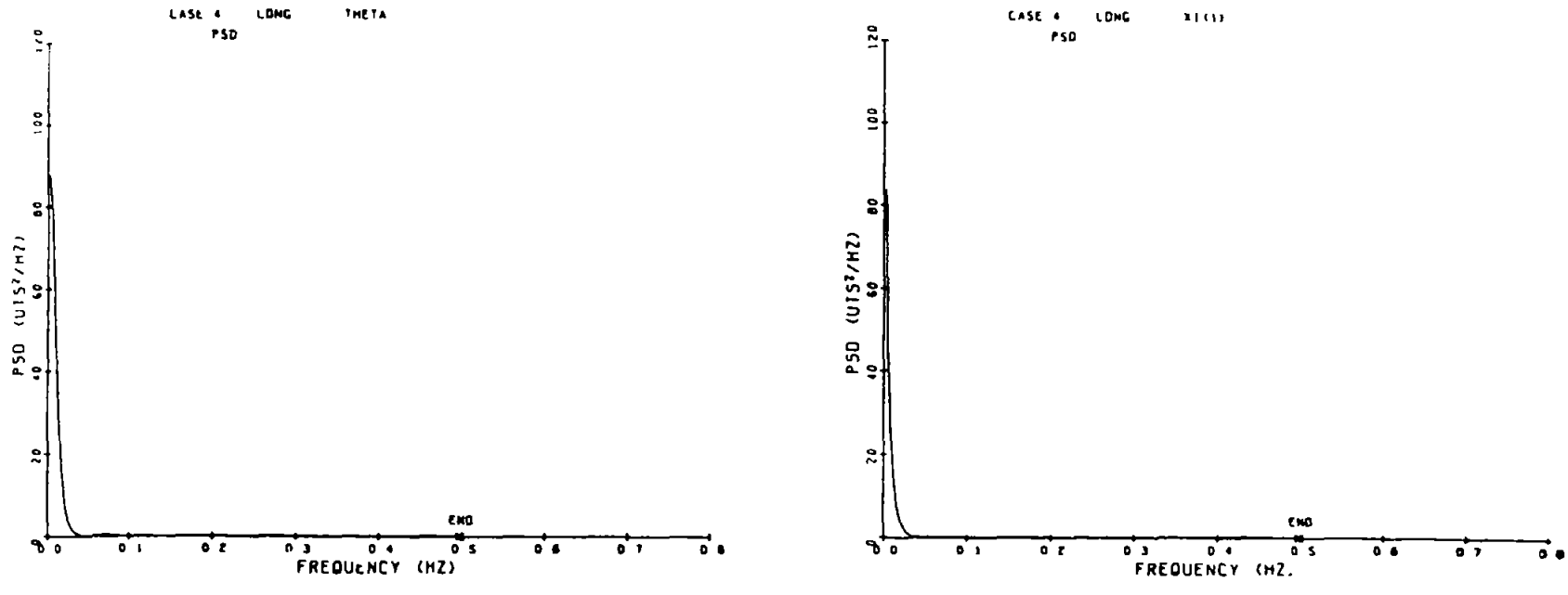

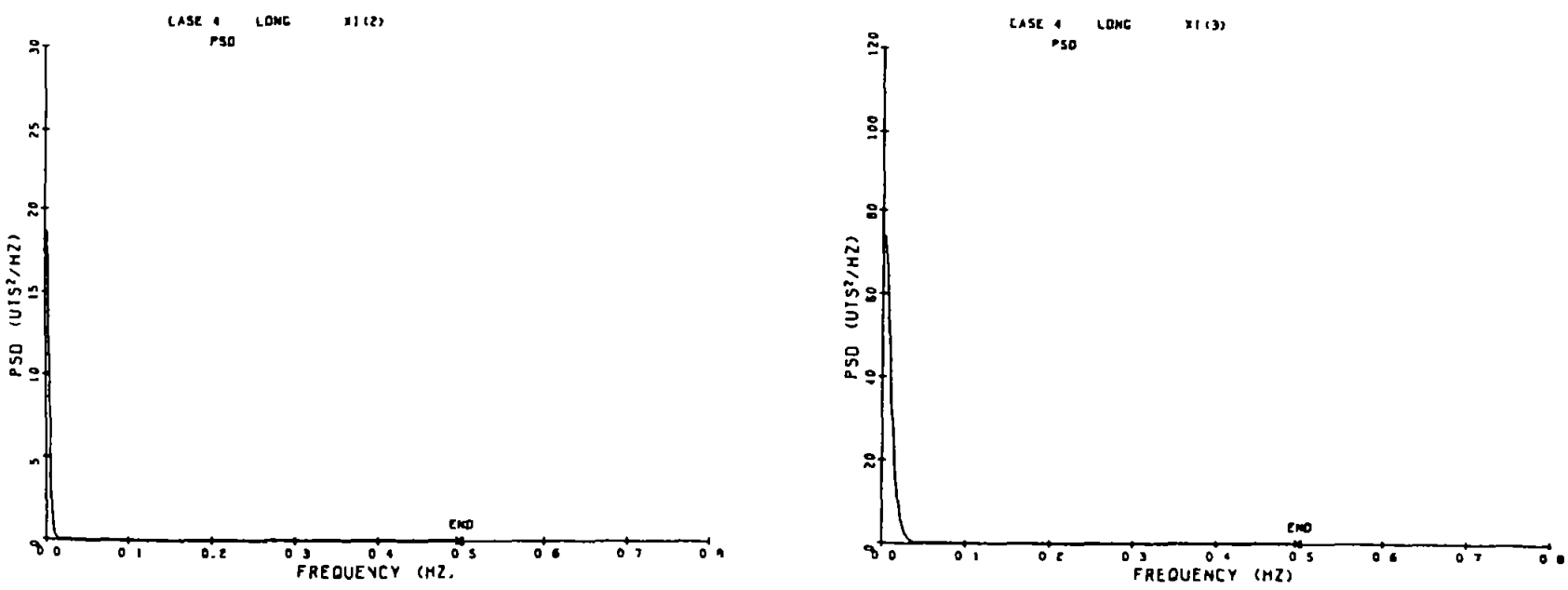

Figure 15. Lateral Case 4, Power Spectral Density

To explain this motion refer to Equation 86 in Appendix A. Neglecting link acceleration terms results in the following equation.

$$F_{\psi} = \left\{ M_S \left[-R_{jm} \epsilon_{33} + R_{km} \epsilon_{23} \right] \left[- R_{km} \right] - I_{YB} \; S\theta + I_{YZB} \; C\theta \; C\phi \right\} \ddot{\phi}$$

$$+ \left\{ M_S \left[-R_{jm} \epsilon_{33} + R_{km} \epsilon_{23} \right]^2 + \left[M_L \; -R_{km} \epsilon_{13} \right]^2 \right.$$

$$+ \left[M_V \; R_{jm} \epsilon_{13} \right]^2 + C^2 \theta \left[I_{XB} \; S^2 \phi + I_{ZB} \; C^2 \phi \right]$$

$$\left. + S^2 \theta \; I_{YB} - S^2 \theta \; C\phi \; I_{YZB} \right\} \ddot{\psi}$$

Substituting a and b for the coefficients of $\ddot{\phi}$ and $\ddot{\psi}$ results in the following equation.

$$F_{\psi} = a \ddot{\phi} + b \ddot{\psi}$$

The equation is solved for

$$\ddot{\psi} = \frac{F_{\psi} - a \ddot{\phi}}{b}$$

where F_{ψ} is the total externally applied balloon yaw moment.

Case 28 parameters have the following values at T = 5.5 seconds (from digital printout of Case 28).

F_{ψ} = -40039 ft-lb	$\ddot{\phi}$ = 3.060 °/sec^2	$\ddot{\psi}$ = 1.207°/sec^2
I_{XB} = 116,000 Slug Ft^2	$\dot{\phi}$ = 2.373 °/sec	$\dot{\psi}$ = 1.989°/sec
I_{YB} = 26,000 Slug Ft^2	ϕ = 0.531°	ψ = 0.426°
I_{ZB} = 119,000 Slug Ft^2		
I_{YZB} = 12,500 Slug Ft^2		

Inspection of the $\ddot{\psi}$ coefficient, b, reveals it to be positive. Since $F\psi$ = -40039 ft-lb and will tend to turn the balloon into the resultant wind, the only term left to cause $\ddot{\psi}$ to be positive is the roll coupling term $a\ddot{\phi}$ In conclusion the initial $\dot{\psi}$ motion away from the resultant wind is caused by roll ($\dot{\phi}$) inertia coupling.

3. EFFECTS OF DESIGN PARAMETERS ON TETHERED BALLOON DESIGN

a. Balloon on Station Performance Parameters

(1) General. As listed in Part 1 of this section a number of tethered balloon design parameters and flight conditions were varied to establish their influence on a tethered balloon design. This subsection summarizes some of the major effects on tethered balloon dynamic behavior as established from the dynamic response calculations presented in Appendix B and an evaluation of these data.

(2) Wind Gust Effects. The response data in Table VII shows the effect of increasing the duration of a horizontal gust on the longitudinal motions of the nominal BJ balloon design for 10,000 foot altitude. It is apparent from an examination of these data that the longer duration of the gust the greater the angle of attack of the balloon becomes. A new equilibrium condition is reached when the gust is left on indefinitely. As a consequence of the increased angle of attack and wind velocity the aerodynamic lift increases and a somewhat more favorable aerodynamic lift to drag ratio is obtained. This serves to increase the altitude of the balloon and reduce the downwind displacement of the balloon. A substantial increase in tether tension is also evident.

A nominal BJ balloon operating at 10,000 feet is subjected to a 20.2 ft/sec, 20 second duration, horizontal gust in Longitudinal Case 4 and to a 20.2 ft/sec, 20 second duration, vertical gust in Longitudinal Case 4A. Table VII also summarizes the results of these two cases.

Table VII. Wind Gust Duration Effects on BJ Nominal Balloon in Longitudinal Plane

Altitude = 10,000 Ft.
Payload Weight = 1,000 Lb.
Trim Angle = 8.5°

Gust Velocity = 20.2 Ft/Sec
Gust Duration = t_G

		Balloon Displacements From Equilibrium			Cable Tensions At Equilibrium		Maximum Cable Tensions	
Case No.	t_G Sec.	Δ Range Down/Up Ft.	Δ Altitude Ft.	Δ Pitch Deg.	Winch Lb.	Bridle Lb.	Winch Lb.	Bridle Lb.
1	∞	-65/800	690	5.7	1650	2210	3630	4200
2	2	-12/16	15	1.9	1650	2210	2250	2830
3	10	-52/73	82	2.9	1650	2210	2650	3210
4	20	-68/146	121	4.7	1650	2210	3180	3740
4A	20	0/451	345	1.25	1650	2210	3582	3947

Specific comments for this comparison are:

(1) The vertical gust displaced the balloon up range approximately three times the horizontal gust up range displacement.

(2) The vertical gust caused the balloon to rise three times higher than the horizontal gust.

(3) The pitch angle change from a vertical gust is only 1/4 the pitch angle change due to a horizontal gust of equal magnitude.

(4) Maximum cable tension increased by 400 pounds due to the vertical gust. It is noted that equilibrium cable tension is slightly different from that listed in Table I. This is a result of different balloon trim angles and number of cable links used in the two analyses.

The effects of gust ramp rise time on the response of a nominal BJ balloon is given in Table VIII. These cases represent BJ nominal balloons at 10,000 feet that are subjected to a steady lateral gust with ramp rise times of 1, 3 and 5 seconds.

Table VIII reveals that gust linear ramp rise times of 1, 3, and 5 seconds have little effect on balloon response, except for balloon roll where the 1 second rise time is 1.8 times larger than the 5 second rise time response.

Table VIII. Wind Gust Ramp Rise Time Effects on BJ Nominal Balloon in Lateral Plane

Case No.	Ramp Rise Time	Gust Velocity Ft/Sec	Balloon Displacements from Initial Equilibrium			Cable Tension At Equilibrium		Maximum Cable Tension	
			Yaw +/- Deg.	Roll +/- Deg.	Lat. Displ. Ft.	At Winch Lb.	At Bridle Lb.	At Winch Lb.	At Bridle Lb.
24	1 sec	12	4 /-13.6	3.9/-0.4	460	1650	2210	1686	2258
25	3 sec	12	4.3/-13.8	3.1/-0.35	460	1650	2210	1680	2250
26	5 sec	12	4 /-13.6	2.2/-0.4	460	1650	2210	1675	2244

The effects of a 50 percent increase in lateral gust velocity on the response of a nominal BJ balloon is given in Table IX. The balloon is operating at 10,000 feet in a steady head wind when subjected to steady lateral gusts of 12 ft/sec and 18 ft/sec. Each gust has a ramp rise time of five seconds. Table IX reveals that a 50 percent increase in steady lateral gust velocity results in approximately a 50 percent increase in balloon lateral displacement, roll, and yaw response.

Table IX. Effect of Increase in Gust Velocity on BJ Nominal Balloon in Lateral Plane

	Balloon Displacements from Initial Equilibrium			Cable Tension At Equilibrium		Maximum Cable Tension	
Case No.	Yaw +/- Deg.	Roll +/- Deg.	Lat. Displ.	At Winch Lb.	At Bridle Lb.	At Winch Lb.	At Bridle Lb.
26	4.0/-13.6	2.2/-0.4	460	1650	2210	1675	2244
27	6.0/-20.0	3.2/-0.6	710	1650	2210	1708	2285

(3) Comparison of Balloon Types. The effects of trim angle on the longitudinal response of BJ nominal, VEE, and GAC single hull balloons is given in Table X. The balloons, in equilibrium with a steady head wind at 10,000 feet, are subjected to a horizontal longitudinal gust of 20.2 feet/second for ten seconds. Table X reveals that:

(1) the down range displacements from equilibrium decreases with an increase in trim angle of attack

(2) the GAC single hull balloon has the smallest displacement from equilibrium of the three balloons

(3) the BJ nominal balloon has the smallest cable tension of the three balloon types

(4) cable tension increases with an increase in trim angle

(5) changes in trim angle have a negligible effect on pitch response to gusts.

The effects of lateral steady wind gusts on the lateral response of BJ nominal, VEE, and GAC single hull balloons are given in Table XI. The balloons are in equilibrium at 10,000 feet with a steady head wind and then subjected to a steady lateral horizontal gust of 12 ft/sec with a three second ramp rise time. Table XI reveals that:

(1) the response of the three balloons is approximately the same in both yaw and roll response

(2) the VEE balloon has 1/3 the lateral displacement of the other balloons

(3) the VEE balloon has 2.5 times more tether load than the BJ balloon as a result of the larger aerodynamic lift of this balloon.

Table X. Effect of Trim Angle of Attack on Longitudinal Response of Three Balloon Types

			Balloon Displacements from Equilibrium			Cable Tensions At Equilibrium		Maximum Cable Tensions	
Type Balloon	Case No.	Trim Angle	Δ Range Down/Up Ft.	Δ Alt. Ft.	Δ Pitch Degree	At Winch Lb.	At Bridle Lb.	At Winch Lb.	At Bridle Lb.
BJ Nom.	6	6.5	-65/65	65	2.8	1350	1880	2070	2610
	3	8.5	-52/73	82	2.9	1650	2210	2650	3210
	7	10.5	-50/75	55	2.9	1950	2525	3220	3800
VEE	19	5.0	-35/135	80	4.2	3450	4500	7500	8600
	18	7.0	-22/119	60	3.7	4620	5802	10100	11300
	20	9.1	-19/105	40	3.3	6000	7200	12900	14000
GAC Single Hull	22	6.0	-60/30	20	0.70	2200	3070	3150	4000
	21	7.9	-48/38	20	0.75	2696	3596	3940	4830
	23	10.0	-40/42	25	0.40	3230	4150	4850	5770

Table XI. Effect of Lateral Wind Gusts on the Lateral Response of the Three Balloon Types

		Balloon Displacements from Equilibrium			Cable Tensions At Equilibrium		Maximum Cable Tensions	
Type Balloon	Case No.	Yaw +/- Deg.	Roll +/- Deg.	Lat. Displ. Ft.	At Winch Lb.	At Bridle Lb.	At Winch Lb.	At Bridle Lb.
BJ	25	4.3/-13.8	3.1/-0.35	460	1650	2210	1680	2250
VEE	37	0.5/-15.5	3.1/-0.4	178	4620	5802	4683	5822
GAC	40	5.5/-14.5	2.7/-0.5	510	2696	3596	2734	3645

(4) Effect of Tail Size. The effect of tail size on the response of nominal BJ balloons subjected to longitudinal gusts is given in Table XII. The effects of tail size on the response of BJ nominal and VEE balloons subjected to lateral gusts are given in Table XIII. The longitudinal cases of Table XII are in equilibrium with a steady headwind and then subjected to 20.2 ft/sec step gust of 10-second duration. The tail sizes investigated were 81%, 100% and 144% of nominal tail area. Table XII reveals that:

(1) both up and down range displacements decrease with increasing tail size

(2) pitch angle response decreases with increasing tail size

(3) the maximum tether load at bridle and winch decrease with increasing tail size.

The lateral cases of Table XIII are in equilibrium with a steady head wind and then subjected to a lateral steady gust of 12 ft/sec with a ramp rise time of three seconds. Table XIII reveals that:

(1) the BJ balloon has larger lateral displacement response and less roll response with increasing tail size

(2) the VEE balloon has smaller response in yaw, roll, and lateral displacement with increasing tail size

(3) tether loads for both types of balloons increase with an increase in tail size.

(5) Effects on Balloon Behavior of Intermediate Altitudes. The effects of intermediate altitude operation on a nominal BJ balloon designed for 10,000 feet are given in Table XIV. The altitudes investigated are 1,000, 4,000 and 10,000 feet. The balloon is in equilibrium with a steady head wind and then is subjected to longitudinal gusts of 10-second duration with varying velocities of 20.2 ft/sec, 13.6 ft/sec, and 7.1 ft/sec for longitudinal dynamics cases 3, 14, and 15, respectively. The wind gust velocities are reduced proportional to the steady wind velocity reductions with altitude. Table XIV reveals the longitudinal responses all decrease with a decrease in altitude andthe maximum tether load at bridle is proportional to the gust velocity.

The effects of intermediate altitude operation on the lateral response of a BJ balloon designed for 10,000 feet are given in Table XV. The balloon is in equilibrium with a steady head wind and then is subjected to lateral steady gusts of 12 ft/sec, 8 ft/sec, and 1 ft/sec corresponding to altitudes of 10,000, 4,000, and 1,000 feet. Table XV reveals that:

(1) the lateral responses of the nominal BJ balloon subjected to lateral steady gusts increase with decreasing altitude

(2) a review of the computer plots of Case 36 (1000 feet) in Appendix B indicates the response is unstable.

A detailed discussion of Lateral Case 36 follows.

Table XII. Longitudinal Response of BJ Balloon With Tail Size Variation

			Balloon Displacements From Equilibrium			Cable Tensions At Equilibrium		Maximum Cable Tensions	
Trim Angle Deg.	Tail Size	Case No.	Range Down/Up Ft.	Alt. Ft.	Pitch Deg.	At Winch Lb.	At Bridle Lb.	At Winch Lb.	At Bridle Lb.
11.0	81%	11	-61/88	70	4.6	1730	1880	3000	3550
8.5	100%	3	-52/73	82	2.9	1650	2210	2650	3210
7.4	144%	12	-50/55	40	1.3	1750	2320	2600	3170

Table XIII. Lateral Response of BJ and VEE Balloons With Tail Size Variation

				Balloon Displacements from Equilibrium			Cable Tensions at Equilibrium		Maximum Cable Tensions	
Type Balloon	Tail Size	Trim Angle	Case No.	Yaw +/- Deg.	Roll +/- Deg.	Lat. Displ. Ft.	At Winch Lb.	At Bridle Lb.	At Winch Lb.	At Bridle Lb.
BJ	81%	10.98°	32	3.4/-13.5	11/-1	420	1700	2283	1818	2400
	100%	8.5°	25	4.3/-13.8	3.1/-0.35	460	1650	2210	1680	2250
	144%	7.37°	33	6.1/-13.3	2.3/-0.6	480	2383	2901	2435	2972
VEE	100%	6.96°	37	0.5/-15	3.1/-0.4	177	4650	4805	4683	4855
	200%	7.23°	38	0 /-11	1.9/-0.2	78	4763	5904	4771	5909
	300%	7.5°	39	0 /-11	0.7/-0.1	72	4874	6017	4883	6021

Table XIV. Effect of Intermediate Altitudes on Longitudinal Response of the BJ Balloon

			Balloon Displacements from Equilibrium			Cable Tensions at Equilibrium		Maximum Cable Tension	
Case No.	Altitude Feet	Gust Velocity Ft/Sec	Range Down/Up Ft.	Alt. Ft.	Pitch Deg.	At Winch Lb.	At Bridle Lb.	At Winch Lb.	At Bridle Lb.
3	10,000	20.2	-52/73	82	2.9	165(	2210	2650	3210
14	4,000	13.6	-30/0	-10	0.6	1420	1650	2040	2260
15	1,000	7 1	-25/10	- 3	0.45	980	1020	1110	1160

Table XV. Effect of Intermediate Altitudes on Lateral Response of the BJ Balloon

			Balloon Displacements from Equilibrium			Cable Tensions at Equilibrium		Maximum Cable Tensions	
Case No.	Gust Velocity Ft/Sec	Alt. Ft.	Yaw +/- Deg.	Roll +/- Deg.	Lat. Displ. Ft.	At Winch Lb.	At Bridle Lb.	At Winch Lb.	At Bridle Lb.
25	12.0	10,000	4.3/-13.8	3.1/-0.35	460	1650	2210	1680	2250
35	8.0	4,000	13.1/-27.0	2.1/-1.26	490	1422	1645	1449	1667
36	1.0	1,000	52./-63.3	10.2/-5.5	570	977	1031	1961	1988

Case 36 represents a nominal BJ Balloon designed for a 10,000-foot operational altitude and operating at 1,000 feet altitude. The balloon is in equilibrium with a steady headwind and then is subjected to a 1 foot/second steady lateral wind.

A lateral stability analysis of this condition is found in Reference 2 Run No. 22. Reference 2 (Figure 42) reveals an unstable mode with a frequency of 0.011 Hz. The shape of this mode is also found in Reference 2 (Figure 11) and has the following relationships between amplitudes and phase angles when the mode is normalized on the balloon yaw angle,

Coordinate		Relative Amplitude*	Phase Angle* Degree
Balloon Yaw	ψ	1.000	0.0
Balloon Roll	ϕ	0.253	101.3
Link 1 Yaw	σ_1	0.340	82.4
Link 2 Yaw	σ_2	0.332	81.9
Link 3 Yaw	σ_3	0.324	80.9

*Data is taken from computer digital printout of Run 22 (this data not included in Reference 2).

The stability analyses also reveals this mode has a rise time to double amplitude of 86.2 seconds.

Turning to the computer plots for lateral case 36 (see Appendix B), the following observations are made:

(1) Tether links are in phase and of approximately equal amplitude.

(2) The balloon roll angle is approximately 90° out of phase with respect to the balloon yaw angle.

(3) The three links are approximately 83 degrees out of phase with respect to the balloon yaw angle.

(4) The rise time to double amplitude for the balloon yaw angle is approximately 85 seconds.

(5) The oscillation has a period of 93 seconds (0.0108 Hz).

(6) Observations (1) through (5) indicate that lateral case 36 is predominantly the unstable 0.011 Hz mode found in the stability analysis run 22.

(7) It should be noted also that the oscillations appear to be diverging, as would be expected, since the 0.011 Hz mode is predominate.

In conclusion lateral case 36 indicates a nominal BJ Balloon designed for a 10,000-foot operating altitude will have lateral instability problems, if it is operated at 1,000 feet. Lateral cases 35 and 37 fly the same balloon at 4,000 and 10,000 feet and reveal no diverging motion. GAC has investigated this type of instability problems in Reference 4. In this Reference the formulation of a method of analysis to predict the instability of short tethered balloons exposed to wind was derived and experimental tests were performed on towed models to verify the analysis. As a result of this work, it can be stated that lateral instability occurs when the inverted pendulum frequency of the balloon on the tether coincides with the balloon yaw frequency. Since the pendulum frequency is inversely proportional to the square root of the tether length, it is obvious that for a certain wind velocity a critical tether length exists. It should also be mentioned that Case 36 is not a winching condition, since the cable was a fixed length in the analysis. However, it does suggest that a possible stability problem will occur when the balloon is winched through the 1,000 foot altitude level.

(6) Effects of Reduced Winds (40 Percent of Nominal Winds). The effects of reducing the steady equilibrium wind and gusts to 40 percent of nominal on response in the longitudinal and lateral planes are summarized in Table XVI. In comparing the effects of a 40 percent reduction in winds, it should be noted that the equilibrium trim angle decreased from 8.5 degrees at 100 percent of nominal wind to 2.96 degrees at 40 percent of nominal wind. The yaw response reveals no change in response, while the other responses are reduced as expected.

Table XVI. Effect of Reducing Winds on Longitudinal and Lateral Response

a) Longitudinal Response

			Balloon Displacements from Equilibrium			Cable Tensions at Equilibrium		Maximum Cable Tensions	
Case No.	Wind And Gusts	Trim Angle Deg.	Range Down/Up Ft.	Alt. Ft.	Pitch Deg.	At Winch Lb.	At Bridle Lb.	At Winch Lb.	At Bridle Lb.
3	Nominal	8.5°	-52/73	82	2.9	1650	2210	2650	3210
13	40% Nom.	2.96°	-38/0.0	8	0.63	315	875	355	910

b) Lateral Response

			Balloon Displacements from Initial Equilibrium			Cable Tension at Equilibrium		Maximum Cable Tension	
Case No.	Wind And Gusts	Trim Angle Deg.	Yaw +/- Deg.	Roll +/- Deg	Lat. Displ. Ft.	At Winch Lb.	At Bridle Lb.	At Winch Lb.	At Bridle Lb.
25	Nominal	8.5	4.3/-13.8	3 1/-0.35	460	1650	2210	1680	2250
34	40% Nom.	2.96	4.9/-13.8	0.91/-0.07	322	316 5	871.6	321 2	874.7

(7) Effects of Nolaro versus Amgal Tethers. The effects of Nolaro and Amgal tethers on the longitudinal response of BJ type balloons are given in Table XVII. The BJ type balloons are at 10,000 feet in equilibrium with a steady head wind and then are subjected to a 20.2 ft/sec horizontal longitudinal gust of 10 seconds duration. The balloon using the Nolaro tether has a volume of 60,000 cu. ft., while the balloon using the Amgal tether has a volume of 75,000 cu. ft. The larger balloon is required because the Amgal tether is heavier than the Nolaro tether. The trim angle for both cases is 8.5°. Table XVII reveals the Nolaro system has slightly more response and smaller tether loads than the Amgal system.

Table XVII. Effect of Nolaro and Amgal Tethers on Longitudinal Response

		Balloon Displacements From Equilibrium			Cable Tensions At Equilibrium		Max Cable Tensions	
Cable Type	Case No.	Range Up/Down Ft	Alt Ft.	Pitch Deg.	Winch Lb	Bridle Lb	Winch Lb	Bridle Lb
Nolaro	3	-52/73	82	2.9	1650	2210	2650	3210
Amgal	10	-60/50	28	2.1	1880	2870	3190	4180

The effects of Nolaro and Amgal tethers on the lateral response of 60 K. Ft^3 and 75K. F^3 BJ type balloon systems are given in Table XVIII. The balloon systems are in equilibrium with a steady head wind and then subjected to a steady lateral horizontal gust of 12 ft/sec with a ramp rise time of three seconds. Table XVIII reveals that

(1) Yaw and roll response of the Nolaro system are slightly larger than the response of the Amgal system

(2) The lateral displacement of the Amgal system is 1.2 times the response of the Nolaro system

(3) The Amgal system has larger tether loads as expected since the Amgal tether is heavier.

Table XVIII. Effect of Nolaro and Amgal Tethers on Lateral Response

			Balloon Displacements From Initial Equilibrium			Cable Tension At Equilibrium		Max Cable Tension	
Case No.	Cable Type	Trim Angle Deg.	Yaw +/- Deg.	Roll +/- Deg.	Lat Displ. Ft.	At Winch Lb	At Bridle Lb	At Winch Lb	At Bridle Lb
25	Nolaro	8.5	4.3/-14	3.1/-.35	460	1650	2210	1680	2250
31	Amgal	8.3	4 /-13	2.1/ -.4	560	1880	2872	1905	2905

(8) Effects of Payload Location. The effects of payload location on the longitudinal response of a nominal BJ balloon at 10,000 ft are given in Table XIX. Case three has the 1,000 pound payload located on the confluence point of the bridle while case sixteen has the payload mounted on the underside of the balloon. The balloons are in equilibrium with a steady head wind and then subjected to a head gust of 20.2 ft/sec with a duration of 10 seconds. Table XIX reveals the configuration with the payload at the bridle confluence point (case 3) has approximately 40 percent more longitudinal response than the payload mounted on the balloon bottom configuration. The tether loads are approximately the same for both configurations.

Table XIX. Effect of Payload Location on Longitudinal Response

		Balloon Displacements From Equilibrium			Cable Tension At Equilibrium		Max Cable Tension	
Case No.	Payload Location	Range Down/Up Ft.	Alt Ft.	Pitch Deg.	At Winch Lb.	At Bridle Lb.	At Winch Lb.	At Bridle Lb.
3	Confl.	-52 /73	82	2.9	1650	2210	2650	3210
16	Underside	-49 /56	48	2.1	1650	2210	2540	3100

(9) Effect of Winch Altitude Location. The effect of winch altitude location on the longitudinal response of a nominal BJ balloon remaining at 10,000 feet MSL is given in Table XX. The winch is located at 0.0 ft and 5,000 ft for cases 3 and 17 respectively. The balloons are in equilibrium with a steady head wind and subjected to a 20.2 ft/sec gust of 10 seconds duration. Table XX reveals that,

(1) the range and altitude responses are reduced when the winch is at 5,000 feet,

(2) the pitching response is slightly larger with the winch at 5,000 feet,

(3) the tether load is maximum when the winch is at 5,000 feet.

Table XX. Effect of Winch Altitude Location on Longitudinal Response

		Balloon Displacements From Equilibrium			Cable Tension At Equilibrium		Max Cable Tension	
Case No.	Winch Alt. Ft.	Range Down/Up Ft.	Alt. Ft.	Pitch Deg.	At Winch Lb.	At Bridle Lb.	At Winch Lb.	At Bridle Lb.
3	0.0	-52 /73	82	2.9	1650	2210	2650	3210
17	5000	-20 /47	24	3.1	1940	2210	3670	3940

(10) Effects of Different Operational Altitudes. The effects of three different operational altitudes on the response of BJ type balloons are given in Table XXII. The design operational altitudes and corresponding balloon volumes are 5,000 ft. and 46,000 cu. ft., 10,000 ft. and 60,000 cu. ft., and 20,000 ft. and 500,000 cu. ft. The balloons are in equilibrium with steady head winds which vary according to wind velocity altitude profile. Longitudina ten second duration gusts of 15.7 ft/ sec , 20.2 ft/sec, and 27.3 ft/sec are applied respectively to the 5,000, 10,000, and 20,000 ft. operational altitude configurations in the longitudinal cases. Lateral three second ramp rise time steady gusts of 9 ft/sec, 12 ft/sec, and 16 ft/sec are applied respectively to the 5,000, 10,000, and 20,000 ft. operational altitude configurations in the lateral cases. Table XXI reveals that

(1) the range displacements from equilibrium increase with an increase in operational altitude

(2) pitch displacements from equilibrium decreases with an increase in operational altitude

(3) the lateral responses show little change due to operational altitude

(4) the tether load increases with altitude as expected.

Table XXI. Effect of Various Design Operational Altitudes

				Balloon Displacement From Equilibrium			Cable Tensions At Equilibrium		Max Cable Tensions	
Case No.	Balloon Volume Ft^3	Equil. Alt. Ft.	Gust* Vel. Ft/Sec	Range Down/Up Ft.	Alt. Ft.	Pitch Deg.	Winch Lb.	Bridle Lb.	Winch Lb.	Bridle Lb.
8	46000	5000	15.7	-12 /38	17	3.8	800	960	1290	1840
3	60000	10000	20.2	-52 /73	82	2.9	1650	2210	2650	3210
9	500000	20000	27.3	-127 /70	80	1.45	8600	15030	10820	17300

		Balloon Displacements From Initial Equilibrium			Cable Tension At Equilibrium		Max Cable Tension	
Case No.	Trim Angle Deg.	Yaw +/- Deg.	Roll +/- Deg.	Lat Displ. Ft.	At Winch Lb.	At Bridle Lb.	At Winch Lb.	At Bridle Lb.
29	5.25	3./-14.5	3.8/-.5	560	803	845	829	866
25	8.50	4.3/-13.8	3.1/-.35	460	1650	2210	1680	2250
30	8.43	5.7/-14	3.6/-1	670	9612	15033	9735	15217

B. Balloon Structural Design Performance Parameters

The balloon structural design performance parameters of interest are the tensions at the winch and bridle and the translational and rotational accelerations of the balloon center of gravity. Tables XXIV and XXV list the maximum variation of these parameters from equilibrium for selected longitudinal and lateral cases. From a design limit load point of view, the values found in Table XXII represent the structural design parameters for the three balloon types subjected to longitudinal gusts of 20.2 ft/sec and 10 second duration and lateral steady gusts of 12 ft/sec.

Table XXII. Structural Design Parameters

Item / Balloon Type	Translational Accelerations ~ Ft/sec^2			Rotational Accelerations ~ Deg/Sec^2			Cable Max. Tensions Lbs.	
	Hor.	Vert.	Lat.	Pitch	Yaw	Roll	Winch	Bridle
BJ Nom	3.8	2.6	8.3	3.4	1.9	2.8	3630	4200
VEE	3.5	2.9	3.0	5.6	1.4	1.2	12900	14000
GAC	3.1	3.8	5.0	.4	.7	.5	4850	5770

C. Balloon Instrumentation Design Performance Parameters

The balloon instrumentation design performance parameters of interest in designing an "on-board" instrumentation package are as follows:

(1) displacements (horizontal, vertical, and lateral)

(2) velocities (horizontal, vertical, and lateral)

(3) angular displacements (pitch, yaw, and roll)

(4) angular velocities (pitch, yaw, and roll)

Tables XXIV and XXV list the maximum variation of these parameters from equilibrium for selected longitudinal and lateral cases.

From an instrumentation design point of view, the values found in Table XXIII represent the instrumentation design parameters for the three balloon types subjected to longitudinal gusts of 20.2 ft/sec and 10 second duration and lateral steady gusts of 12 ft/sec.

Table XXIII. Instrumentation Design Parameters

Item / Ballon Type	Displacements Ft.			Velocity Ft/Sec			Angular Displ. Degree			Angular Velocities Deg/Sec		
	Hor.	Vert.	Lat.	Hor.	Vert.	Lat.	Pitch	Yaw	Roll	Pitch	Yaw	Roll
BJ Nom	73	82	560	6.2	3.5	16.9	2.2	13.8	3.9	1.14	1.74	2.2
VEE	135	80	177	9.3	4.1	11.5	4.3	15.4	3.2	1.73	2.4	1.2
GAC	60	25	506	6.6	2.1	18.5	.8	14.3	2.7	.10	1.5	.5

TABLE XXIV

MAXIMUM VARIATIONS OF STRUCTURAL AND INSTRUMENTATION DESIGN PERFORMANCE PARAMETERS
LONGITUDINAL CASES

EFFECT		DESCRIPTION TYPE BALLOON	GUST	CASE NUMBER	CHANGE IN PITCH DEG	PITCH VELOCITY DEG/SEC	PITCH ACC. DEG/SEC^2	HOR. DISP. FT.	HOR. VEL. FT/SEC.	HOR. ACC. FT/SEC^2	VERT. DISP. FT.	VERT. VEL. FT/SEC	VERT. ACC. FT/SEC^2	MAX. TETHER WINCH LB.	LOADS BRIDLE LB.
GUST DURATION	2 Sec.	BJ Nominal	20.2 Ft/Sec	2	1.89	1.14	3.09	16	-4.13	-3.09	15	3.25	2.29	2250	2830
	10 Sec.			3	2.24	1.14	3.09	73	-6.22	-3.09	82	3.47	2.29	2650	3210
	20 Sec.			4	4.73	1.14	3.09	146	9.34	-3.09	121	5.12	2.29	3180	3740
				1	5.67	1.14	3.09	800	9.53	-3.09	690	7.32	2.29	3630	4200
TAIL SIZE	81%	BJ Nominal	20.2 Ft/Sec 10 Sec	11	4.59	2.15	5.18	88	-7.09	-3.80	70	4.13	2.21	3000	3550
	100%			3	2.24	1.14	3.09	73	-6.22	-3.09	82	3.47	2.29	2650	3210
	144%			12	1.29	.63	1.77	55	-5.46	-2.36	40	2.96	2.77	2600	3170
OPER. ALTITUDE	5000 Ft	BJ Type	15.7 Ft/Sec 10 Sec	8	3.79	.93	2.04	38	3.77	-2.06	17	1.18	.78	1290	1840
	1000 Ft		20.2 Ft/Sec 10 Sec	3	4.73	1.14	3.09	73	-6.22	-3.09	82	3.47	2.29	2650	3210
	20,000 Ft		27.3 Ft/Sec 10 Sec	9	1.42	.62	1.31	70	-12.1	-2.53	80	4.88	2.37	10,820	17,300
TRIM ANGLE	$\alpha = 7.0^\circ$	Vee	20.2 Ft/Sec 10 Sec.	18	3.78	1.73	5.59	119	9.32	-3.30	60	3.56	2.92	10,100	11,300
	$\alpha = 5.0^\circ$			19	4.27	1.70	5.50	135	9.10	-3.38	80	4.11	2.65	7500	8600
	$\alpha = 9.1^\circ$			20	3.34	1.62	5.35	105	9.24	-3.51	40	2.98	2.93	12,900	14,000
TRIM ANGLE	$\alpha = 7.9^\circ$	GAC	20.2 Ft/Sec 10 Sec.	21	.68	.097	.31	-48	-5.78	-2.04	20	2.00	3.28	3940	4830
	$\alpha = 6.0^\circ$			22	.75	.092	.35	-60	-6.58	-2.31	20	1.81	2.74	3150	4000
	$\alpha = 10.0^\circ$			23	.40	.103	.14	-40	5.21	-1.88	25	2.10	3.75	4850	5770
TRIM ANGLE	$\alpha = 8.5$	BJ Nominal	20.2 Ft/Sec 10 Sec.	3	2.24	1.14	3.09	73	-6.22	-3.09	82	3.47	2.29	2650	3210
	$\alpha = 6.5$			6	2.8	1.04	2.65	65	-6.85	-3.02	65	3.40	1.87	2070	2610
	$\alpha = 10.5$			7	2.9	1.24	3.44	75	-5.77	-3.11	55	3.42	2.64	3220	3800

TABLE XXV

MAXIMUM VARIATIONS OF STRUCTURAL AND INSTRUMENTATION DESIGN PERFORMANCE PARAMETERS
LATERAL CASES

EFFECT		DESCRIPTION TYPE BALLOON	GUST	CASE NUMBER	CHANGE IN YAW DEG.	YAW VELOCITY DEG/SEC	YAW ACC. DEG/SEC.^{2}	CHANGE IN ROLL DEG.	ROLL VELOCITY DEG/SEC	ROLL ACC. DEG/SEC^2	LATERAL DISPL. FT.	LATERAL VELOCITY FT/SEC	LATERAL ACC. FT/SEC^2	MAX. TETHER WINCH LB	LOADS BRIDLE LB
RAMP RISE TIME	1 Sec	BJ	12 Ft/Sec	24	-13.8	1.74	1.86	3.88	2.63	2.83	460	16.9	8.29	1686	2258
	3 Sec	Nominal	Steady	25	-13.8	1.19	.62	3.13	1.33	.94	460	16.8	4.83	1680	2250
	5 Sec			26	-13.8	.85	.37	2.10	.80	.57	460	16.6	3.29	1675	2244
TAIL SIZE	81%	BJ	12 Ft/Sec	32	-13.5	.74	.70	10.95	4.94	3.63	420	15.9	4.10	1818	2400
	100%	Nominal	Steady	25	-13.8	1.19	.62	3.13	1.33	.94	460	16.8	4.83	1680	2250
	144%			33	-13.4	1.77	.84	2.33	.90	.57	480	20.4	5.96	2435	2972
OPER ALTITUDE	5000 Ft	BJ Type	9 Ft/Sec Steady	29	-19.0	1.00	.66	5.18	2.24	1.68	560	15 8	4.18	829	866
	10,000 Ft		12 Ft/Sec Steady	25	-13.8	1.19	.62	3.13	1.33	.94	460	16.8	4.83	1680	2250
	20,000 Ft		16 Ft/Sec Steady	30	-10.6	1.08	.43	2.78	.59	41	670	18.6	4 60	9735	15,217
GUST	10 Sec. Step	BJ	12 Ft/Sec	28	4.38	-2.27	1.21	3.99	-3.04	3.07	161	16.9	7.80	1687	2256
	Steady	Nominal	18 Ft/Sec	27	-20.4	1.31	.56	3.25	1.20	.85	706	25.1	5 00	1708	2285
TAIL SIZE	100%	VEE	12 Ft/Sec	37	-15.4	-.80	.132	3.16	1.21	.67	177	11.5	2 94	4683	4855
	200%			38	-11.1	-2.07	-.96	.98	.41	.29	78	5.36	1 97	4771	5909
	300%			39	-10.9	-2.41	-1.35	.70	.31	.23	72	4.71	1.88	4883	6021
GUST	Steady	GAC	12 Ft/Sec	40	-14.3	1.49	.65	2.70	.47	.25	506	18.5	4.98	2735	3645

SECTION V

CONCLUSIONS AND RECOMMENDATIONS ON TETHERED BALLOON DYNAMIC BEHAVIOR

Mathematical tools have been developed to analyze the dynamic behavior of tethered balloon systems. The techniques used are determination of the roots of the linearized characteristics equations which incorporate the physical, aerodynamic, and mass characteristics of the system, and dynamic simulation of the tethered balloon systems to determine response of the systems to wind disturbances. The techniques are complementary and each helps to obtain insight into the behavior of tethered balloon systems.

Exploratory analysis of significant design and operational parameters, including balloon type, balloon pitch trim angle, tail size, behavior at altitudes intermediate to the design altitude, and operational design altitude, have been conducted. Generally, an inspection of the data for dynamic response of tethered balloon systems to wind gust and the preliminary power spectral density analysis indicate that the lower frequency modes of motion are excited. Consequently, these modes of motion should be favored in establishing tethered balloon system designs. Specific comments and recommendations for design based on these and other parameters are summarized in the paragraphs that follow. In view of the greater interest expressed for the BJ balloon at the beginning of this program, greater emphasis has been placed on exploring the characteristics of tethered balloon systems employing this type of balloon.

1. GUST EFFECTS ON NOMINAL BJ BALLOON

Horizontal gusts with a magnitude 30% greater than the steady-state operational wind, cause increases in downrange displacement, altitude, balloon pitch, and tether cable tension. These increases are a function of the duration of the gusts, and if applied for an extended period of time, result in substantial increases in displacements and tether tensions. A 30% increase in velocity above operational wind for an extended period of time is equivalent to the survival wind design condition and results in dynamic tether tension loads which are twice the equilibrium operational condition. Dynamic load factors of two should be considered for design. Vertical gusts of magnitude equal to that of horizontal gusts have greater effects on balloon displacements and tether tensions. If gusts of greater magnitude than 30% above operational winds in the horizontal direction and of long duration are to be encountered, methods for alleviation of tether tensions and balloon displacements will be desirable. Angle of attack control mechanisms for the balloon system, such as bridle geometry change mechanisms, or aerodynamic surfaces, controlled by autopilots, should be considered for severe wind conditions or strict station keeping requirements to limit tension and displacements. Aerodynamic control surfaces for severe lateral wind disturbances and station keeping requirements can also be considered.

2. COMPARISON OF BALLOON TYPES

The BJ balloon, with ram air filled ballonet and fins, provides the smallest size tethered balloon system to fly a 1000-pound payload at 10,000 feet. However, it has the greatest downrange displacement from the ground tether point. Equilibrium tether tensions are the lowest. Longitudinal excursions around equilibrium are moderate, but lateral displacements due to side gusts are substantial as compared to the Vee-type balloon.

Generally the Vee balloon investigated has a somewhat greater angle-of-attack excursion about static equilibrium for a given input, but with the high aerodynamic lift configuration, results in less overall downrange displacement from the tether point. Lateral excursion is a minimum for this balloon type. Overall, the Vee offers the least excursion with wind variation but at the expense of relatively high tether tension. Elastic devices can be built into the suspension system to limit angle of attack and tether tension. However, analysis of elastic suspension is beyond the scope of the reported analysis. The Vee-type balloon then offers a configuration for applications where the tethered system should be nearer vertical with respect to the tether point, and where displacement from the tether point should be minimized.

The GAC single-hull balloon provides a greater aerodynamic lift and aerodynamic lift-to-drag ratio and less downrange displacement from the tether point than the BJ balloon, and not much greater than that for the Vee for the 10,000-foot altitude system (4950 feet as compared to 7377 feet for the BJ and 4594 feet for the Vee). The equilibrium cable tension is moderate (3800 pounds). Longitudinal motions of this balloon are substantially less for given input wind disturbances than for the other types. Lateral displacements are comparable to those for the BJ balloon for an equal disturbance. The first longitudinal and lateral modes of GAC single-hull balloon type are notably more stable (see Figures 31 and 51 of Reference 2) than the other balloon types.

Structural and onboard payload design parameters for particular wind gust inputs are listed in Tables XXIV and XXV.

3. INFLUENCE OF TRIM ANGLE ON LONGITUDINAL AND LATERAL DYNAMIC BEHAVIOR

Considering the BJ balloon, longitudinal dynamic response data indicates that trim angle-of-attack does not significantly change the response of the balloon in longitudinal translation and rotation.

In view of the lateral dynamic response, analysis indicates that the two lower modes of motion are excited (i.e., pendulum motion of the balloon and tether as a whole, and balloon roll). Trim angle change does not substantially influence these modes for the BJ balloon. However, the vertical location of the confluence point affects the second mode (balloon roll). The apex closer to the balloon results in greater damping of this mode while not greatly affecting the damping of the first mode (Figure 36 of Reference 2).

Longitudinal dynamic response of the Vee balloon is somewhat more sensitive to design trim angle-of-attack. A tethered balloon system, employing the Vee balloon, should be designed to fly at moderate angle-of-attack (say 7 degrees) inasmuch as longitudinal instability tendencies exist at low angle-of-attack. This tendency is indicated in the linearized stability analysis by the lack of damping in the roots of the characteristic equation for the lowest frequency mode of motion. From the stability analysis, first and second longitudinal and lateral modes of motion for the GAC single hull balloon are stable and well damped (Figures 31 and 51 of Reference 2). The first two longitudinal modes are, respectively, a pitching motion of tether and balloon, and a pitching of the balloon. The first two lateral modes are a coupled balloon yaw and lateral link rotation, and a coupled balloon yaw and roll and lateral link rotation. These modes of motion are relatively insensitive to trim angle of attack and vertical location of the bridle confluence point. Dynamic response data also verify that longitudinal linear and angular displacements from equilibrium are relatively insensitive to trim angle-of-attack changes.

4. EFFECT OF TAIL SIZE ON LONGITUDINAL AND LATERAL DYNAMIC BEHAVIOR

Tail size for the BJ balloon was varied by proportionally changing all dimensions to obtain tail area of 81%, 100% and 144% of the nominal design values. Stability analysis indicates that tail size increase to 144% is required to give longitudinal stability for the first oscillatory mode,but that all tail sizes provide lateral stability in the first lateral mode. Also, the tether dynamic load factor reduces with larger tail sizes because of reduced angle-of-attack excursions. However, increased tail sizes increase the side displacements somewhat. It appears that 100% tails should be adequate since near neutral stability is present about the equilibrium point for the first longitudinal mode, and dynamic response data does not show displacement divergence for any of the tail sizes for the 180 seconds of response that were calculated.

The Vee balloon investigation was confined to determining the effect of increasing vertical tail area only. Consequently, longitudinal dynamic characteristics are not greatly affected. The vertical tails on the lower side of the two hulls are increased in area from the 100% nominal size to 300%. An examination of the roots of the characteristic equations for lateral stability (Figure 49 of Reference 2) indicates that the larger tails give somewhat greater damping and lower frequency for the first mode, and an inverse effect for the second mode. The lateral dynamic response data indicate that lateral displacements of yaw, roll, and side motion are all reduced with the larger tail sizes. Tail areas of 200% of nominal then appears to be most desirable.

5. EFFECT OF ALTITUDES INTERMEDIATE TO THE DESIGN ALTITUDE ON BEHAVIOR OF THE BJ TETHERED BALLOON SYSTEM

As the BJ tethered balloon system designed for 10,000 feet is brought to lower and lower altitudes, the wind speed it sees is reduced and the trim angle of attack changes inasmuch as the suspension bridle geometry remains unchanged. Generally, the longitudinal modes of motion become less damped at the lower altitudes. Dynamic response data indicates that longitudinal response is diminished, as might be expected, with the lower steady winds and gusts used in the analysis.

The lateral stability analysis reveals an unstable lateral first mode consisting of coupled balloon yaw and lateral displacement of the 1000-foot altitude. Generally, damping of all lateral modes is reduced substantially at the lower altitudes. A divergent lateral motion is revealed in the dynamic response analysis at 1000 feet altitude for the 10,000-foot design. Comparing dynamic response and stability data, it is concluded that the unstable first lateral mode consists of a coupled yaw lateral displacement. This mode oscillates at a frequency which is approximately equal to an inverted pendulum mode where the frequency is established by the pendulum length and the restoring forces consisting of the net buoyancy and the aerodynamic forces. The divergent motion was not revealed at the 4000-foot altitude. Design features which improve the damping of this mode, such as larger tails and/or automatically actuated stabilizing aerodynamic surfaces, are required. A more detailed investigation and analysis is required to make specific recommendations to improve the dynamic characteristics exposed by this exploratory analysis.

6. EFFECTS OF REDUCED WIND ON THE BEHAVIOR OF THE BJ TETHERED BALLOON SYSTEM

The longitudinal and lateral dynamic characteristics consisting of frequencies and damping qualities change considerably as the wind is reduced. The trim angle of attack steadily decreases as wind decreases. Generally, damping of the tethered balloon system also reduces substantially as wind is reduced. As steady winds and wind gusts reduce yaw response is unchanged but other balloon motion responses reduce as might be expected.

7. NOLARO VS AMGAL TETHERS

The BJ balloon system employing a NOLARO type tether offers the advantage of a smaller balloon to meet the requirements of supporting a 1000-pound payload at 10,000 feet. Dynamic response of the balloon longitudinal and lateral degrees of freedom are not greatly influenced by the different tethers with the exception of lateral displacements. Greater lateral displacements result with the system employing AMGAL. This may be attributed to the lesser lateral damping of the smaller diameter AMGAL tether. For 20,000 foot altitude designs, a single balloon tethered system can not be achieved with a reasonable size balloon using AMGAL tether material. Considering these factors, the NOLARO type tether generally will provide a more favorable tethered balloon system.

8. EFFECT OF PAYLOAD LOCATION

The configuration with payload located at the confluence point of the bridle has somewhat greater longitudinal response than that with the payload located at the underside of the balloon. However, longitudinal response changes are relatively minor and need not influence a decision on payload location. Lateral dynamic response characteristics were not determined for this design variation.

9. EFFECT OF WINCH ALTITUDE LOCATION

In this comparison the BJ balloon is still flown at 10,000 feet altitude, M.S.L., but the winch is at 5000 feet M.S.L. Dynamic response is somewhat larger in the longitudinal plane with the winch at 5000 feet. Lateral dynamic response characteristics were not determined for this design variation. Lateral stability analysis indicates that one of the overdamped modes becomes oscillatory when the winch is located at 5000 feet.

10. BJ TETHERED BALLOON SYSTEMS DESIGNED FOR VARIOUS ALTITUDES

Tethered balloon system designs for altitudes of 5000, 10,000 and 20,000 feet have been defined. As commented elsewhere, it was not possible to obtain a reasonably sized single balloon system with AMGAL tether for the 20,000 foot condition. Dynamic response analysis indicates that longitudinal displacements are somewhat reduced for higher altitude designs and lateral displacements are somewhat increased. However, substantial changes have not bee observed. Dynamic load factors for tether cable design are significantly less for the higher altitude design.

Longitudinal stability analysis indicates that the second and third oscillatory modes, which are balloon pitching modes, reduce in frequency for the higher altitude designs. The lower frequencies might be somewhat attributed to the larger pitching inertia associated with the larger balloons.

It is recommended that the mathematical techniques developed be investigated further by comparing analytical predictions of the tools with experimental data. After this correlation has been completed, more comprehensive analysis of tethered balloon systems of specific interest with wind conditions and gusts to be expected in operations can be conducted.

REFERENCES

1. Definition of Tethered Balloon Systems, Scientific Report No. 1 AFCRL-71-0213, 31 March 1971.

2. Investigation of Stability Characteristics of Tethered Balloon Systems, Scientific Report No. 2, AFCRL-71-0406, 30 July 1971.

3. Doyle, George R., Jr.: Mathematical Model for the Ascent and Descent of a High-Altitude Tethered Balloon; Journal of Aircraft, Vol. 6, No. 5, September-October 1969.

4. GER-13668, Prediction of Flight Stability of Tethered Balloons, Goodyear Aerospace Corporation, Akron, Ohio, February 1968

APPENDIX A

EQUATIONS OF MOTION FOR DYNAMIC SIMULATION

TABLE OF CONTENTS

Section		Page
I	INTRODUCTION	A-3
II	LONGITUDINAL EQUATIONS OF MOTION FOR SMALL ANGULAR VELOCITIES.	A-20
III	NON LINEAR LONGITUDINAL EQUATIONS OF MOTION	A-30
IV	LATERAL EQUATIONS OF MOTION FOR SMALL ANGULAR VELOCITIES	A-40

SECTION I
INTRODUCTION

In Appendix A of the Second Scientific Report*, the equations of motion of a tethered balloon were derived in three dimensions. The initial derivation assumed that angular velocities were small so that products of angular velocities could be neglected. This assumption reduced the complexity of the equations (especially the lateral equations) by a considerable amount, but each equation remained nonlinear and coupled in each degree of freedom. It is assumed that the reader has read Ref. 2 Appendix A, Section II and has a clear understanding of the derivation of the equation of motion, for this discussion will begin with the results of that section.

Many of the terms used in this derivation are defined in the listing which follows.

*Reference 2

FORTRAN	STANDARD	DESCRIPTION	UNITS
AA(4,4)		A four by four array of variables used to define incremental velocities in the numerical integration	rad/sec
AAG(8)		An array of eight variables signifying the angle of the gust to the horizon corresponding to TTG(8)	deg
AALP(16)		An array of sixteen variables signifying the angle-of-attack of the balloon	rad
AALPD(16)		An array of sixteen variables signifying the angle-of-attack of the balloon	deg
AALT(8)		An array of eight variables signifying altitudes of steady state wind velocities	ft
AG	αg	Gust angle off the horizon interpolated from AAG(8) and TTG(8)	deg
AGR	αg	Gust angle off the horizon	rad
ALPB	α_B	Angle-of-attack of balloon	rad
ALPBD	$\dot{\alpha}_B$	$d\ \alpha_B/dt$	rad/sec
ALPBDD	$\dot{\alpha}_B$	$d\ \alpha_B/dt$	deg/sec
ALPBDE	α_B	Angle-of-attack of balloon	deg
ALPSL		A ratio of two angle-of-attack differences used in interpolation of aerodynamic coefficients of the balloon at some α	
ALTSL		A ratio of two altitude differences used in interpolation of steady state wind velocities	
AXB	a_{XB}	The inertial force acting on the balloon along the lateral axis of the balloon	slug-ft sec^2
AYB	a_{YB}	The inertial force acting on the balloon along the longitudinal axis of the balloon	slug-ft sec^2

FORTRAN	STANDARD	DESCRIPTION	UNITS
AZB	a_{ZB}	The inertial force acting on the balloon along the vertical axis of the balloon	slug-ft/ sec^2
BBET(8)		An array of eight variables signifying the sideslip angle of the balloon	rad
BBETD(8)		An array of eight variables signifying the sideslip angle of the balloon	deg
BETB	β	Sideslip angle of balloon (positive-wind to the right of balloon's centerline)	rad
BETBD	$\dot{\beta}$	d β/dt	rad/sec
BETBDD	$\dot{\beta}$	d β/dt	deg/sec
BETBDE	β	Sideslip angle of balloon (positive-wind to the right of balloon's centerline)	deg
BETSL		A ratio of two sideslip angle differences used in interpolation of aerodynamic coefficients of the balloon at some β	
C(3)	C_r	Non-dimensional center-of-pressure of "r" th link	
CCDB(16)		An array of sixteen variables signifying drag coefficients of the balloon corresponding to AALPD(16)	
CCLB(16)		An array of sixteen variables signifying lift coefficients of the balloon in the longitudinal program corresponding to AALPD(16)	
CCLB(8)		An array of eight variables signifying roll moment coefficients of the balloon in the lateral program corresponding to BBETD(8)	
CCLLB(16)		An array of sixteen variables signifying lift coefficients of the balloon in the lateral program corresponding to AALPD(16)	

FORTRAN	STANDARD	DESCRIPTION	UNITS
CCMB(16)		An array of sixteen variables signifying pitch moment coefficients of the balloon corresponding to AALPD(16)	
CCNB(8)		An array of eight variables signifying yaw moment coefficients of the balloon corresponding to BBETD(8)	
CDB	C_{DB}	Drag coefficients of balloon	
CDC	C_{DC}	Drag coefficient of link (infinite cylinder)	
CDTDB	$C_{D\dot{\theta}B}$	Balloon drag coefficient due to pitch velocity	rad^{-1}
CGAMB	$C\ \gamma_B$	$\cos \gamma_B$	
CLB	C_{LB}	Lift coefficient of balloon in longitudinal program	
CLB	$C_{\ell B}$	Balloon roll moment coefficient in lateral program	
CLLB	C_{LB}	Lift coefficient of balloon in lateral program	
CLPHDB	$C_{\ell\dot{\phi}B}$	Balloon roll moment coefficient due to roll velocity	rad^{-1}
CLPSDB	$C_{\ell\dot{\psi}B}$	Balloon roll moment coefficient due to yaw velocity	rad^{-1}
CLTDB	$C_{L\dot{\theta}B}$	Balloon lift coefficient due to pitch velocity	rad^{-1}
CMB	C_{mB}	Balloon pitch moment coefficient	
CMTDB	$C_{m\dot{\theta}B}$	Balloon pitch moment coefficient due to pitch velocity	rad^{-1}
CNB	C_{nB}	Balloon yaw moment coefficient	
CNPHDB	$C_{n\dot{\phi}B}$	Balloon yaw moment coefficient due to roll velocity	rad^{-1}

FORTRAN	STANDARD	DESCRIPTION	UNITS
CNPSDB	$C_{n\dot{\psi}B}$	Balloon yaw moment coefficient due to yaw velocity	rad^{-1}
COM1		Input data defining computer run	
CPHI	$C\phi$	$\cos\phi$	
CPHI2	$C^2\phi$	$\cos^2\phi$	
CPSI	$C\psi$	$\cos\psi$	
CSIG(3)	$C\sigma_i$	$\cos\sigma_i$,(i = 1, 2, 3)	
CSIG2(3)	$C^2\sigma_i$	$\cos^2\sigma_i$,(i = 1, 2, 3)	
CTHE	$C\theta$	$\cos\theta$	
CTHE2	$C^2\theta$	$\cos^2\theta$	
CTPX(3)	$C(\theta+\xi_i)$	$\cos(\theta+\xi_i)$,(i = 1, 2, 3)	
CTPX2(3)	$C^2(\theta+\xi_i)$	$\cos^2(\theta+\xi_i)$,(i = 1, 2, 3)	
CXI(3)	$C\xi_i$	$\cos\xi_i$,(i = 1, 2, 3)	
CXI2(3)	$C^2\xi_i$	$\cos^2\xi i$, (i = 1,2,3)	
CXMX(3,3)	$C(\xi_i-\xi_j)$	$\cos(\xi_i-\xi_j)$,(i = 1,2,3,; j= 1,2,3)	
CYB	C_{YB}	Side force coefficient	
CYPHDB	$Cy_{\dot{\phi}B}$	Side force coefficient of balloon due to roll velocity	rad^{-1}
CYPSDB	$Cy_{\dot{\psi}B}$	Side force coefficient of balloon due to yaw velocity	rad^{-1}
DB	d_B	Aerodynamic reference length of balloon ($\forall^{1/3}$)	ft
DC		Diameter of tether	ft
DCH(3)	D_{CHi}	Horizontal aerodynamic force acting on the center-of-pressure of the "i"th link, (i = 1,2,3)	lb_f

FORTRAN	STANDARD	DESCRIPTION	UNITS
DCS(3)	D_{CSi}	Lateral aerodynamic force acting on the center-of-pressure of the "i"th link, (i = 1,2,3)	lb_f
DCV(3)	D_{CVi}	Vertical aerodynamic force acting on the center-of-pressure of the "i"th link, (i = 1,2,3)	lb_f
DD(4,4)		A four by four array of variables signifying the coefficients of the second derivatives in the equations of motion	$slug\text{-}ft^2$
DRAGB	DRAGB	Aerodynamic drag acting on balloon	
DT		Integration time increment	sec
DTP		Number of integrations between data printouts	
DTP1		Number of integrations between data printouts when DT = DT1	
DTP2		Number of integrations between data printouts when DT = DT2	
DT1		Integration time increment when T < TDTC	sec
DT2		Integration time increment when T ≥ TDTC	sec
DYPRB	q_B	Effective dynamic pressure acting on c.g. of balloon	lb_f/ft^2
DYPRH(4)	q_{Hi}	Effective dynamic pressure acting on the "i"th link hinge, (i = 1,2,3,4). The first hinge is at the winch	lb_f/ft^2

FORTRAN	STANDARD	DESCRIPTION	UNITS
EE(4)		An array of four variables signifying the generalized forces plus terms containing products of angular velocities if this option is chosen. See FF	$ft\text{-}lb_f$
EEPS(3,3)	ε_{ij}	A three by three array representing the transformation matrix between the balloon body unit vectors and the inertia frame unit vectors	
FBHA	F_{BHA}	Horizontal aerodynamic forces acting on balloon	lb_f
FBSA	F_{BSA}	Lateral aerodynamic forces acting on balloon	lb_f
FBVA	F_{BVA}	Vertical aerodynamic forces acting on balloon	lb_f
FCH(3)	F_{CHi}	Horizontal component of tension acting on the "i"th link, (i = 1,2,3)	lb_f
FCN(3)	F_{CNi}	Aerodynamic force acting normal to "i"th link, (i = 1,2,3)	lb_f
FCS(3)	F_{CSi}	Lateral component of tension acting on the "i"th link, (i = 1,2,3)	lb_f
FCV(3)	F_{CVi}	Vertical component of tension acting on the "i"th link, (i = 1,2,3)	lb_f
FF		Input variable which gives the option of including inertia terms containing products of angular velocities in the longitudinal program. If these terms are not wanted set FF = 0.. If the terms are to be included, set FF to any number except "0.".	

FORTRAN	STANDARD	DESCRIPTION	UNITS
FPHI	F_{ϕ}	Generalized force acting on balloon's roll degree-of-freedom	$ft\text{-}lb_f$
FPSI	F_{ψ}	Generalized force acting on balloon's yaw degree-of-freedom	$ft\text{-}lb_f$
FSIG(3)	$F_{\sigma i}$	Generalized force acting on the "i"th link's yaw degree-of-freedom, (i = 1,2,3)	$ft\text{-}lb_f$
FTHE	F_{θ}	Generalized force acting on balloon's pitch degree-of-freedom	$ft\text{-}lb_f$
FWH		Horizontal component of tether tension acting at winch	lb_f
FWS		Lateral component of tether tension acting at winch	lb_f
FWV		Vertical component of tether tension acting at winch	lb_f
FXI(3)	$F_{\xi i}$	Generalized force acting on the "i"th link's pitch degree-of-freedom, (i = 1,2,3)	$ft\text{-}lb_f$
G	g	Acceleration of gravity = 32.17 ft/sec^2	ft/sec^2
GAMB	γ_B, Γ_B	In the longitudinal program γ_B is the relative flight path angle of the balloon in the longitudinal plane; in the lateral program Γ_B is the relative flight path angle of the balloon in the horizontal plane	rad
GAMBD	$\dot{\gamma}_B$, $\dot{\Gamma}_B$	$d\gamma_B/dt$ or $d\Gamma_B/dt$	rad/sec
GAMBDE	γ_B, Γ_B	See GAMB	deg
GAMBDD	$\ddot{\gamma}_B$, $\ddot{\Gamma}_B$	$d\gamma_B/dt$ or $d\Gamma_B/dt$	deg/sec
IXB	I_{XB}	Apparent pitch moment of inertia of balloon	$slug\text{-}ft^2$

FORTRAN	STANDARD	DESCRIPTION	UNITS
IYB	I_{YB}	Apparent roll moment of inertia of balloon	slug-ft^2
IYZB	I_{YZB}	Apparent product of inertia of balloon with respect to roll and yaw body axis	slug-ft^2
IZB	I_{ZB}	Apparent yaw moment of inertia of balloon	slug-ft^2
L	ℓ	Length of one tether link	ft
LIFTB	LIFTB	Aerodynamic lift acting on balloon	lb_f
LS	L_S	Buoyant lift of balloon = weight of displaced air	lb_f
M	m	Mass of one tether link	slugs
MAL		Added mass of balloon along its longitudinal axis	slugs
MAS		Added mass of balloon along its lateral axis	slugs
MAV		Added mass of balloon along its vertical axis	slugs
ML	M_L	Apparent mass of balloon along its longitudinal axis. Apparent mass equals total static mass associated with the balloon plus air mass being accelerated in a particular direction.	slugs
MPHIB	$M_{\phi B}$	Aerodynamic rolling moment acting on balloon	ft-lb_f
MPL	m_{PL}	Mass of payload-located at bridle tether connection	slugs
MPSIB	$M_{\psi B}$	Aerodynamic yawing moment acting on balloon	ft-lb_f
MS	M_S	Apparent mass of balloon along its lateral axis	slugs
MTHEB	$M_{\theta B}$	Aerodynamic pitching moment acting on balloon	ft-lb_f

FORTRAN	STANDARD	DESCRIPTION	UNITS
MV	M_V	Apparent mass of balloon along its vertical axis	slugs
PHI	ϕ	Roll angle of balloon (positive-right wing down)	rad
PHID	$\dot{\phi}$	$d\phi/dt$	rad/sec
PHIDD	$\ddot{\phi}$	$d^2\phi/dt^2$	rad/sec^2
PHIDDD	$\ddot{\phi}$	$d^2\phi/dt^2$	deg/sec^2
PHIDDE	$\dot{\phi}$	$d\phi/dt$	deg/sec
PHIDEG	ϕ	Roll angle of balloon (positive-right wing down)	deg
PHID2	$\dot{\phi}^2$	$\dot{\phi}^2$	rad^2/sec^2
PR		Atmospheric pressure (not used in program)	lb/ft^2
PSI	ψ	Yaw angle of balloon (positive-nose to right)	rad
PSID	$\dot{\psi}$	$d\psi/dt$	rad/sec
PSIDD	$\ddot{\psi}$	$d^2\psi/dt^2$	rad/sec^2
PSIDDD	$\ddot{\psi}$	$d^2\psi/dt^2$	deg/sec^2
PSIDDE	$\dot{\psi}$	$d\psi/dt$	deg/sec
PSIDEG	ψ	Yaw angle of balloon (positive-nose to right)	deg
PSID2	$\dot{\psi}^2$	$\dot{\psi}^2$	rad^2/sec^2
RHOB	ρ_B	Air density at Z_B	slug/ft^3
RHOC(3)	ρ_{ci}	Air density at Z_{ci}, (i=1,2,3)	slug/ft^3
RHOCH(3)	ρ_{Hi}	Air density at Z_{cHi}, (i=1,2,3,4)	slug/ft^3
RJA	R_{jA}	Distance along longitudinal axis of balloon from aerodynamic reference center to bridle apex (positive toward nose)	ft

FORTRAN	STANDARD	DESCRIPTION	UNITS
RJB	R_{jB}	Distance along longitudinal axis of balloon from center of buoyancy to bridle apex (positive toward nose)	ft
RJG	R_{jg}	Distance along longitudinal axis of balloon from center of gravity to bridle apex (positive toward nose)	ft
RJM	R_{jm}	Distance along longitudinal axis of balloon from dynamic mass center to bridle apex (positive toward nose)	ft
RKA	R_{kA}	Distance along vertical axis of balloon from aerodynamic reference center to bridle apex (positive up)	ft
RKB	R_{kB}	Distance along vertical axis of balloon from center of buoyancy to bridle apex (positive up)	ft
RKG	R_{kg}	Distance along vertical axis of balloon from center of gravity to bridle apex (positive up)	ft
RKM	R_{km}	Distance along vertical axis of balloon from dynamic mass center to bridle apex (positive up)	ft
SB	S_B	Aerodynamic reference area of balloon ($\forall^{2/3}$)	ft^2
SC(3)	S_{ci}	Aerodynamic reference area of one tether link = $(\ell)(dc)$, $(i = 1,2,3)$	ft^2
SGAMB	$S\gamma_B$	$\sin \gamma_B$	
SIG(3)	σ_i	Yaw angle of "i"th link, $(i = 1,2,3)$ (positive-counter-clockwise looking down range)	rad
SIGD(3)	$\dot{\sigma}_i$	$d\sigma_i/dt$, $(i = 1,2,3)$	rad/sec

FORTRAN	STANDARD	DESCRIPTION	UNITS
SIGDD(3)	$\ddot{\sigma}_i$	$d^2\sigma_i/dt^2$,(i = 1,2,3)	rad/sec^2
SIGDDD(3)	$\ddot{\sigma}_i$	$d^2\sigma_i/dt^2$,(i = 1,2,3)	deg/sec^2
SIGDDE(3)	$\dot{\sigma}_i$	$d\sigma_i/dt$,(i = 1,2,3)	deg/sec
SIGDEG(3)	σ_i	Yaw angle of "i"th link, (i = 1,2,3) (positive-counterclockwise looking down range)	deg
SIGD2(3)	$\dot{\sigma}_i^{\,2}$	$\dot{\sigma}_i^{\,2}$,(i = 1,2,3)	rad^2/sec^2
SPHI	$S\phi$	$\sin\phi$	
SPHI2	$S^2\phi$	$\sin^2\phi$	
SPSI	$S\psi$	$\sin\psi$	
SSIG(3)	$S\sigma_i$	$\sin\sigma_i$,(i = 1,2,3)	
STHE	$S\theta$	$\sin\theta$	
STHE2	$S^2\theta$	$\sin^2\theta$	
STPX(3)	$S(\theta+\xi_i)$	$\sin(\theta+\xi_i)$,(i = 1,2,3)	
STPX2(3)	$S^2(\theta+\xi_i)$	$\sin^2(\theta+\xi_i)$,(i = 1,2,3)	
SXI(3)	$S\xi_i$	$\sin\xi_i$,(i = 1,2,3)	
SXI2(3)	$S^2\xi_i$	$\sin^2\xi_i$,(i = 1,2,3)	
SXMX(3,3)	$S(\xi_i-\xi_j)$	$\sin(\xi_i-\xi_j)$,(i=1,2,3; j=1,2,3)	
S2THE	$S2\theta$	$\sin 2\theta$	
T	t	Flight time	sec
TDTC		Flight time at which DT is changed from DT1 to DT2 and DTP is changed from DTP1 to DTP2	sec
TENS(3)	T_i	Tension in tether at top of "i"th link ,(i = 1,2,3)	lb_f
TENSW	T_w	Tension in tether at winch	lb_f

FORTRAN	STANDARD	DESCRIPTION	UNITS
TETH		Total length of tether	ft
THE	θ	Pitch angle of balloon (positive-nose up)	rad
THED	$\dot{\theta}$	$d\theta/dt$	rad/sec
THEDD	$\ddot{\theta}$	$d^2\theta/dt$	rad/sec^2
THEDDD	$\dddot{\theta}$	$d^2\theta/dt$	deg/sec^2
THEDDE	$\dot{\theta}$	$d\theta/dt$	deg/sec
THEDEG	θ	Pitch angle of balloon (positive-nose up)	deg
THED2	$\dot{\theta}^2$	$\dot{\theta}^2$	rad^2/sec^2
THEODE	θ_o	Equilibrium pitch angle of balloon	deg
TSL		A ratio of two time differences used in interpolation of gust velocities and gust angles	
TTG(8)		An array of eight variables signifying the time history of the gust	sec
TTT		Flight time at which computer simulation ends	sec
VBR	V_{BR}	Relative velocity of balloon's c.g. with respect to the air	ft/sec
VC(3)	V_{ci}	Relative velocity of the c.p. of the "i"th link with respect to the air, (i=1,2,3)	ft/sec
VG	V_g	Gust velocity	ft/sec
VGH	V_{gH}	Component of gust in Y_B direction	ft/sec
VGS	V_{gs}	Component of gust in X_B direction	ft/sec

FORTRAN	STANDARD	DESCRIPTION	UNITS
VGV	V_{gv}	Component of gust in Z_B direction	ft/sec
VHR(4)	V_{Hri}	Relative wind velocity of "i"th link hinge in the Y_B direction,(i=1,2,3,4). The first hinge is at the winch.	ft/sec
VS		Speed of sound (not used in program)	ft/sec
VVG(8)		An array of eight variables signifying gust velocity acting on balloon and corresponding to TTG(8)	ft/sec
VVW(8)		An array of eight variables signifying steady state wind profile and corresponding to AALT(8)	ft/sec
VW	V_w	Steady state wind velocity at Z_B	ft/sec
VWC(3)	V_{wci}	Steady state wind velocity at Z_{ci},(i = 1,2,3)	ft/sec
VWH(4)	V_{wHi}	Steady state wind velocity at Z_{cHi},(i = 1,2,3,4)	ft/sec
WB	W_B	Total weight of balloon - includes balloon and bridle material, and enclosed gases	lbs
WPL		Weight of payload located at bridle tether connection	lb
WTC		Weight of tether	lb
XB	X_B	Lateral displacement of balloon's c.g. in the inertia reference frame	ft
XBD	$\dot{X}_B$	dX_B/dt	ft/sec
XBDD	$\ddot{X}_B$	d^2X_B/dt^2	ft/sec^2
XBDDR		Lateral acceleration of balloon's c.g. relative to air	ft/sec^2

FORTRAN	STANDARD	DESCRIPTION	UNITS
XBDR		Lateral velocity of balloon's c.g. relative to air	ft/sec
XCD(3)	$\dot{X}_{ci}$	Lateral velocity of c.p. of "i"the link,(i = 1,2,3)	ft/sec
XCDD(3)	$\ddot{X}_{ci}$	Lateral acceleration of c.g. of "i"th link,(i = 1,2,3)	ft/sec^2
XCHD(4)	$\dot{X}_{cHi}$	Lateral velocity of "i"th link hinge,(i = 1,2,3,4). The first hinge is at the winch	ft/sec
XI(3)	ξ_i	Pitch angle of "i"th link, (i = 1,2,3) (positive-rotated up from the horizon, clockwise)	rad
XID(3)	$\dot{\xi}_i$	$d\xi_i/dt$,(i = 1,2,3)	rad/sec
XIDD(3)	$\ddot{\xi}_i$	$d^2\xi_i/dt^2$,(i = 1,2,3)	rad/sec^2
XIDDDE(3)	$\ddot{\xi}_i$	$d^2\xi_i/dt^2$,(i = 1,2,3)	deg/sec^2
XIDDEG(3)	$\dot{\xi}_i$	$d\xi_i/dt$,(i = 1,2,3)	deg/sec
XIDEG(3)	ξ_i	Pitch angle of "i"th link, (i = 1,2,3) (positive-rotated up from the horizon, clockwise)	deg
XID2(3)	$\dot{\xi}^2_i$	$\dot{\xi}^2_i$ (i = 1,2,3)	rad^2/sec^2
XIODEG(3)	ξ_{io}	Equilibrium pitch angle of "i"th link,(i = 1,2,3)	deg
XPLDD	$\ddot{X}_{PL}$	Lateral acceleration of payload	ft/sec^2
YB	Y_B	Down range displacement of balloon's c.g. in the inertia reference frame	ft
YBD	$\dot{Y}_B$	dY_B/dt	ft/sec
YBDD	$\ddot{Y}_B$	d^2Y_B/dt^2	ft/sec^2

FORTRAN	STANDARD	DESCRIPTION	UNITS
YBDDR		Down range acceleration of balloon's c.g. relative to air	ft/sec^2
YBDR		Down range velocity of balloon's c.g. relative to air	ft/sec
YCD(3)	$\dot{Y}_{ci}$	Down range velocity of C.P. of "i"th link ,(i = 1,2,3)	ft/sec
YCDD(3)	$\ddot{Y}_{ci}$	Down range acceleration of c.g. of "i"th link, (i = 1,2,3)	ft/sec
YCHD(4)	$\dot{Y}_{cHi}$	Down range velocity of "i"th link hinge,(i = 1,2,3,4) The first hinge is at the winch	ft/sec
YPLDD	$\ddot{Y}_{PL}$	Down range acceleration of payload	ft/sec^2
ZB	Z_B	Altitude of balloons c.g. in inertia reference frame	ft
ZBD	$\dot{Z}_B$	dZ_B/dt	ft/sec
ZBDD	$\ddot{Z}_B$	d^2Z_B/dt^2	ft/sec^2
ZBDDR		Vertical acceleration of balloon's c.g. relative to air	ft/sec^2
ZBDR		Vertical velocity of balloon's c.g. relative to air	ft/sec
ZC(3)	Z_{ci}	Altitude of C.P. of "i"th link ,(i = 1,2,3)	ft
ZCD(3)	$\dot{Z}_{ci}$	Vertical velocity of C.P. of "i"th link ,(i = 1,2,3)	ft/sec
ZCDD(3)	$\ddot{Z}_{ci}$	Vertical accleration of c.g. of "i"th link ,(i = 1,2,3)	ft/sec^2
ZCH(4)	Z_{cHi}	Altitude of "i"th link hinge ,(i = 1,2,3,4) The first hinge is at the winch	ft

FORTRAN	STANDARD	DESCRIPTION	UNITS
ZCHD(4)	$\dot{Z}_{CHi}$	Vertical velocity of "i"th link hinge ,(i = 1,2,3,4) The first hinge is at the winch	ft/sec
ZPLDD	$\ddot{Z}_{PL}$	Vertical acceleration of payload	ft/sec^2

SECTION II

LONGITUDINAL EQUATIONS OF MOTION FOR SMALL ANGULAR VELOCITIES

First consider the longitudinal equation of motion. The dependent variables (see Figure 1) are θ (pitch of the balloon) and ξ_r (pitch of the "r" the link), where r is a particular link.

The appropriate equations of motion in the Second Scientific Report, Appendix A, Section II are (80) and (97). Since these equations were derived in three dimensions, they contain the lateral degrees-of-freedom, ψ (yaw of balloon), ϕ (roll of balloon), and σ_r (yaw of "r" th link). It will be assumed that the balloon remains in equilibrium in the lateral degrees-of-freedom. Therefore, $\psi \equiv \phi \equiv \sigma_r \equiv 0$. With this assumption Equation (80) and (97) are rewritten as follows:

$$M_L \Big\langle \ell R_{km} \sum_{i=1}^{N} \Big\{ \ddot{\xi}_i \big[S\xi_i C\theta + C\xi_i S\theta \big] \Big\} + R_{km}^2 \ddot{\theta} \Big\rangle$$

$$+ M_V \Big\langle \ell R_{jm} \sum_{i=1}^{N} \Big\{ -\ddot{\xi}_i \big[-S\xi_i S\theta + C\xi_i C\theta \big] \Big\} + R_{jm}^2 \ddot{\theta} \Big\rangle + I_{xB} \ddot{\theta} = F_\theta \qquad (1)$$

$$\sum_{n=n+1}^{N} m\ell^2 \Big\{ \sum_{i=1}^{n-1} \ddot{\xi}_i C(\xi_n - \xi_i) + \tfrac{1}{2} \ddot{\xi}_n C(\xi_n - \xi_n) \Big\} + \tfrac{m}{2} \ell^2 \sum_{i=1}^{n-1} \ddot{\xi}_i C(\xi_n - \xi_i) + \tfrac{m}{3} \ell^2 \ddot{\xi}_n$$

$$+ m_{PL} \ell^2 \sum_{i=1}^{N} \ddot{\xi}_i C(\xi_n - \xi_i) + M_L \Big\langle \ell^2 \sum_{i=1}^{N} \ddot{\xi}_i \big[S\xi_i C\theta + C\xi_i S\theta \big] \big[S\xi_n C\theta + C\xi_n S\theta \big]$$

$$+ R_{km} \ell \ddot{\theta} \big[S\xi_n C\theta + C\xi_n S\theta \big] \Big\rangle + M_V \Big\langle \ell^2 \sum_{i=1}^{N} \ddot{\xi}_i \big[-S\xi_i S\theta + C\xi_i C\theta \big] \big[-S\xi_n S\theta + C\xi_n C\theta \big] .$$

$$- R_{jm} \ell \dot{\theta} \big[-S\xi_n S\theta + C\xi_n C\theta \big] \Big\rangle = F_{\xi_n} \qquad (2)$$

where $S\theta = \sin\theta$ and $C\theta = \cos\theta$, etc.

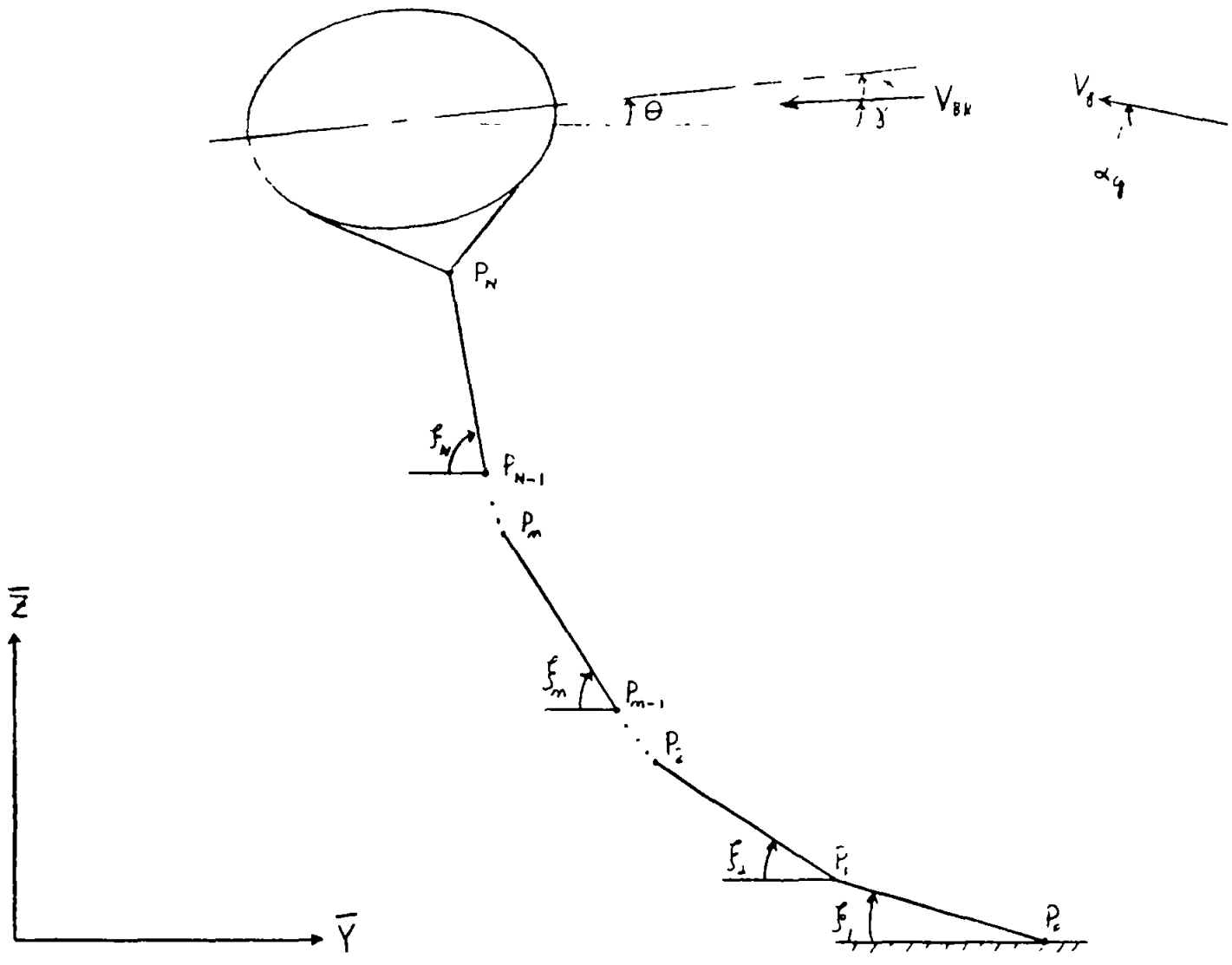

FIGURE 1 - BALLOON TETHER MODEL IN LONGITUDINAL PLANE

In order to solve Equations (1) and (2), it will be assumed that N = 3. Rewrite Equations (1) and (2) with this assumption and substitute in the trigometric identities for the sums of angles.

$$
\begin{aligned}
&\left[M_L R_{km}^2 + M_V R_{jm}^2 + I_{YB}\right]\ddot{\theta} + \left[M_L \ell R_{km}\, s(\xi_1+\theta) - M_V \ell R_{jm}\, c(\xi_1+\theta)\right]\ddot{\xi}_1 \\
&+ \left[M_L \ell R_{km}\, s(\xi_2+\theta) - M_V \ell R_{jm}\, c(\xi_2+\theta)\right]\ddot{\xi}_2 \qquad (3) \\
&+ \left[M_L \ell R_{km}\, s(\xi_3+\theta) - M_V \ell R_{jm}\, c(\xi_3+\theta)\right]\ddot{\xi}_3 = F_\theta
\end{aligned}
$$

For r = 1,

$$[M_L \ell R_{km} s(\xi_1+\theta) - M_V \ell R_{gm} c(\xi_1+\theta)]\ddot{\theta}$$

$$+\ell^2\left[\frac{7m}{3} + m_{pL} + M_L s^2(\xi_1+\theta) + M_V c^2(\xi_1+\theta)\right]\ddot{\xi}_1$$

$$+\ell^2\left[\left(\frac{3m}{2}+m_{pL}\right)c(\xi_1-\xi_2) + M_L s(\xi_1+\theta)s(\xi_2+\theta) + M_V c(\xi_1+\theta)c(\xi_2+\theta)\right]\ddot{\xi}_2$$

$$+\ell^2\left[\left(\frac{m}{2}+m_{pL}\right)c(\xi_1-\xi_3) + M_L s(\xi_1+\theta)s(\xi_3+\theta) + M_V c(\xi_1+\theta)c(\xi_3+\theta)\right]\ddot{\xi}_3 = F_{\xi_1} \qquad (4)$$

For r = 2,

$$[M_L \ell R_{km} s(\xi_2+\theta) - M_V \ell R_{gm} c(\xi_2+\theta)]\ddot{\theta}$$

$$+\ell^2\left[\left(\frac{3m}{2}+m_{pL}\right)c(\xi_1-\xi_2) + M_L s(\xi_1+\theta)s(\xi_2+\theta) + M_V c(\xi_1+\theta)c(\xi_2+\theta)\right]\ddot{\xi}_1$$

$$+\ell^2\left[\frac{4m}{3} + m_{pL} + M_L s^2(\xi_2+\theta) + M_V c^2(\xi_2+\theta)\right]\ddot{\xi}_2$$

$$+\ell^2\left[\left(\frac{m}{2}+m_{pL}\right)c(\xi_2-\xi_3) + M_L s(\xi_2+\theta)s(\xi_3+\theta) + M_V c(\xi_2+\theta)c(\xi_3+\theta)\right]\ddot{\xi}_3 = F_{\xi_2} \qquad (5)$$

For r = 3,

$$[M_L \ell R_{km} s(\xi_3+\theta) - M_V \ell R_{gm} c(\xi_3+\theta)]\ddot{\theta}$$

$$\ell^2\left[\left(\frac{m}{2}+m_{PL}\right)c(\xi_1-\xi_3)+M_L\, s(\xi_1+\theta)\, s(\xi_3+\theta)+M_V\, c(\xi_1+\theta)\, c(\xi_3+\theta)\right]\ddot{\xi}_1$$

$$\ell^2\left[\left(\frac{m}{2}+m_{PL}\right)c(\xi_2-\xi_3)+M_L\, s(\xi_2+\theta)\, s(\xi_3+\theta)+M_V\, c(\xi_2+\theta)\, c(\xi_3+\theta)\right]\ddot{\xi}_2$$

$$+\ell^2\left[\frac{m}{3}+m_{PL}+M_L\, s^2(\xi_3+\theta)+M_V\, c^2(\xi_3+\theta)\right]\ddot{\xi}_3 = F_{\xi_3} \qquad (6)$$

The generalized forces (F_θ, F_{ξ_1}, F_{ξ_2}, F_{ξ_3}) were derived in Section III, Appendix A of the Second Scientific Report*. The following necessary equations are taken from that section.

$$F_\theta = \left[L_S R_{kB} - W_B R_{kg} + F_{BVA} R_{kA} - F_{BHA} R_{jA}\right] s\theta$$

$$+\left[-L_S R_{jB} + W_B R_{jg} - F_{BVA} R_{jA} - F_{BHA} R_{kA}\right] c\theta + M_{\theta B} \qquad (7)$$

$$F_{\xi_1} = \left[L_S - W_B + F_{BVA} - m_{PL}\, g - D_{PLV} - \frac{5}{3} mg\right] \ell\, c\xi_1$$

$$+\left[-F_{BHA} - D_{PLH}\right] \ell\, s\xi_1 - \ell\, C_1 \left[D_{CH1}\, s^2\xi_1 + D_{CV1}\, c^2\xi_1\right]$$

$$-\ell\left[\left(D_{CH2}\, s^2\xi_2 + D_{CV2}\, c^2\xi_2\right) c(\xi_1-\xi_2) + \left(D_{CH3}\, s^2\xi_3\right.\right.$$

$$\left.\left. + D_{CV3}\, c^2\xi_3\right) c(\xi_1-\xi_3)\right] \qquad (8)$$

*Reference 2

$$F_{\xi_2} = \left[L_S - W_B + F_{BVA} - m_{PL} g - D_{PLV} - \frac{3m}{2} g \right] \ell \, C\xi_2 + \left[-F_{BHA} - D_{PLH} \right] \ell \, S\xi_2$$

$$- \ell \left\{ C_2 \left[D_{CH2} S^2 \xi_2 + D_{CV2} C^2 \xi_2 \right] + \left[D_{CH3} S^2 \xi_3 + D_{CV3} C^2 \xi_3 \right] C(\xi_2 - \xi_3) \right\} \tag{9}$$

$$F_{\xi_3} = \left[L_S - W_B + F_{BVA} - m_{PL} g - D_{PLV} - \frac{m}{2} g \right] \ell \, C\xi_3$$

$$+ \left[-F_{BHA} - D_{PLH} \right] \ell \, S\xi_3 - \ell \, C_3 \left[D_{CH3} S^2 \xi_3 + D_{CV3} C^2 \xi_3 \right] \tag{10}$$

$$F_{BHA} = DRAGB \, (C\gamma_B) + LIFTB \, (S\gamma_B) \tag{11}$$

$$F_{BVA} = LIFTB \, (C\gamma_B) - DRAGB \, (S\gamma_B) \tag{12}$$

$$DRAGB = q_B S_B \left[C_{LB} + C_{L_{\dot\theta B}} \left(\frac{d_B}{V_{BR}} \right) \dot\theta \right] \tag{13}$$

$$LIFTB = q_B S_B \left[C_{DB} + C_{D_{\dot\theta B}} \left(\frac{d_B}{V_{BR}} \right) \dot\theta \right] \tag{14}$$

$$M_{\theta B} = q_B S_B d_B \left[C_{m_B} + C_{m_{\dot\theta B}} \left(\frac{d_B}{V_{BR}} \right) \dot\theta \right] \tag{15}$$

$$D_{CHi} = \frac{1}{2} \rho_{Ci} S_{Ci} C_{DC} V_{Ci} \left(V_{WCi} + \dot{Y}_{Ci} \right) \tag{16}$$

$$D_{CVi} = \frac{1}{2} \rho_{Ci} S_{Ci} C_{DC} V_{Ci} \left(\dot{Z}_{Ci} \right) \tag{17}$$

The drag on the payload is neglected.

$$D_{PLH} = D_{PLV} = 0 \tag{18}$$

$$C_n = \frac{1}{3}\left(\frac{q_{Hn} + 2q_{Hn+1}}{q_{Hn} + q_{Hn+1}}\right) \tag{19}$$

$$q_B = \frac{1}{2}\rho_B V_{Bn}^2 \tag{20}$$

$$V_{BR}^2 = (\dot{Y}_B + V_w + V_{qH})^2 + (\dot{Z}_B - V_{qV})^2 \tag{21}$$

$$\gamma_B = \tan^{-1}\left[(\dot{Z}_B - V_{qV})/(\dot{Y}_B + V_w + V_{qH})\right] \tag{22}$$

$$\alpha_B = \theta - \gamma_B \tag{23}$$

See Figure 1

In order to show the load distribution along the tether at any time, the tension in the tether is calculated at the end of each link. This is done by summing forces in the vertical and horizontal directions at each hinge. Before summing forces, consider the inertia forces acting on the balloon. Figure 2 shows the balloon and with the apparent inertia forces acting along and normal to the centerline.

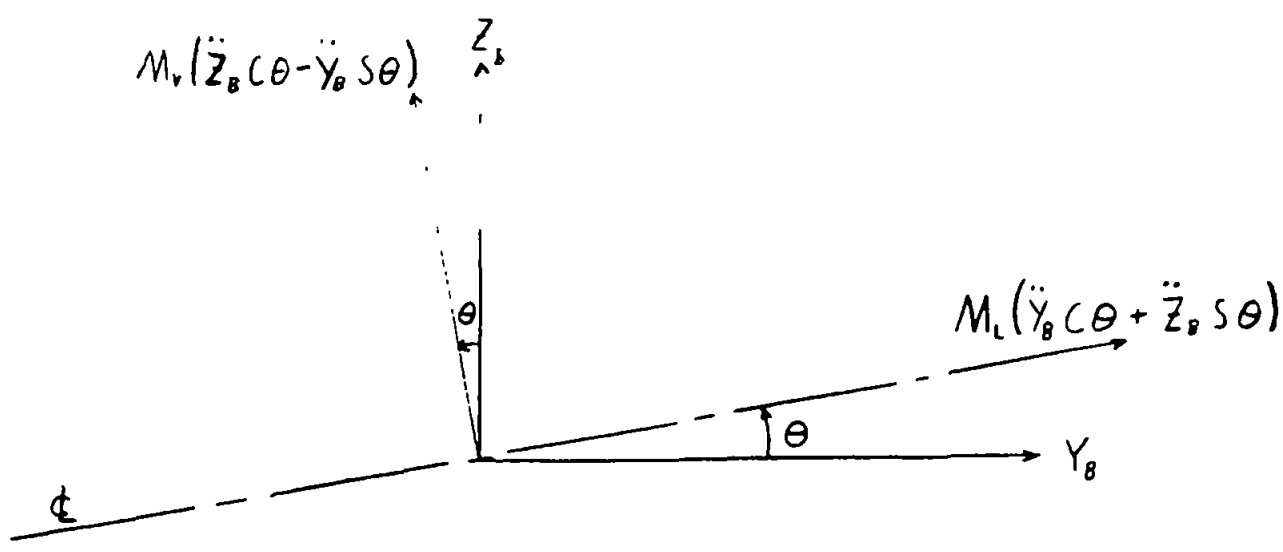

FIGURE 2 INERTIA FORCES ACTING ON BALLOON IN LONGITUDINAL PLANE

$$\sum F_z = M_V(\ddot{z}_B C\theta - \ddot{y}_B S\theta)C\theta + M_L(\ddot{y}_B C\theta + \ddot{z}_B S\theta)S\theta$$

$$= \ddot{z}_B[M_V C^2\theta + M_L S^2\theta] + \ddot{y}_B[M_L - M_V]S\theta C\theta \tag{24}$$

$$\sum F_y = M_L(\ddot{y}_B C\theta + \ddot{z}_B S\theta)C\theta - M_V(\ddot{z}_B C\theta - \ddot{y}_B S\theta)S\theta$$

$$= \ddot{z}_B[M_L - M_V]S\theta C\theta + \ddot{y}_B[M_V S^2\theta + M_L C^2\theta] \tag{25}$$

The summation of forces acting on the balloon are:

$$\sum F_z = L_S + F_{BVA} - W_B - T_{BV} \tag{26}$$

$$\sum F_y = T_{BH} - F_{BHA} \tag{27}$$

where: T_{BV} and T_{BH} are the vertical and horizontal tension forces at the bridle-tether confluence point respectively

Note that the payload forces are not included in these summations but will be included shortly. Equating Equations (24) and (26), and Equations (25) and (27) gives the following expressions for T_{BV} and T_{BH}.

$$T_{BV} = L_S + F_{BVA} - W_B - \ddot{z}_B[M_V C^2\theta + M_L S^2\theta] - \ddot{y}_B[M_L - M_V]S\theta C\theta \tag{28}$$

$$T_{BH} = F_{BHA} + \ddot{z}_B[M_L - M_V]S\theta C\theta + \ddot{y}_B[M_V S^2\theta + M_L C^2\theta] \tag{29}$$

Equations (28) and (29) give the tensions on the tether at a point just above the payload. Figure 3 shows the payload with all forces acting on it.

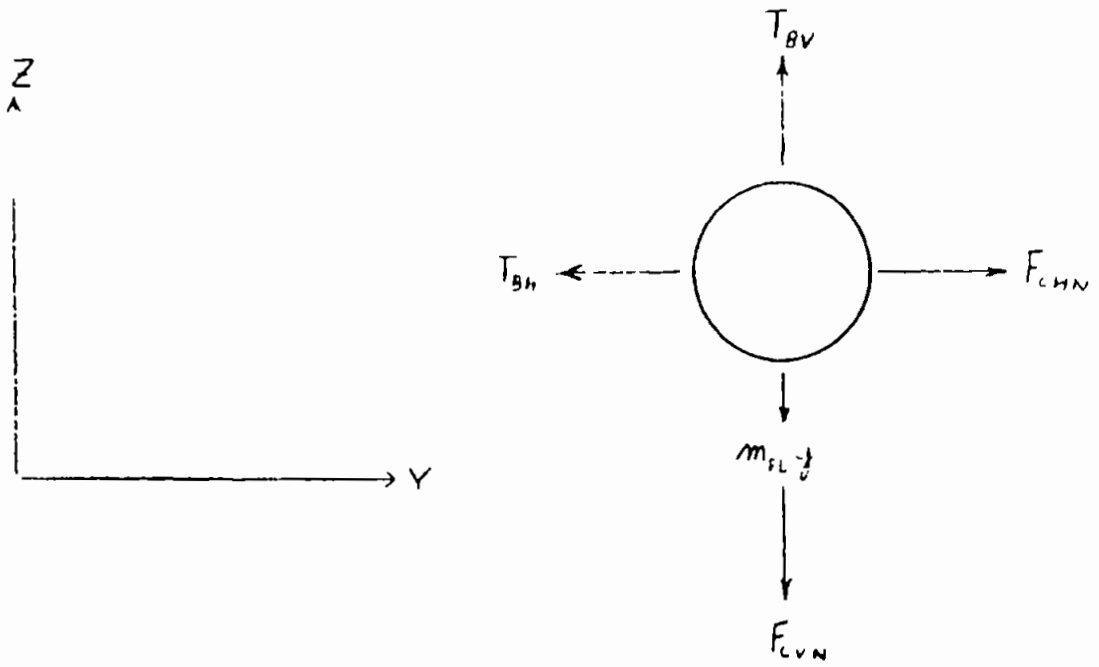

FIGURE 3 APPLIED FORCES ACTING ON PAYLOAD IN LONGITUDINAL PLANE

Summing forces in the vertical and horizontal directions gives:

$$\sum F_z = m_{PL}\ddot{z}_{PL} = T_{BV} - m_{PL}g - F_{CVN} \tag{30}$$

$$\sum F_y = m_{PL}\ddot{y}_{PL} = F_{CHN} - T_{BH} \tag{31}$$

where F_{CV_N} and F_{CH_N} are the vertical and horizontal components of tension at the top of the tether below the payload. Substituting Equation (28) into (30) and (29) into (31) and solving for the vertical and horizontal components of tension at the top of the tether results in the following equations.

$$F_{CVN} = L_S + F_{BVA} - W_B - \ddot{z}_B \left[M_V C^2\theta + M_L S^2\theta \right]$$

$$- \ddot{y}_B \left[M_L - M_V \right] S\theta C\theta - m_{PL}\, g - m_{PL}\, \ddot{z}_{PL} \tag{32}$$

$$F_{CHN} = F_{BHA} + \ddot{z}_B \left[M_L - M_V \right] S\theta C\theta + \ddot{y}_B \left[M_V S^2\theta + M_L C^2\theta \right] + m_{PL}\, \ddot{y}_{PL} \tag{33}$$

The total tension at the top of the tether is:

$$T_N = \sqrt{F_{CHN}^{\,2} + F_{CVN}^{\,2}} \tag{34}$$

Figure 4 shows the applied forces acting on the "N"th link

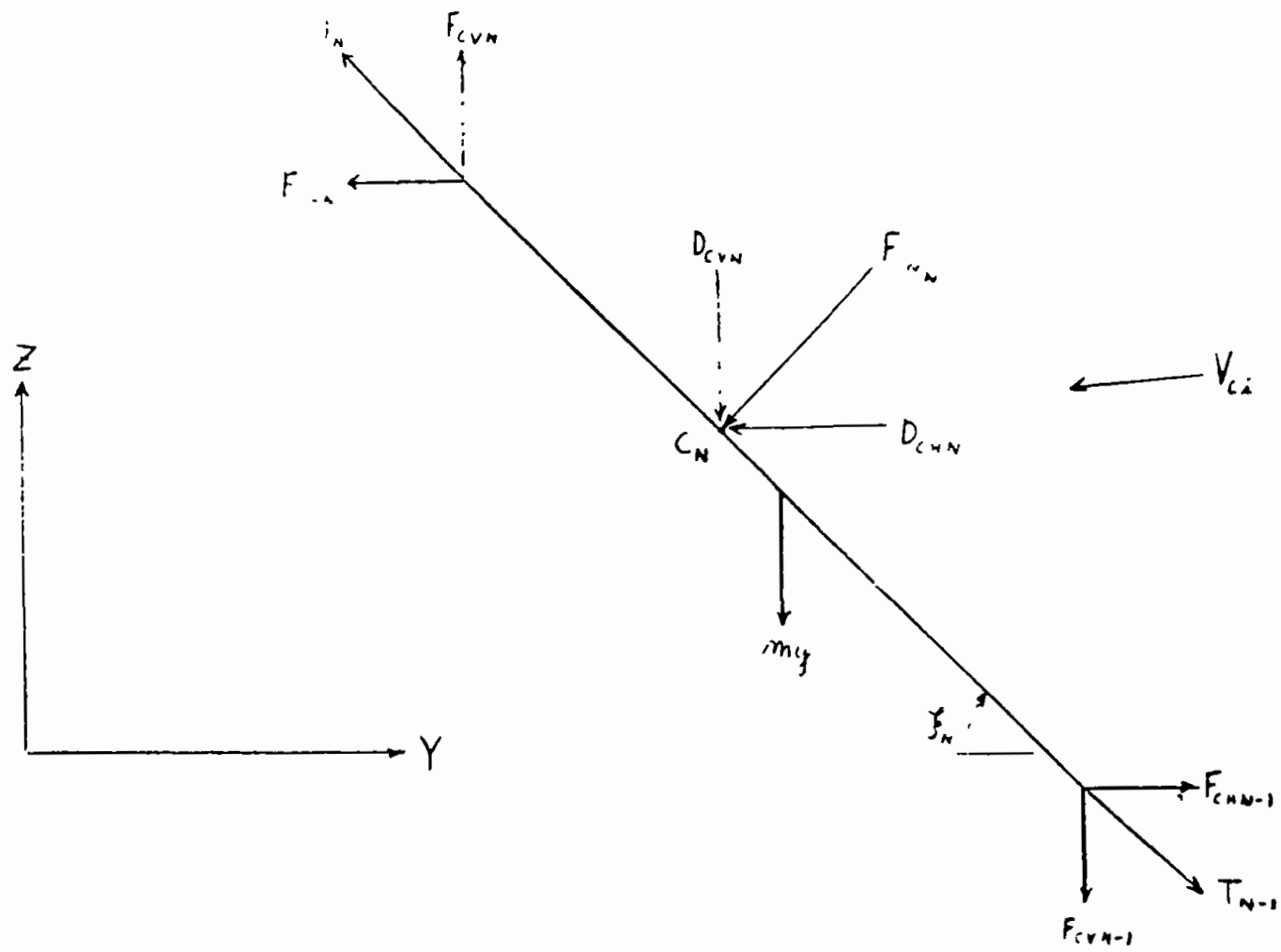

FIGURE 4 APPLIED FORCES ACTING ON "N"TH LINK IN LONGITUDINAL P

The aerodynamic forces D_{CH_N} and D_{CV_N} are the horizontal and vertical components respectively of the normal aerodynamic force (F_{CN_N}) acting at the c.p. of the "N"th link due to the relative motion of the "N"th link with respect to the air. This relative motion takes into account both the steady state wind and the horizontal and vertical inertial velocities of the link. Expressions for D_{CH_N} and D_{CV_N} are given in Equations (16) and (17). The normal force acting on the link is given by:

$$F_{CN_N} = D_{CH_N} S^2 \xi_N + D_{CV_N} C^2 \xi_N \tag{35}$$

Summing vertical and horizontal forces on the "N" link:

$$\sum F_z = m \ddot{z}_{CN} = F_{CVN} - F_{CN_N} C \xi_N - mg - F_{CVN-1} \tag{36}$$

$$\sum F_y = m \ddot{y}_{CN} = -F_{CH_N} - F_{CN_N} S \xi_N + F_{CHN-1} \tag{37}$$

Solving for the tension forces at the bottom of the "N"th link gives the following equations.

$$F_{CVN-1} = F_{CVN} - F_{CN_N} C \xi_N - mg - m \ddot{z}_{CN} \tag{38}$$

$$F_{CHN-1} = F_{CHN} + F_{CN_N} S \xi_N + m \ddot{y}_{CN} \tag{39}$$

$$F_{CVr-1} = F_{CV_r} - F_{CN_r} C \xi_r - m(g + \ddot{z}_{Cr}) \tag{40}$$

$$F_{CHr-1} = F_{CHR} + F_{CN_r} S \xi_r + m \ddot{y}_{Cr} \tag{41}$$

$$T_{r-1} = \sqrt{F_{CVr-1}^2 + F_{CHr-1}^2} \tag{42}$$

The tension at the winch is found by setting r = 1.

SECTION III

NON LINEAR LONGITUDINAL EQUATIONS OF MOTION

Section II of this Appendix contains the longitudinal equations of motion of a tethered balloon if angular velocities are small and products of angular velocities are negligible. This assumption was made in the derivation in Appendix A of the Second Scientific Report*. It is now desirable to examine the equations of motion when large angular velocities are allowed. As in Section II, appropriate equations will be extracted from Appendix A of the Second Scientific Report*. These equations are (41), (79) and (96). Equation (41) is the total kinetic energy of the system: Equation (79) and (96) are terms that are needed for Lagrange's equations. However, these equations are functions of both the longitudinal and lateral degrees-of-freedom. Therefore, before rewriting Equations (41), (79) and (96) of Appendix A* set all lateral degrees-of-freedom equal to zero ($\psi \equiv \phi \equiv \sigma_r \equiv 0$).

The total kinetic energy of the system in the longitudinal plane is:

$$\bar{T} = \sum_{n=1}^{N} \left[\frac{1}{2} m \left(\vec{V}^{P_n^*} \right)^2 + \frac{1}{24} m \ell^2 \dot{\xi}_n^{\,2} \right] + \frac{1}{2} m_{P_L} \left(\vec{V}^{P_L} \right)^2$$

$$+ \frac{1}{2} M_L \left(\vec{V}^{Q} \cdot \vec{j}_B \right)^2 + \frac{1}{2} M_V \left(\vec{V}^{U} \cdot \vec{k}_B \right)^2 + \frac{1}{2} I_{xB} \dot{\theta}^2 \tag{43}$$

where

$$\vec{V}^{P_n^*} = \ell \left[\sum_{i=1}^{n-1} \dot{\xi}_i \, \vec{e}_i + \frac{1}{2} \dot{\xi}_n \, \vec{e}_n \right] \tag{44}$$

*Reference 2

$$\vec{V}^{PL} = \ell \sum_{i=1}^{N} \dot{\xi}_i \vec{e}_i \tag{45}$$

$$\vec{V}^{G} = \ell \sum_{i=1}^{N} \dot{\xi}_i \vec{e}_i + \left[R_{km} \vec{j}_B - R_{jm} \vec{k}_B \right] \dot{\theta} \tag{46}$$

Now write Equation (79) of Appendix A*

$$\frac{\partial \bar{T}}{\partial \dot{\theta}} = M_L \left\{ \ell \sum_{i=1}^{N} \dot{\xi}_i s(\theta + \xi_i) + R_{km} \dot{\theta} \right\} R_{km}$$

$$+ M_V \left\{ \ell \sum_{i=1}^{N} \dot{\xi}_i c(\theta + \xi_i) - R_{jm} \dot{\theta} \right\} \left\{ -R_{jm} \right\} + I_{xB} \dot{\theta} \tag{47}$$

Rewriting Equation (96) of Appendix A*:

$$\frac{\partial \bar{T}}{\partial \dot{\xi}_n} = \sum_{m=n+1}^{N} m \ell^2 \left\{ \sum_{i=1}^{n-1} \dot{\xi}_i c(\xi_n - \xi_i) + \frac{1}{2} \dot{\xi}_n c(\xi_n - \xi_n) \right\}$$

$$+ m \ell^2 \left\{ \frac{1}{2} \sum_{i=1}^{n-1} \dot{\xi}_i c(\xi_n - \xi_i) + \frac{1}{3} \dot{\xi}_n \right\} + m_{PL} \ell^2 \left\{ \sum_{i=1}^{N} \dot{\xi}_i c(\xi_n - \xi_i) \right\}$$

$$+ M_L \left\{ \ell^2 \sum_{i=1}^{N} \dot{\xi}_i s(\theta + \xi_i) + \ell R_{km} \dot{\theta} \right\} s(\theta + \xi_n)$$

$$+ M_V \left\{ \ell^2 \sum_{i=1}^{N} \dot{\xi}_i c(\theta + \xi_i) - \ell R_{jm} \dot{\theta} \right\} c(\theta + \xi_n) \tag{48}$$

Langrange's equations for the system are:

$$\frac{d}{dt}\left(\frac{\partial \bar{T}}{\partial \dot{\theta}} \right) - \frac{\partial \bar{T}}{\partial \theta} = F_\theta \tag{49}$$

$$\frac{d}{dt}\left(\frac{\partial \bar{T}}{\partial \dot{\xi}_n} \right) - \frac{\partial \bar{T}}{\partial \xi_n} = F_{\xi_n} \tag{50}$$

*Reference 2

First derive the terms in Equation (49). Using Equation (47) the following term is formed.

$$\frac{d}{dt}\left(\frac{\partial \bar{T}}{\partial \dot{\theta}}\right) = M_L\left\{\ell\left[\sum_{i=1}^{N} \ddot{\xi}_i\, s(\theta+\xi_i) + \sum_{i=1}^{N} \dot{\xi}_i(\dot{\theta}+\dot{\xi}_i)\, c(\theta+\xi_i)\right] + R_{km}\ddot{\theta}\right\} R_{km}$$

$$+ M_V\left\{\ell\left[\sum_{i=1}^{N} \ddot{\xi}_i\, c(\theta+\xi_i) - \sum_{i=1}^{N} \dot{\xi}_i(\dot{\theta}+\dot{\xi}_i)\, s(\theta+\xi_i)\right] - R_{jm}\ddot{\theta}\right\}\left\{-R_{jm}\right\}$$

$$+ I_{xB}\,\ddot{\theta} \tag{51}$$

From Equation (43)

$$\frac{\partial \bar{T}}{\partial \theta} = M_L\left(\vec{V}^{a}\cdot\vec{j}_B\right)\left[\frac{\partial \vec{V}^{a}}{\partial \theta}\cdot\vec{j}_B + \vec{V}^{a}\cdot\frac{\partial \vec{j}_B}{\partial \theta}\right]$$

$$+ M_V\left(\vec{V}^{a}\cdot\vec{k}_B\right)\left[\frac{\partial \vec{V}^{a}}{\partial \theta}\cdot\vec{k}_B + \vec{V}^{a}\cdot\frac{\partial \vec{k}_B}{\partial \theta}\right] \tag{52}$$

From Equation (46)

$$\vec{V}^{a}\cdot\vec{j}_B = \ell\sum_{i=1}^{N} \dot{\xi}_i\, \vec{\ell}_i\cdot\vec{j}_B + R_{km}\dot{\theta} \tag{53}$$

$$\vec{V}^{a}\cdot\vec{j}_B = \ell\sum_{i=1}^{N} \dot{\xi}_i\, s(\theta+\xi_i) + R_{km}\dot{\theta} \tag{54}$$

$$\vec{V}^{a}\cdot\vec{k}_B = \ell\sum_{i=1}^{N} \dot{\xi}_i\, c(\theta+\xi_i) - R_{jm}\dot{\theta} \tag{55}$$

$$\frac{\partial \vec{V}^{a}}{\partial \theta} = \left[R_{km}\frac{\partial \vec{j}_B}{\partial \theta} - R_{jm}\frac{\partial \vec{k}_B}{\partial \theta}\right]\dot{\theta} = \left[R_{km}\vec{k}_B + R_{jm}\vec{j}_B\right]\dot{\theta} \tag{56}$$

$$\frac{\partial \vec{V}^{a}}{\partial \theta}\cdot\vec{j}_B = R_{0m}\dot{\theta} \tag{57}$$

$$\frac{\partial \vec{V}^{a}}{\partial \theta} \cdot \vec{k}_{b} = R_{km}\dot{\theta} \tag{58}$$

$$\vec{V}^{a} \cdot \frac{\partial \vec{j}_{b}}{\partial \theta} = \ell \sum_{i=1}^{N} \dot{\xi}_{i}\, c(\theta+\xi_{i}) - R_{jm}\dot{\theta} \tag{59}$$

$$\vec{V}^{a} \cdot \frac{\partial \vec{k}_{b}}{\partial \theta} = \ell \sum_{i=1}^{N} -\dot{\xi}_{i}\, s(\theta+\xi_{i}) - R_{km}\dot{\theta} \tag{60}$$

Substitute Equations (53) to (60) into (52):

$$\begin{aligned}\frac{\partial \bar{T}}{\partial \theta} = {} & M_{L}\Big[\ell \sum_{i=1}^{N} \dot{\xi}_{i}\, s(\theta+\xi_{i}) + R_{km}\dot{\theta}\Big]\Big[R_{jm}\dot{\theta} + \ell \sum_{i=1}^{N} \dot{\xi}_{i}\, c(\theta+\xi_{i}) - R_{jm}\dot{\theta}\Big] \\ & + M_{V}\Big[\ell \sum_{i=1}^{N} \dot{\xi}_{i}\, c(\theta+\xi_{i}) - R_{jm}\dot{\theta}\Big]\Big[R_{km}\dot{\theta} - \ell \sum_{i=1}^{N} \dot{\xi}_{i}\, s(\theta+\xi_{i}) - R_{km}\dot{\theta}\Big]\end{aligned} \tag{61}$$

$$\begin{aligned}\frac{\partial \bar{T}}{\partial \theta} = {} & [M_{L} - M_{V}]\Big[\ell^{2} \sum_{i=1}^{N} \dot{\xi}_{i}\, s(\theta+\xi_{i}) \sum_{i=1}^{N} \dot{\xi}_{i}\, c(\theta+\xi_{i})\Big] \\ & + M_{L}\ell R_{km}\dot{\theta} \sum_{i=1}^{N} \dot{\xi}_{i}\, c(\theta+\xi_{i}) + M_{V}\ell R_{jm}\dot{\theta} \sum_{i=1}^{N} \dot{\xi}_{i}\, s(\theta+\xi_{i})\end{aligned} \tag{62}$$

Substituting Equations (51) and (62) into Eqation (49) yields the final nonlinear balloon pitching equation. Note, F_{θ} is the same for both the nonlinear equation that follows, and Equation (1) which assumed small angular velocities. The expression for F_{θ} is given by Equation (7).

$$\begin{aligned}& M_{L}\ell R_{km} \sum_{i=1}^{N} \ddot{\xi}_{i}\, s(\theta+\xi_{i}) - M_{V}\ell R_{jm} \sum_{i=1}^{N} \ddot{\xi}_{i}\, c(\theta+\xi_{i}) + [M_{L}R_{km}^{2} + M_{V}R_{jm}^{2} + I_{xb}]\ddot{\theta} \\ & = [M_{L} - M_{V}]\Big[\ell^{2} \sum_{i=1}^{N} \dot{\xi}_{i}\, s(\theta+\xi_{i}) \sum_{i=1}^{N} \dot{\xi}_{i}\, c(\theta+\xi_{i})\Big] \\ & \quad - M_{L}\ell R_{km} \sum_{i=1}^{N} \dot{\xi}_{i}^{2}\, c(\theta+\xi_{i}) - M_{V}\ell R_{jm} \sum_{i=1}^{N} \dot{\xi}_{i}^{2}\, s(\theta+\xi_{i}) + F_{\theta}\end{aligned} \tag{63}$$

Now consider the tether equation of motion (50). From Equation (48) it follows:

$$\frac{d}{dt}\left(\frac{\partial \bar{T}}{\partial \dot{\xi}_n}\right) = \sum_{m=n+1}^{N} m\ell^2 \Big\{ \sum_{i=1}^{m-1} \ddot{\xi}_i\, c(\xi_n-\xi_i) - \sum_{i=1}^{m-1} \dot{\xi}_i (\dot{\xi}_n-\dot{\xi}_i)\, s(\xi_n-\xi_i)$$

$$+\tfrac{1}{2}\ddot{\xi}_m\, c(\xi_n-\xi_m) - \tfrac{1}{2}\dot{\xi}_m(\dot{\xi}_n-\dot{\xi}_m)\, s(\xi_n-\xi_m)\Big\} + m\ell^2\Big\{\tfrac{1}{2}\sum_{i=1}^{n-1}\ddot{\xi}_i\, c(\xi_n-\xi_i)$$

$$-\tfrac{1}{2}\sum_{i=1}^{n-1}\dot{\xi}_i(\dot{\xi}_n-\dot{\xi}_i)\, s(\xi_n-\xi_i) + \tfrac{1}{3}\ddot{\xi}_n\Big\} + m_{PL}\ell^2\Big\{\sum_{i=1}^{N}\ddot{\xi}_i\, c(\xi_n-\xi_i)$$

$$-\sum_{i=1}^{N}\dot{\xi}_i(\dot{\xi}_n-\dot{\xi}_i)\, s(\xi_n-\xi_i)\Big\}$$

$$+M_L\Big\{\Big[\ell^2\sum_{i=1}^{N}\ddot{\xi}_i\, s(\theta+\xi_i) + \ell^2\sum_{i=1}^{N}\dot{\xi}_i(\dot{\theta}+\dot{\xi}_i)\, c(\theta+\xi_i) + \ell R_{fm}\ddot{\theta}\Big] s(\theta+\xi_n)$$

$$+\Big[\ell^2\sum_{i=1}^{N}\xi_i\, s(\theta+\xi_i) + \ell R_{fm}\dot{\theta}\Big]\Big[\dot{\theta}+\dot{\xi}_n\Big]\, c(\theta+\xi_n)\Big\}$$

$$+M_V\Big\{\Big[\ell^2\sum_{i=1}^{N}\ddot{\xi}_i\, c(\theta+\xi_i) - \ell^2\sum_{i=1}^{N}\dot{\xi}_i(\dot{\theta}+\dot{\xi}_i)\, s(\theta+\xi_i) - \ell R_{fm}\ddot{\theta}\Big] c(\theta+\xi_n)$$

$$-\Big[\ell^2\sum_{i=1}^{N}\xi_i\, c(\theta+\xi_i) - \ell R_{fm}\dot{\theta}\Big]\Big[\dot{\theta}+\dot{\xi}_n\Big]\, s(\theta+\xi_n) \qquad (64)$$

From Equation (43):

$$\frac{\partial \bar{T}}{\partial \xi_n} = \sum_{m=1}^{N} m\left(\vec{V}^{P_m^*}\cdot\frac{\partial \vec{V}^{P_m^*}}{\partial \xi_n}\right) + m_{PL}\left(\vec{V}^{PL}\cdot\frac{\partial \vec{V}^{PL}}{\partial \xi_n}\right)$$

$$+M_L\left(\vec{V}^{Q}\cdot\vec{j}_B\right)\left(\frac{\partial \vec{V}^{Q}}{\partial \xi_n}\cdot\vec{j}_B\right) + M_V\left(\vec{V}^{Q}\cdot\vec{k}_B\right)\left(\frac{\partial \vec{V}^{Q}}{\partial \xi_n}\cdot\vec{k}_B\right) \qquad (65)$$

From Equation (44):

$$\frac{\partial \vec{V}^{P_n^*}}{\partial \xi_n} = \begin{cases} -\ell\, \dot{\xi}_n\, \vec{e}_n & m > n \\ -\frac{1}{2}\ell\, \dot{\xi}_n\, \vec{e}_n & m = n \\ 0 & m < n \end{cases} \tag{66}$$

$$\sum_{m=1}^{N} \vec{V}^{P_m^*} \cdot \frac{\partial \vec{V}^{P_m^*}}{\partial \xi_n} = -\ell^2 \sum_{m=n+1}^{N} \left[\sum_{i=1}^{m-1} \dot{\xi}_i \dot{\xi}_n\, \vec{e}_i \cdot \vec{e}_n + \frac{1}{2} \dot{\xi}_n \dot{\xi}_n\, \vec{e}_n \cdot \vec{e}_n \right.$$

$$\left. -\ell^2 \left[\frac{1}{2} \sum_{i=1}^{n-1} \dot{\xi}_i \dot{\xi}_n\, \vec{e}_i \cdot \vec{e}_n - \frac{1}{4} \dot{\xi}_n^2\, \vec{e}_n \cdot \vec{e}_n \right] \right. \tag{67}$$

From Equation (45):

$$\frac{\partial \vec{V}^{P_L}}{\partial \xi_n} = -\ell\, \dot{\xi}_n\, \vec{e}_n \tag{68}$$

$$\vec{V}^{P_L} \cdot \frac{\partial \vec{V}^{P_L}}{\partial \xi_n} = -\ell^2 \sum_{i=1}^{N} \dot{\xi}_i \dot{\xi}_n\, \vec{e}_n \cdot \vec{e}_i \tag{69}$$

From Equation (46):

$$\frac{\partial \vec{V}^{Q}}{\partial \xi_n} = -\ell\, \dot{\xi}_n\, \vec{e}_n \tag{70}$$

$$\frac{\partial \vec{V}^{Q}}{\partial \xi_n} \cdot \vec{j}_B = -\ell\, \dot{\xi}_n \left[-c\xi_n c\theta + s\xi_n s\theta \right] \tag{71}$$

$$\frac{\partial \vec{V}^{Q}}{\partial \xi_n} \cdot \vec{k}_B = -\ell\, \dot{\xi}_n \left[c\xi_n s\theta + s\xi_n c\theta \right] \tag{72}$$

Substituting Equations (67), (69), (71), (72), (54), and (55) into Equation (65) yields

$$\frac{\partial \bar{T}}{\partial \xi_n} = \ell^2 m \Big\{ \sum_{m=n+1}^{N} \Big[\sum_{i=1}^{m-1} \dot{\xi}_i \dot{\xi}_n s(\xi_i - \xi_n) + \frac{1}{2} \dot{\xi}_m \dot{\xi}_n s(\xi_m - \xi_n) \Big]$$

$$+ \frac{1}{2} \sum_{i=1}^{n-1} \dot{\xi}_i \dot{\xi}_n s(\xi_i - \xi_n) \Big\} + m_{PL} \ell^2 \sum_{i=1}^{N} \dot{\xi}_i \dot{\xi}_n s(\xi_i - \xi_n)$$

$$+ M_L \ell \dot{\xi}_n c(\theta + \xi_n) \Big[\ell \sum_{i=1}^{N} \dot{\xi}_i s(\theta + \xi_i) + R_{km} \dot{\theta} \Big]$$

$$- M_V \ell \dot{\xi}_n s(\theta + \xi_n) \Big[\ell \sum_{i=1}^{N} \dot{\xi}_i c(\theta + \xi_i) - R_{jm} \dot{\theta} \Big] \tag{73}$$

Substitute Equations (64) and (73) into Equation (50) to give the final nonlinear tether pitching equation. F_{ξ_n} has already been found in Equations (8), (9) and (10).

$$\sum_{m=n+1}^{N} m \ell^2 \Big\{ \sum_{i=1}^{m-1} \ddot{\xi}_i c(\xi_n - \xi_i) + \frac{1}{2} \ddot{\xi}_m c(\xi_n - \xi_m) \Big\} + m \ell^2 \Big\{ \frac{1}{2} \sum_{i=1}^{n-1} \ddot{\xi}_i c(\xi_n - \xi_i) + \frac{1}{3} \ddot{\xi}_n \Big\}$$

$$+ m_{PL} \ell^2 \sum_{i=1}^{N} \ddot{\xi}_i c(\xi_n - \xi_i) + M_L \Big[\ell^2 \sum_{i=1}^{N} \ddot{\xi}_i s(\theta + \xi_i) + \ell R_{km} \ddot{\theta} \Big] s(\theta + \xi_n)$$

$$+ M_V \Big[\ell^2 \sum_{i=1}^{N} \ddot{\xi}_i c(\theta + \xi_i) - \ell R_{jm} \ddot{\theta} \Big] c(\theta + \xi_n)$$

$$= \sum_{m=n+1}^{N} m \ell^2 \Big\{ \sum_{i=1}^{m-1} \dot{\xi}_i^2 s(\xi_i - \xi_n) + \frac{1}{2} \dot{\xi}_m^2 s(\xi_m - \xi_n) \Big\} + \frac{m \ell^2}{2} \sum_{i=1}^{n-1} \dot{\xi}_i^2 s(\xi_i - \xi_n)$$

$$+ m_{PL} \ell^2 \sum_{i=1}^{N} \dot{\xi}_i^2 s(\xi_i - \xi_n) + M_L \Big\{ \ell^2 \Big[\sum_{i=1}^{N} - \dot{\xi}_i (\dot{\theta} + \dot{\xi}_i) c(\theta + \xi_i) s(\theta + \xi_n)$$

$$- \sum_{i=1}^{N} \dot{\xi}_i \dot{\theta} s(\theta + \xi_i) c(\theta + \xi_n) \Big] - \ell R_{km} \dot{\theta}^2 c(\theta + \xi_n) \Big\}$$

$$+M_V\Big\{\ell^2\Big[\sum_{i=1}^{N}\dot{\varphi}_i(\dot{\theta}+\dot{\varphi}_i)\,s(\theta+\varphi_i)\,c(\theta+\varphi_r)$$

$$+\sum_{i=1}^{N}\dot{\varphi}_i\dot{\theta}\,c(\theta+\varphi_i)\,s(\theta+\varphi_r)-\ell R_{jm}\dot{\theta}^2 s(\theta+\varphi_r)\Big\}+F_{\varphi_r} \tag{74}$$

Now assume the tether is composed of three links (N = 3). Rewriting the balloon pitching Equation (63) gives:

$$\{I_{xB}+M_L R_{km}^2+M_V R_{jm}^2\}\ddot{\theta}$$

$$+\ell\{M_L R_{km}\,s(\theta+\varphi_1)-M_V R_{jm}\,c(\theta+\varphi_1)\}\ddot{\varphi}_1$$

$$+\ell\{M_L R_{km}\,s(\theta+\varphi_2)-M_V R_{jm}\,c(\theta+\varphi_2)\}\ddot{\varphi}_2$$

$$+\ell\{M_L R_{km}\,s(\theta+\varphi_3)-M_V R_{jm}\,c(\theta+\varphi_3)\}\ddot{\varphi}_3$$

$$=[M_L-M_V]\Big[\ell^2\sum_{i=1}^{3}\dot{\varphi}_i\,s(\theta+\varphi_i)\sum_{i=1}^{3}\dot{\varphi}_i\,c(\theta+\varphi_i)\Big]$$

$$-M_L\ell R_{km}\sum_{i=1}^{3}\dot{\varphi}_i^2\,c(\theta+\varphi_i)-M_V\ell R_{jm}\sum_{i=1}^{3}\dot{\varphi}_i^2\,s(\theta+\varphi_i)+F_\theta \tag{75}$$

For N = 3 and r = 1, Equation (74) becomes:

$$\{M_L\ell R_{km}\,s(\theta+\varphi_1)-M_V\ell R_{jm}\,c(\theta+\varphi_1)\}\ddot{\theta}$$

$$+\ell^2\Big\{\frac{7m}{3}+m_{PL}+M_L s^2(\theta+\varphi_1)+M_V c^2(\theta+\varphi_1)\Big\}\ddot{\varphi}_1$$

$$+\ell^2\Big\{\Big[\frac{3m}{2}+m_{PL}\Big]c(\varphi_1-\varphi_2)+M_L s(\theta+\varphi_2)s(\theta+\varphi_1)+M_V c(\theta+\varphi_2)\,c(\theta+\varphi_1)\Big\}\ddot{\varphi}_2$$

$$+\ell^2\left\{\left[\frac{m}{2}+m_{PL}\right]c(\varphi_1-\varphi_3)+M_L s(\theta+\varphi_3)s(\theta+\varphi_1)+M_V c(\theta+\varphi_3)c(\theta+\varphi_1)\right\}\ddot{\varphi}_3$$

$$=m\ell^2\left\{\frac{3}{2}\dot{\varphi}_2^2 s(\varphi_2-\varphi_1)+\frac{1}{2}\dot{\varphi}_3^2 s(\varphi_3-\varphi_1)\right\}+m_{PL}\ell^2\sum_{i=2}^{3}\dot{\varphi}_i^2 s(\varphi_i-\varphi_1)$$

$$+[M_V-M_L]\ell^2\left\{s(\theta+\varphi_1)\sum_{i=1}^{3}\dot{\varphi}_i\dot{\theta}c(\theta+\varphi_i)+c(\theta+\varphi_1)\sum_{i=1}^{3}\dot{\varphi}_i\dot{\theta}s(\theta+\varphi_i)\right\}$$

$$+M_V\ell^2 c(\theta+\varphi_1)\sum_{i=1}^{3}\dot{\varphi}_i^2 s(\theta+\varphi_i)-M_L\ell^2 s(\theta+\varphi_1)\sum_{i=1}^{3}\dot{\varphi}_i^2 c(\theta+\varphi_i)$$

$$-\ell\left[M_L R_{km}c(\theta+\varphi_1)+M_L R_{jm}s(\theta+\varphi_1)\right]\dot{\theta}^2+F_{\varphi_1} \tag{76}$$

For N = 3 and r = 2, Equation (74) becomes:

$$\left\{M_L\ell R_{km}s(\theta+\varphi_2)-M_V\ell R_{jm}c(\theta+\varphi_2)\right\}\ddot{\theta}$$

$$+\ell^2\left\{\left[\frac{3m}{2}+m_{PL}\right]c(\varphi_1-\varphi_2)+M_L s(\theta+\varphi_1)s(\theta+\varphi_2)+M_V c(\theta+\varphi_1)c(\theta+\varphi_2)\right\}\ddot{\varphi}_1$$

$$+\ell^2\left\{\frac{4m}{3}+m_{PL}+M_L s^2(\theta+\varphi_2)+M_V c^2(\theta+\varphi_2)\right\}\ddot{\varphi}_2$$

$$+\ell^2\left\{\left[\frac{m}{2}+m_{PL}\right]c(\varphi_2-\varphi_3)+M_L s(\theta+\varphi_2)s(\theta+\varphi_3)+M_V c(\theta+\varphi_2)c(\theta+\varphi_3)\right\}\ddot{\varphi}_3$$

$$=m\ell^2\left\{\frac{3}{2}\dot{\varphi}_1^2 s(\varphi_1-\varphi_2)+\frac{1}{2}\dot{\varphi}_3^2 s(\varphi_3-\varphi_2)\right\}+m_{PL}\ell^2\sum_{i=1}^{3}\dot{\varphi}_i^2 s(\varphi_i-\varphi_2)$$

$$+[M_V-M_L]\ell^2\left\{s(\theta+\varphi_2)\sum_{i=1}^{3}\dot{\varphi}_i\dot{\theta}c(\theta+\varphi_i)+c(\theta+\varphi_2)\sum_{i=1}^{3}\dot{\varphi}_i\dot{\theta}s(\theta+\varphi_i)\right\}$$

$$+M_V\ell^2 c(\theta+\varphi_2)\sum_{i=1}^{3}\dot{\varphi}_i^2 s(\theta+\varphi_i)-M_L\ell^2 s(\theta+\varphi_2)\sum_{i=1}^{3}\dot{\varphi}_i^2 c(\theta+\varphi_i)$$

$$-\ell\left[M_L R_{km}c(\theta+\varphi_2)+M_V R_{jm}s(\theta+\varphi_2)\right]\dot{\theta}^2+F_{\varphi_2} \tag{77}$$

For N = 3 and r = 3, Equation (74) becomes:

$$
\begin{aligned}
&\{M_L \ell R_{km} s(\theta+\varphi_3) - M_V \ell R_{jm} c(\theta+\varphi_3)\}\ddot{\theta} \\
&+\ell^2\{[\tfrac{m}{2}+m_{pL}]c(\varphi_1-\varphi_3)+M_L s(\theta+\varphi_1)s(\theta+\varphi_3)+M_V c(\theta+\varphi_1)c(\theta+\varphi_3)\}\ddot{\varphi}_1 \\
&+\ell^2\{[\tfrac{m}{2}+m_{pL}]c(\varphi_2-\varphi_3)+M_L s(\theta+\varphi_2)s(\theta+\varphi_3)+M_V c(\theta+\varphi_2)c(\theta+\varphi_3)\}\ddot{\varphi}_2 \\
&+\ell^2\{\tfrac{m}{3}+m_{pL}+M_L s^2(\theta+\varphi_3)+M_V c^2(\theta+\varphi_3)\}\ddot{\varphi}_3 \\
&=\ell^2[\tfrac{m}{2}+m_{pL}]\sum_{i=1}^{2}\dot{\varphi}_i^2 s(\varphi_i-\varphi_3) \\
&+[M_V-M_L]\ell^2\{s(\theta+\varphi_3)\sum_{i=1}^{3}\dot{\varphi}_i\dot{\theta}c(\theta+\varphi_i)+c(\theta+\varphi_3)\sum_{i=1}^{3}\dot{\varphi}_i\dot{\theta}s(\theta+\varphi_i)\} \\
&+M_V\ell^2 c(\theta+\varphi_3)\sum_{i=1}^{3}\dot{\varphi}_i^2 s(\theta+\varphi_i)-M_L\ell^2 s(\theta+\varphi_3)\sum_{i=1}^{3}\dot{\varphi}_i^2 c(\theta+\varphi_i) \\
&-\ell[M_L R_{km} c(\theta+\varphi_3)+M_V R_{jm} s(\theta+\varphi_3)]\dot{\theta}^2 + F_{\varphi_3}
\end{aligned}
\tag{78}
$$

SECTION IV

LATERAL EQUATIONS OF MOTION FOR SMALL ANGULAR VELOCITIES

Sections II and III considered the equations of motion of a tethered balloon in the longitudinal plane. This section will consider the equations of motion of a tethered balloon when the longitudinal degrees-of-freedom are fixed at their equilibrium value and the system is allowed to move only in the lateral degrees-of-freedom. Figure 5 displays a front and top view of the tethered balloon. All angles are shown positive. The lateral degrees-of-freedom are: ψ (yaw of balloon), ϕ (roll of balloon), and σ_r (yaw of "r"th link).

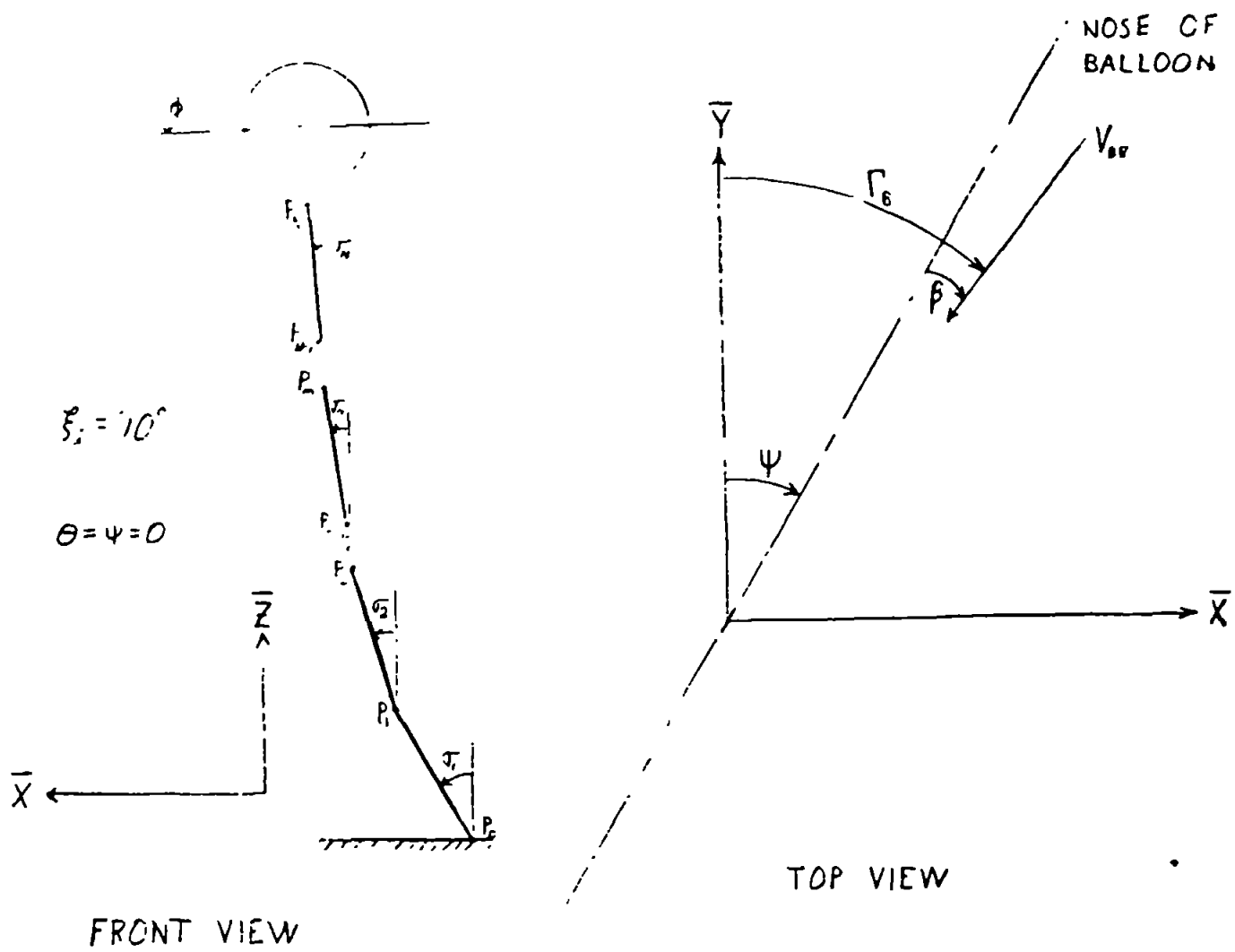

FIGURE 5 - BALLOON TETHER MODEL IN LATERAL PLANE

The appropriate equations of motion are Equations (73), (86), and (108) of Appendix A of the Second Scientific Report*. These three equations will be rewritten below remembering that θ (pitch of balloon) and ζ_r (pitch of "r"th link) are constants. The first equation is the balloon yaw equation of motion.

$$
\begin{aligned}
&M_s\Big\{\ell\sum_{i=1}^{N}\ddot{\sigma}_i\big[c\sigma_i(s\phi s\theta s\psi+c\phi c\psi)+s\sigma_i c\xi_i(s\phi s\theta c\psi-c\phi s\psi)-s\sigma_i s\xi_i(-s\phi c\theta)\big] \\
&+\big[R_{jm}(-\ddot{\psi}c\theta c\phi)-R_{km}(-\ddot{\psi}s\theta+\ddot{\phi})\big]\Big\}\big\{-R_{jm}c\theta c\phi+R_{km}s\theta\big\} \\
&+M_s\Big\{\ell\sum_{i=1}^{N}\ddot{\sigma}_i\big[c\sigma_i(c\theta s\psi)+s\sigma_i c\xi_i(c\theta c\psi)-s\sigma_i s\xi_i(s\theta)\big]+\big[R_{km}(\ddot{\psi}s\phi c\theta)\big]\Big\}\big\{R_{km}s\phi c\theta\big\} \\
&+M_s\Big\{\ell\sum_{i=1}^{N}\ddot{\sigma}_i\big[c\sigma_i(-c\phi s\theta s\psi+s\phi c\psi)+s\sigma_i c\xi_i(-c\phi s\theta c\psi-s\phi s\psi)-s\sigma_i s\xi_i(c\phi c\theta)\big] \\
&+\big[-R_{jm}(\ddot{\psi}s\phi c\theta)\big]\Big\}\big\{-R_{jm}s\phi c\theta\big\}+\ddot{\phi}\big[-I_{YB}s\theta+I_{YZB}c\theta c\phi\big] \\
&+\big[c^2\theta(I_{XB}s^2\phi+I_{ZB}c^2\phi)+s^2\theta I_{YB}-s2\theta c\phi I_{YZB}\big]=F_\psi
\end{aligned}
\tag{79}
$$

The second equation is the balloon roll equation.

$$
\begin{aligned}
&M_s\Big\{\ell\sum_{i=1}^{N}\ddot{\sigma}_i\big[c\sigma_i(s\phi s\theta s\psi+c\phi c\psi)+s\sigma_i c\xi_i(s\phi s\theta c\psi-c\phi s\psi)-s\sigma_i s\xi_i(-s\phi c\theta)\big] \\
&+\big[R_{jm}(-\ddot{\psi}c\theta c\phi)-R_{km}(-\ddot{\psi}s\theta+\ddot{\phi})\big]\Big\}\big\{-R_{km}\big\} \\
&+\ddot{\phi}\big[I_{YB}\big]+\ddot{\psi}\big[-I_{YB}s\theta+I_{YZB}c\theta c\phi\big]=F_\phi
\end{aligned}
\tag{80}
$$

*Reference 2

The equation for the tether link yaw equation of motion is given as follows:

$$
\begin{aligned}
&\sum_{m=n+1}^{N} m\ell^2\Big\{\sum_{i=1}^{n-1}\ddot{\sigma}_i\left[c\sigma_i\, c\sigma_n + s\sigma_i\, s\sigma_n\, c(\xi_n-\xi_i)\right] + \tfrac{1}{2}\ddot{\sigma}_n\left[c\sigma_m\, c\sigma_n + s\sigma_m\, s\sigma_n\, c(\xi_n-\xi_m)\right]\Big\} \\
&+\frac{m}{2}\ell^2\sum_{i=1}^{n-1}\ddot{\sigma}_i\left[c\sigma_i\, c\sigma_n + s\sigma_i\, s\sigma_n\, c(\xi_n-\xi_i)\right] + \frac{m}{3}\ell^2\ddot{\sigma}_n \\
&+m_{PL}\,\ell^2\sum_{i=1}^{N}\ddot{\sigma}_i\left[c\sigma_i\, c\sigma_n + s\sigma_i\, s\sigma_n\, c(\xi_n-\xi_i)\right] \\
&+M_s\Big\{\ell\sum_{i=1}^{N}\ddot{\sigma}_i\left[c\sigma_i(s\phi\, s\theta\, s\psi + c\phi\, c\psi) + s\sigma_i\, c\xi_i(s\phi\, s\theta\, c\psi - c\phi\, s\psi) - s\sigma_i\, s\xi_i(-s\phi\, c\theta)\right] \\
&+\left[R_{jm}(-\ddot{\psi}c\theta\, c\phi) - R_{km}(-\ddot{\psi}s\theta + \ddot{\phi})\right]\Big\}\Big\{\ell\Big[c\sigma_n(s\phi\, s\theta\, s\psi + c\phi\, c\psi) \\
&+s\sigma_n\, c\xi_n(s\phi\, s\theta\, c\psi - c\phi\, s\psi) - s\sigma_n\, s\xi_n(-s\phi\, c\theta)\Big]\Big\} \\
&+M_L\Big\{\ell\sum_{i=1}^{N}\ddot{\sigma}_i\left[c\sigma_i(c\theta\, s\psi) + s\sigma_i\, c\xi_i(c\theta\, c\psi) - s\sigma_i\, s\xi_i(s\theta)\right] \\
&+\left[R_{km}(\ddot{\psi}s\phi\, c\theta)\right]\Big\}\Big\{\ell\Big[c\sigma_n(c\theta\, s\psi) + s\sigma_n\, c\xi_n(c\theta\, c\psi) - s\sigma_n\, s\xi_n(s\theta)\Big]\Big\} \\
&+M_V\Big\{\ell\sum_{i=1}^{N}\ddot{\sigma}_i\left[c\sigma_i(-c\phi\, s\theta\, s\psi + s\phi\, c\psi) + s\sigma_i\, c\xi_i(-c\phi\, s\theta\, c\psi - s\phi\, s\psi)\right. \\
&\left.-s\sigma_i\, s\xi_i(c\phi\, c\theta)\right] + \left[-R_{jm}(\ddot{\psi}s\phi\, c\theta)\right]\Big\}\Big\{\ell\Big[c\sigma_n(-c\phi\, s\theta\, s\psi + s\phi\, c\psi) \\
&+s\sigma_n\, c\xi_n(-c\phi\, s\theta\, c\psi - s\phi\, s\psi) - s\sigma_n\, s\xi_n(c\phi\, c\theta)\Big]\Big\} = F_{\sigma_n}
\end{aligned}
\tag{81}
$$

In Equations (79), (80), and (81), there are several trignometric combinations of the balloon angles ψ, θ, ϕ. These terms are the elements of a matrix (Equation (51)) given in Appendix A of the Second Scientific Report*. The matrix (ϵ_{ij}) gives the relation between the balloon unit vectors and the inertia frame.

$$\epsilon_{ij} = \begin{bmatrix} s\phi\, s\theta\, s\psi + c\phi\, c\psi & s\phi\, s\theta\, c\psi - c\phi\, s\psi & -s\phi\, c\theta \\ c\theta\, s\psi & c\theta\, c\psi & s\theta \\ -c\phi\, s\theta\, s\psi + s\phi\, c\psi & -c\phi\, s\theta\, c\psi - s\phi\, s\psi & c\phi\, c\theta \end{bmatrix} \tag{82}$$

The balloon yaw Equation (79) is rewritten as:

$$\begin{aligned}
&M_S \Big\{ \ell \sum_{i=1}^{N} \ddot{\sigma}_i \left[c\sigma_i\, \epsilon_{11} + s\sigma_i\, c\xi_i\, \epsilon_{12} - s\sigma_i\, s\xi_i\, \epsilon_{13} \right] \Big] \left[-R_{jm}\, \epsilon_{33} + R_{km}\, \epsilon_{23} \right] \\
&+ M_L \Big\{ \ell \sum_{i=1}^{N} \ddot{\sigma}_i \left[c\sigma_i\, \epsilon_{21} + s\sigma_i\, c\xi_i\, \epsilon_{22} - s\sigma_i\, s\xi_i\, \epsilon_{23} \right] \Big] \left[-R_{km}\, \epsilon_{13} \right] \\
&+ M_V \Big\{ \ell \sum_{i=1}^{N} \ddot{\sigma}_i \left[c\sigma_i\, \epsilon_{31} + s\sigma_i\, c\xi_i\, \epsilon_{32} - s\sigma_i\, s\xi_i\, \epsilon_{33} \right] \Big] \left[R_{jm}\, \epsilon_{13} \right] \\
&+ \ddot{\psi} \Big\{ \left[-R_{jm}\, \epsilon_{33} + R_{km}\, \epsilon_{23} \right]^2 M_S + \left[-R_{km}\, \epsilon_{13} \right]^2 M_L + \left[R_{jm}\, \epsilon_{13} \right]^2 M_V \\
&+ c^2\theta \left[I_{xB}\, s^2\phi + I_{zB}\, c^2\phi \right] + s^2\theta\, I_{yB} - s2\theta\, c\phi\, I_{yzB} \Big\} \\
&+ \ddot{\phi} \Big\{ -R_{km} \left[-R_{jm}\, \epsilon_{33} + R_{km}\, \epsilon_{23} \right] M_S - I_{yB}\, s\theta + I_{yzB}\, c\theta\, c\phi \Big\} = F_\psi
\end{aligned} \tag{83}$$

The balloon roll Equation (80) is rewritten as:

*Reference 2

$$M_S\left\{\ell\sum_{i=1}^{N}\ddot{\sigma}_i\left[c\sigma_i\,\epsilon_{11}+s\sigma_i\,c\xi_i\,\epsilon_{12}-s\sigma_i\,s\xi_i\,\epsilon_{13}\right]\left[-R_{km}\right]\right\}$$

$$+\ddot{\psi}\left\{\left[-R_{jm}\,\epsilon_{33}+R_{km}\,\epsilon_{23}\right]\left[-R_{km}\right]M_S-I_{YB}\,s\theta+I_{YZB}\,c\theta c\phi\right\}$$

$$+\ddot{\phi}\left\{M_S\left[R_{km}\right]^2+I_{YB}\right\}=F_\phi \tag{84}$$

The tether yaw Equation (81) is rewritten as:

$$\sum_{n=n+1}^{N}m\ell^2\left\{\sum_{i=1}^{n-1}\ddot{\sigma}_i\left[c\sigma_i\,c\sigma_n+s\sigma_i\,s\sigma_n\,c(\xi_n-\xi_i)\right]+\frac{1}{2}\ddot{\sigma}_n\left[c\sigma_n\,c\sigma_n+s\sigma_n\,s\sigma_n\,c(\xi_n-\xi_n)\right]\right\}$$

$$+\frac{m}{2}\ell^2\sum_{i=1}^{n-1}\ddot{\sigma}_i\left[c\sigma_i\,c\sigma_n+s\sigma_i\,s\sigma_n\,c(\xi_n-\xi_i)\right]+\frac{m}{3}\ell^2\ddot{\sigma}_n$$

$$+m_{PL}\ell^2\sum_{i=1}^{N}\ddot{\sigma}_i\left[c\sigma_i\,c\sigma_n+s\sigma_i\,s\sigma_n\,c(\xi_n-\xi_i)\right]$$

$$+M_S\left\{\ell^2\sum_{i=1}^{N}\ddot{\sigma}_i\left[c\sigma_i\,\epsilon_{11}+s\sigma_i\,c\xi_i\,\epsilon_{12}-s\sigma_i\,s\xi_i\,\epsilon_{13}\right]\left[c\sigma_n\,\epsilon_{11}+s\sigma_n\,c\xi_n\,\epsilon_{12}-s\sigma_n\,s\xi_n\,\epsilon_{13}\right]\right\}$$

$$+M_L\left\{\ell^2\sum_{i=1}^{N}\ddot{\sigma}_i\left[c\sigma_i\,\epsilon_{21}+s\sigma_i\,c\xi_i\,\epsilon_{22}-s\sigma_i\,s\xi_i\,\epsilon_{23}\right]\left[c\sigma_n\,\epsilon_{21}+s\sigma_n\,c\xi_n\,\epsilon_{22}-s\sigma_n\,s\xi_n\,\epsilon_{23}\right]\right\}$$

$$+M_V\left\{\ell^2\sum_{i=1}^{N}\ddot{\sigma}_i\left[c\sigma_i\,\epsilon_{31}+s\sigma_i\,c\xi_i\,\epsilon_{32}-s\sigma_i\,s\xi_i\,\epsilon_{33}\right]\left[c\sigma_n\,\epsilon_{31}+s\sigma_n\,c\xi_n\,\epsilon_{32}-s\sigma_n\,s\xi_n\,\epsilon_{33}\right]\right\}$$

$$+\ddot{\psi}\left\{\ell M_S\left[-R_{jm}\,\epsilon_{33}+R_{km}\,\epsilon_{13}\right]\left[c\sigma_n\,\epsilon_{11}+s\sigma_n\,c\xi_n\,\epsilon_{12}-s\sigma_n\,s\xi_n\,\epsilon_{13}\right]\right.$$

$$+\ell M_L\left[-R_{km}\,\epsilon_{13}\right]\left[c\sigma_n\,\epsilon_{21}+s\sigma_n\,c\xi_n\,\epsilon_{22}-s\sigma_n\,s\xi_n\,\epsilon_{23}\right]+\ell M_V\left[R_{jm}\,\epsilon_{13}\right]\left[c\sigma_n\,\epsilon_{31}\right.$$

$$\left.\left.+s\sigma_n\,c\xi_n\,\epsilon_{32}-s\sigma_n\,s\xi_n\,\epsilon_{33}\right]\right\}+\ddot{\phi}\left\{\ell M_S\left[-R_{km}\right]\left[c\sigma_n\,\epsilon_{11}+s\sigma_n\,c\xi_n\,\epsilon_{12}-s\sigma_n\,s\xi_n\,\epsilon_{13}\right]\right\}=F_{\sigma_n} \tag{85}$$

In order to solve Equations (83), (84), and (85), assume N = 3. The balloon yaw equation is:

$$
\begin{aligned}
&\ell\{M_s[c\sigma_1 \epsilon_{11} + s\sigma_1 c\beta_1 \epsilon_{12} - s\sigma_1 s\beta_1 \epsilon_{13}][-R_{jm}\epsilon_{33} + R_{km}\epsilon_{23}] \\
&+ M_L[c\sigma_1 \epsilon_{21} + s\sigma_1 c\beta_1 \epsilon_{22} - s\sigma_1 s\beta_1 \epsilon_{23}][-R_{km}\epsilon_{13}] \\
&+ M_v[c\sigma_1 \epsilon_{31} + s\sigma_1 c\beta_1 \epsilon_{32} - s\sigma_1 s\beta_1 \epsilon_{33}][R_{jm}\epsilon_{13}]\}\ddot{\sigma}_1 \\
&+ \ell\{M_s[c\sigma_2 \epsilon_{11} + s\sigma_2 c\beta_2 \epsilon_{12} - s\sigma_2 s\beta_2 \epsilon_{13}][-R_{jm}\epsilon_{33} + R_{km}\epsilon_{23}] \\
&+ M_L[c\sigma_2 \epsilon_{21} + s\sigma_2 c\beta_2 \epsilon_{22} - s\sigma_2 s\beta_2 \epsilon_{23}][-R_{km}\epsilon_{13}] \\
&+ M_v[c\sigma_2 \epsilon_{31} + s\sigma_2 c\beta_2 \epsilon_{32} - s\sigma_2 s\beta_2 \epsilon_{33}][R_{jm}\epsilon_{13}]\}\ddot{\sigma}_2 \\
&+ \ell\{M_s[c\sigma_3 \epsilon_{11} + s\sigma_3 c\beta_3 \epsilon_{12} - s\sigma_3 s\beta_3 \epsilon_{13}][-R_{jm}\epsilon_{33} + R_{km}\epsilon_{23}] \\
&+ M_L[c\sigma_3 \epsilon_{21} + s\sigma_3 c\beta_3 \epsilon_{22} - s\sigma_3 s\beta_3 \epsilon_{23}][-R_{km}\epsilon_{13}] \\
&+ M_v[c\sigma_3 \epsilon_{31} + s\sigma_3 c\beta_3 \epsilon_{32} - s\sigma_3 s\beta_3 \epsilon_{33}][R_{jm}\epsilon_{13}]\}\ddot{\sigma}_3 \\
&+ \{M_s[-R_{jm}\epsilon_{33} + R_{km}\epsilon_{23}]^2 + M_L[-R_{km}\epsilon_{13}]^2 + M_v[R_{jm}\epsilon_{13}]^2 \\
&+ c^2\theta[I_{xB}s^2\phi + I_{zB}c^2\phi] + s^2\theta I_{yB} - s2\theta\, c\phi\, I_{yzB}\}\ddot{\psi} \\
&+ \{M_s[-R_{jm}\epsilon_{33} + R_{km}\epsilon_{23}][-R_{km}] - I_{yB}s\theta + I_{yzB}\, c\theta\, c\phi\}\ddot{\phi} = F_v
\end{aligned}
\tag{86}
$$

The balloon roll equation is:

$$\ell\{M_s[c\sigma_1\epsilon_{11}+s\sigma_1 c\beta_1\epsilon_{12}-s\sigma_1 s\beta_1\epsilon_{13}][-R_{km}]\}\ddot{\sigma}_1$$

$$+\ell\{M_s[c\sigma_2\epsilon_{11}+s\sigma_2 c\beta_2\epsilon_{12}-s\sigma_2 s\beta_2\epsilon_{13}][-R_{km}]\}\ddot{\sigma}_2$$

$$+\ell\{M_s[c\sigma_3\epsilon_{11}+s\sigma_3 c\beta_3\epsilon_{12}-s\sigma_3 s\beta_3\epsilon_{13}][-R_{km}]\}\ddot{\sigma}_3$$

$$+\{M_s[-R_{jm}\epsilon_{33}+R_{km}\epsilon_{33}][-R_{km}]-I_{yB}s\theta+I_{yzB}c\theta c\phi\}\ddot{\psi}$$

$$+\{M_s[R_{km}]^2+I_{yB}\}\ddot{\phi}=F_\phi \tag{87}$$

From Equation (85), three equations will be generated (one for each link) by assuming r = 1, r = 2, r = 3 consecutively.

For r = 1,

$$\ell^2\{\tfrac{7m}{3}+m_{PL}+M_s[c\sigma_1\epsilon_{11}+s\sigma_1 c\beta_1\epsilon_{12}-s\sigma_1 s\beta_1\epsilon_{13}]^2$$

$$+M_L[c\sigma_1\epsilon_{21}+s\sigma_1 c\beta_1\epsilon_{22}-s\sigma_1 s\beta_1\epsilon_{23}]^2+M_V[c\sigma_1\epsilon_{31}+s\sigma_1 c\beta_1\epsilon_{32}-s\sigma_1 s\beta_1\epsilon_{33}]^2\}\ddot{\sigma}_1$$

$$+\ell^2\{[c\sigma_2 c\sigma_1+s\sigma_2 s\sigma_1 c(\beta_1-\beta_2)][\tfrac{3m}{2}+m_{PL}]$$

$$+M_s[c\sigma_2\epsilon_{11}+s\sigma_2 c\beta_2\epsilon_{12}-s\sigma_2 s\beta_2\epsilon_{13}][c\sigma_1\epsilon_{11}+s\sigma_1 c\beta_1\epsilon_{12}-s\sigma_1 s\beta_1\epsilon_{13}]$$

$$+M_L[c\sigma_2\epsilon_{21}+s\sigma_2 c\beta_2\epsilon_{22}-s\sigma_2 s\beta_2\epsilon_{23}][c\sigma_1\epsilon_{21}+s\sigma_1 c\beta_1\epsilon_{22}-s\sigma_1 s\beta_1\epsilon_{23}]$$

$$+M_v[c\sigma_2\,\epsilon_{31}+s\sigma_2\,c\varphi_2\,\epsilon_{32}-s\sigma_2\,s\varphi_2\,\epsilon_{33}][c\sigma_1\,\epsilon_{31}+s\sigma_1\,c\varphi_1\,\epsilon_{32}-s\sigma_1\,s\varphi_1\,\epsilon_{33}]\}\ddot{\sigma}_2$$

$$+\ell^2\{[c\sigma_3\,c\sigma_1+s\sigma_3\,s\sigma_1\,c(\varphi_1-\varphi_3)][\tfrac{m}{2}+m_{pl}]$$

$$+M_s[c\sigma_3\,\epsilon_{11}+s\sigma_3\,c\varphi_3\,\epsilon_{12}-s\sigma_3\,s\varphi_3\,\epsilon_{13}][c\sigma_1\,\epsilon_{11}+s\sigma_1\,c\varphi_1\,\epsilon_{12}-s\sigma_1\,s\varphi_1\,\epsilon_{13}]$$

$$+M_L[c\sigma_3\,\epsilon_{21}+s\sigma_3\,c\varphi_3\,\epsilon_{22}-s\sigma_3\,s\varphi_3\,\epsilon_{23}][c\sigma_1\,\epsilon_{21}+s\sigma_1\,c\varphi_1\,\epsilon_{22}-s\sigma_1\,s\varphi_1\,\epsilon_{23}]$$

$$+M_v[c\sigma_3\,\epsilon_{31}+s\sigma_3\,c\varphi_3\,\epsilon_{32}-s\sigma_3\,s\varphi_3\,\epsilon_{33}][c\sigma_1\,\epsilon_{31}+s\sigma_1\,c\varphi_1\,\epsilon_{32}-s\sigma_1\,s\varphi_1\,\epsilon_{33}]\}\ddot{\sigma}_3$$

$$+\ell\{M_s[-R_{jm}\,\epsilon_{33}+R_{km}\,\epsilon_{23}][c\sigma_1\,\epsilon_{11}+s\sigma_1\,c\varphi_1\,\epsilon_{12}-s\sigma_1\,s\varphi_1\,\epsilon_{13}]$$

$$+M_L[-R_{km}\,\epsilon_{13}][c\sigma_1\,\epsilon_{21}+s\sigma_1\,c\varphi_1\,\epsilon_{22}-s\sigma_1\,s\varphi_1\,\epsilon_{23}]$$

$$+M_v[R_{jm}\,\epsilon_{13}][c\sigma_1\,\epsilon_{31}+s\sigma_1\,c\varphi_1\,\epsilon_{32}-s\sigma_1\,s\varphi_1\,\epsilon_{33}]\}\ddot{\psi}$$

$$+\ell\{M_s[-R_{km}][c\sigma_1\,\epsilon_{11}+s\sigma_1\,c\varphi_1\,\epsilon_{12}-s\sigma_1\,s\varphi_1\,\epsilon_{13}]\}\ddot{\phi}=F_{\sigma_1} \tag{88}$$

For r = 2,

$$\ell^2\{[c\sigma_1\,c\sigma_2+s\sigma_1\,s\sigma_2\,c(\varphi_2-\varphi_1)][\tfrac{3m}{2}+m_{pl}]$$

$$+M_s[c\sigma_1\,\epsilon_{11}+s\sigma_1\,c\varphi_1\,\epsilon_{12}-s\sigma_1\,s\varphi_1\,\epsilon_{13}][c\sigma_2\,\epsilon_{11}+s\sigma_2\,c\varphi_2\,\epsilon_{12}-s\sigma_2\,s\varphi_2\,\epsilon_{13}]$$

$$+M_L\left[c\sigma_1 \epsilon_{21} + s\sigma_1 c\beta_1 \epsilon_{22} - s\sigma_1 s\beta_1 \epsilon_{23}\right]\left[c\sigma_2 \epsilon_{21} + s\sigma_2 c\beta_2 \epsilon_{22} - s\sigma_2 s\beta_2 \epsilon_{23}\right]$$

$$+M_V\left[c\sigma_1 \epsilon_{31} + s\sigma_1 c\beta_1 \epsilon_{32} - s\sigma_1 s\beta_1 \epsilon_{33}\right]\left[c\sigma_2 \epsilon_{31} + s\sigma_2 c\beta_2 \epsilon_{32} - s\sigma_2 s\beta_2 \epsilon_{33}\right]\Big\}\ddot{\sigma}_1$$

$$+\ell^2\Big\{\frac{4m}{3} + m_{p_2} + M_S\left[c\sigma_2 \epsilon_{11} + s\sigma_2 c\beta_2 \epsilon_{12} - s\sigma_2 s\beta_2 \epsilon_{13}\right]^2$$

$$+M_L\left[c\sigma_2 \epsilon_{21} + s\sigma_2 c\beta_2 \epsilon_{22} - s\sigma_2 s\beta_2 \epsilon_{23}\right]^2 + M_V\left[c\sigma_2 \epsilon_{31} + s\sigma_2 c\beta_2 \epsilon_{32} - s\sigma_2 s\beta_2 \epsilon_{33}\right]^2\Big\}\ddot{\sigma}_2$$

$$+\ell^2\Big\{\left[c\sigma_3 c\sigma_2 + s\sigma_3 s\sigma_2 c(\beta_2 - \beta_3)\right]\left[\frac{m}{2} + m_{p_2}\right]$$

$$+M_S\left[c\sigma_3 \epsilon_{11} + s\sigma_3 c\beta_3 \epsilon_{12} - s\sigma_3 s\beta_3 \epsilon_{13}\right]\left[c\sigma_2 \epsilon_{11} + s\sigma_2 c\beta_2 \epsilon_{12} - s\sigma_2 s\beta_2 \epsilon_{13}\right]$$

$$+M_L\left[c\sigma_3 \epsilon_{21} + s\sigma_3 c\beta_3 \epsilon_{22} - s\sigma_3 s\beta_3 \epsilon_{23}\right]\left[c\sigma_2 \epsilon_{21} + s\sigma_2 c\beta_2 \epsilon_{22} - s\sigma_2 s\beta_2 \epsilon_{23}\right]$$

$$+M_V\left[c\sigma_3 \epsilon_{31} + s\sigma_3 c\beta_3 \epsilon_{32} - s\sigma_3 s\beta_3 \epsilon_{33}\right]\left[c\sigma_2 \epsilon_{31} + s\sigma_2 c\beta_2 \epsilon_{32} - s\sigma_2 s\beta_2 \epsilon_{33}\right]\Big\}\ddot{\sigma}_3$$

$$+\ell\Big\{M_S\left[-R_{jm} \epsilon_{33} + R_{km} \epsilon_{23}\right]\left[c\sigma_2 \epsilon_{11} + s\sigma_2 c\beta_2 \epsilon_{12} - s\sigma_2 s\beta_2 \epsilon_{13}\right]$$

$$+M_L\left[-R_{km} \epsilon_{13}\right]\left[c\sigma_2 \epsilon_{21} + s\sigma_2 c\beta_2 \epsilon_{22} - s\sigma_2 s\beta_2 \epsilon_{23}\right]$$

$$+M_V\left[R_{jm} \epsilon_{13}\right]\left[c\sigma_2 \epsilon_{31} + s\sigma_2 c\beta_2 \epsilon_{32} - s\sigma_2 s\beta_2 \epsilon_{33}\right]\Big\}\ddot{\psi}$$

$$+\ell\Big\{M_S\left[-R_{km}\right]\left[c\sigma_2 \epsilon_{11} + s\sigma_2 c\beta_2 \epsilon_{12} - s\sigma_2 s\beta_2 \epsilon_{13}\right]\Big\}\ddot{\phi} = F_{\sigma_2} \tag{89}$$

For r = 3,

$$\ell^2\{[c\sigma_1 c\sigma_3 + s\sigma_1 s\sigma_3 c(\varphi_3-\varphi_1)][\tfrac{m}{2}+m_{pl}]$$

$$+M_s[c\sigma_1\epsilon_{11}+s\sigma_1 c\varphi_1\epsilon_{12}-s\sigma_1 s\varphi_1\epsilon_{13}][c\sigma_3\epsilon_{11}+s\sigma_3 c\varphi_3\epsilon_{12}-s\sigma_3 s\varphi_3\epsilon_{13}]$$

$$+M_L[c\sigma_1\epsilon_{21}+s\sigma_1 c\varphi_1\epsilon_{22}-s\sigma_1 s\varphi_1\epsilon_{23}][c\sigma_3\epsilon_{21}+s\sigma_3 c\varphi_3\epsilon_{22}-s\sigma_3 s\varphi_3\epsilon_{23}]$$

$$+M_V[c\sigma_1\epsilon_{31}+s\sigma_1 c\varphi_1\epsilon_{32}-s\sigma_1 s\varphi_1\epsilon_{33}][c\sigma_3\epsilon_{31}+s\sigma_3 c\varphi_3\epsilon_{32}-s\sigma_3 s\varphi_3\epsilon_{33}]\}\ddot{\sigma}_1$$

$$+\ell^2\{[c\sigma_2 c\sigma_3 + s\sigma_2 s\sigma_3 c(\varphi_3-\varphi_2)][\tfrac{m}{2}+m_{pl}]$$

$$+M_s[c\sigma_2\epsilon_{11}+s\sigma_2 c\varphi_2\epsilon_{12}-s\sigma_2 s\varphi_2\epsilon_{13}][c\sigma_3\epsilon_{11}+s\sigma_3 c\varphi_3\epsilon_{12}-s\sigma_3 s\varphi_3\epsilon_{13}]$$

$$+M_L[c\sigma_2\epsilon_{21}+s\sigma_2 c\varphi_2\epsilon_{22}-s\sigma_2 s\varphi_2\epsilon_{23}][c\sigma_3\epsilon_{21}+s\sigma_3 c\varphi_3\epsilon_{22}-s\sigma_3 s\varphi_3\epsilon_{23}]$$

$$+M_V[c\sigma_2\epsilon_{31}+s\sigma_2 c\varphi_2\epsilon_{32}-s\sigma_2 s\varphi_2\epsilon_{33}][c\sigma_3\epsilon_{31}+s\sigma_3 c\varphi_3\epsilon_{32}-s\sigma_3 s\varphi_3\epsilon_{33}]\}\ddot{\sigma}_2$$

$$+\ell^2\{\tfrac{m}{3}+m_{pl}+M_s[c\sigma_3\epsilon_{11}+s\sigma_3 c\varphi_3\epsilon_{12}-s\sigma_3 s\varphi_3\epsilon_{13}]^2$$

$$+M_L[c\sigma_3\epsilon_{21}+s\sigma_3 c\varphi_3\epsilon_{22}-s\sigma_3 s\varphi_3\epsilon_{23}]^2+M_V[c\sigma_3\epsilon_{31}+s\sigma_3 c\varphi_3\epsilon_{32}-s\sigma_3 s\varphi_3\epsilon_{33}]^2\}\ddot{\sigma}_3$$

$$+\ell\{M_s[-R_{jm}\epsilon_{33}+R_{km}\epsilon_{23}][c\sigma_3\epsilon_{11}+s\sigma_3 c\varphi_3\epsilon_{12}-s\sigma_3 s\varphi_3\epsilon_{13}]$$

$$+M_L[-R_{km}\epsilon_{13}][c\sigma_3\epsilon_{21}+s\sigma_3 c\varphi_3\epsilon_{22}-s\sigma_3 s\varphi_3\epsilon_{23}]$$

$$+M_v\left[R_{jm}\epsilon_{13}\right]\left[c\sigma_3\epsilon_{31}+s\sigma_3\, c\beta_3\,\epsilon_{32}-s\sigma_3\, s\beta_3\,\epsilon_{33}\right]\Big\}\ddot{\psi}$$

$$+\ell\Big\{M_s\left[-R_{km}\right]\left[c\sigma_3\,\epsilon_{11}+s\sigma_3\, c\beta_3\,\epsilon_{12}-s\sigma_3\, s\beta_3\,\epsilon_{13}\right]\Big\}\ddot{\phi} = F_{\sigma_3} \tag{90}$$

The generalized forces (F_ψ, F_ϕ, F_{σ_1}, F_{σ_2}, F_{σ_3}) were derived in Section V, Appendix A of the Second Scientific Report*. The following equations are taken from that section.

$$F_\psi = F_{BSA}\left[(-R_{jA}\epsilon_{33}+R_{kA}\epsilon_{23})\epsilon_{11}+(R_{kA}\epsilon_{13})\epsilon_{21}+(R_{jA}\epsilon_{13})\epsilon_{31}\right]+M_{\psi B} \tag{91}$$

$$F_\phi = \left[W_B R_{kg}-L_S R_{kB}\right]\epsilon_{13}+\left[-F_{BSA}R_{kA}\right]\epsilon_{11}+M_{\phi B} \tag{92}$$

$$F_{\sigma_1} = \ell\Big\{\left[L_S-W_B-\left(m_{PL}+\tfrac{S_m}{2}\right)g\right]\left[-s\sigma_1\, s\beta_1\right]+\left[F_{BSA}\right]\left[c\sigma_1\right]$$

$$+\left[D_{CS1}\right]\left[C_1\, c^2\sigma_1\right]+\left[D_{CS2}\right]\left[c^2\sigma_2\left(c\sigma_2\, c\sigma_1+s\sigma_2\, s\sigma_1\, c(\beta_1-\beta_2)\right)\right]$$

$$+\left[D_{CS3}\right]\left[c^2\sigma_3\left(c\sigma_3\, c\sigma_1+s\sigma_3\, s\sigma_1\, c(\beta_1-\beta_3)\right)\right]\Big\} \tag{93}$$

$$F_{\sigma_2} = \ell\Big\{\left[L_S-W_B-\left(m_{PL}+\tfrac{3m}{2}\right)g\right]\left[-s\sigma_2\, s\beta_2\right]+\left[F_{BSA}\right]\left[c\sigma_2\right]$$

$$+\left[D_{CS2}\right]\left[C_2\, c^2\sigma_2\right]+\left[D_{CS3}\right]\left[c^2\sigma_3\left(c\sigma_3\, c\sigma_2+s\sigma_3\, s\sigma_2\, c(\beta_2-\beta_3)\right)\right]\Big\} \tag{94}$$

$$F_{\sigma_3} = \ell\Big\{\left[L_S-W_B-\left(m_{PL}+\tfrac{m}{2}\right)g\right]\left[-s\sigma_3\, s\beta_3\right]+\left[F_{BSA}\right]\left[c\sigma_3\right]+\left[D_{CS3}\right]\left[C_3\, c^2\sigma_3\right] \tag{95}$$

The aerodynamic forces and moments are:

$$F_{BSA} = q_B S_B\left[C_{YB}+C_{Y\dot{\psi}B}\left(\frac{d_B}{V_{BE}}\right)\dot{\psi}+C_{Y\dot{\phi}B}\left(\frac{d_B}{V_{BE}}\right)\dot{\phi}\right] \tag{96}$$

*Reference 2

$$M_{\psi B} = q_B S_B d_B \left[C_{mB} + C_{m\dot{\psi}B}\left(\frac{d_B}{V_{BR}}\right)\dot{\psi} + C_{m\dot{\phi}B}\left(\frac{d_B}{V_{BR}}\right)\dot{\phi} \right] \tag{97}$$

$$M_{\phi B} = q_B S_B d_B \left[C_{\ell B} + C_{\ell\dot{\psi}B}\left(\frac{d_B}{V_{BR}}\right)\dot{\psi} + C_{\ell\dot{\phi}B}\left(\frac{d_B}{V_{BR}}\right)\dot{\phi} \right] \tag{98}$$

$$D_{csi} = -\frac{1}{2}\rho_{ci} S_{ci} C_{Dc} V_{ci} \dot{X}_{ci} \tag{99}$$

$$q_B = \frac{1}{2}\rho_B V_{BR}^2 \tag{100}$$

$$V_{BR}^2 = (\dot{x}_B - V_{gs})^2 + (\dot{y}_B + V_w)^2 + (\dot{z}_B - V_{gv})^2 \tag{101}$$

$$\Gamma_B = \tan^{-1}(\dot{x}_{BR}/\dot{y}_{BR}) \tag{102}$$

$$\beta = \Gamma_B - \psi \tag{103}$$

$$C_n = \frac{1}{3}\left(\frac{g_{nn} + 2g_{nn+1}}{g_{nn} + g_{nn+1}}\right) \tag{104}$$

As in the longitudinal dynamics, it is desirable to know the tension in the tether. This is done by summing forces at each hinge point. First consider the apparent inertia forces acting on the balloon along and normal to the centerline.

$$a_{xB} = M_S\left[\ddot{x}_B \epsilon_{11} + \ddot{y}_B \epsilon_{12} + \ddot{z}_B \epsilon_{13}\right] \tag{105}$$

$$a_{yB} = M_L\left[\ddot{x}_B \epsilon_{21} + \ddot{y}_B \epsilon_{22} + \ddot{z}_B \epsilon_{23}\right] \tag{106}$$

$$a_{zB} = M_V\left[\ddot{x}_B \epsilon_{31} + \ddot{y}_B \epsilon_{32} + \ddot{z}_B \epsilon_{33}\right] \tag{107}$$

In Equations (105), (106), and (107), $\ddot{X}_B$, $\ddot{Y}_B$ and $\ddot{Z}_B$ are inertia accelerations of the balloon: a_{XB}, a_{YB}, and a_{ZB} are inertia forces in the positive direction of the balloon's lateral, longitudinal, and vertical axes. ϵ_{ij} are elements of the matrix defined in Equation (82). Summing the apparent inertia forces in the lateral, longitudinal, and vertical directions gives:

$$\sum F_x = \epsilon_{11} a_{XB} + \epsilon_{21} a_{YB} + \epsilon_{31} a_{ZB} \tag{108}$$

$$\sum F_y = \epsilon_{12} a_{XB} + \epsilon_{22} a_{YB} + \epsilon_{32} a_{ZB} \tag{109}$$

$$\sum F_z = \epsilon_{13} a_{XB} + \epsilon_{23} a_{YB} + \epsilon_{33} a_{ZB} \tag{110}$$

The forces acting on the balloon above the payload are:

$$\sum F_x = F_{BSA} - T_{BS} \tag{111}$$

$$\sum F_y = T_{BH} - F_{BHA} \tag{112}$$

$$\sum F_z = L_S - W_B + F_{BVA} - T_{BV} \tag{113}$$

Now equate Equations (108), (109), and (110) with Equations (111), (112), and (113) respectively, and the following expressions for T_{BS}, T_{BH}, and T_{BV} are found.

$$T_{BS} = F_{BSA} - (\epsilon_{11} a_{XB} + \epsilon_{21} a_{YB} + \epsilon_{31} a_{ZB}) \tag{114}$$

$$T_{BH} = F_{BHA} + (\epsilon_{11} a_{xB} + \epsilon_{22} a_{yB} + \epsilon_{32} a_{zB}) \tag{115}$$

$$T_{BV} = F_{BVA} + L_S - W_B - (\epsilon_{13} a_{xB} + \epsilon_{23} a_{yB} + \epsilon_{33} a_{zB}) \tag{116}$$

If forces are summed at the payload location, the components of tension at the top of the tether results.

$$F_{CSN} = F_{BSA} - (\epsilon_{11} a_{xB} + \epsilon_{21} a_{yB} + \epsilon_{31} a_{zB}) - m_{PL} \ddot{x}_{PL} \tag{117}$$

$$F_{CHN} = F_{BHA} + (\epsilon_{12} a_{xB} + \epsilon_{22} a_{yB} + \epsilon_{32} a_{zB}) + m_{PL} \ddot{y}_{PL} \tag{118}$$

$$F_{CVN} = F_{BVA} + L_S - W_B - (\epsilon_{13} a_{xB} + \epsilon_{23} a_{yB} + \epsilon_{33} a_{zB}) - m_{PL} g - m_{PL} \ddot{z}_{PL} \tag{119}$$

The vertical and horizontal forces on the "N"th link are the same as they were in the longitudinal dynamics program. The force in the lateral direction is given in Equation (99). In general for the "r"th link.

$$F_{CS,r-1} = F_{CS,r} - D_{CS,r} - m \ddot{x}_{cr} \tag{120}$$

$$F_{CH,r-1} = F_{CH,r} + F_{CN_r} S \xi_r + m \ddot{y}_{cr} \tag{121}$$

$$F_{CV,r-1} = F_{CV_r} - F_{CN_r} C \xi_r - mg - m \ddot{z}_{cr} \tag{122}$$

$$T_{r-1} = \sqrt{(F_{CS,r-1})^2 + (F_{CH,r-1})^2 + (F_{CV,r-1})^2} \tag{123}$$

The tension at the winch is found by setting r = 1.

APPENDIX B

DYNAMIC RESPONSE INPUT AND OUTPUT DATA

LONGITUDINAL AND LATERAL DYNAMIC SIMULATIONS

CASES 1 THROUGH 40

SECTION I

INTRODUCTION

Appendix B consists of the input data used in making the computer run cases 1 through 40, and computer constructed plots of selected output variables for these cases.

Table B-1 lists input data for the longitudinal dynamic cases 1 through 23, and Table B-II lists the input data for the lateral dynamic cases 24 through 40. Tables B-III and B-IV list the balloon longitudinal and lateral static aerodynamic coefficients respectively.

Computer constructed plots (3 plots per case are included on each page) for cases 1 through 40 follow Table B-IV. The parameters plotted with respect to time are listed below.

<u>Longitudinal Cases 1 through 23</u>

Balloon pitch angle Link 3 pitch angle Link 2 pitch angle Link 1 pitch angle	Plot 1
Tension at bridle Tension at winch Balloon altitude Balloon range	Plot 2
Wind gust velocity Pitching velocity of balloon Wind angle of attack Relative velocity of balloon	Plot 3

<u>Lateral Cases 24 through 40</u>

Balloon roll angle Balloon yaw angle Balloon yaw rate Balloon sideslip angle	Plot 1
Balloon lateral displacement Link 3 yaw angle Link 2 yaw angle Link 1 yaw angle	Plot 2
Wind gust velocity Relative velocity of Balloon Tension at bridle Tension at winch	Plot 3

Table B-1. Input Data for Longitudinal Cases

Run No.	Balloon Type	Altitude Feet	Tether Type	Tail Config.	Volume Ft^3	Wind Profile	WB Lb	LS Lb	MPL Slugs	WTC Lb	IXB Slug-Ft^2	MAL Slugs	MAV Slugs	FF	$SB=V^{2/3}$ Ft^2	$DB=V^{1/3}$ Ft^2	CDC	DC Ft	Teth Ft	CMTDB Rad^{-1}	CLTDB Rad^{-1}
1	BJ	10,000	Nolard	Nominal	60K	100%	2157	3942	31.06	708	116,000	15.7	110.0	0	1533	39.15	1.1	0.0342	12,639	-2 01	1.68
2																					
3																					
4 *																					
5																					
6																					
7		10,000			60K		2157	3942	31.06	708	116,000	15 7	110.0		1533	39.15	1 1	0.0342	12,639		
8		5,000			46K		1627	3526	46.58	183	75,000	12.0	86.0		1284	35.83		0.0268	5,692		
9		20,000	Nolard		500K		15624	23715	18.63	8900	3,204,000	95.0	666.0		6300	79.37		0.0828	27,436		
10.		10,000	Amgal	Nominal	75K		2665	4928	31.06	1128	167,000	20.0	138.0		1778	42.17		0.0208	11,305	-2.01	1.68
11			Nolard	81%	60K		1970	3811		708	104,100	14.7	103.0		1533	39.15		0 0342	12,639	-1.58	1.25
12				144%		100%	2680	4340			142,000	18.8	131.0							-2.61	2.14
13		10,000		Nominal		40%	2157	3942		708	116,000	15.7	110.0						12,639	-2.01	1.68
14		4,000				100%	2877	4720		234	142,000	31.7	222.0						4,170		
15		1,000					3358	5190		54.0	159,400	35.5	249.0						970		
16 (Payload on Underside)		10,000					3157	942		708	171,300	15.7	110 0						12,639		
17 (Winch at 5000 Feet)	BJ				60K		2157	3942		314	116,000	15.7	110.0		1533	39.15		0 0342	5,600	-2.01	1.68
18	Vee				80K		2334	4822		1260	166,300	47.0	189.0		1856.7	43.09		0.0488	11,060	-2.483	2.495
19																					
20	Vee						2334	4822		1260	166,300	47.0	189 0					0.0488	11,060	-2.483	2.495
21	GAC						2788	5016		1015	249,400	14.7	169.4					0 0433	11,274	-2.07	1.49
22																					
23	GAC	10,000	Nolard	Nominal	80K	100%	2788	5016	31.06	1015	249,400	14.7	169 4	0	1856.7	43.09	1.1	0.0433	11,274	-2.07	1 49

* Case 4A is identical to Case 4 except gust is applied vertically up in Case 4A rather than horizontally aft

Table B-I. (Continued)

Run No.	RJM Ft	RKM Ft	RJA Ft	RKA Ft	RJG Ft	RKG Ft	RJB Ft	RKB Ft	THE DEG DEG	XIDEG (1) DEG	XIDEG (2) DEG	XIDEG (3) DEG	THEDDE DEG	XIDDEG (I) I= 1, 2, 3 DEG	DT1 Sec	DT2 Sec	DTP1	DTP2	TDTC Sec	TTT Sec	T Sec
1	19.6	-44.6	6.7	-46.0	23.7	-42.3	12.6	-45.4	8.5030	41.6466	51.5297	65.4682	0.0	0.0	.5	1.	1.	5.	60.	180.	0.0
2																					
3																					
4																					
5																					
6	21.4	-44.6	8.5	-46.0	25.5	-42.3	14.4	-45.4	6.4289	36.9724	48.2677	64.0386			.5	1.	1.	5.	60.	180.	
7	17.9	-44.6	5.0	-46.0	22.0	-42.3	10.9	-45.4	10.4826	45.0979	53.9550	66.5133									
8	16.9	-41.1	4.9	-42.1	21.7	-39.2	10.3	-41.5	5.2536	55.3565	60.0976	66.8154									
9	45.6	-89.7	19.9	-93.3	51.4	-84.7	31.9	-92.0	8.4342	30.0426	48.4859	67.6940									
10	20.7	-48.4	6.8	-49.6	25.1	-45.6	13.2	-48.9	8.3106	53.9520	62.2320	70.9677									
11	19.5	-44.6	8.9	-46.0	23.8	-42.5	13.4	-45.6	10.9832	41.6977	51.1670	64.5175									
12	21.5	-44.4	4.5	-46.0	25.4	-42.0	13.3	-44.9	7.3693	43.4984	53.1029	66.6907									
13	19.6	-44.6	6.7	-46.0	23.7	-42.3	12.6	-45.4	2.9646	57.3521	71.4708	81.0848									
14	21.4	-44.2	6.7	-46.0	23.8	-41.4	12.6	-45.4	8.7908	69.8457	72.2866	75.5869									
15	20.9	-44.1	6.7	-46.0	22.5	-41.5	12.6	-45.4	7.3067	83.2441	83.6630	84.1377			.25	.5	2.	10.			
16 (Payload on Underside)	20.7	-38.0	9.7	-46.0	21.3	-28.9	15.6	-45.4	8.5076	41.6310	51.5191	65.4645			.5	.1	1.	5.			
17 (Winch at 5000 Feet)	19.6	-44.6	6.7	-46.0	23.7	-42.3	12.6	-45.4	8.5103	56.4410	62.6544	69.4930									
18	21.3	-37.5	9.4	-38.6	17.0	-34.5	11.7	-38.5	6.9577	58.5433	64.1700	71.7230									
19	24.2	-37.5	12.3	-38.6	19.9	-34.5	14.6	-38.5	4.9941	52.7234	59.9523	69.3939									
20	18.6	-37.5	6.7	-38.6	14.3	-34.5	9.0	-38.5	9.1072	62.8254	67.3040	73.4503									
21	18.3	-56.6	-.5	-57.5	18.4	-54.7	4.7	-57.5	7.9176	53.9442	62.0587	72.9344									
22	22.5	-56.6	3.7	-57.5	22.6	-54.7	8.7	-57.5	5.9761	49.0389	58.4903	70.9483									
23	14.6	-56.6	-4.2	-57.5	14.7	-54.7	.8	-57.5	10.0287	58.0898	65.0961	74.6215									

Table B-I. (Continued)

	Time (seconds)						Velocity (feet per second)					
Run No.	TTG (1)	TTG (2)	TTG (3)	TTG (4)	TTG (5)	TTG (6)	VVG (1)	VVG (2)	VVG (3)	VVG (4)	VVG (5)	VVG (6)
1	0.0	4.99	5.0	1000.			0.0	0.0	20.2	20.2		
2				7.0	7.01	1000.					0.0	0.0
3				15.0	15.01							
4				25.0	25.01							
5												
6				15.0	15.01	1000.			20.2	20.2	0.0	0.0
7												
8									15.7	15.7		
9									27.3	27.3		
10									20.2	20.2		
11												
12												
13									8.0	8.0		
14									13.6	13.6		
15									7.1	7.1		
16									20.2	20.2		
17												
18												
19												
20												
21												
22												
23												

Table B-II. Input Data for Lateral Cases

Run. No.	Balloon Type	Altitude FT	Tether Type	Tail Conf	Volume Ft^3	Wind Profile	WB Lb	LS Lb	MPL Slugs	WTC Lb	IZB Slugs-Ft^2	IYB Slugs-Ft^2	IYZB Slugs Ft^2	IXB Slugs Ft^2
24	BJ	10,000	Nolard	Nominal	60K	100%	2157.	3942.	31.06	708.	119,000.	26,000.	12,500.	116,000.
25														
26														
27														
28														
29		5,000			46K		1627.	3526.	46.58	183.	75,300.	17,000	8,200	75,000.
30		20,000			500K		15624.	23715.	18.63	8900.	3,374,000.	771,000	296,000	3,204,000.
31		10,000	Amgal		75K		2665.	4928	31.06	1128.	172,000.	40,000	18,000	167,000.
32			Nolard	81%	60K		1970.	3811.		708.	106,400.	17,600	10,200	104,100
33				144%			2680.	4340.			145,000.	53,900	18,600	142,000
34				Nominal		40%	2157.	3942.		602.	119,000.	26,000	12,500	116,000
35		4,000				100%	2877.	4740.	31.06	234.	146,800.	35,800	13,400	142,400
36		1,000					3358.	5190.		54.0	164,700.	39,300	14,500	159,400
37	VEE	10,000			80K		2334.	4822.		1260.	173,300.	84,000	3,900	166,300
38				200%			2408.	4832.			187,000.	86,200	7,500	167,900
39				300%			2476.	4842.			198,700.	88,300	10,700	170,000
40	GAC			Nominal			2788.	5016.		1015.	228,800.	106,500	10,500	249,400

Table B-II. (Continued)

Run No.	THEODE DEG	X±0 DEG (1) DEG	XIO DEG (2) DEG	XIO DEG (3) DEG	RJM	RKM	RJA	RKA	RJG	RKG	RJB	RKB
24	8.5030	41.6466	51.5297	65.4682	20.5	-42.6	6.7	-46.0	23.7	-42.3	12.6	-45.4
25	↓	↓	↓	↓	↓	↓	↓	↓	↓	↓	↓	↓
26	↓	↓	↓	↓	↓	↓	↓	↓	↓	↓	↓	↓
27	↓	↓	↓	↓	↓	↓	↓	↓	↓	↓	↓	↓
28	↓	↓	↓	↓	↓	↓	↓	↓	↓	↓	↓	↓
29	5.2536	55.3565	60.0976	66.8153	17.8	-39.1	4.9	-42.1	21.7	-39.2	10.3	-41.5
30	8.4342	30.0426	48.4859	67.6940	47.2	-85.8	19.9	-93.3	51.4	-84.7	31.9	-92.0
31	8.3106	53.9520	62.2320	70.9677	21.7	-45.9	6.8	-49.6	25.1	-45.6	13.2	-48.9
32	10.9832	41.6977	51.1670	64.5175	18.3	-43.2	8.9	-46.0	23.8	-42.5	13.4	-45.6
33	7.3693	43.4984	53.1029	66.6907	24.7	-41.3	4.5	-46.0	25.4	-42.0	13.3	-44.9
34	2.9646	57.3521	71.4708	81.0848	20.5	-42.6	6.7	-46.0	23.7	-42.3	12.6	-45.4
35	8.7908	69.8457	72.2866	75.5869	22.3	-42.2	6.7	-46.0	23.8	-41.4	12.6	-45.4
36	7.3067	83.2441	83.6630	84.1377	21.8	-42.2	6.7	-46.0	22.5	-41.5	12.6	-45.4
37	6.9577	58.5433	64.1700	71.7230	13.7	-36.7	9.4	-38.6	17.0	-34.5	11.7	-38.5
38	7.2273	58.8436	64.3656	71.7906	13.8	-36.0	9.4	-38.6	17.5	-34.3	11.7	-38.5
39	7.5040	59.1800	64.5910	71.8802	14.0	-35.4	9.4	-38.6	18.1	-33.9	11.7	-38.5
40	7.9176	53.9442	62.0587	72.9344	16.2	-55.0	-.5	-57.5	18.4	-54.7	4.7	-57.5

Table B-II. (Continued)

Run No.	SB= $V^{2/3}$ FT^2	DB= $V^{1/3}$ FT	CDC	DC FT	TETH FT	MAL Slugs	MAV Slugs	MAS Slugs	CYPSDB rad^{-1}	CYPHDB rad^{-1}	CNPSDB rad^{-1}	CNPHDB rad^{-1}	CLPSDB rad^{-1}	CLPHDB rad^{-1}	DT1 Sec	DT2 Sec	DTP1	DTP2	TDTC Sec	TTT Sec	T Sec
24	1533	39.15	1.1	.0342	12639.	15.7	110.0	115.0	1.79	.142	-2.31	-.122	-.347	-.327	.5	1.	1.	5.	30.	300.	0.
25																			60.		
26																					
27																					
28																					
29	1284.	35.83		.0268	5692.	12.0	86.0	86.0											30.		
30	6300.	79.37		.0828	27436.	95.0	666.0	690.0											30.		
31	1778.	42.17		.0208	11305.	20.0	138.0	143.0											60.		
32	1533	39.15		.0342	12639.	14.7	103.0	107.0	1.55	.104	-2.08	-.096	-.280	-.210					30.		
33						18.8	131.0	140.0	2.27	.224	-2.67	-.170	-.484	-.609							
34					10740.	15.7	110.0	115.0	1.79	.142	-2.31	-.122	-.347	-.327							
35					4170.	31.7	222.0	227.0											60.	720.	
36					970.	35.5	249.0	255.0							.25	.25	2.	20	120.	360.	
37	1856.7	43.09		.0488	11060.	47.0	189.0	127.0	.439	.054	-.482	-.0505	-.0212	-.3758	.5	1.	1.	5.	30.		
38								135.0	.718	.108	-.784	-.1010	-.0494	-.3930							
39								143.0	.997	.162	-1.086	-.1615	-.0810	-.4120							
40				.0433	11274.	14.7	169.4	154.4	1.94	0.0	-2.07	0.0	-.298	-.508							

Table B-II. (Continued)

Run No.	Time (seconds) TT G (1)	TTG (2)	TTG (3)	TTG (4)	TTG (5)	TTG (6)	Velocity (Feet per second) VVG (1)	VVG (2)	VVG (3)	VVG (4)	VVG (5)	VVG (6)
24	0.0	5.0	6.0	1000.			0.0	0.0	12.0	12.0		
25			8.0									
26			10.0									
27									18.0	18.0		
28			5.01	15.0	15.01	1000.			12.0	12.0	0.0	0.0
29			8.0	1000.					9.0	9.0		
30									16.0	16.0		
31									12.0	12.0		
32												
33												
34									4.8	4.8		
35									8.0	8.0		
36									1.0	1.0		
37									12.0	12.0		
38												
39												
40												

TABLE B-III. LONGITUDINAL STATIC AERODYNAMIC COEFFICIENTS

Angle-Of-Attack		-5	0	5	10	12	15	20	25
BJ (Nominal)	C_m	.0137	.0103	-.0005	.0044	.0050	-.0075	-.0410	-.0780
	C_L	-.1100	.0063	.1368	.2514	.2991	.3710	.5100	.6200
	C_D	.1100	.0764	.0865	.1133	.1279	.1527	.2200	.3000
BJ (81% Tail)	C_m	-.0099	.0103	.0231	.0515	.0615	.0632	.0532	.0398
	C_L	-.0838	.0063	.1106	.1990	.2363	.2925	.4053	.4891
	C_D	.1094	.0764	.0857	.1103	.1236	.1460	.2077	.2814
BJ (144% Tail)	C_m	.0490	.0103	-.0358	-.0663	-.0798	-.1135	-.1824	-.2547
	C_L	-.1528	.0063	.1796	.3369	.4017	.4993	.6810	.8338
	C_D	.1115	.0764	.0883	.1198	.1372	.1672	.2464	.3402
VEE (Nominal)	C_m	-.010	.030	.103	.110	.113	.102	.090	.022
	C_L	-.400	0.0	.400	.800	.970	1.210	1.610	2.030
	C_D	.150	.160	.170	.230	.265	.340	.510	.740
GAC (Nominal)	C_m	.070	-.010	-.074	-.120	-.170	-.190	-.310	-.460
	C_L	-.240	0.0	.210	.380	.450	.560	.830	1.080
	C_D	.105	.085	.090	.100	.110	.140	.230	.390

TABLE B-IV. LATERAL STATIC AERODYNAMIC COEFFICIENTS

Sideslip Angle		-20	0	20
BJ (Nominal)	C_y	.7260	0.0	-.726
	C_m	-.0366	0.0	.0366
	C_l	-.1226	0.0	.1226
BJ (81% Tail)	C_y	.646	0.0	-.646
	C_m	.0279	0.0	-.0279
	C_l	.0907	0.0	-.0907
BJ (144% Tail)	C_y	.923	0.0	-.923
	C_m	-.174	0.0	.174
	C_l	-.193	0.0	.193
VEE (Nominal)	C_y	.299	0.0	-.299
	C_m	-.0014	0.0	.0014
	C_l	-.002	0.0	.002
VEE (200% Bottom Tail)	C_y	.502	0.0	-.502
	C_m	-.154	0.0	.154
	C_l	-.0471	0.0	.0741
VEE (300% Bottom Tail)	C_y	.706	0.0	-.706
	C_m	-.3065	0.0	.3065
	C_l	-.0768	0.0	.0768
GAC (Nominal)	C_y	.663	0.0	-.663
	C_m	-.0768	0.0	.0768
	C_l	-.1305	0.0	.1305

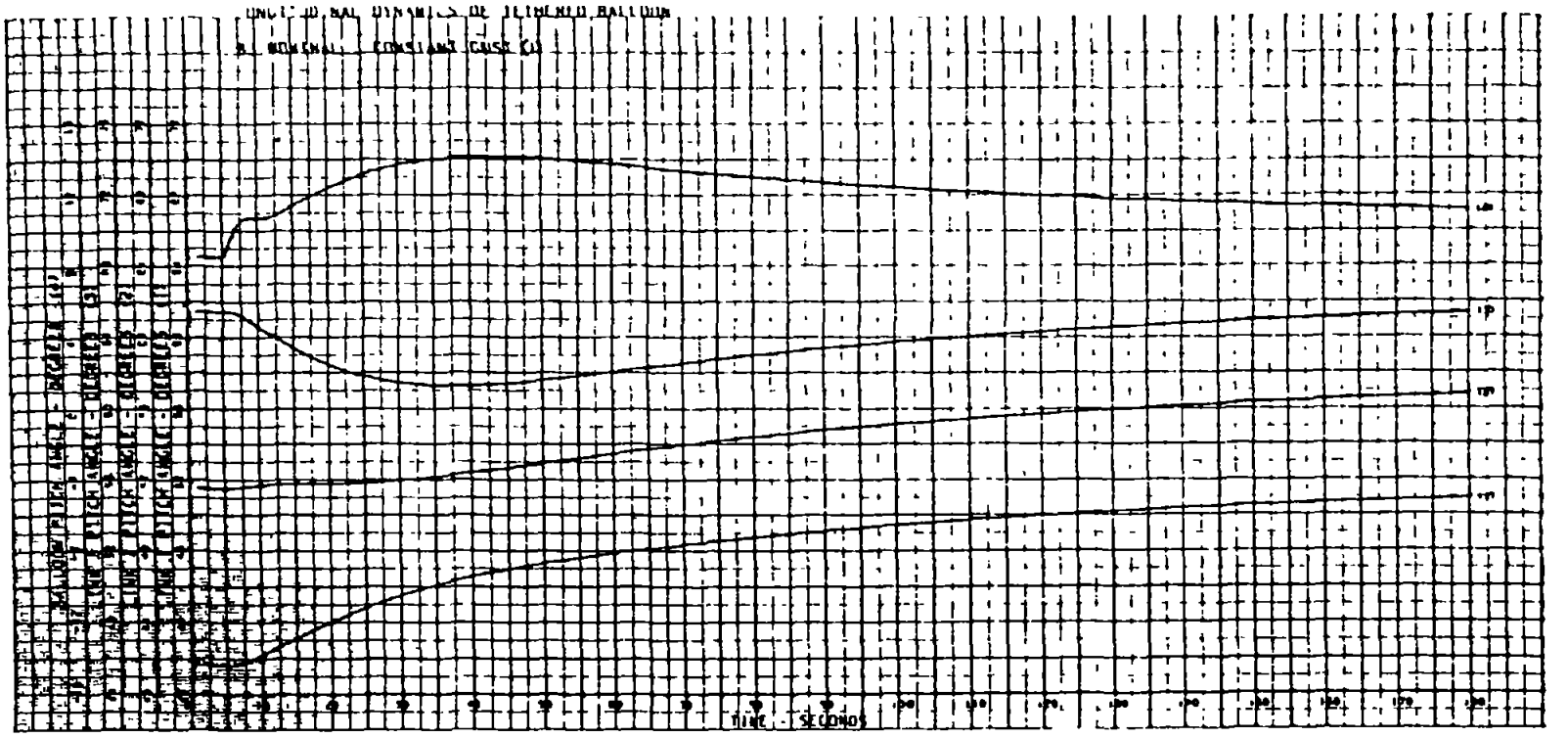
LONGITUDINAL DYNAMICS OF TETHERED BALLOON
TIME - SECONDS

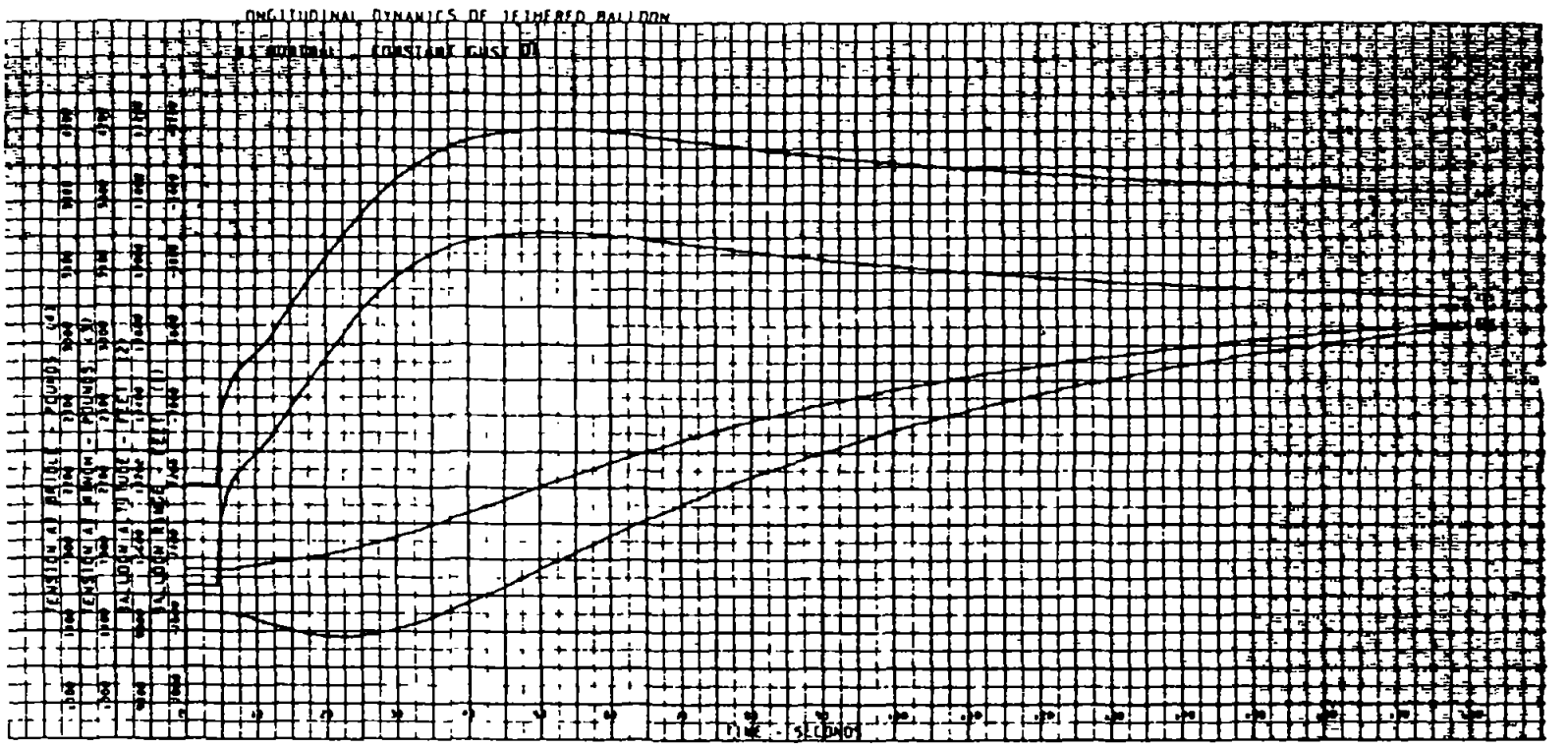
LONGITUDINAL DYNAMICS OF TETHERED BALLOON
TIME - SECONDS

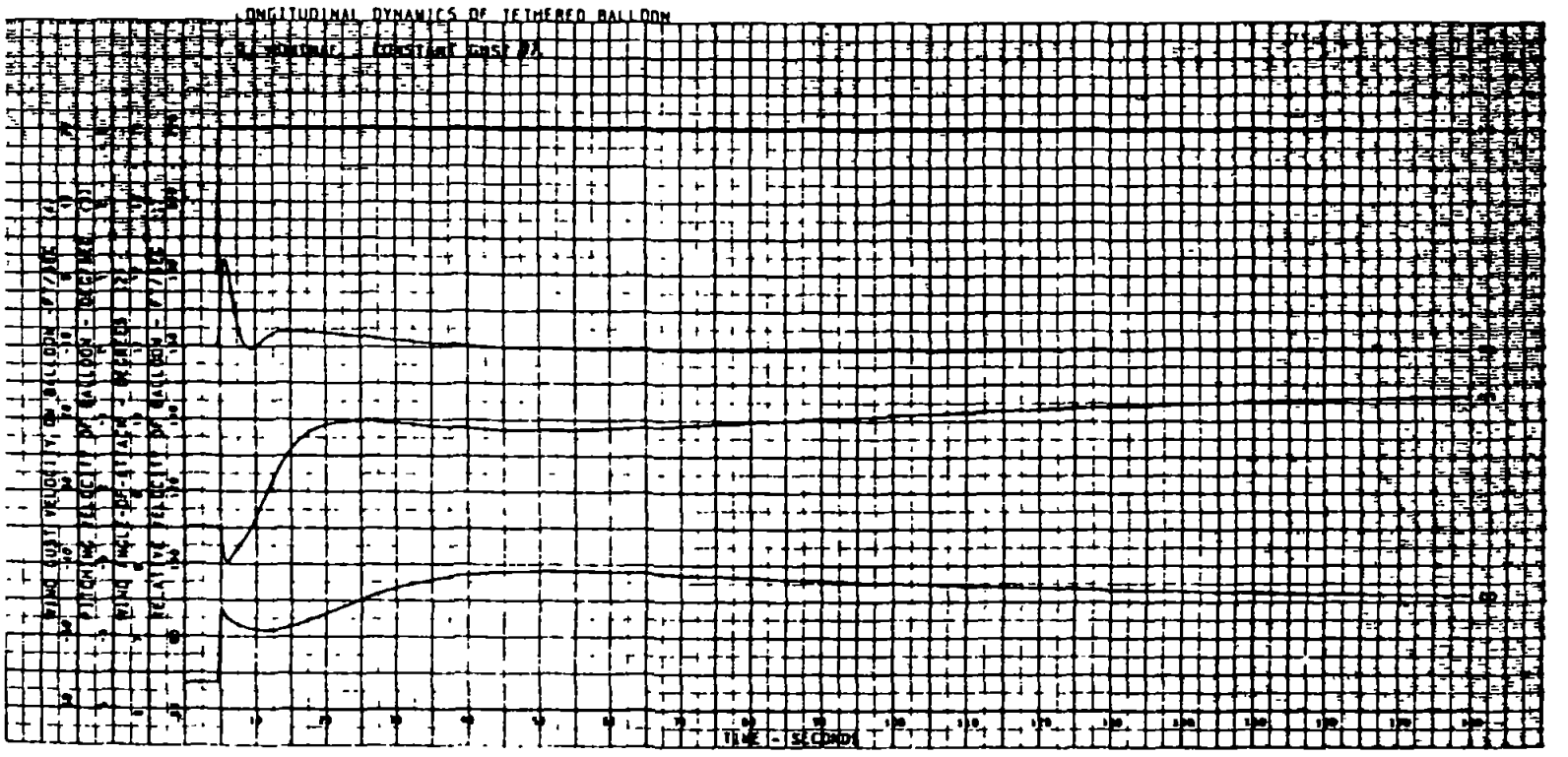
LONGITUDINAL DYNAMICS OF TETHERED BALLOON
TIME - SECONDS

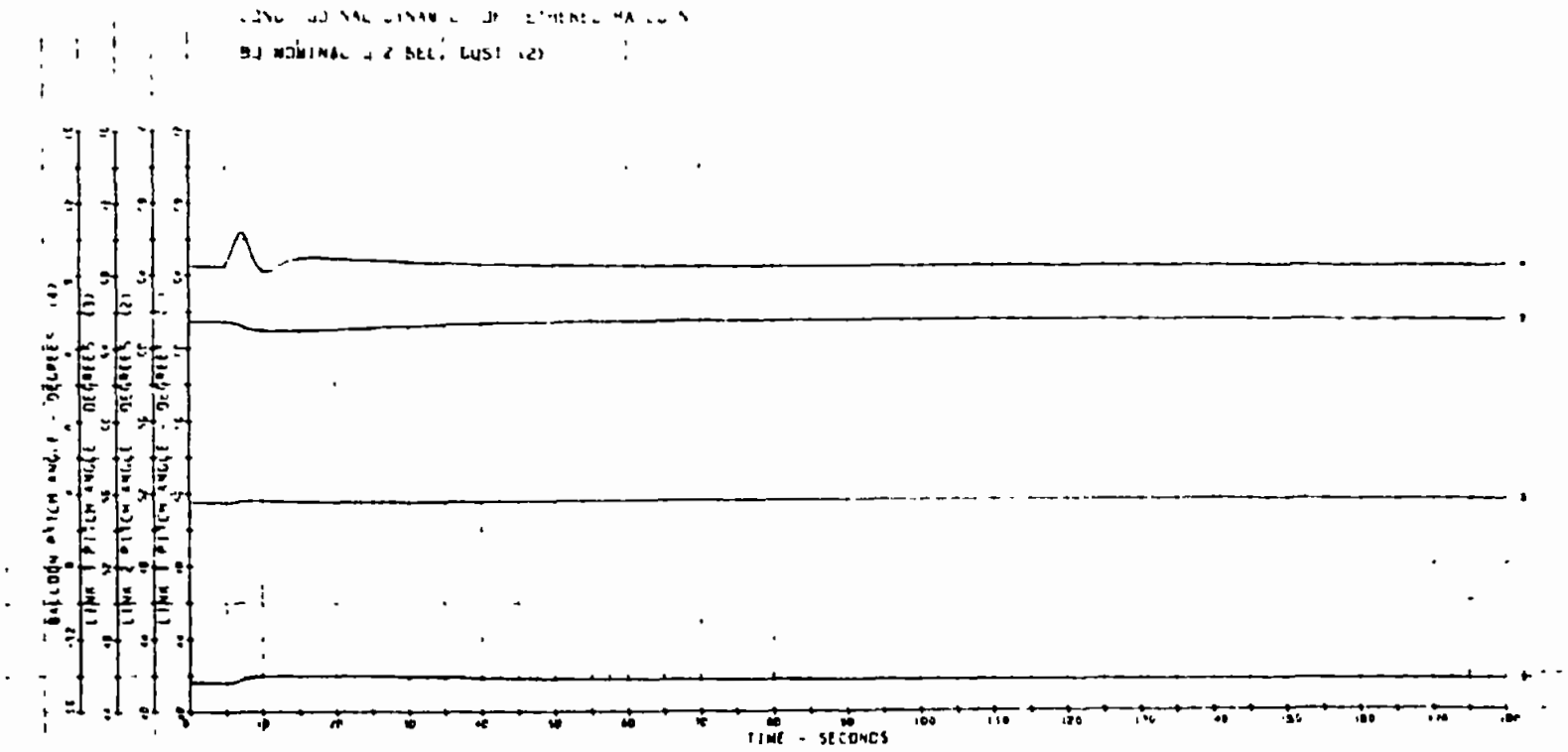
TIME - SECONDS

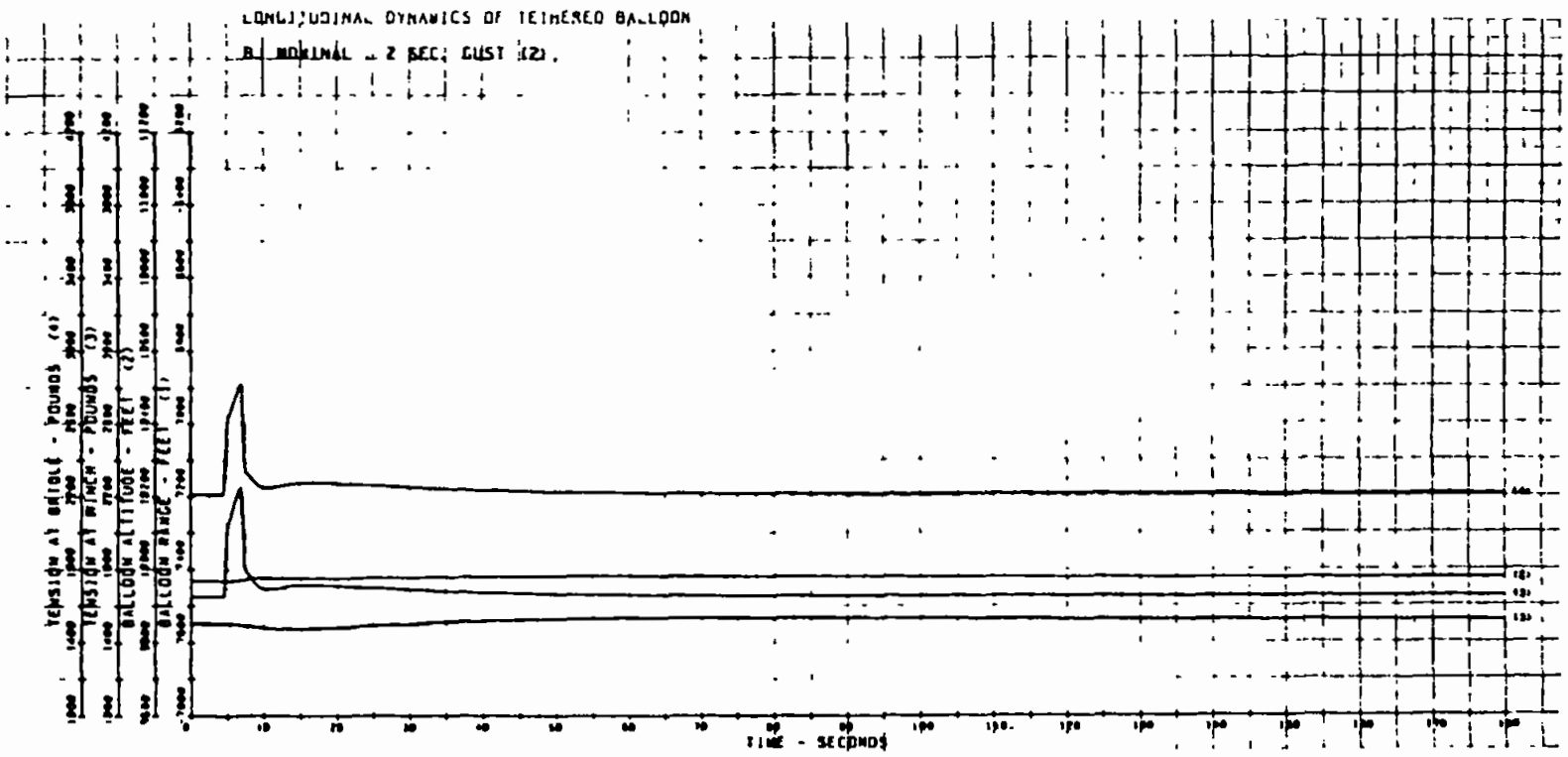
LONGITUDINAL DYNAMICS OF TETHERED BALLOON
TIME - SECONDS

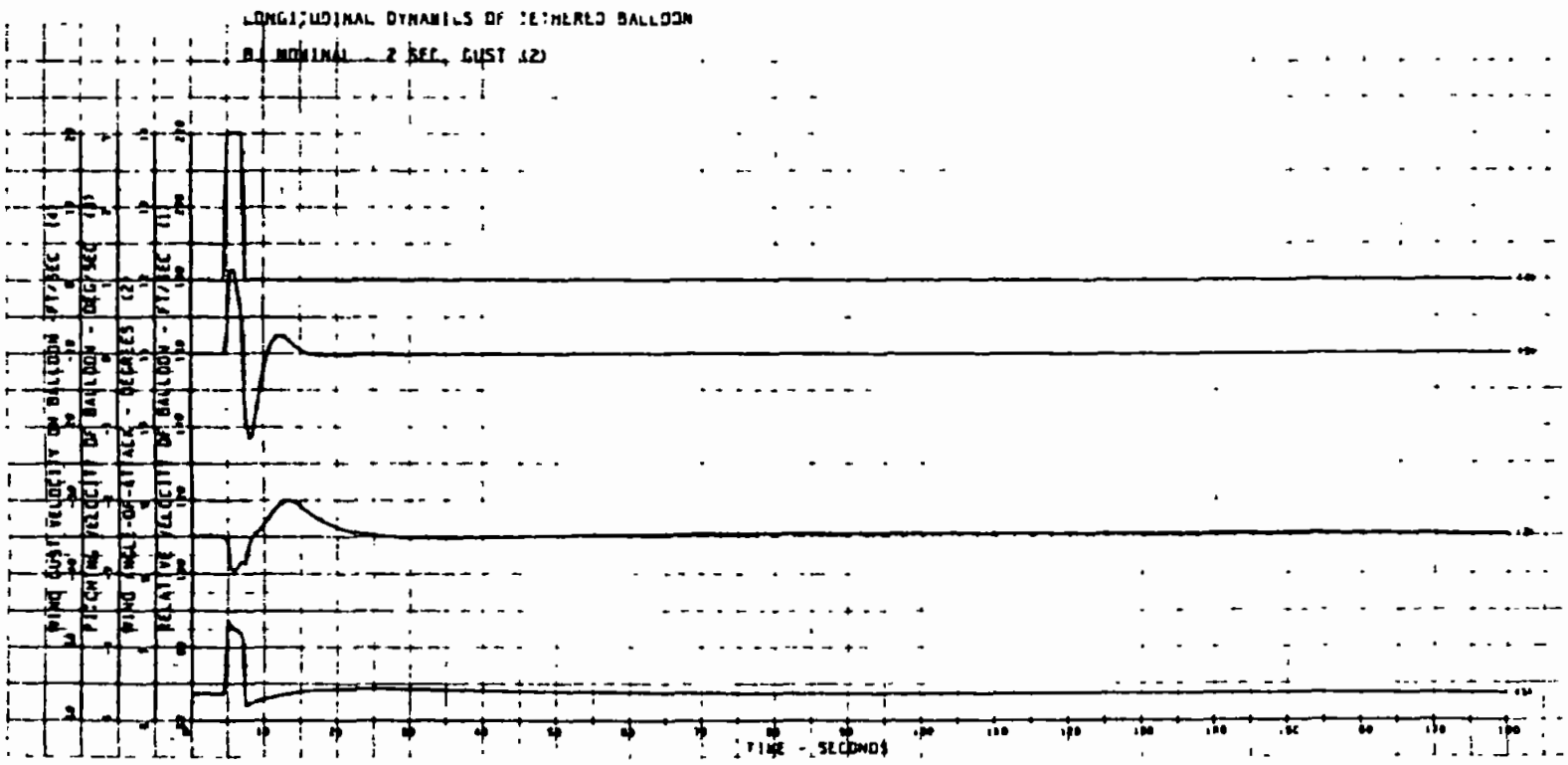
LONGITUDINAL DYNAMICS OF TETHERED BALLOON
TIME - SECONDS

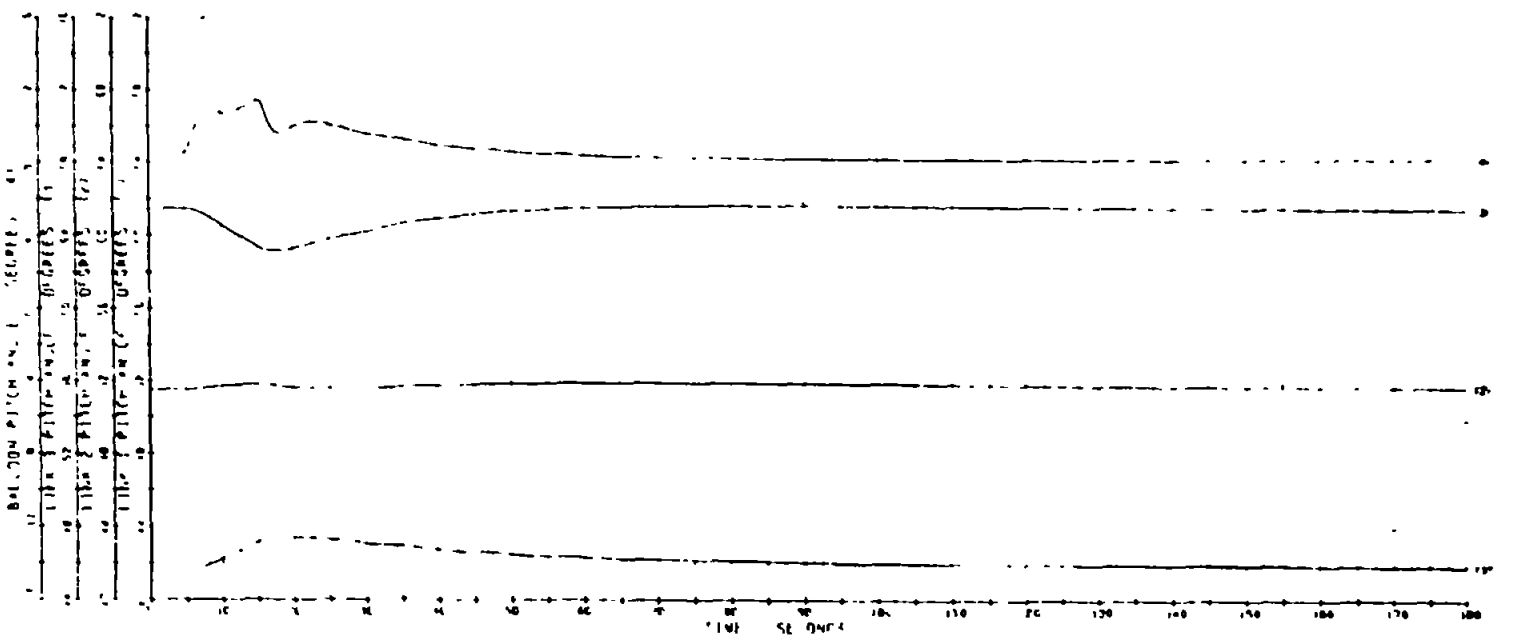

LONGITUDINAL DYNAMICS OF TETHERED BALLOON

BJ NOMINAL . 10 SEC. GUST (3)

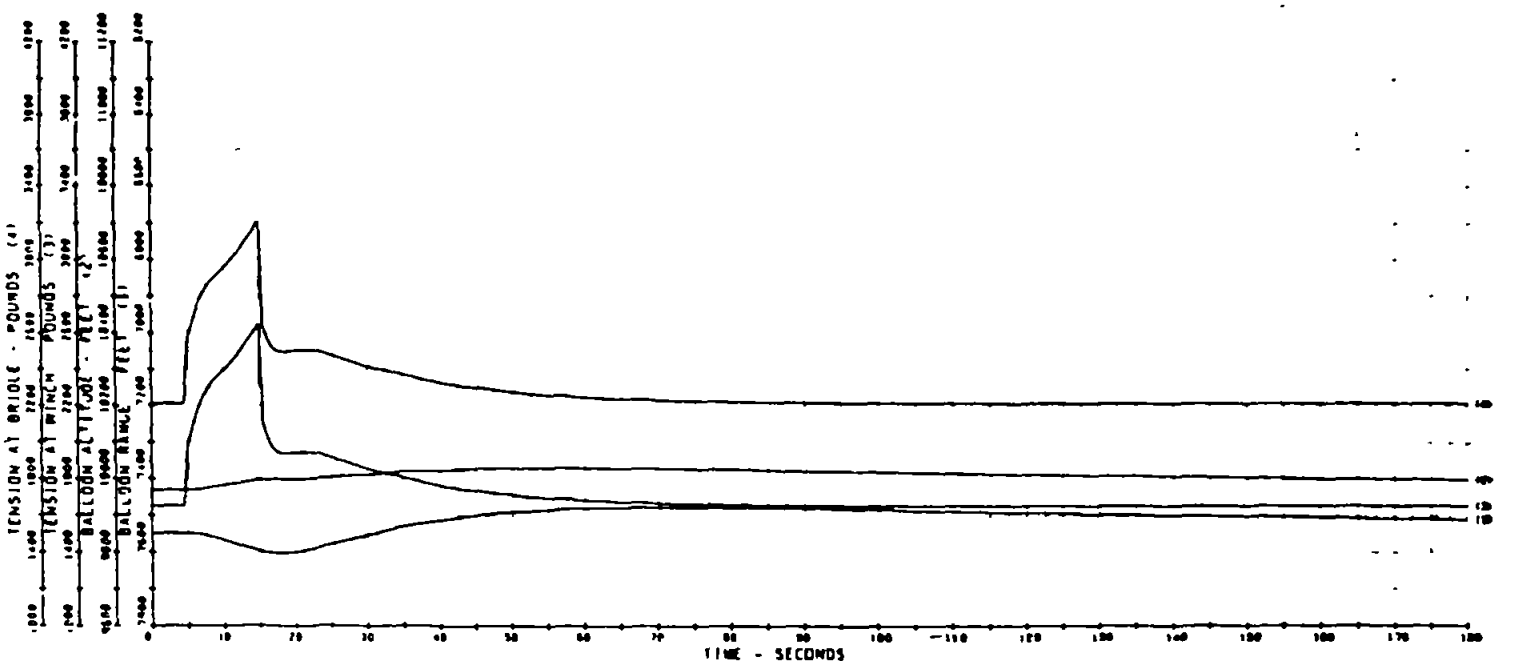

LONGITUDINAL DYNAMICS OF TETHERED BALLOON

BJ NOMINAL . 10 SEC. GUST (3)

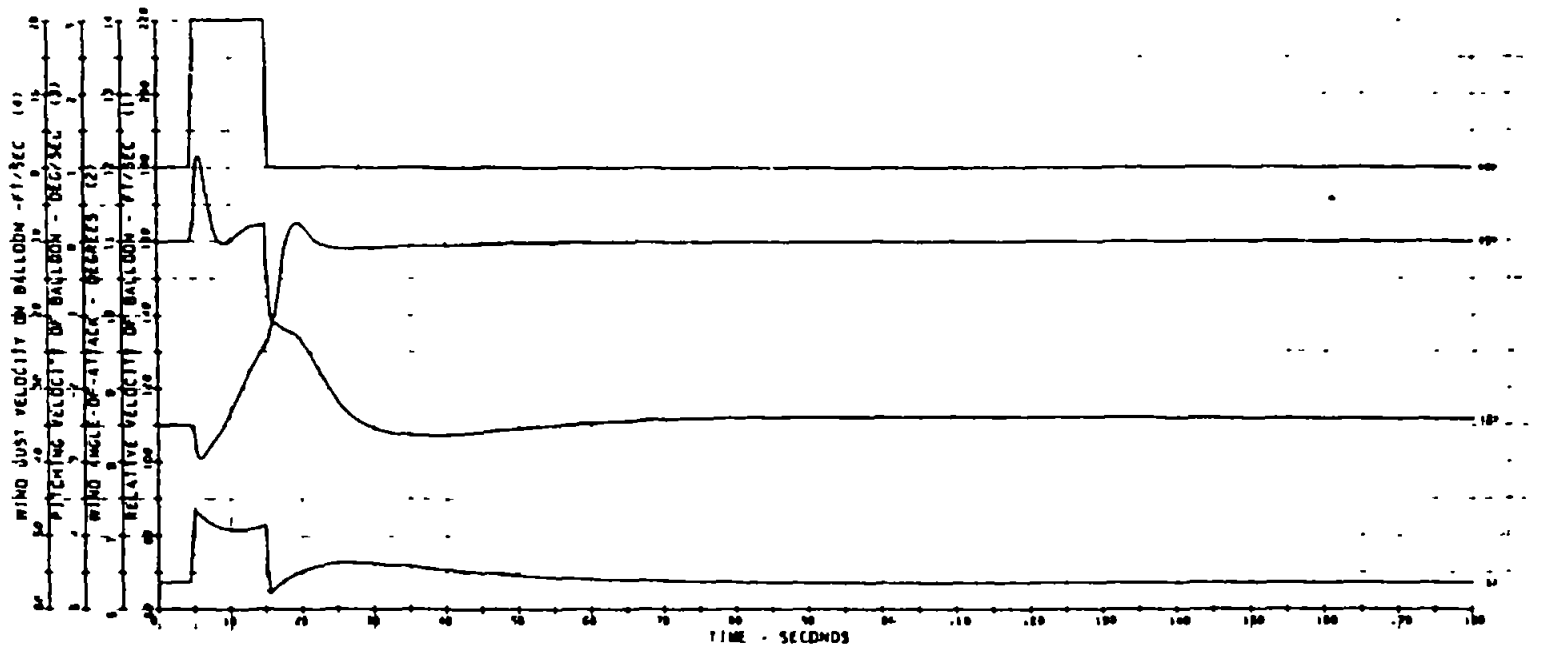

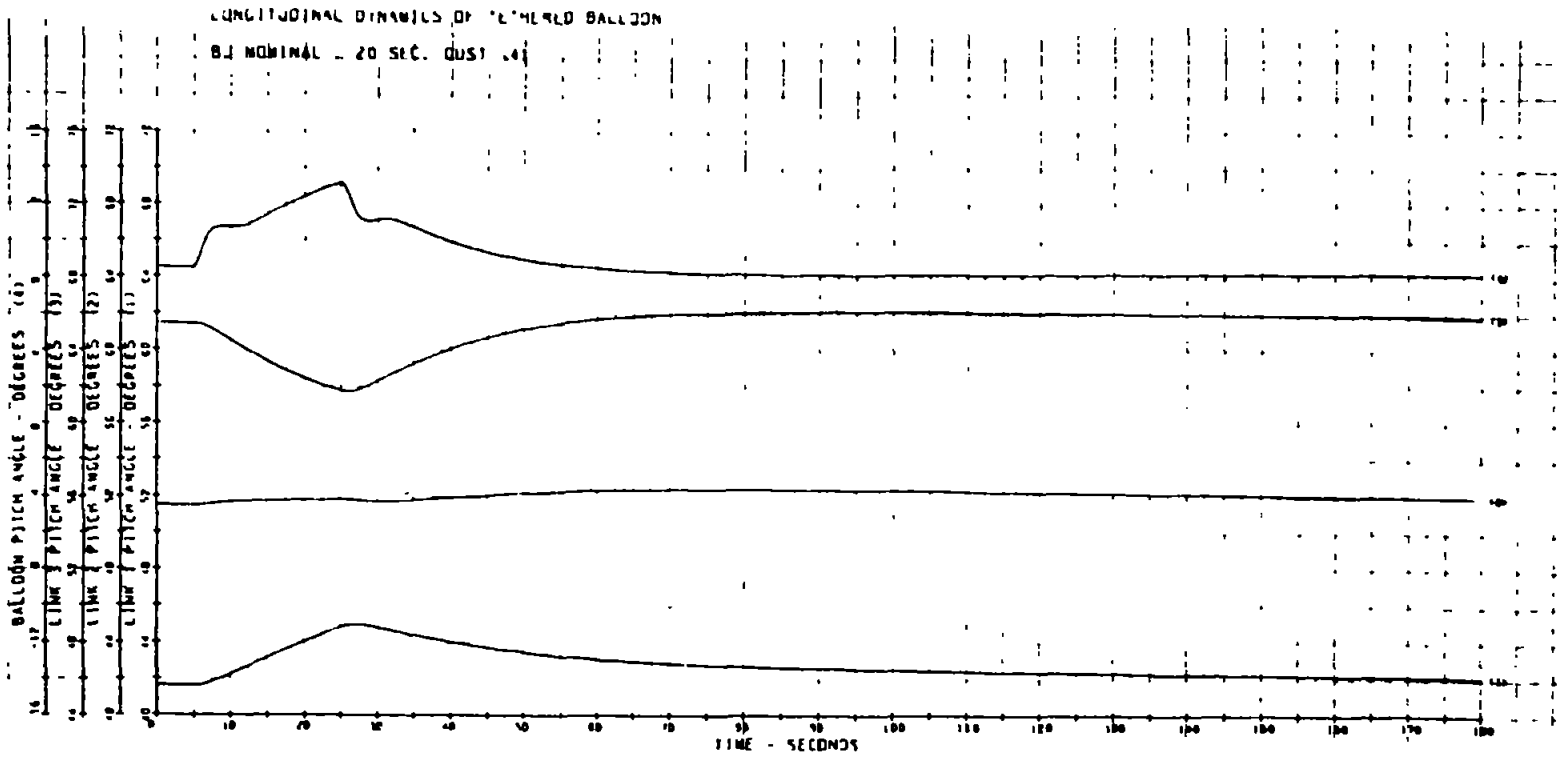
LONGITUDINAL DYNAMICS OF TETHERED BALLOON
B.I NOMINAL - 20 SEC. GUST (4)
BALLOON PITCH ANGLE - DEGREES (4)
LINK 3 PITCH ANGLE - DEGREES (3)
LINK 2 PITCH ANGLE - DEGREES (2)
LINK 1 PITCH ANGLE - DEGREES (1)
TIME - SECONDS

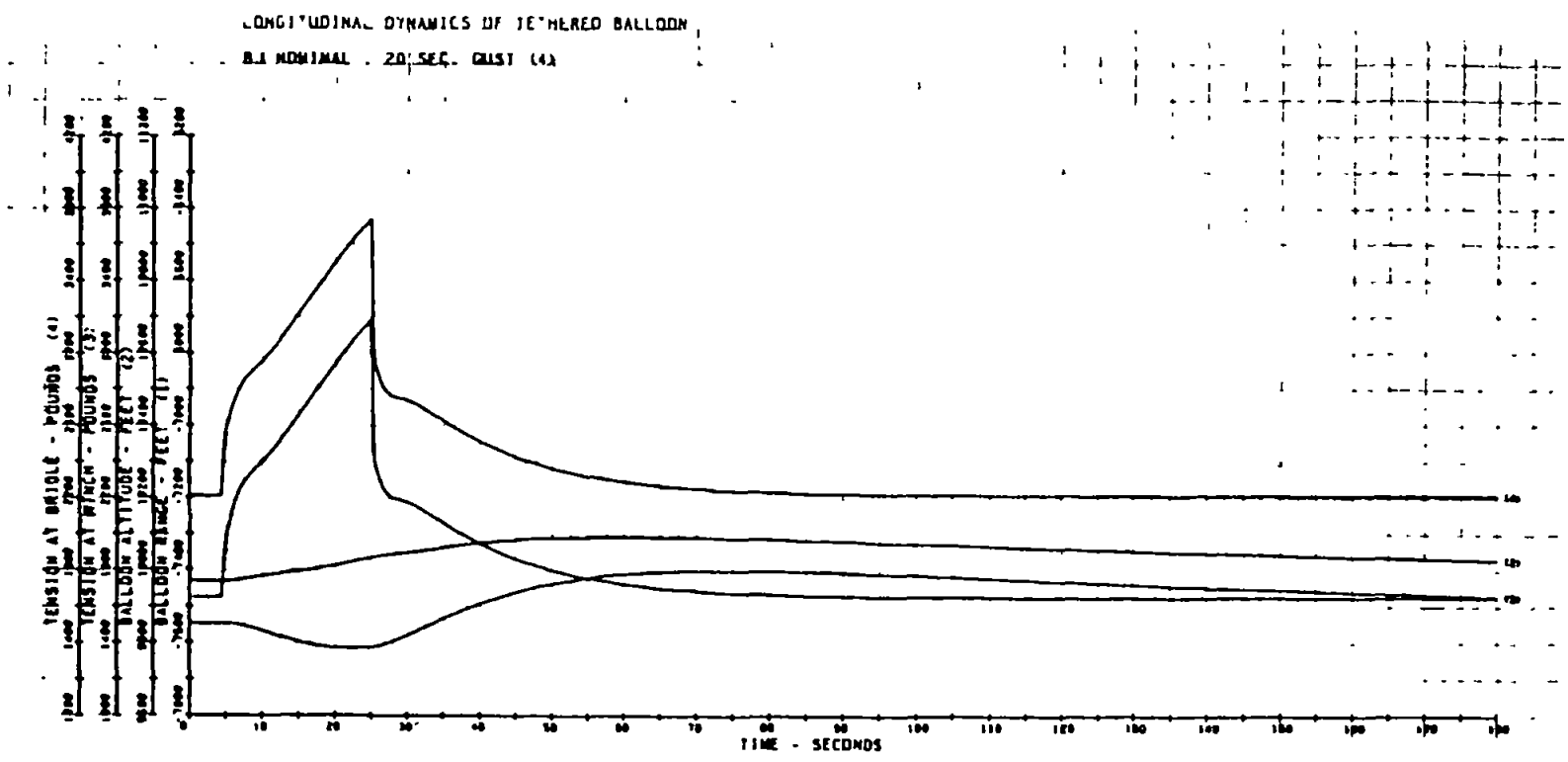
LONGITUDINAL DYNAMICS OF TETHERED BALLOON
B.I NOMINAL - 20 SEC. GUST (4)
TENSION AT BRIDLE - POUNDS (4)
TENSION AT WINCH - POUNDS (3)
BALLOON ALTITUDE - FEET (2)
BALLOON RANGE - FEET (1)
TIME - SECONDS

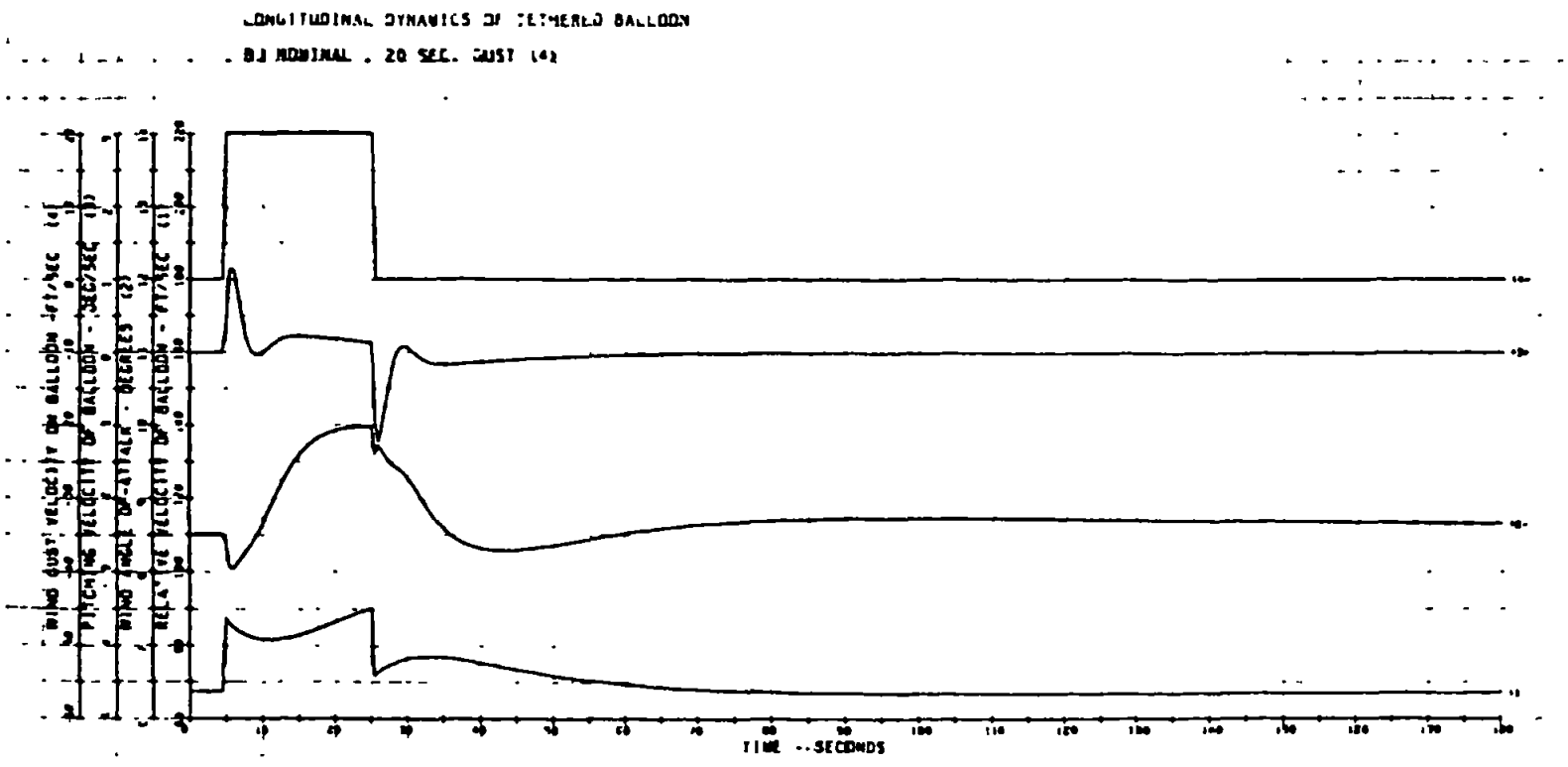
LONGITUDINAL DYNAMICS OF TETHERED BALLOON
B.I NOMINAL - 20 SEC. GUST (4)
WIND GUST VELOCITY ON BALLOON - FT/SEC (4)
PITCHING VELOCITY OF BALLOON - DEG/SEC (3)
WIND ANGLE OF ATTACK - DEGREES (2)
RELATIVE VELOCITY OF BALLOON - FT/SEC (1)
TIME - SECONDS

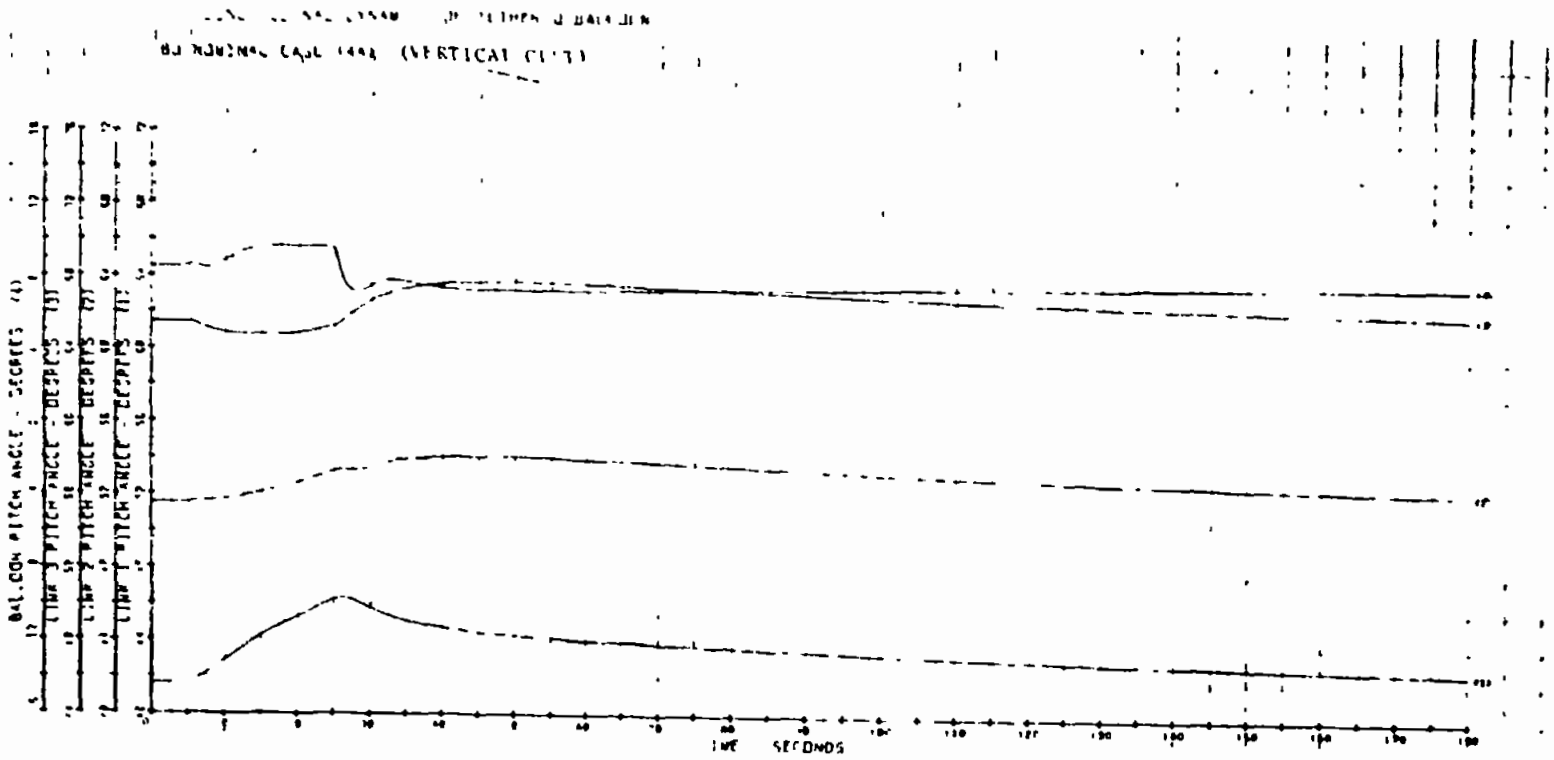
(VERTICAL GUST)
BALLOON PITCH ANGLE - DEGREES
TIME - SECONDS

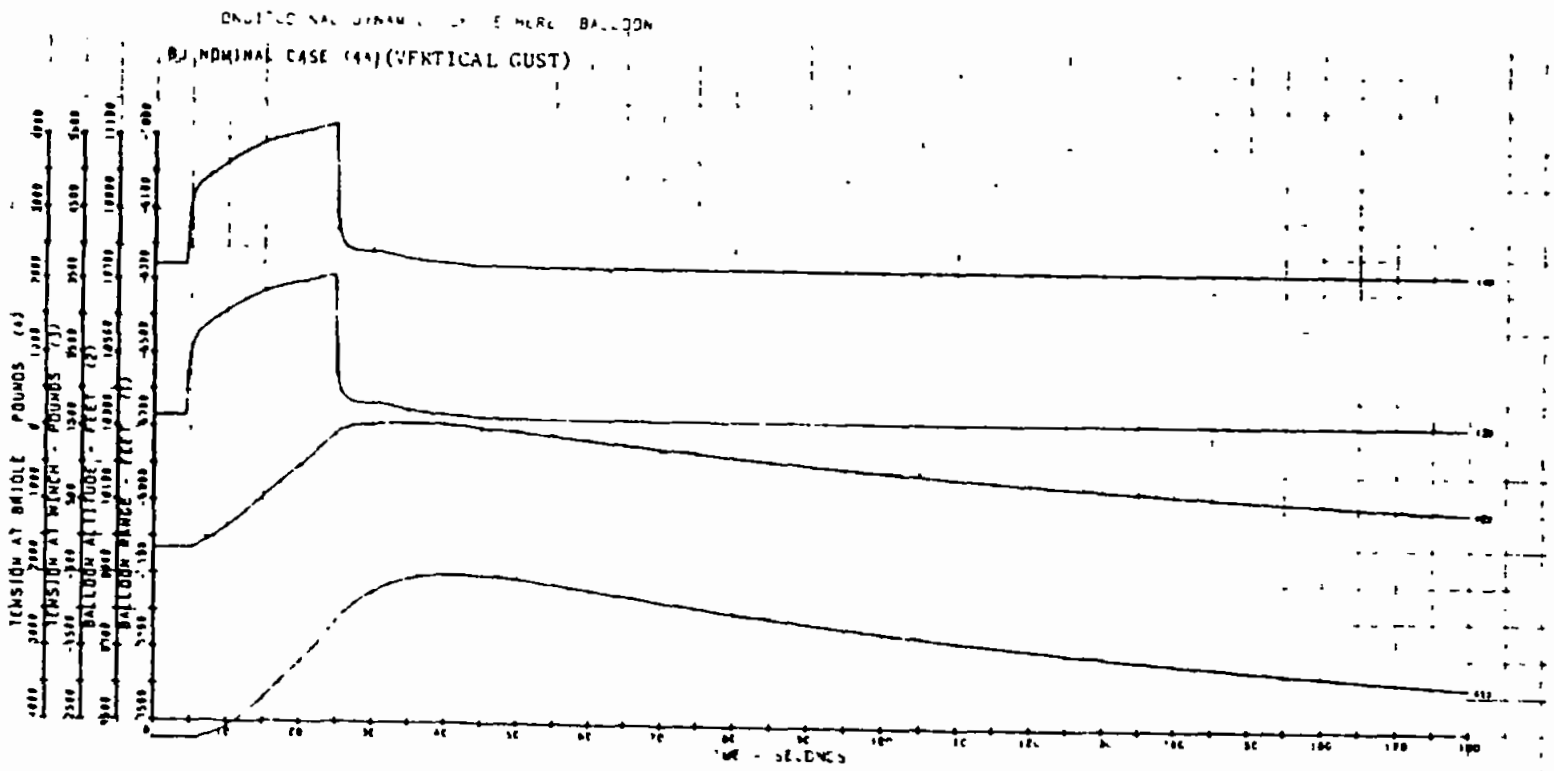
NOMINAL CASE (4A) (VERTICAL GUST)
TENSION AT BRIDLE - POUNDS
TENSION AT WINCH - POUNDS
BALLOON ALTITUDE - FEET
BALLOON RANGE - FEET
TIME - SECONDS

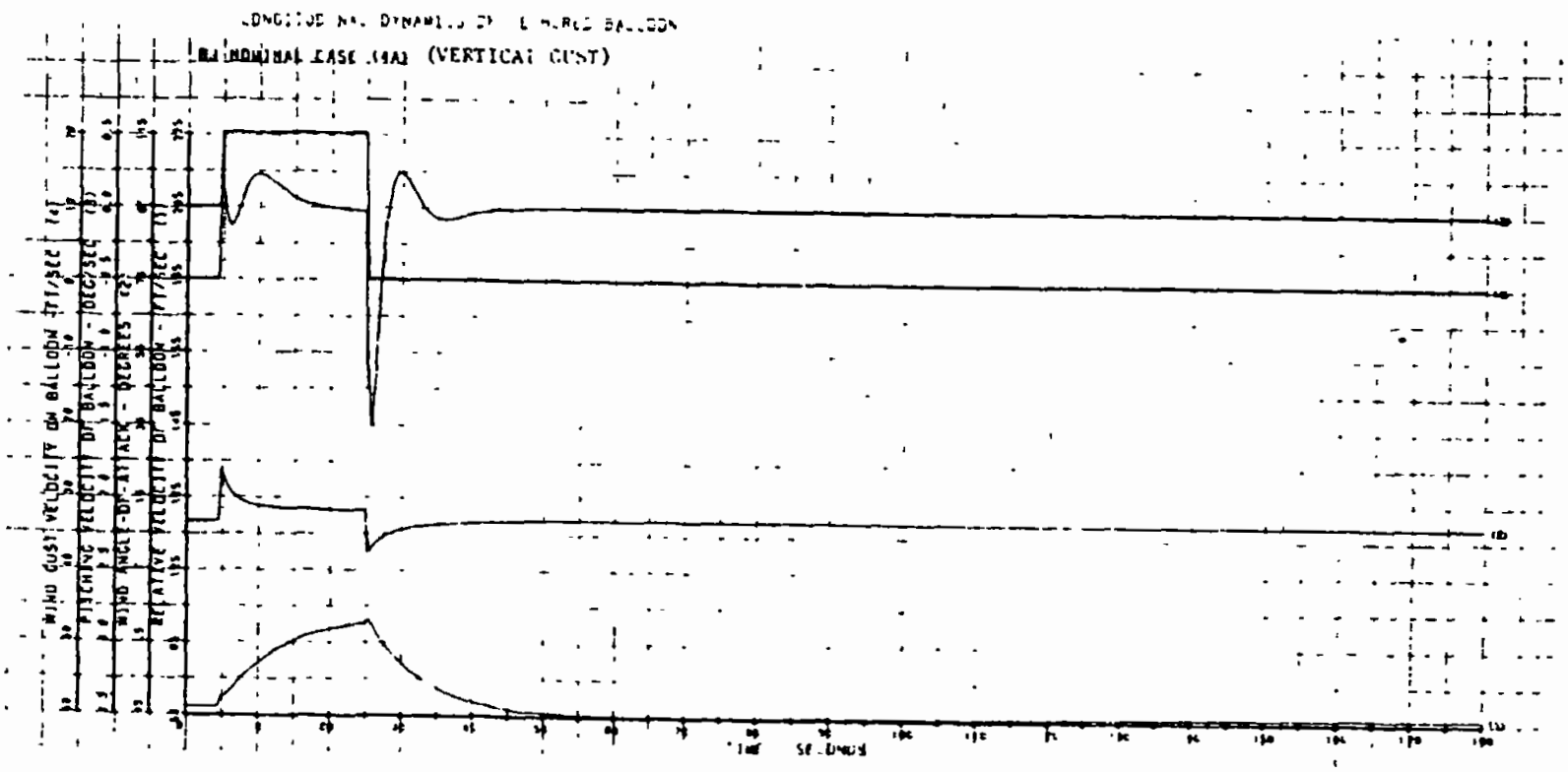
NOMINAL CASE (4A) (VERTICAL GUST)
WIND GUST VELOCITY ON BALLOON - FT/SEC
PITCHING VELOCITY OF BALLOON - DEG/SEC
WIND ANGLE-OF-ATTACK - DEGREES
RELATIVE VELOCITY OF BALLOON - FT/SEC
TIME - SECONDS

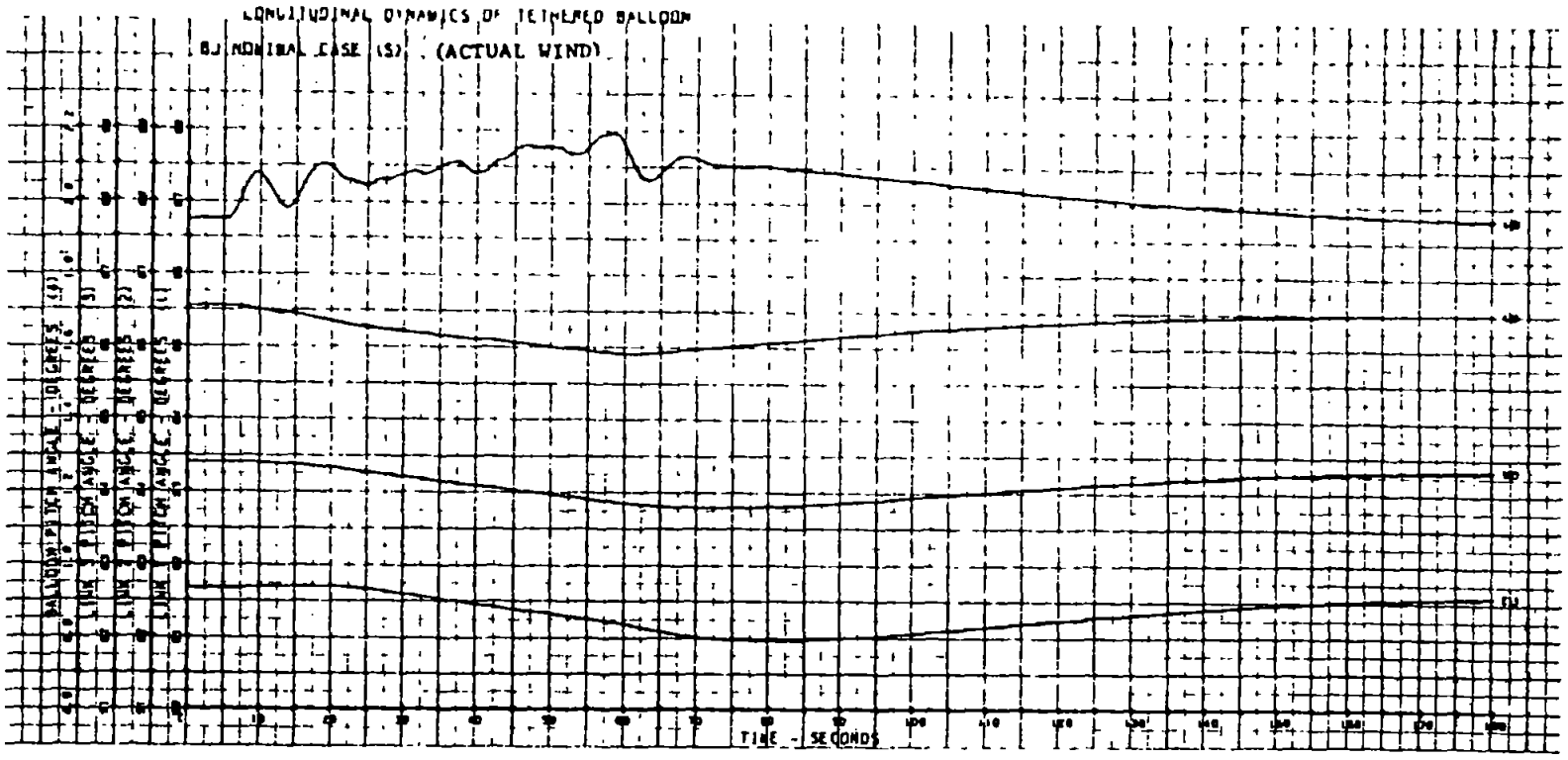
LONGITUDINAL DYNAMICS OF TETHERED BALLOON
BJ NOMINAL CASE (S) (ACTUAL WIND)
TIME - SECONDS

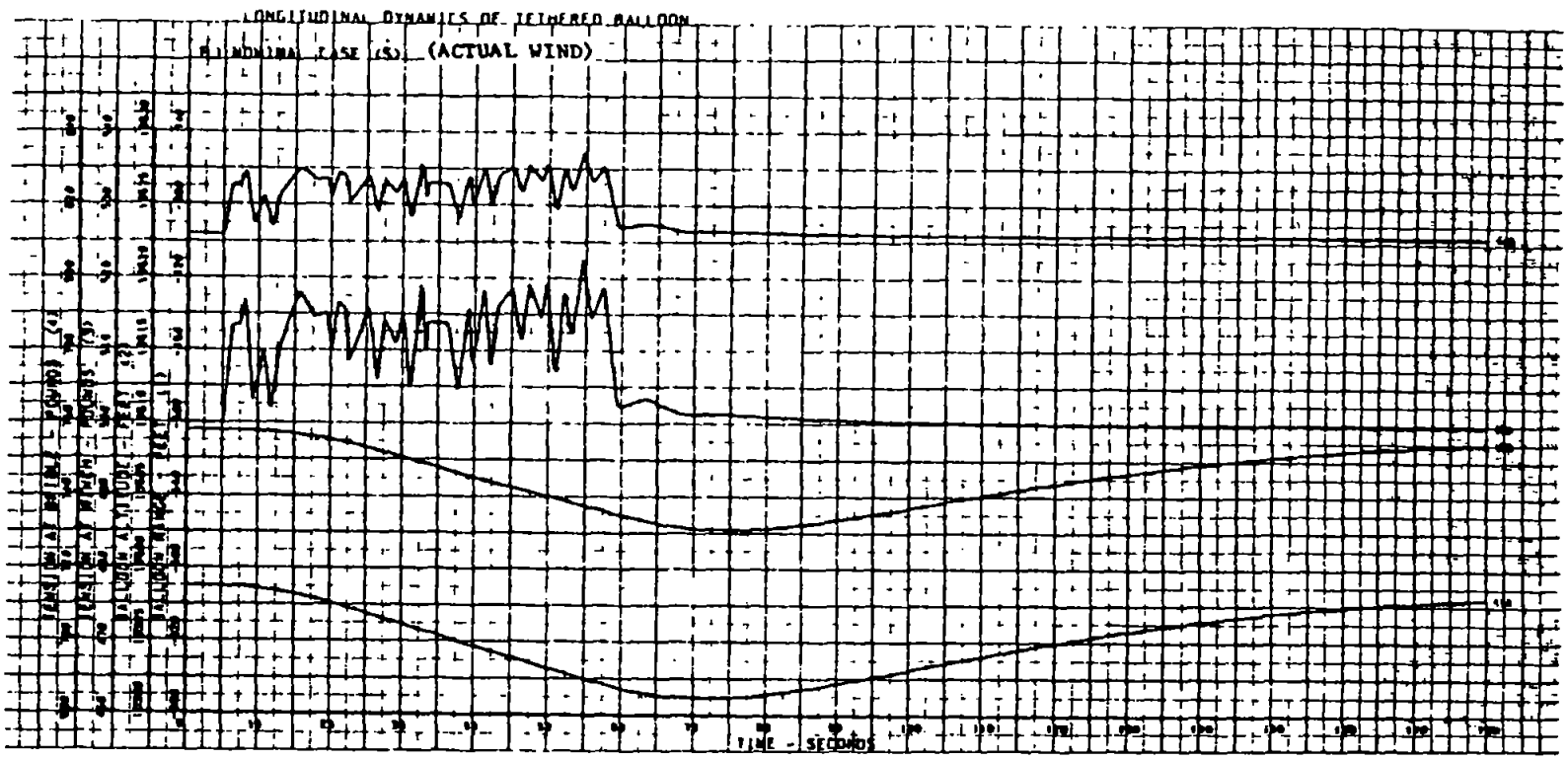
LONGITUDINAL DYNAMICS OF TETHERED BALLOON
BJ NOMINAL CASE (S) (ACTUAL WIND)
TIME - SECONDS

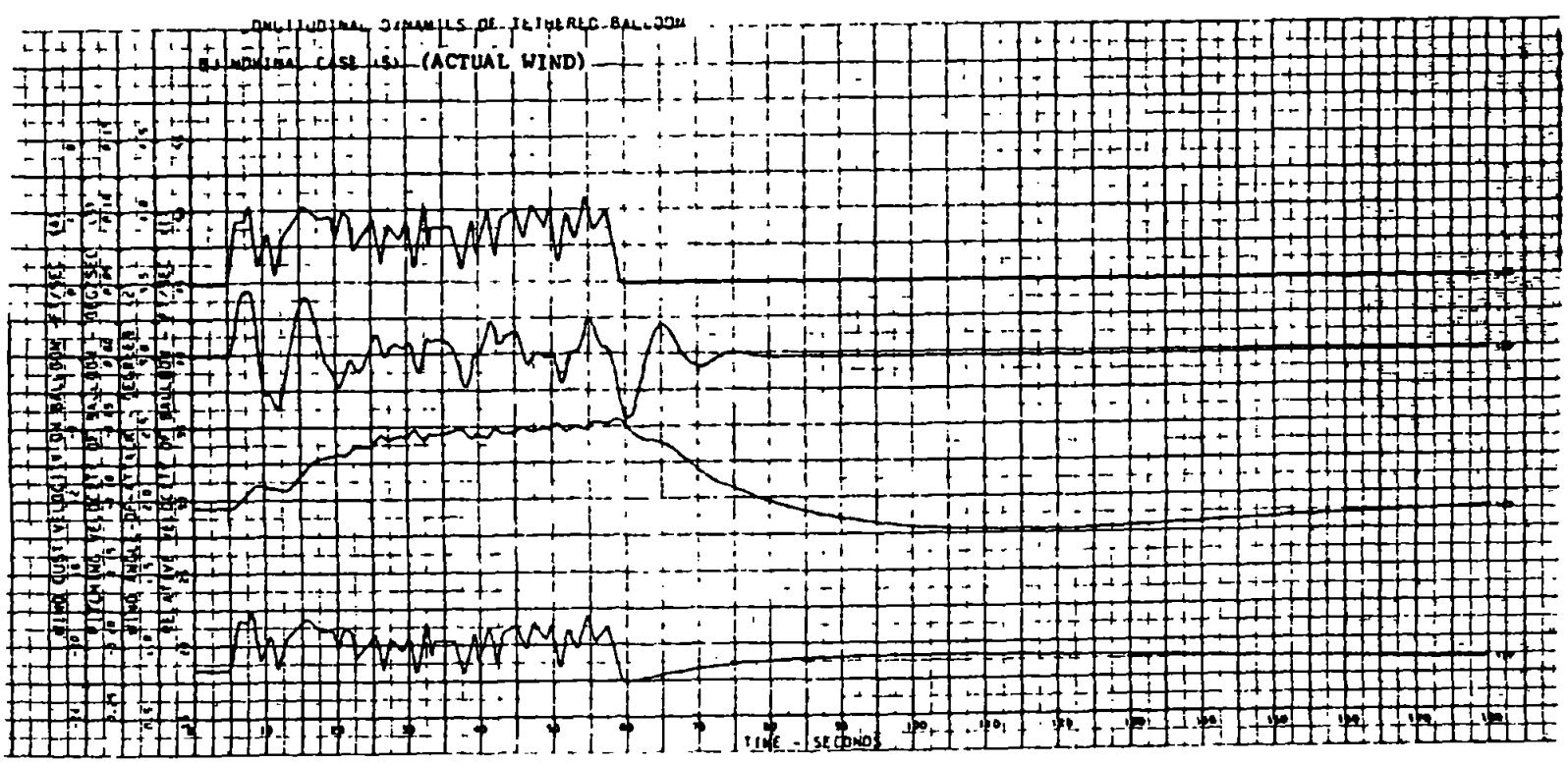
LONGITUDINAL DYNAMICS OF TETHERED BALLOON
BJ NOMINAL CASE (S) (ACTUAL WIND)
TIME - SECONDS

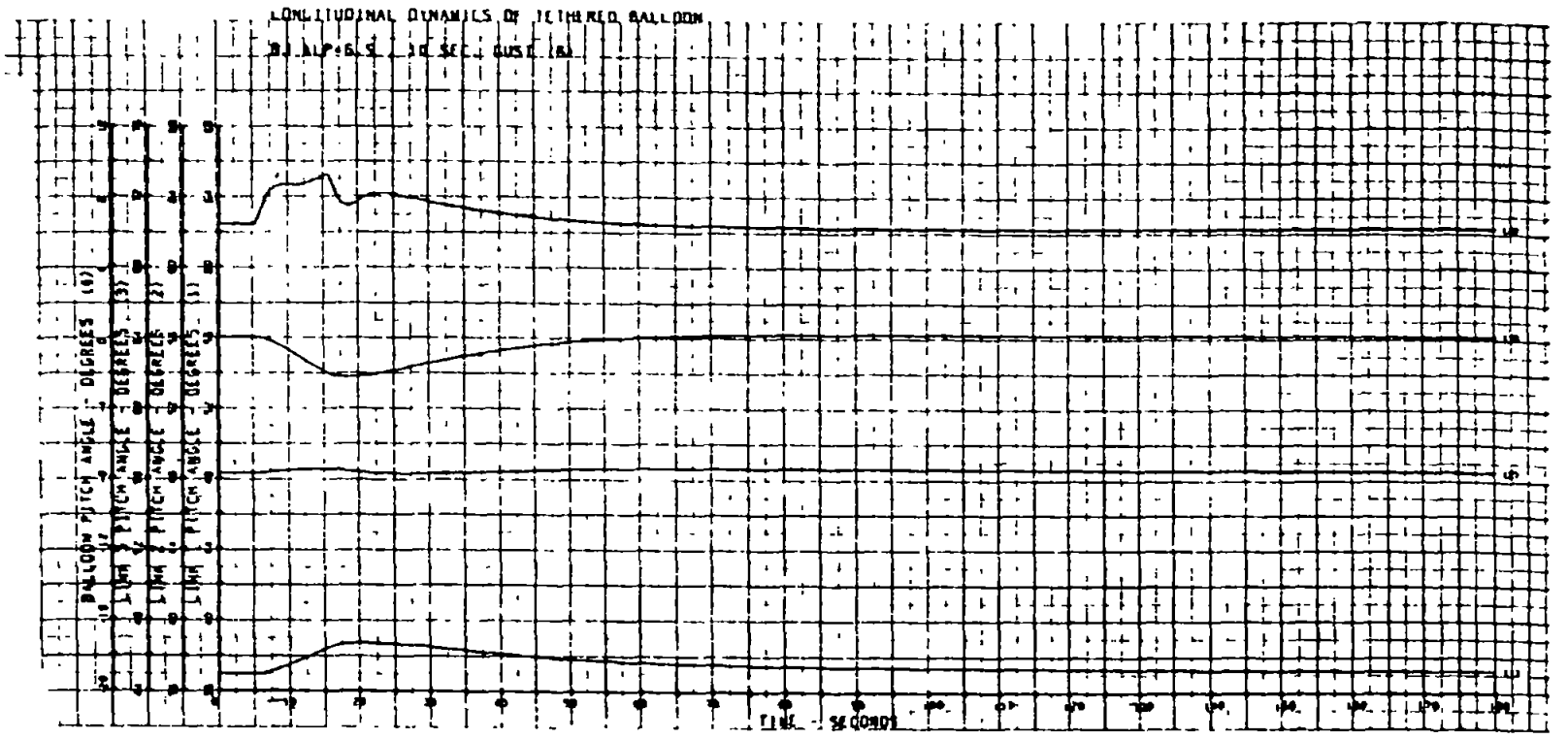
LONGITUDINAL DYNAMICS OF TETHERED BALLOON
TIME - SECONDS

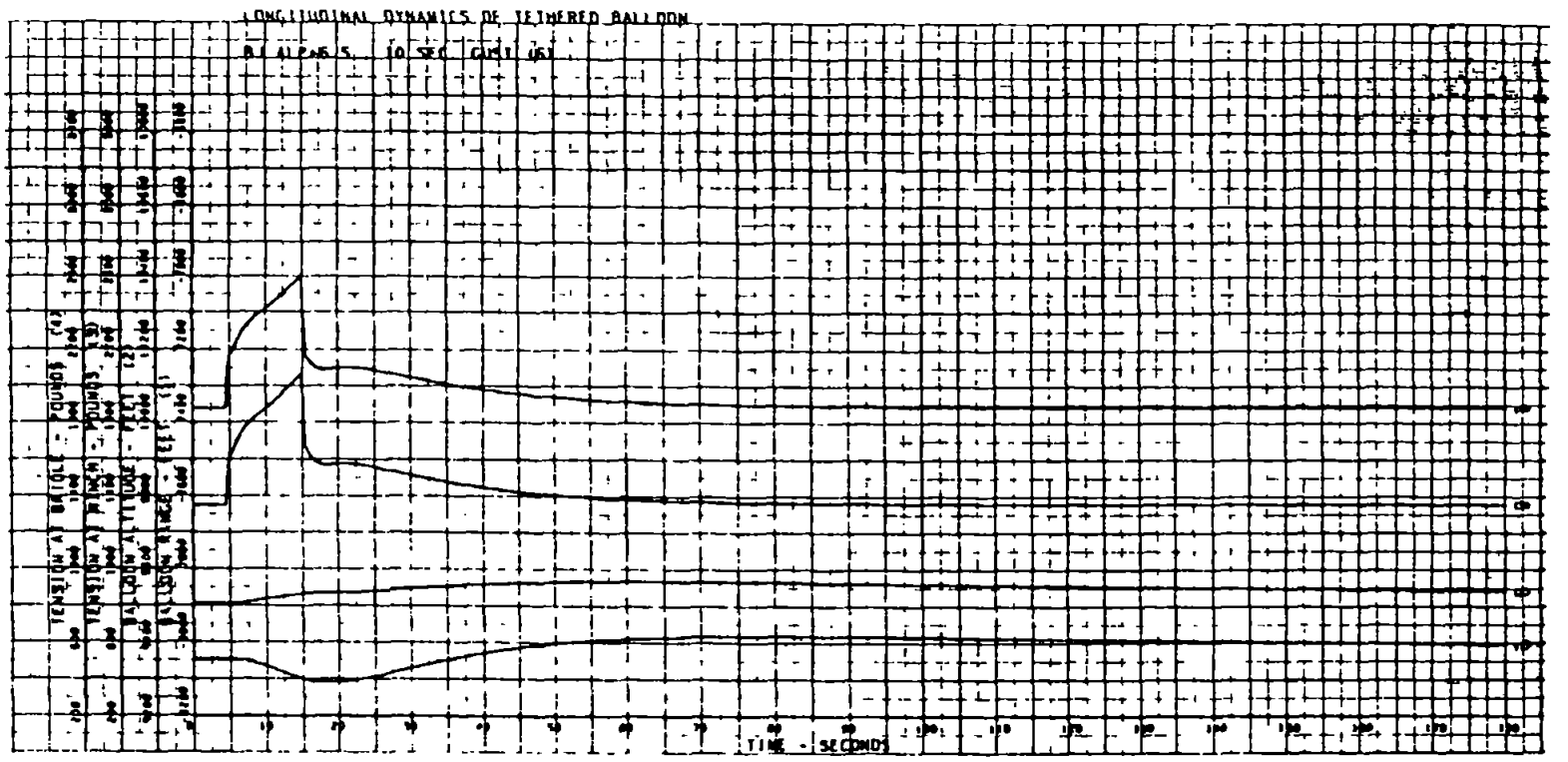
LONGITUDINAL DYNAMICS OF TETHERED BALLOON
TIME - SECONDS

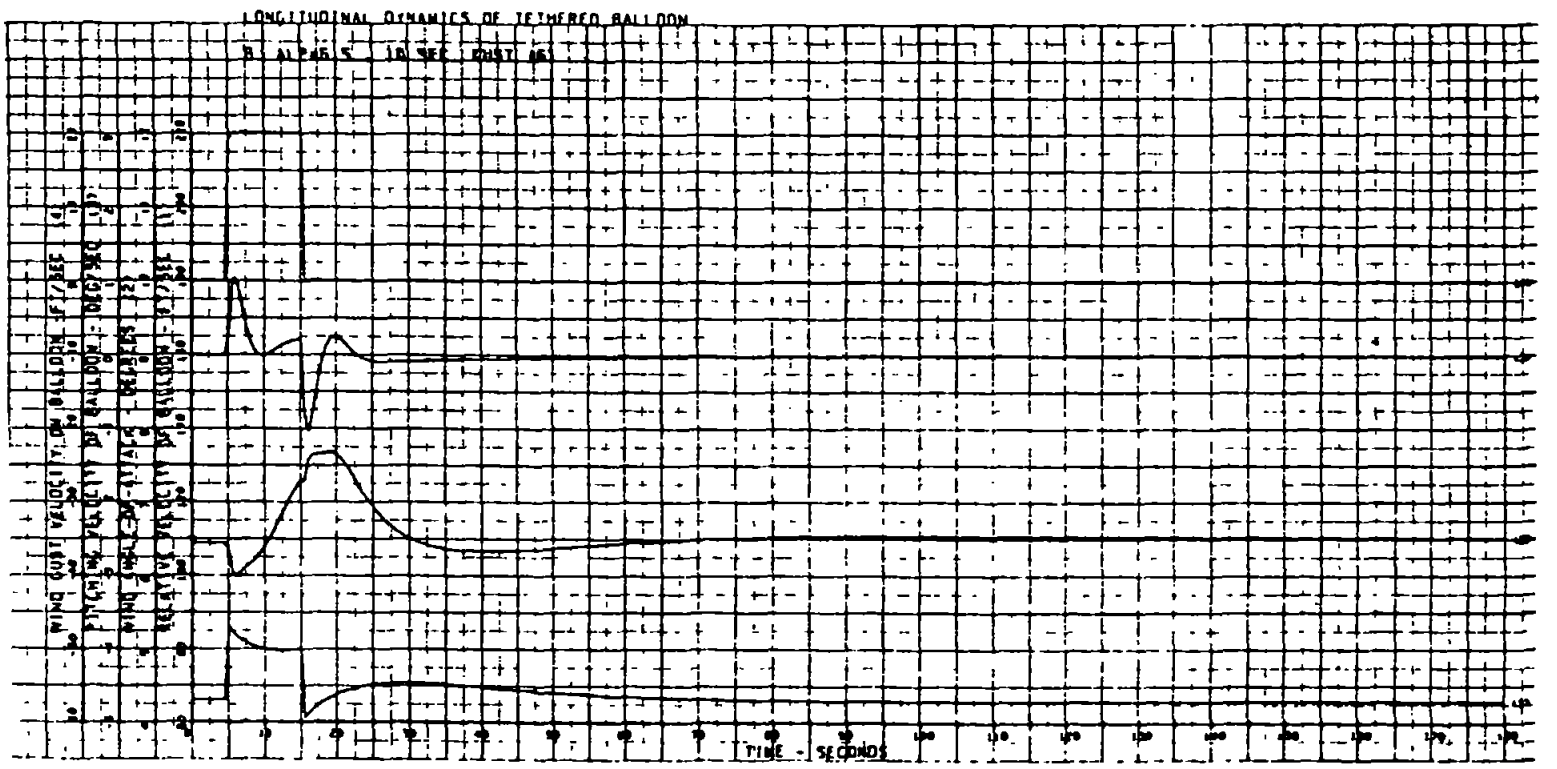
LONGITUDINAL DYNAMICS OF TETHERED BALLOON
TIME - SECONDS

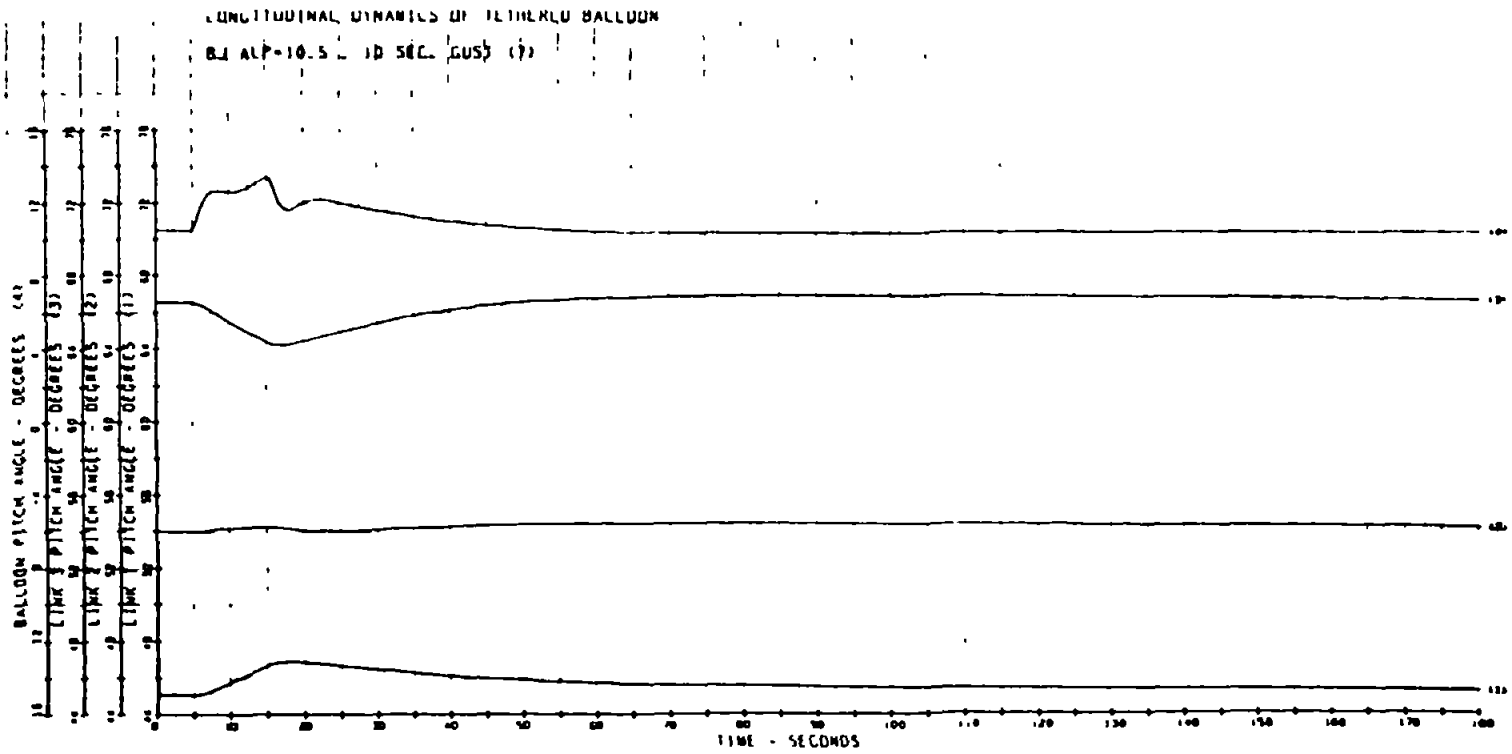
LONGITUDINAL DYNAMICS OF TETHERED BALLOON
BJ ALP=10.5 , 10 SEC. GUST (7)
BALLOON PITCH ANGLE - DEGREES (4)
LINK 3 PITCH ANGLE - DEGREES (3)
LINK 2 PITCH ANGLE - DEGREES (2)
LINK 1 PITCH ANGLE - DEGREES (1)
TIME - SECONDS

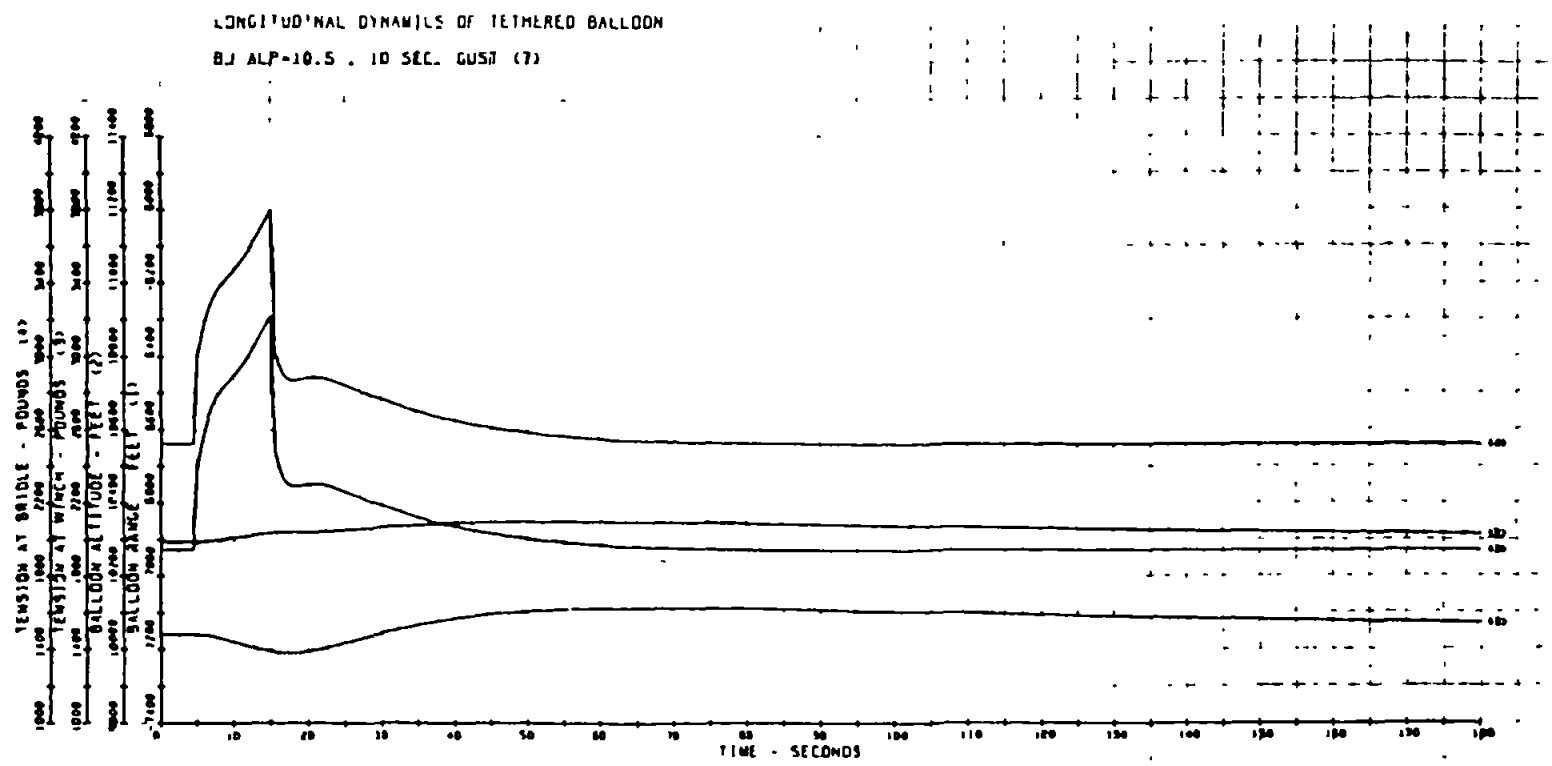
LONGITUDINAL DYNAMICS OF TETHERED BALLOON
BJ ALP=10.5 , 10 SEC. GUST (7)
TENSION AT BRIDLE - POUNDS (4)
TENSION AT WINCH - POUNDS (3)
BALLOON ALTITUDE - FEET (2)
BALLOON RANGE - FEET (1)
TIME - SECONDS

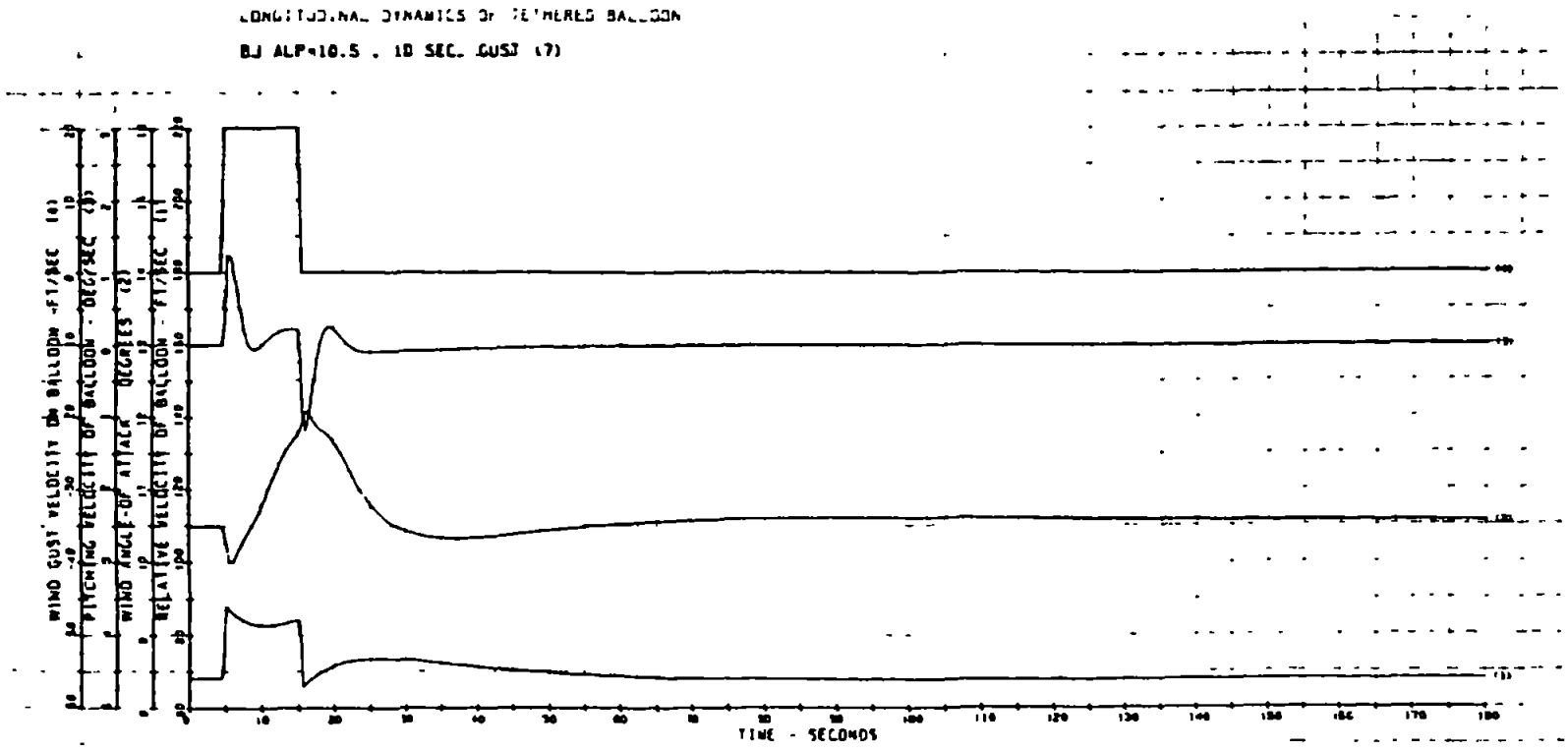
LONGITUDINAL DYNAMICS OF TETHERED BALLOON
BJ ALP=10.5 , 10 SEC. GUST (7)
WIND GUST VELOCITY ON BALLOON -FT/SEC (4)
PITCHING VELOCITY OF BALLOON - DEG/SEC (3)
WIND ANGLE-OF-ATTACK - DEGREES (2)
RELATIVE VELOCITY OF BALLOON - FT/SEC (1)
TIME - SECONDS

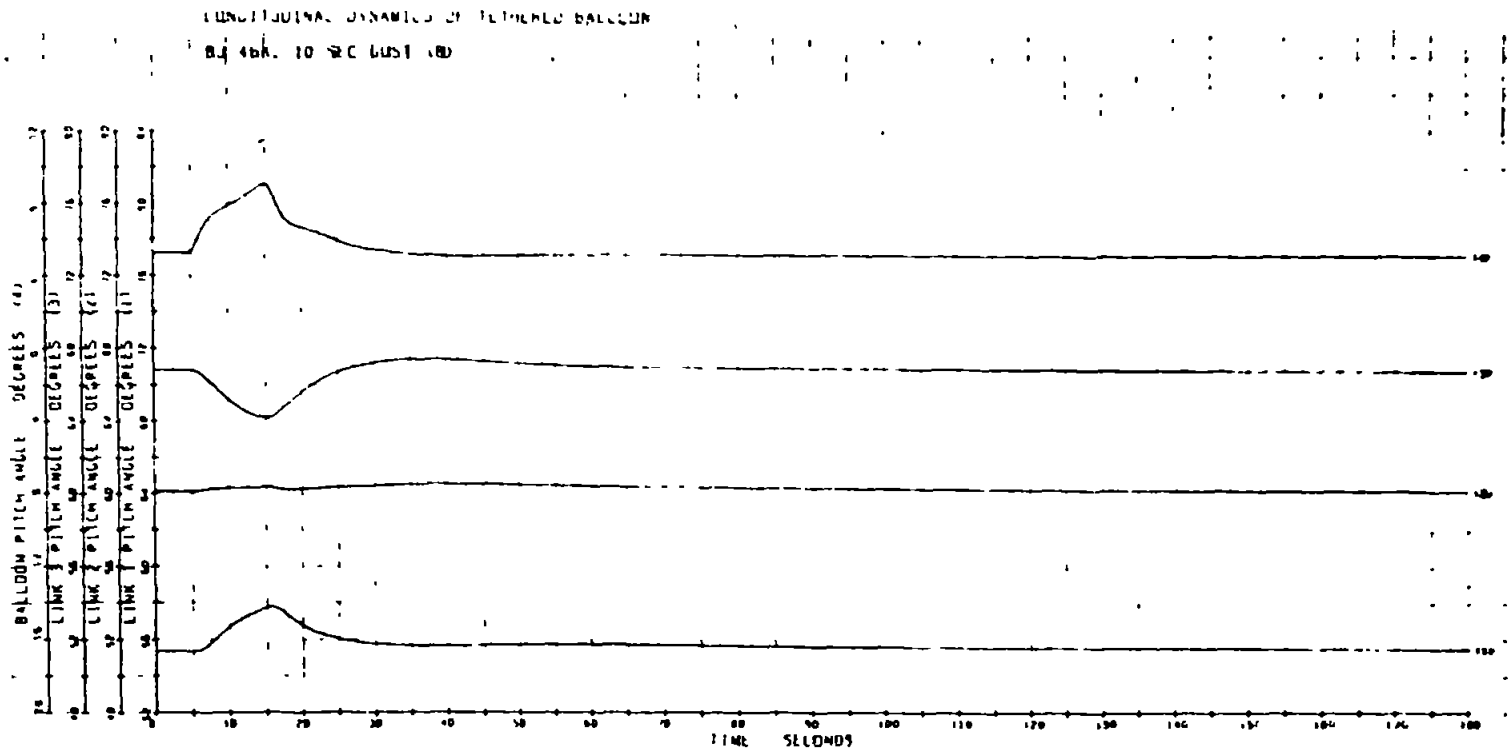
LONGITUDINAL DYNAMICS OF TETHERED BALLOON
BALLOON PITCH ANGLE DEGREES
LINK 3 PITCH ANGLE DEGREES
LINK 2 PITCH ANGLE DEGREES
LINK 1 PITCH ANGLE DEGREES
TIME SECONDS

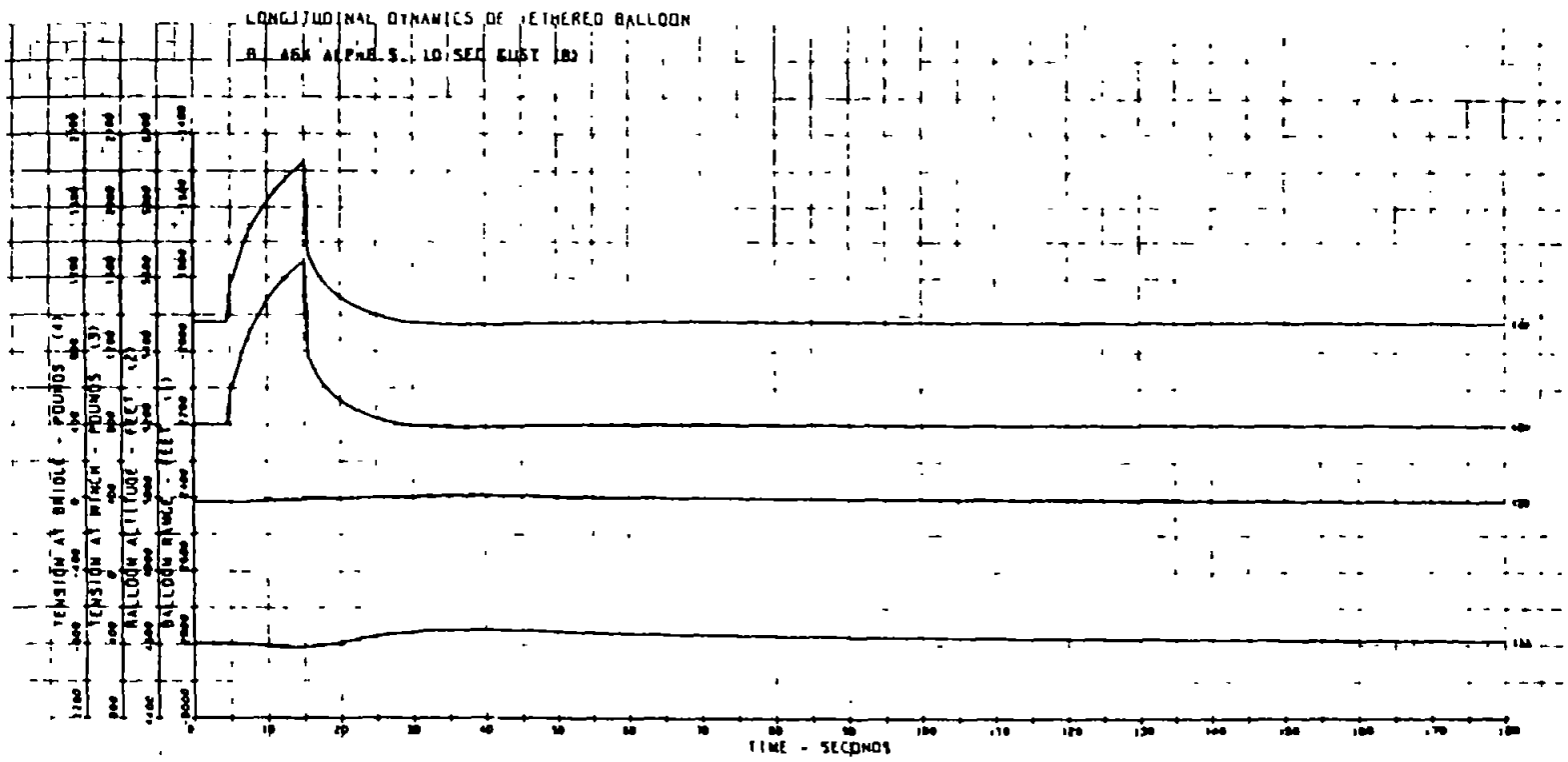
LONGITUDINAL DYNAMICS OF TETHERED BALLOON
TENSION AT BRIDLE - POUNDS
TENSION AT WINCH - POUNDS
BALLOON ALTITUDE - FEET
BALLOON RANGE - FEET
TIME - SECONDS

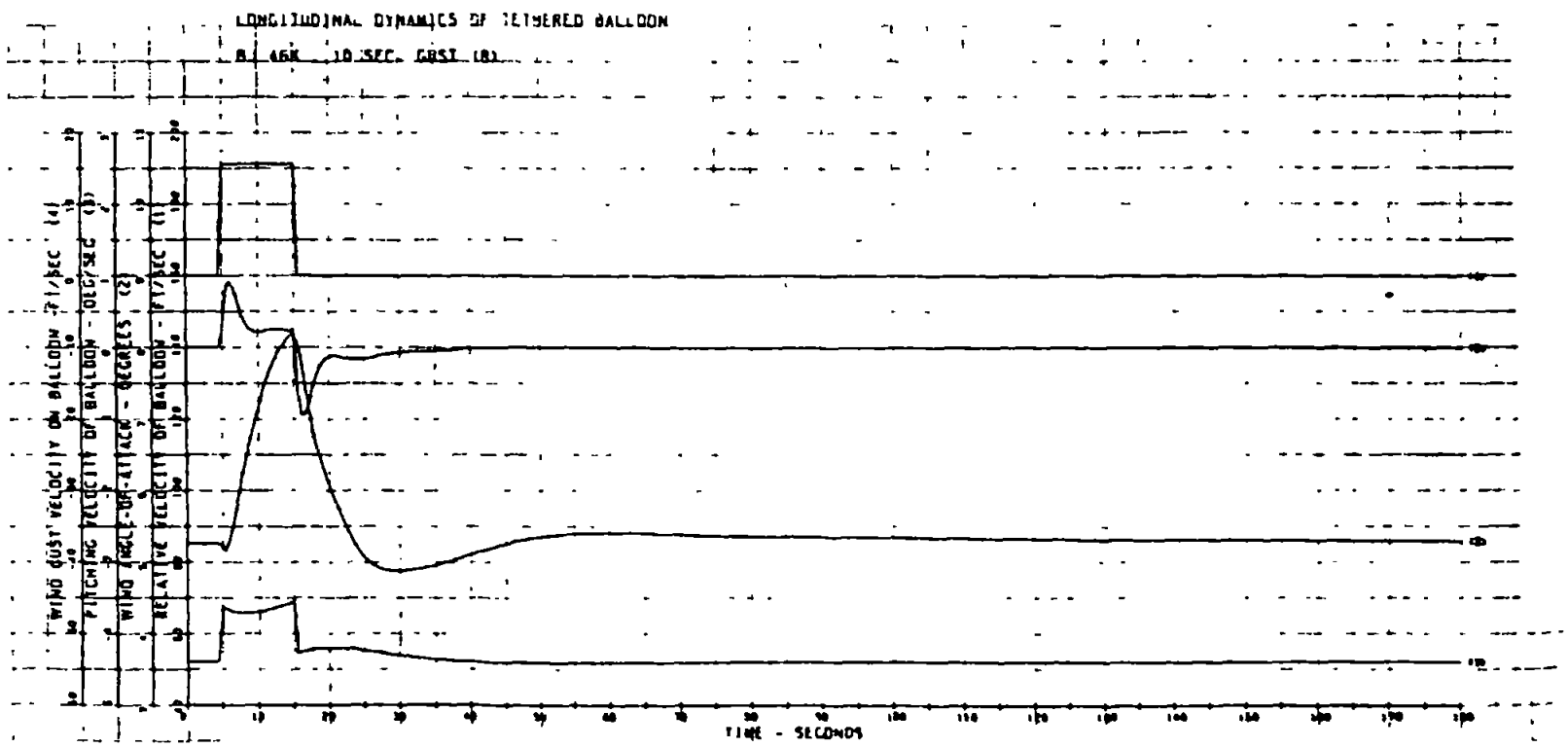
LONGITUDINAL DYNAMICS OF TETHERED BALLOON
WIND GUST VELOCITY ON BALLOON - FT/SEC
PITCHING VELOCITY OF BALLOON - DEG/SEC
WIND ANGLE-OF-ATTACK - DEGREES
RELATIVE VELOCITY OF BALLOON - FT/SEC
TIME - SECONDS

LONGITUDINAL DYNAMICS OF TETHERED BALLOON

BJ 500K 10 SEC GUST (9)

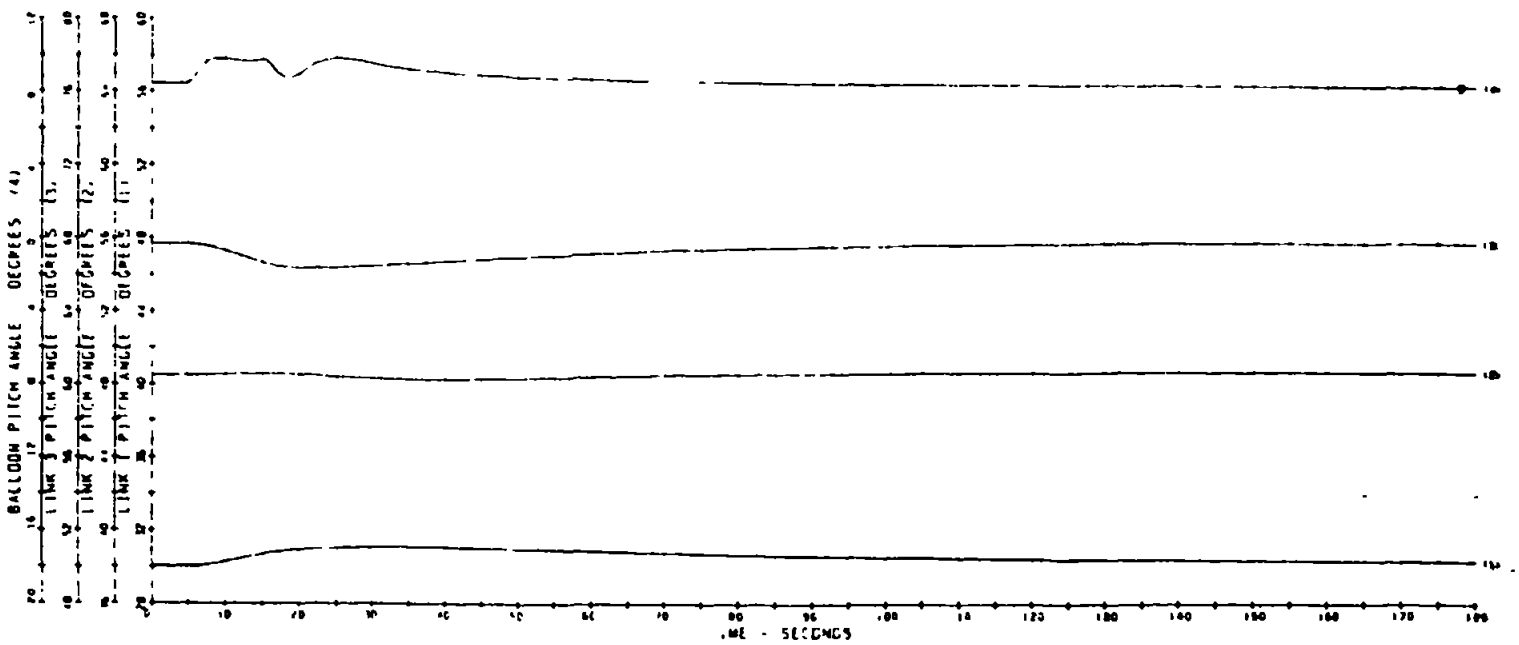

LONGITUDINAL DYNAMICS OF TETHERED BALLOON

BJ 500K. 10 SEC GUST (9)

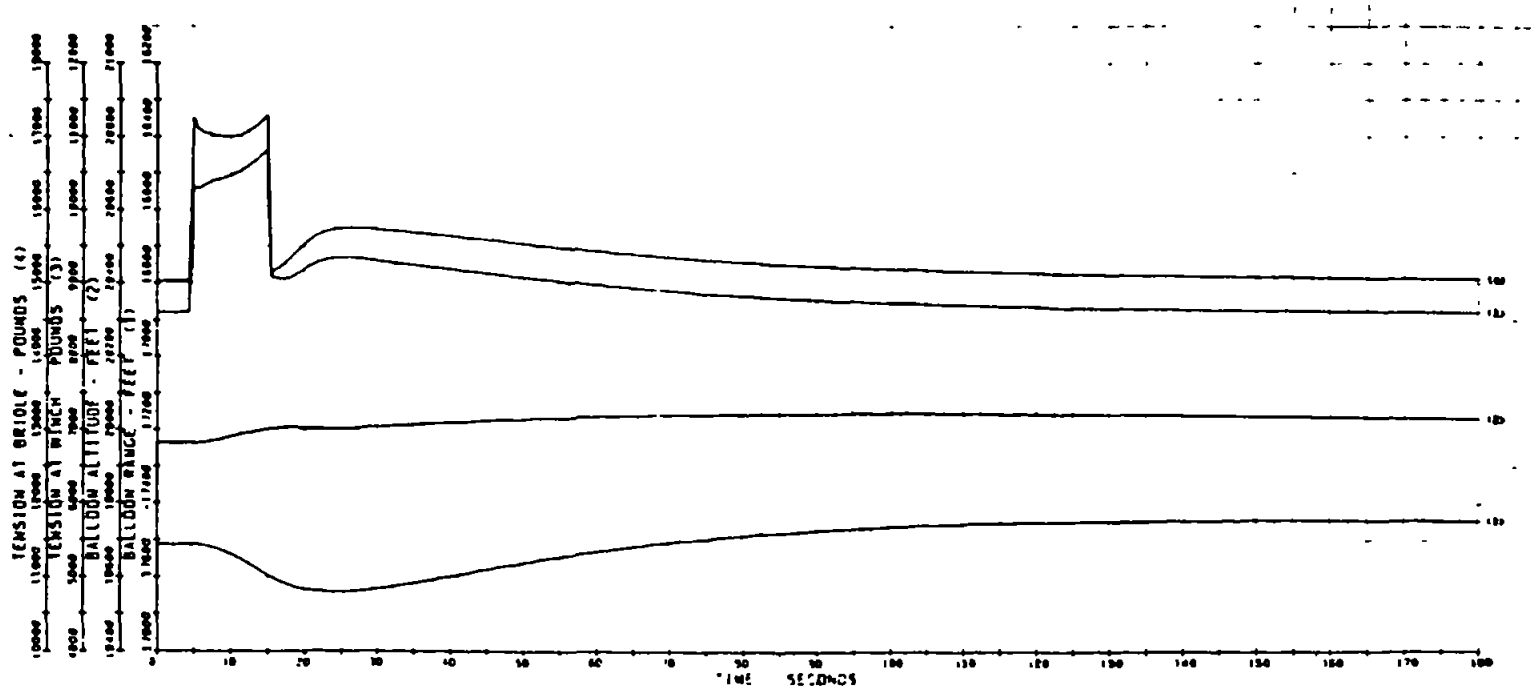

LONGITUDINAL DYNAMICS OF TETHERED BALLOON

BJ 500 K . 10 SEC. GUST (B)

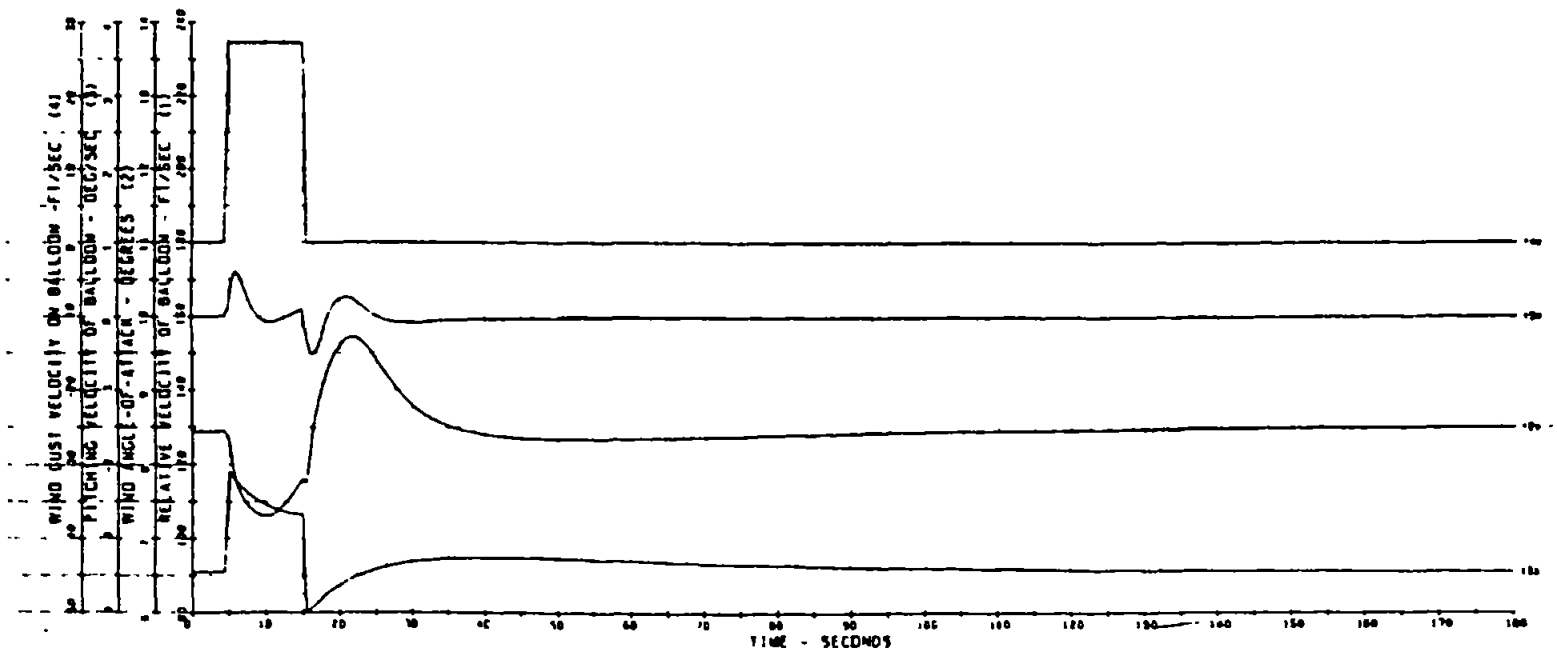

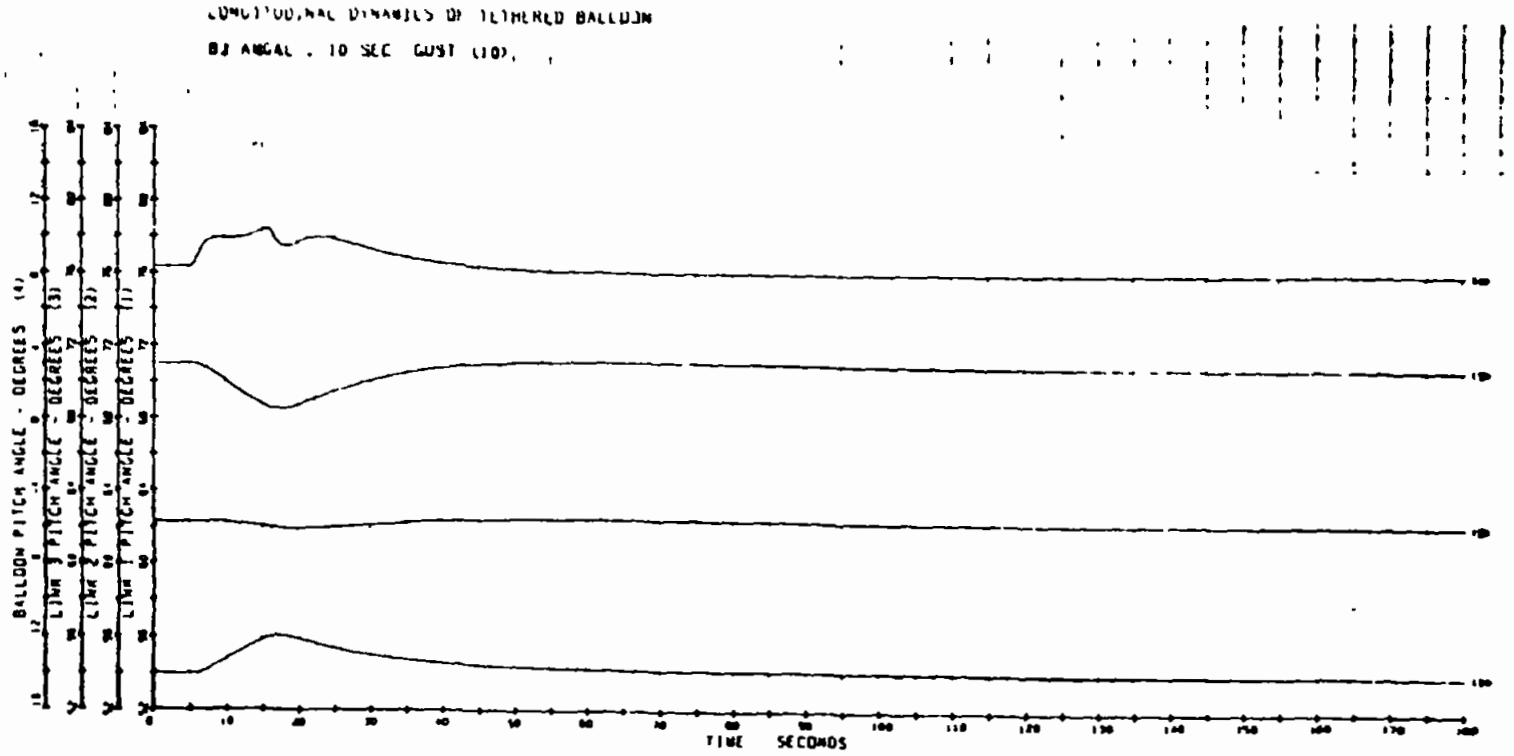
LONGITUDINAL DYNAMICS OF TETHERED BALLOON
BJ ANGAL . 10 SEC GUST (10)
BALLOON PITCH ANGLE - DEGREES (4)
LINK 3 PITCH ANGLE - DEGREES (3)
LINK 2 PITCH ANGLE - DEGREES (2)
LINK 1 PITCH ANGLE - DEGREES (1)
TIME SECONDS

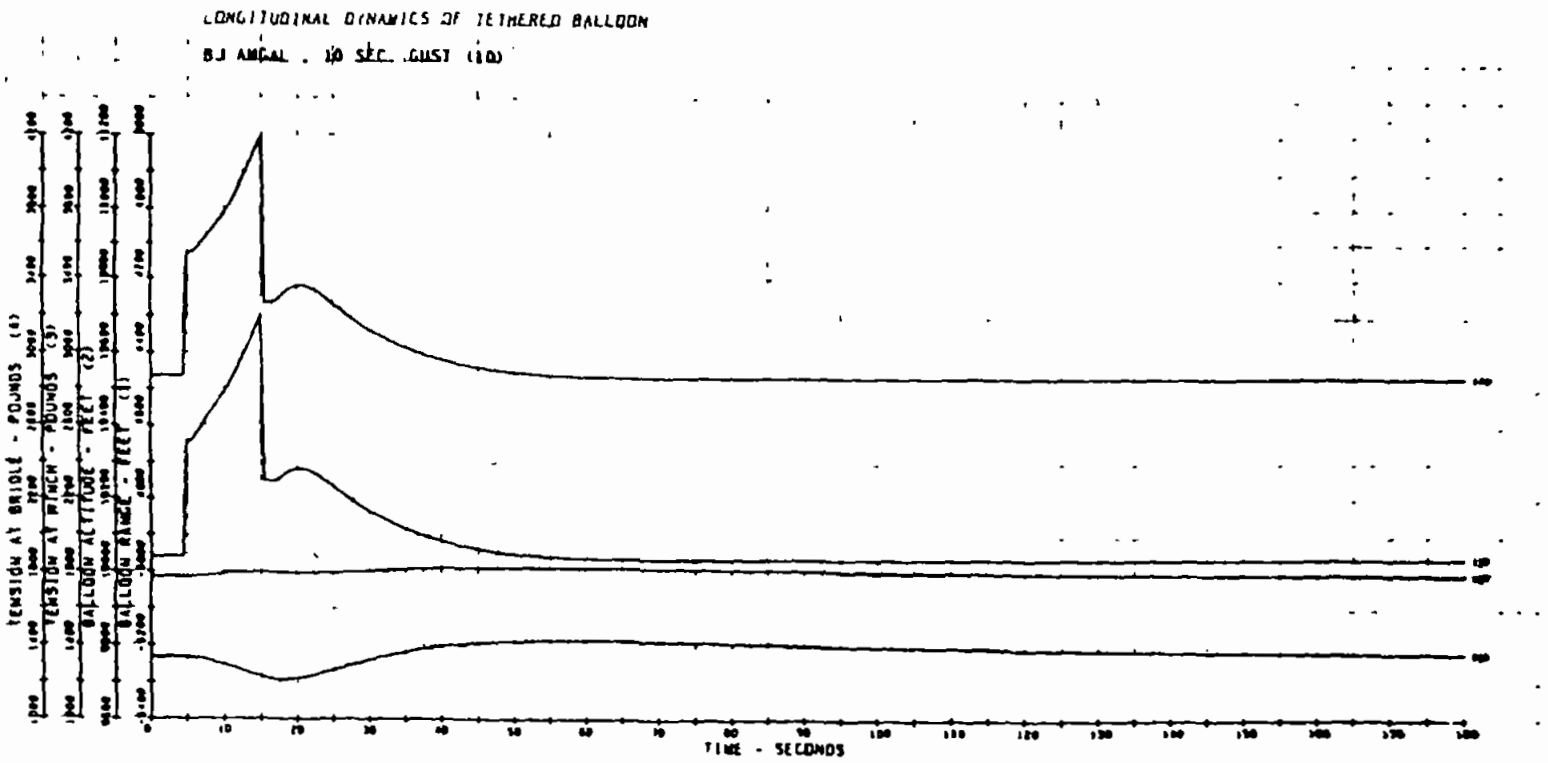
LONGITUDINAL DYNAMICS OF TETHERED BALLOON
BJ ANGAL . 10 SEC. GUST (10)
TENSION AT BRIDLE - POUNDS (4)
TENSION AT WINCH - POUNDS (3)
BALLOON ALTITUDE - FEET (2)
BALLOON RANGE - FEET (1)
TIME - SECONDS

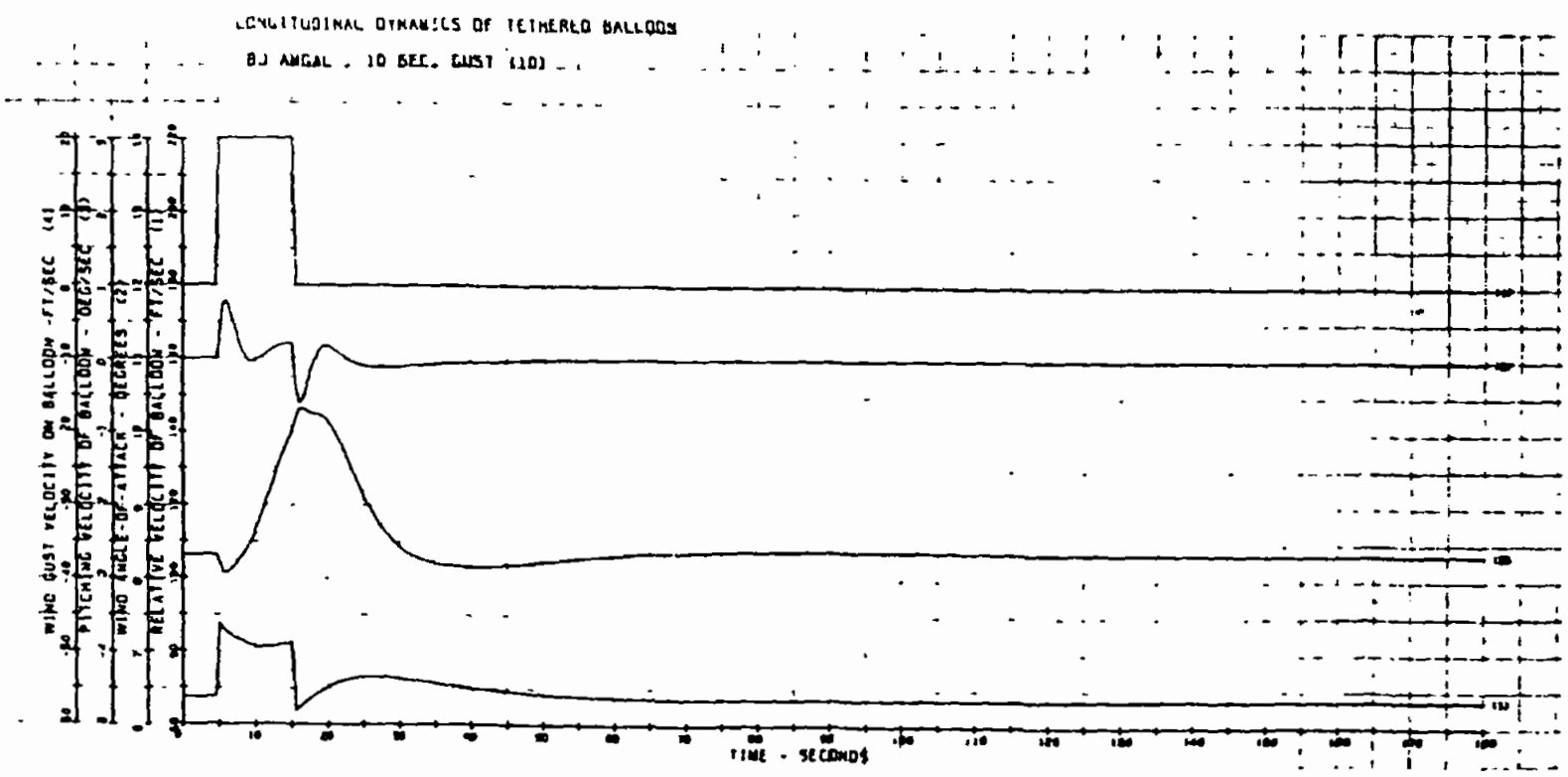
LONGITUDINAL DYNAMICS OF TETHERED BALLOON
BJ ANGAL . 10 SEC. GUST (10)
WIND GUST VELOCITY ON BALLOON - FT/SEC (4)
PITCHING VELOCITY OF BALLOON - DEG/SEC (3)
WIND ANGLE-OF-ATTACK - DEGREES (2)
RELATIVE VELOCITY OF BALLOON - FT/SEC (1)
TIME - SECONDS

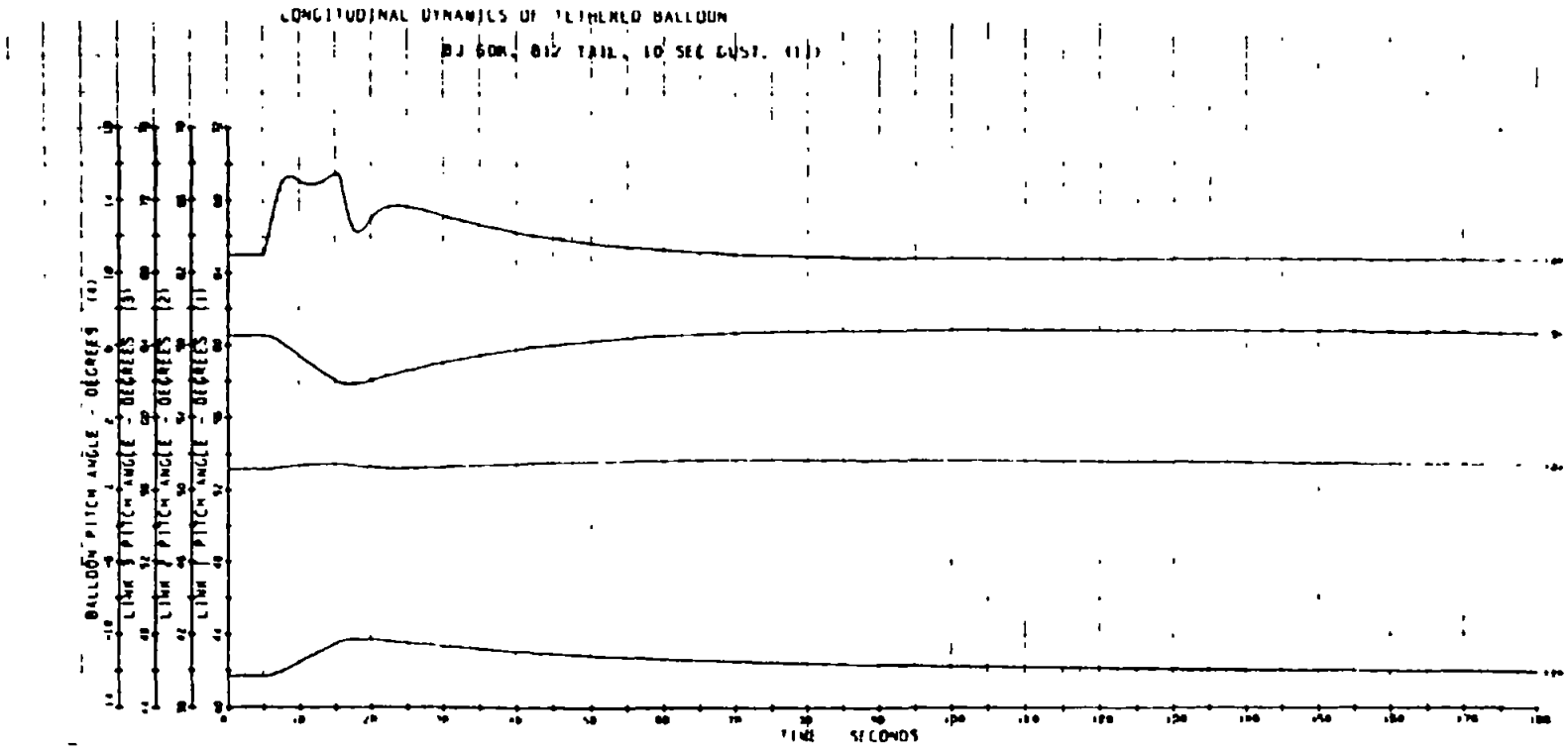
LONGITUDINAL DYNAMICS OF TETHERED BALLOON
BALLOON PITCH ANGLE - DEGREES
LINK 3 PITCH ANGLE - DEGREES
LINK 2 PITCH ANGLE - DEGREES
LINK 1 PITCH ANGLE - DEGREES
TIME - SECONDS

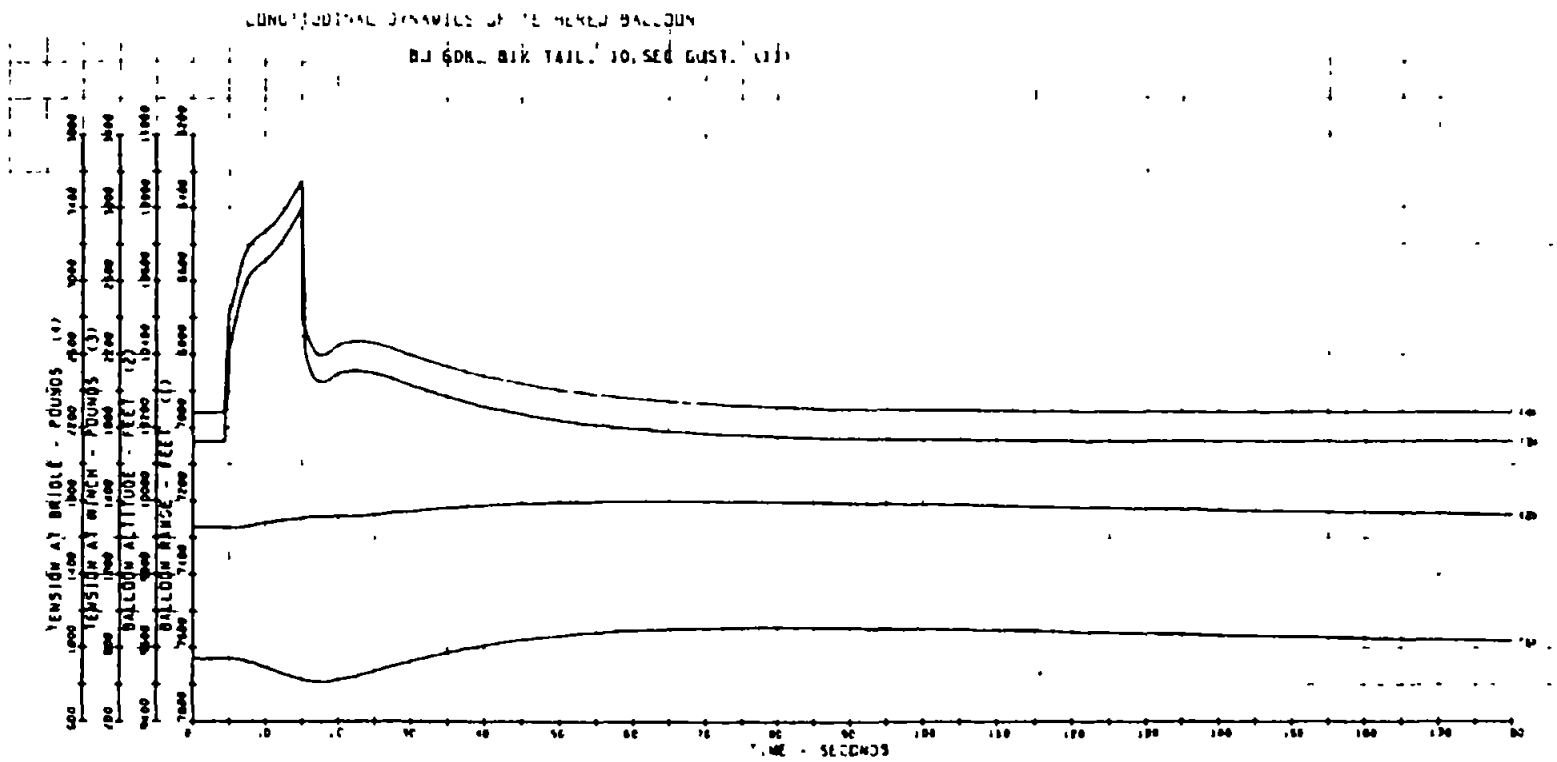
LONGITUDINAL DYNAMICS OF TETHERED BALLOON
TENSION AT BRIDLE - POUNDS
TENSION AT WINCH - POUNDS
BALLOON ALTITUDE - FEET
BALLOON RANGE - FEET
TIME - SECONDS

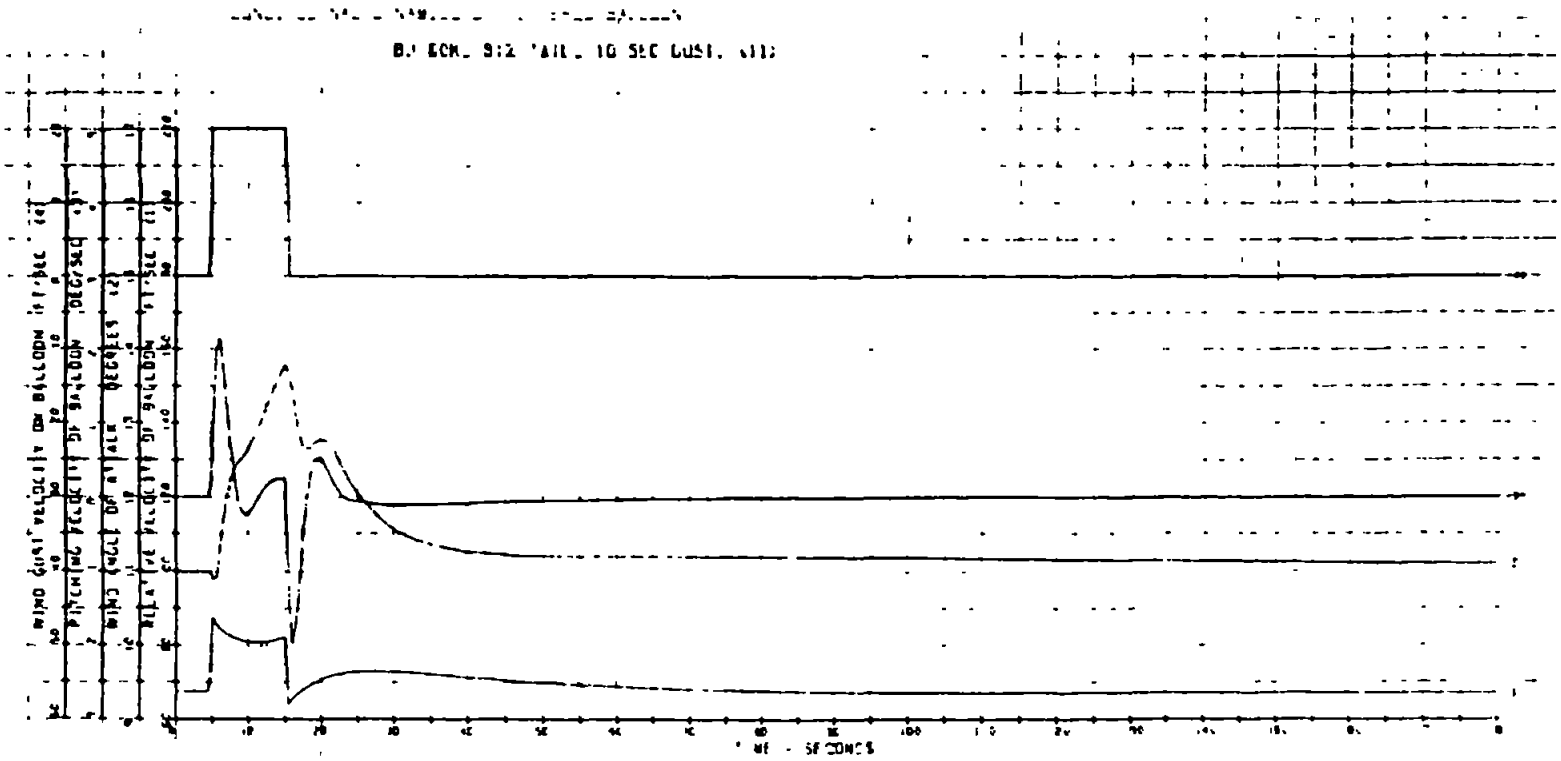
TIME - SECONDS

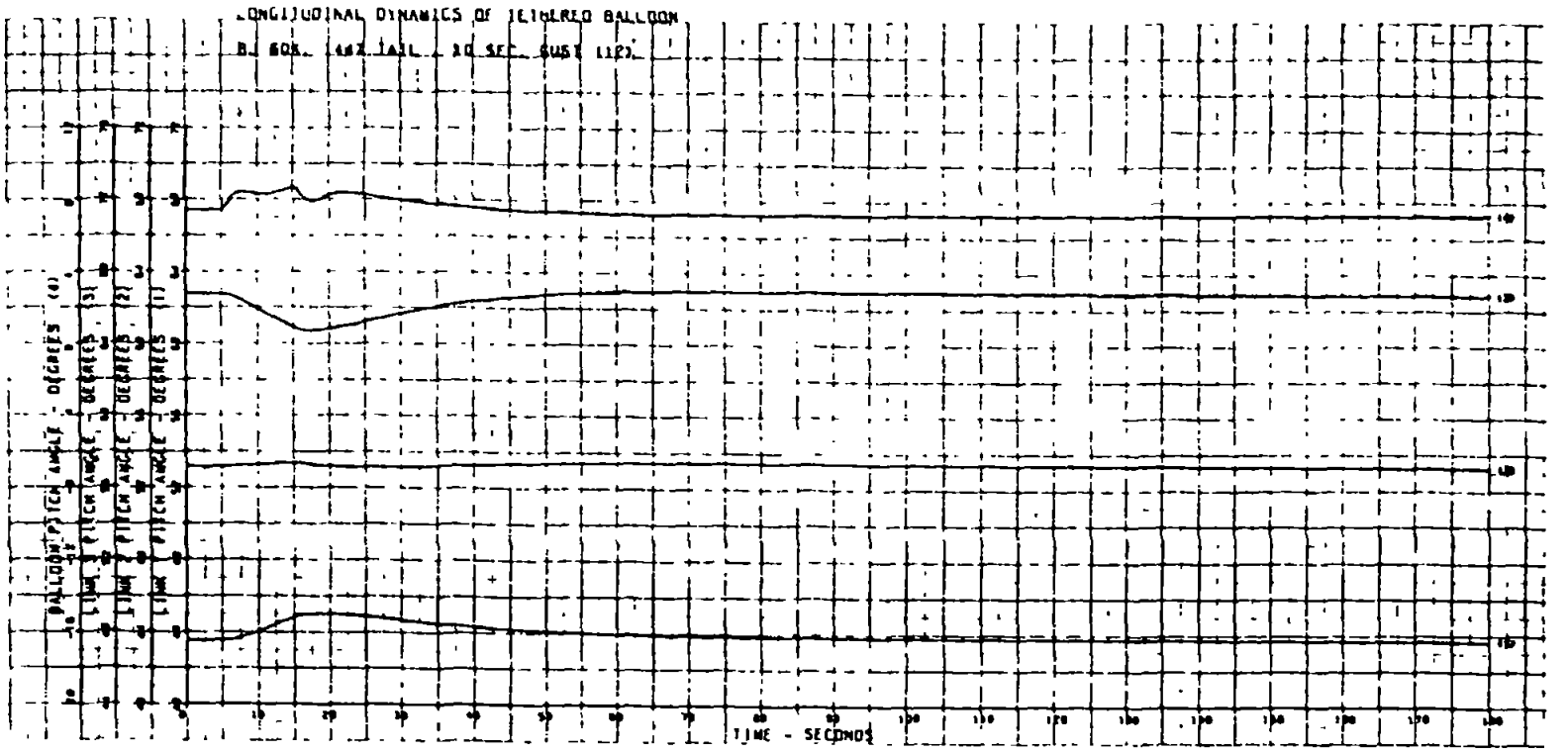
LONGITUDINAL DYNAMICS OF TETHERED BALLOON
TIME - SECONDS

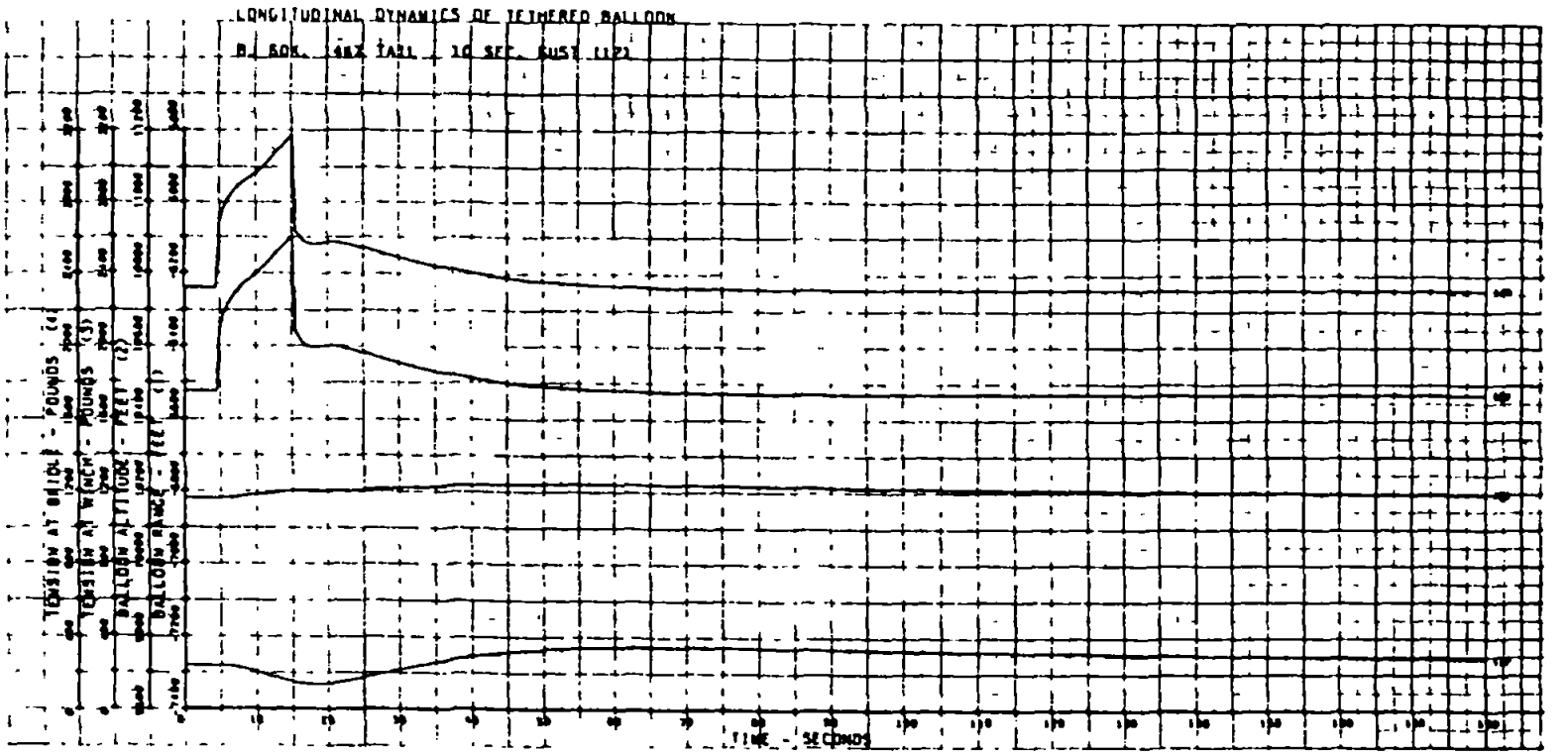
LONGITUDINAL DYNAMICS OF TETHERED BALLOON
TIME - SECONDS

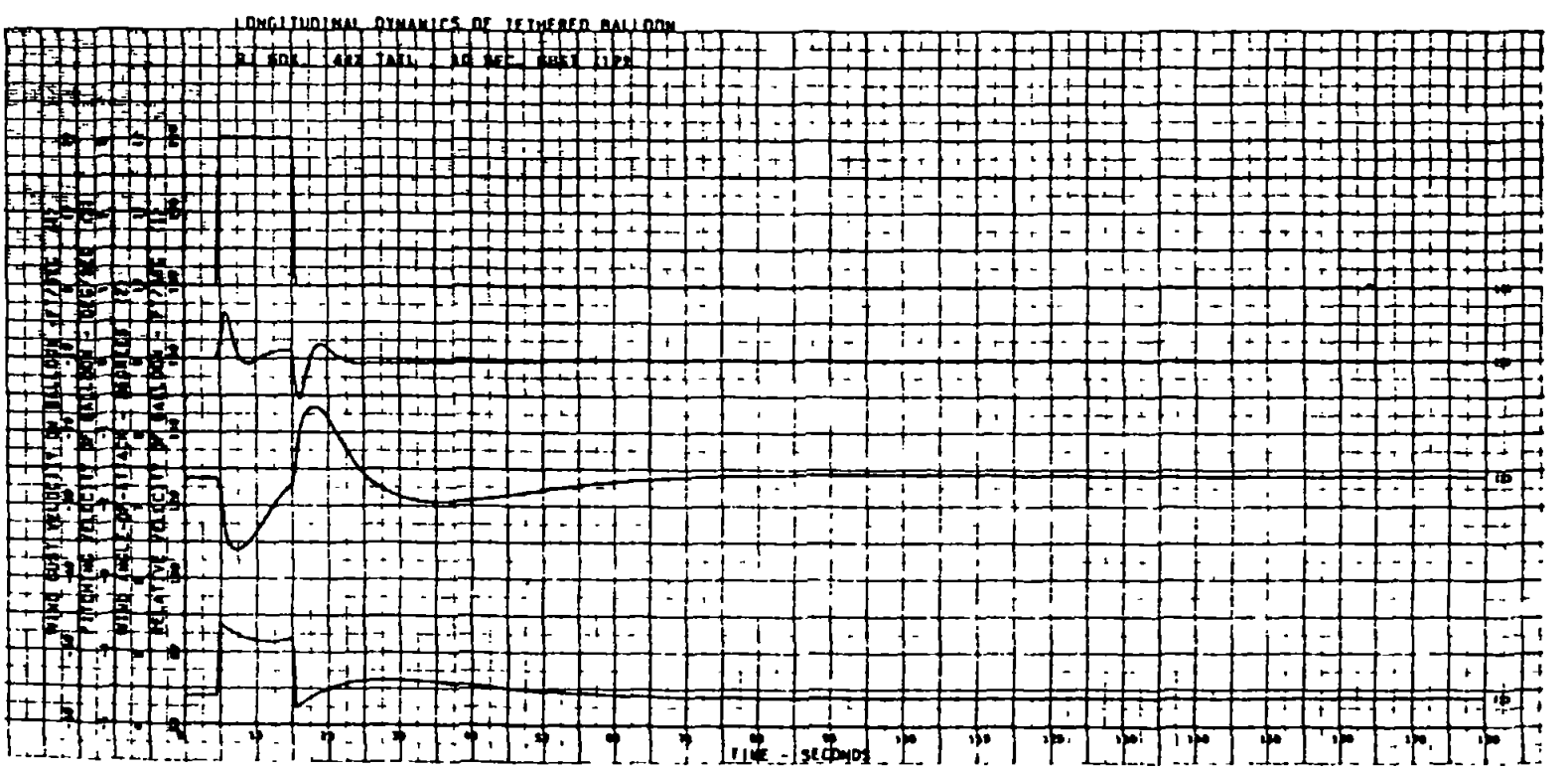
LONGITUDINAL DYNAMICS OF TETHERED BALLOON
TIME - SECONDS

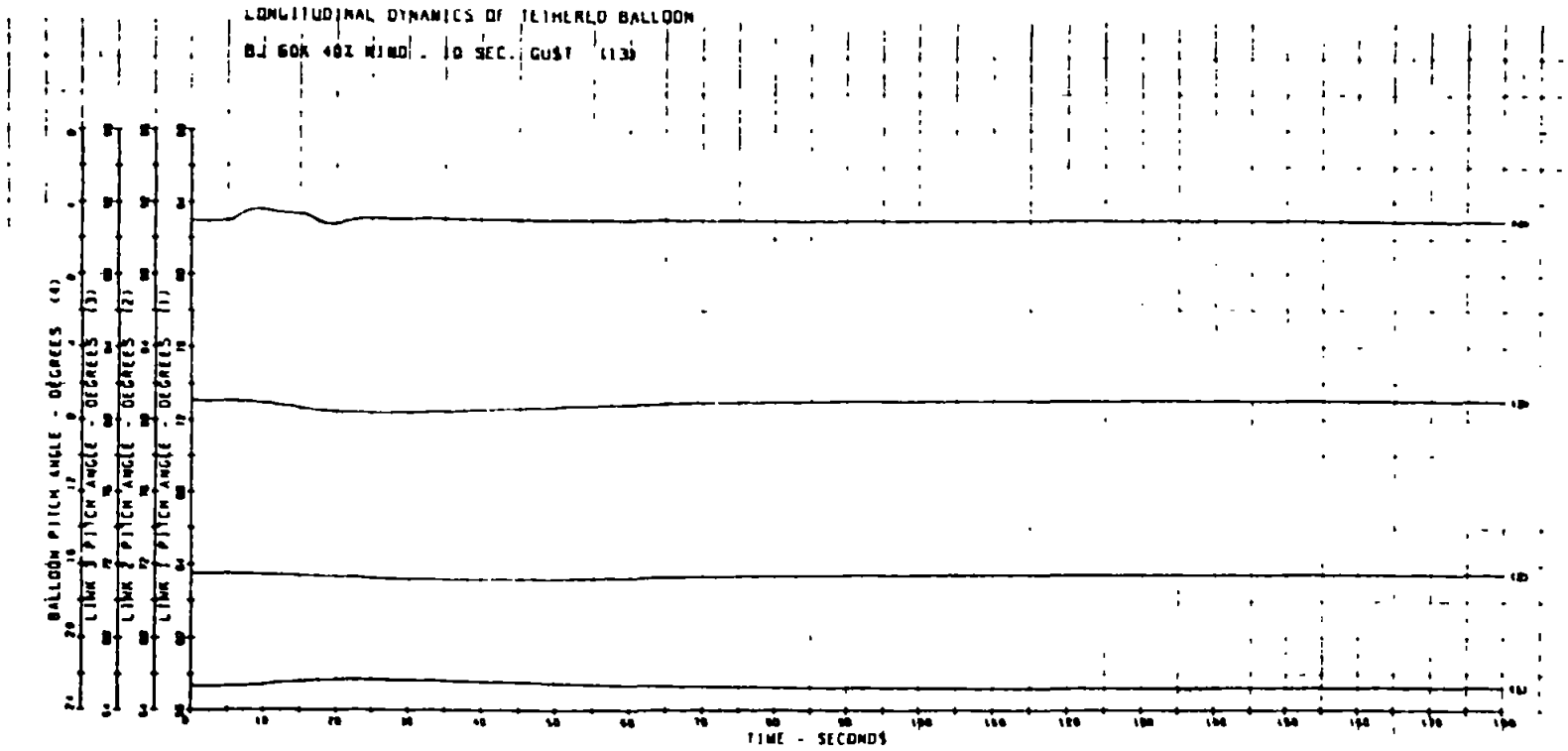
LONGITUDINAL DYNAMICS OF TETHERED BALLOON
BJ 60K 40Z WIND . 10 SEC. GUST (13)
BALLOON PITCH ANGLE - DEGREES (4)
LINK 3 PITCH ANGLE - DEGREES (3)
LINK 2 PITCH ANGLE - DEGREES (2)
LINK 1 PITCH ANGLE - DEGREES (1)
TIME - SECONDS

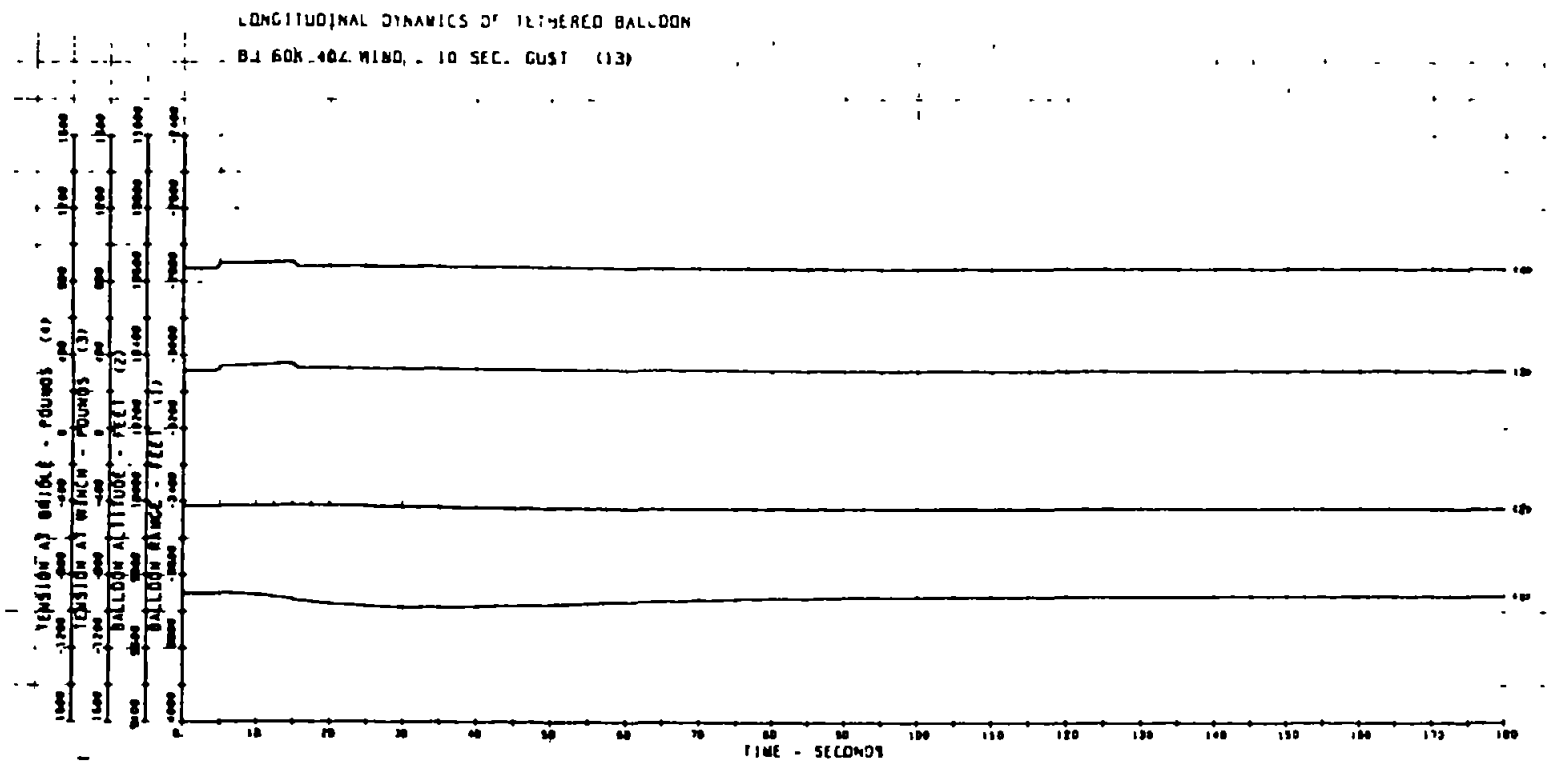
LONGITUDINAL DYNAMICS OF TETHERED BALLOON
BJ 60K 40Z WIND . 10 SEC. GUST (13)
TENSION AT WINCH - POUNDS (3)
BALLOON ALTITUDE - FEET (2)
BALLOON RANGE - FEET (1)
TIME - SECONDS

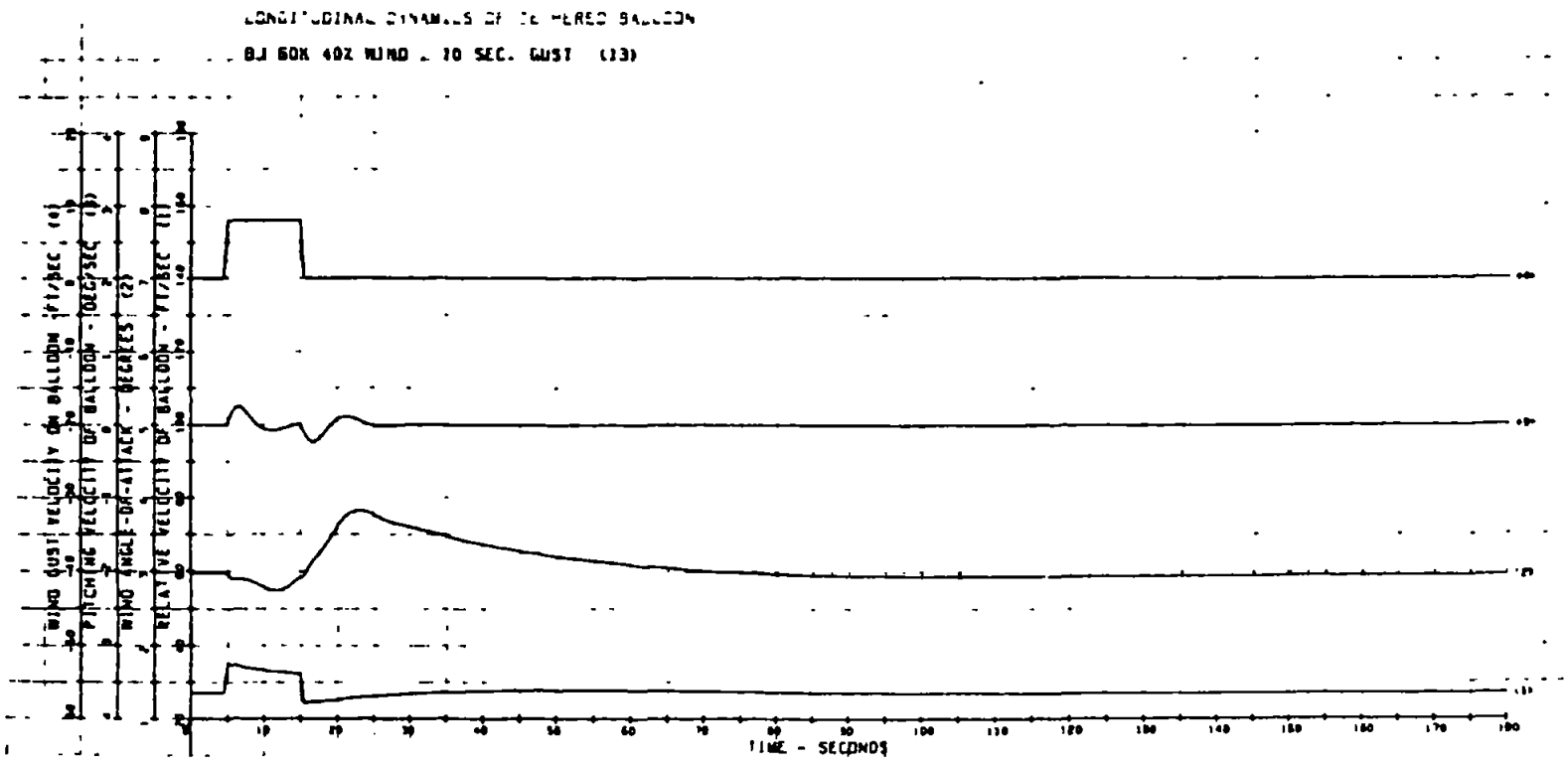
LONGITUDINAL DYNAMICS OF TETHERED BALLOON
BJ 60K 40Z WIND . 10 SEC. GUST (13)
WIND GUST VELOCITY ON BALLOON (FT/SEC) (4)
PITCHING VELOCITY OF BALLOON - DEG/SEC (3)
WIND ANGLE-OF-ATTACK - DEGREES (2)
RELATIVE VELOCITY OF BALLOON - FT/SEC (1)
TIME - SECONDS

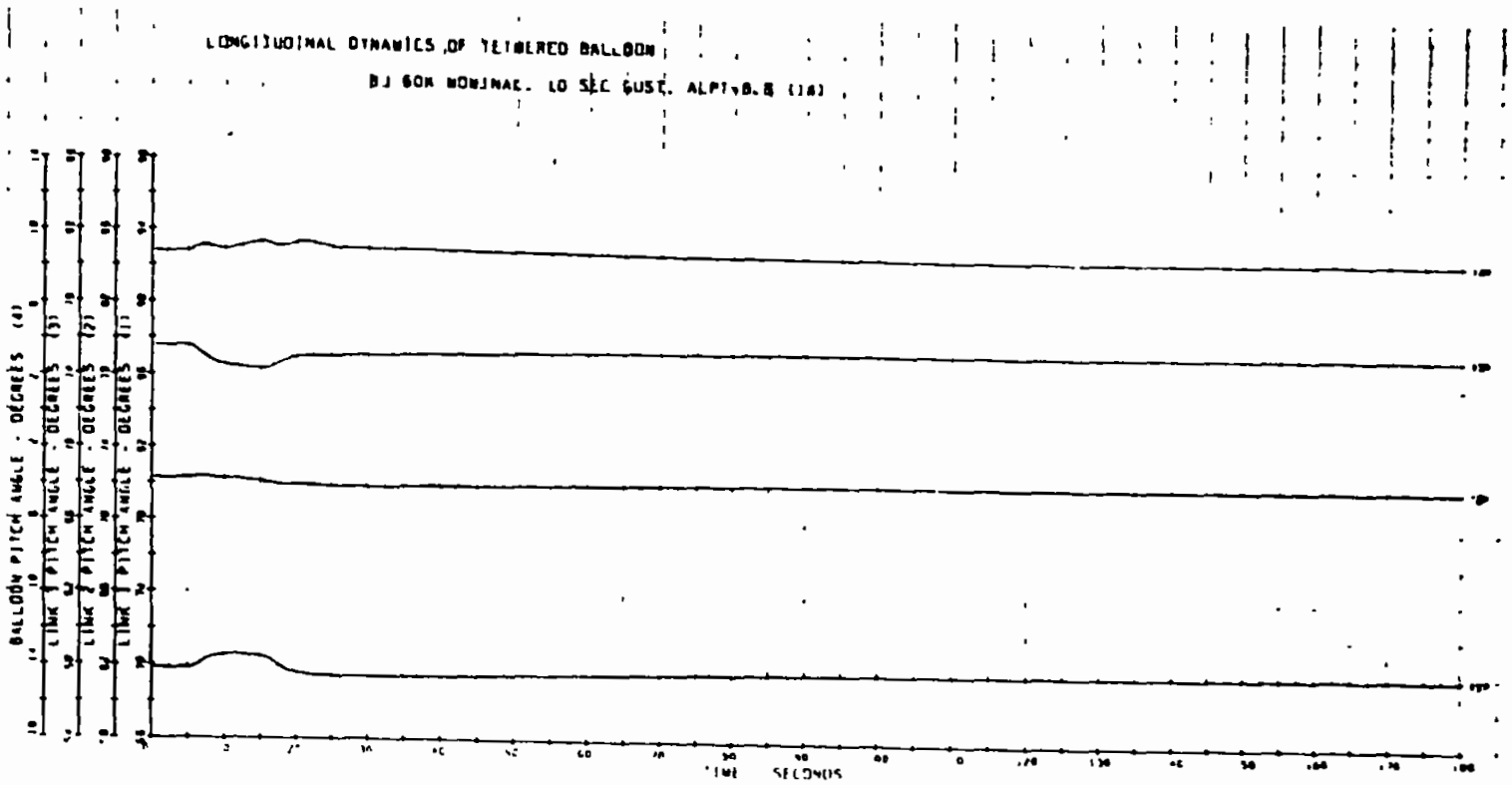
LONGITUDINAL DYNAMICS OF TETHERED BALLOON
BALLOON PITCH ANGLE - DEGREES
TIME - SECONDS

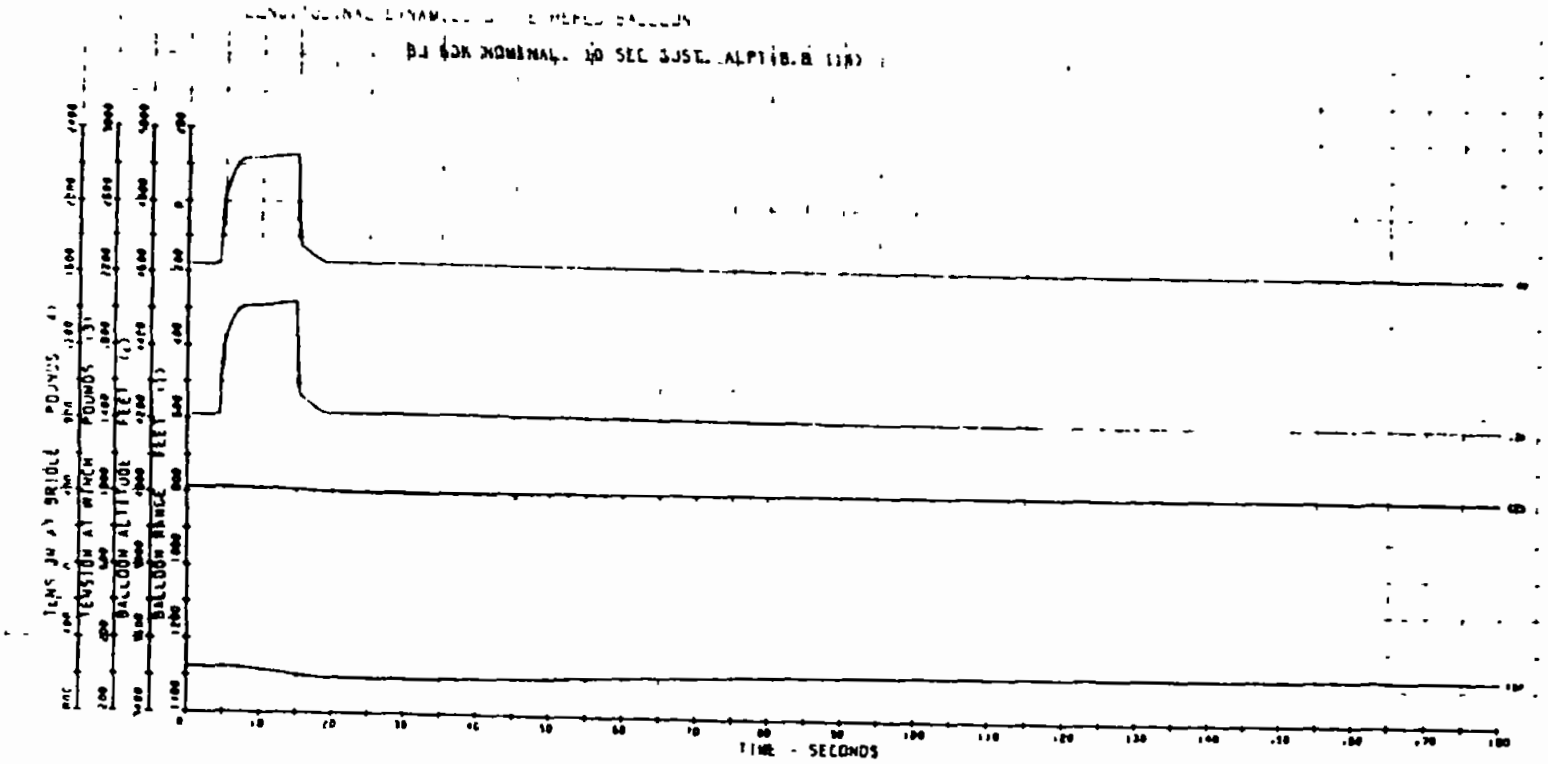
TIME - SECONDS

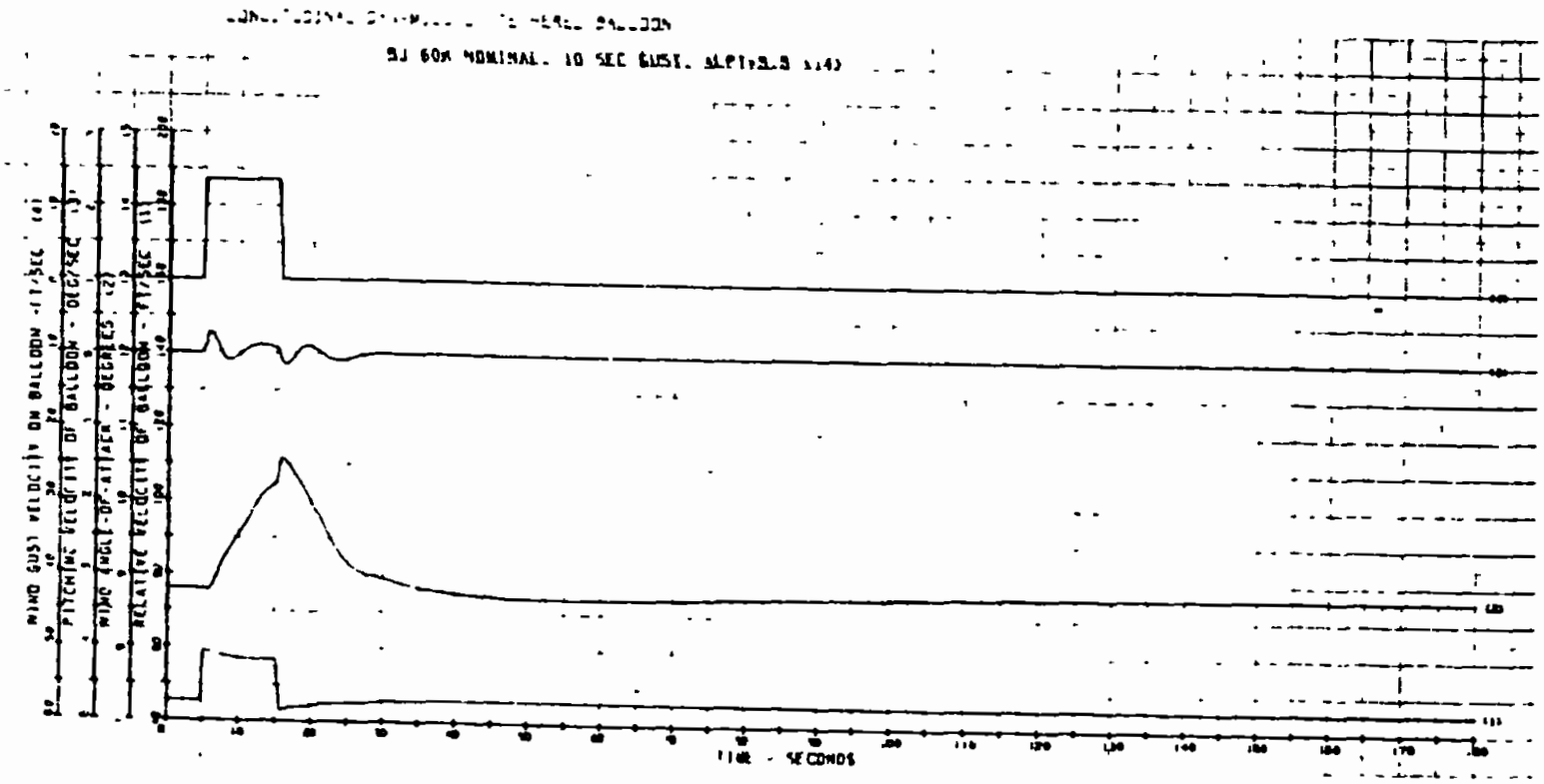
TIME - SECONDS

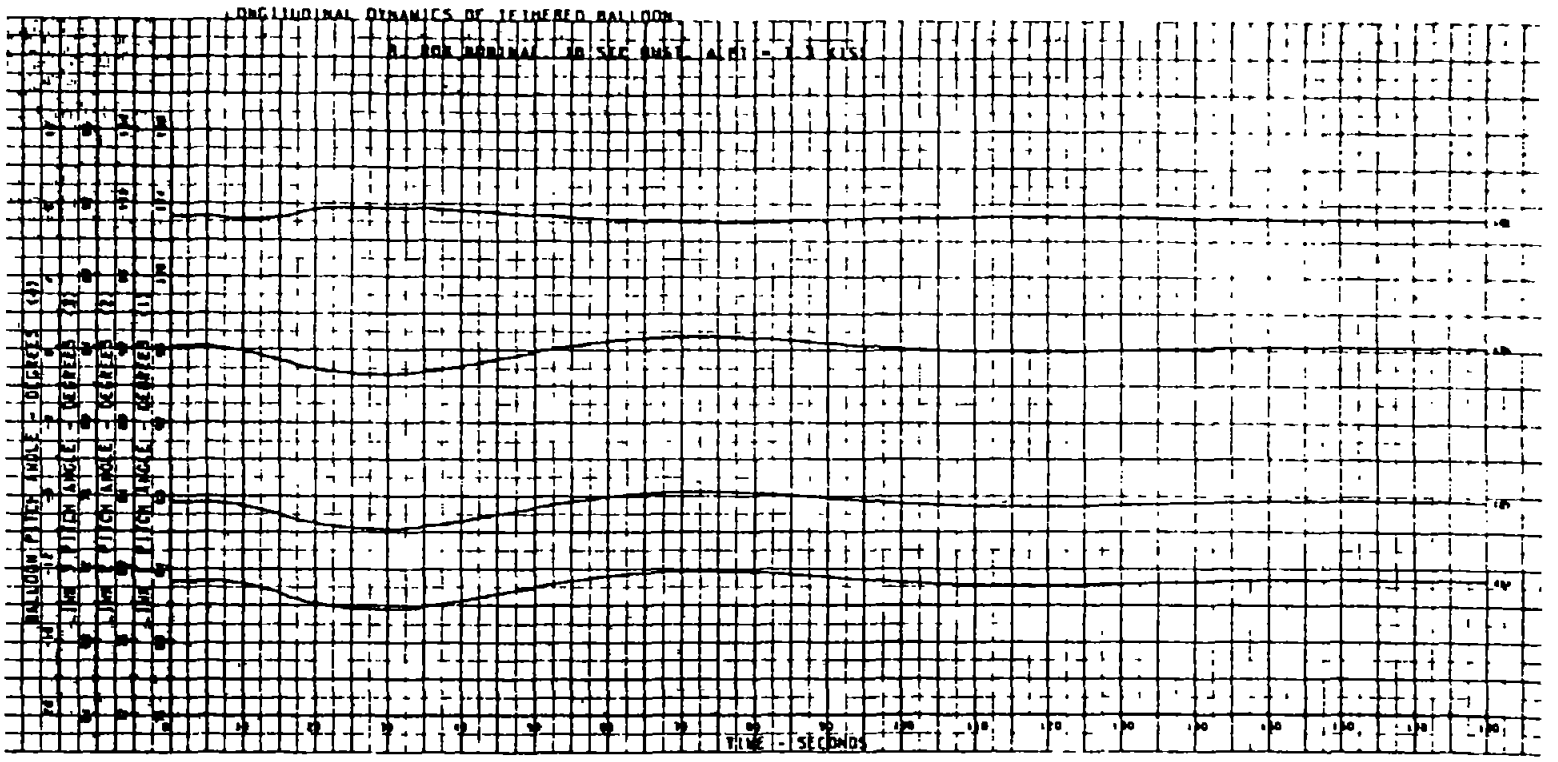
LONGITUDINAL DYNAMICS OF TETHERED BALLOON
TIME - SECONDS

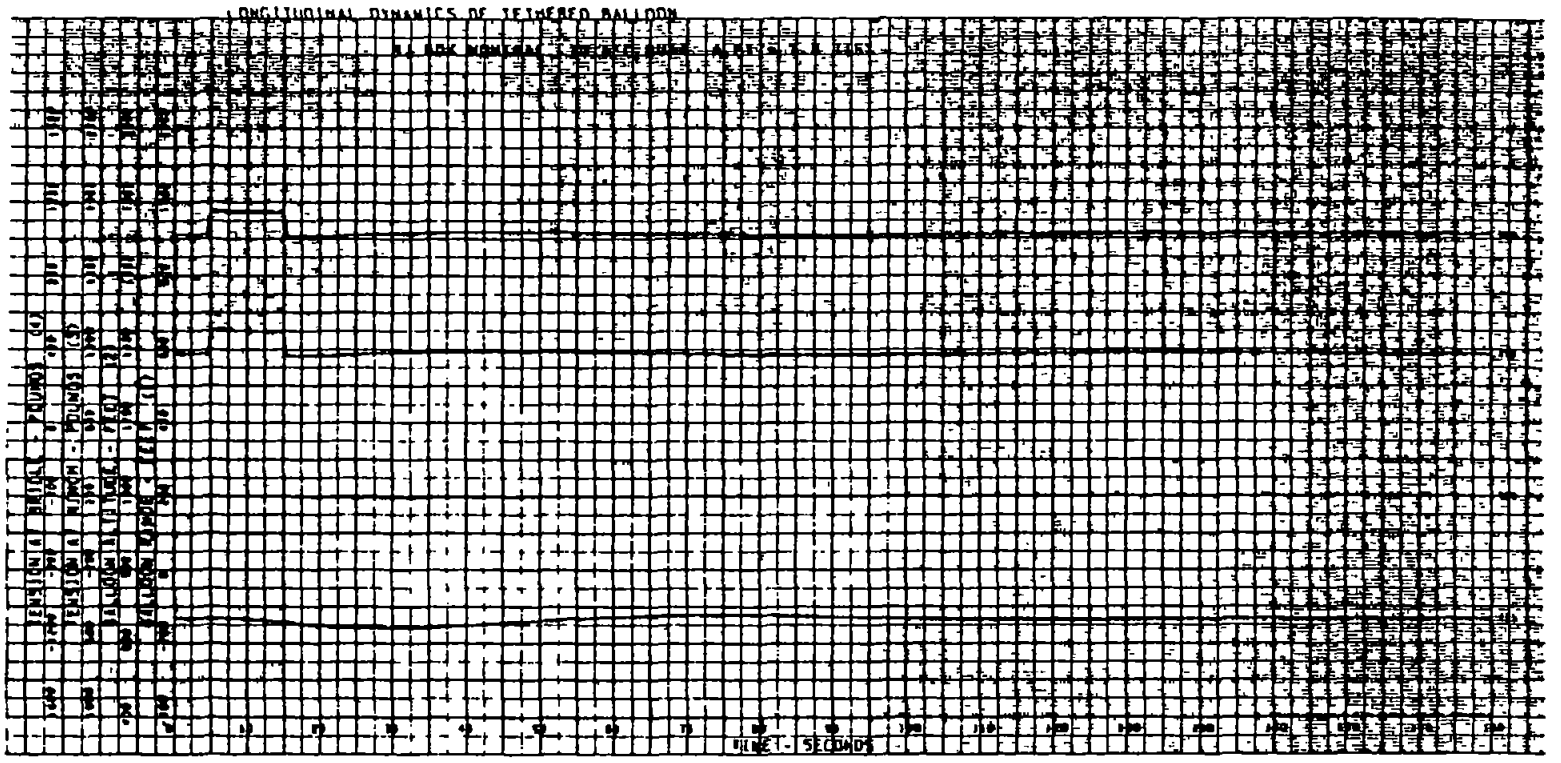
LONGITUDINAL DYNAMICS OF TETHERED BALLOON
TIME - SECONDS

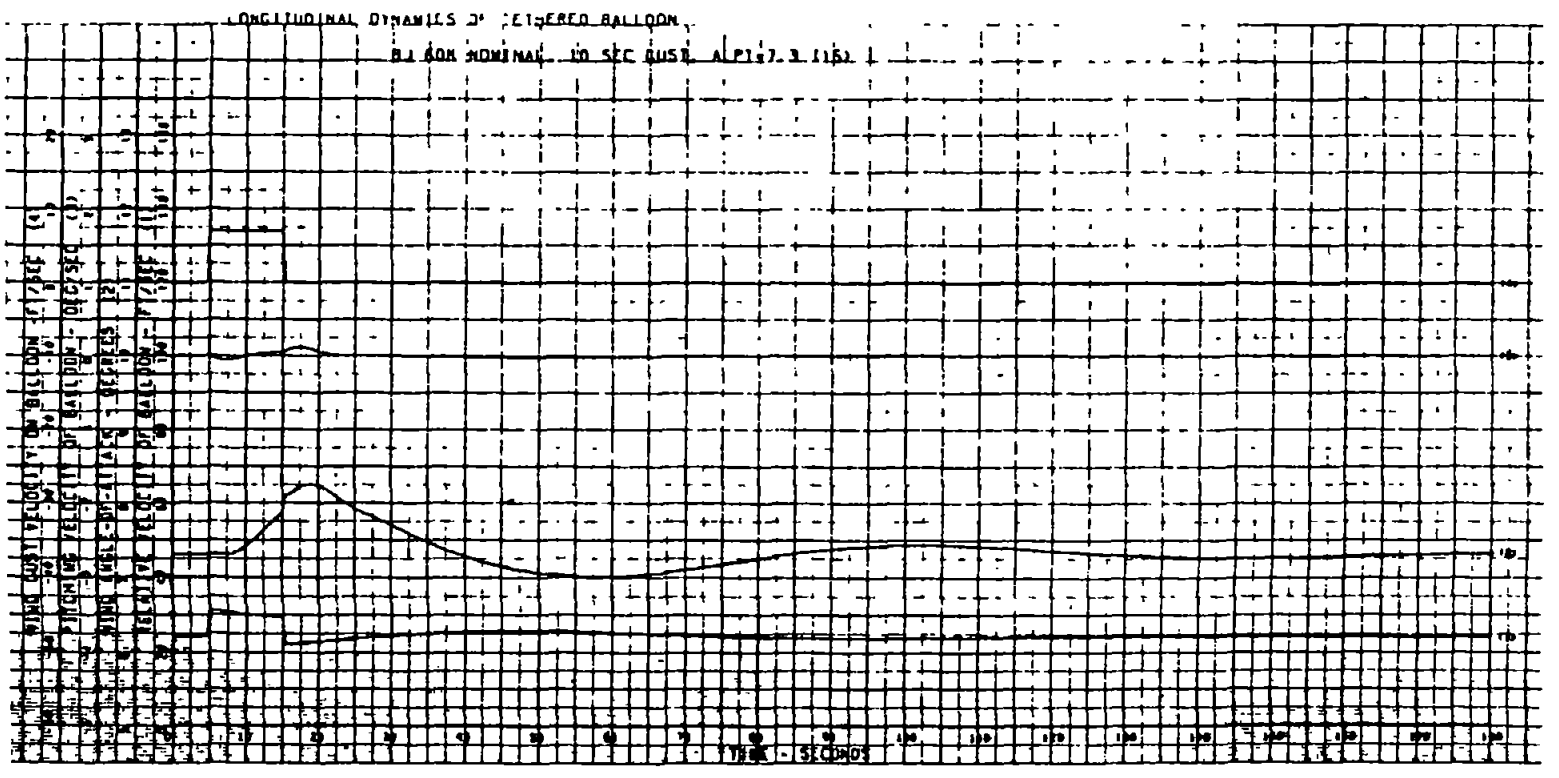
LONGITUDINAL DYNAMICS OF TETHERED BALLOON
TIME - SECONDS

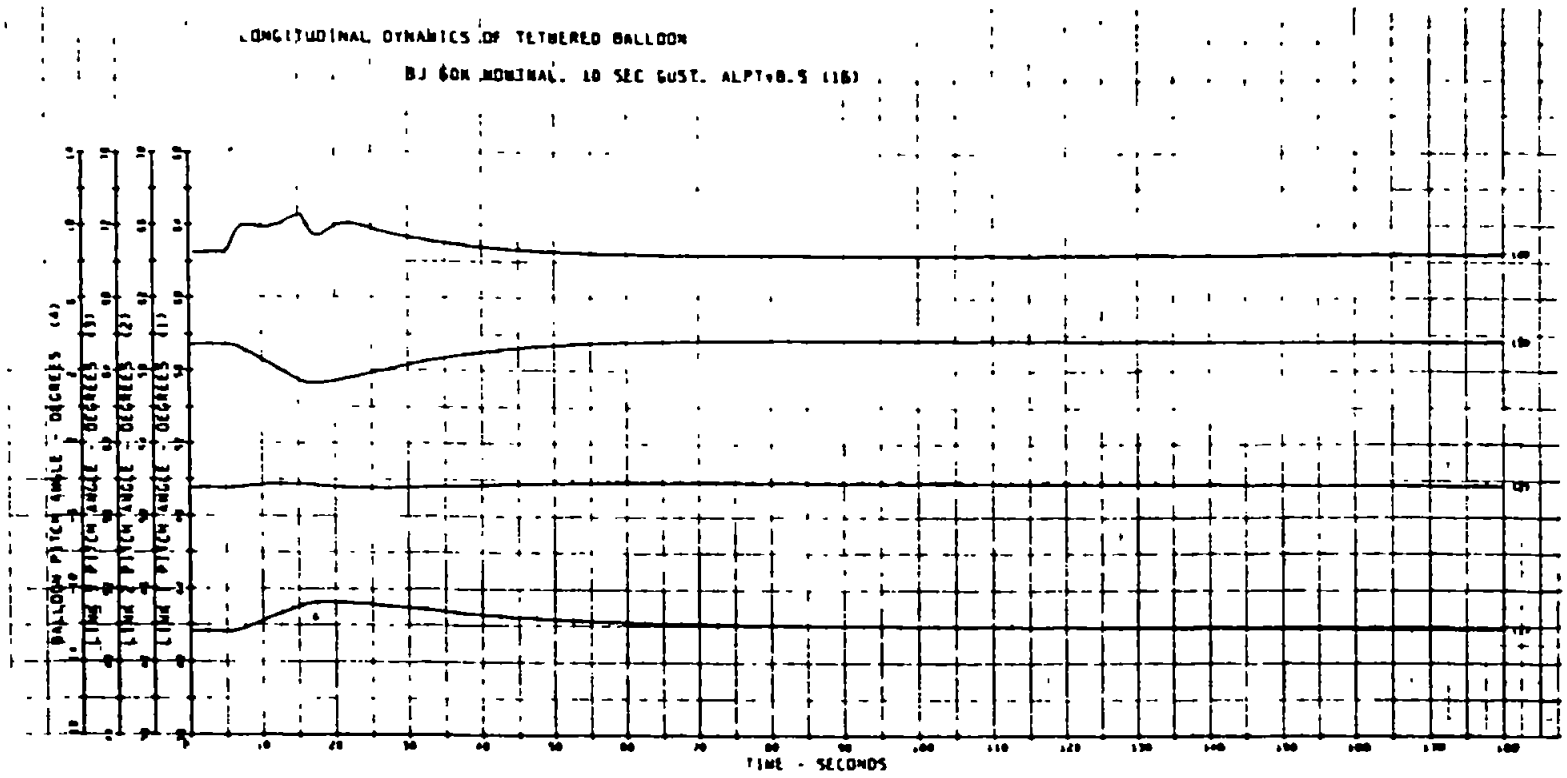
LONGITUDINAL DYNAMICS OF TETHERED BALLOON
BJ 60K NOMINAL. 10 SEC GUST. ALPT=8.5 (16)
BALLOON PITCH ANGLE - DEGREES (4)
LINE PITCH ANGLE - DEGREES (3)
LINE PITCH ANGLE - DEGREES (2)
LINE PITCH ANGLE - DEGREES (1)
TIME - SECONDS

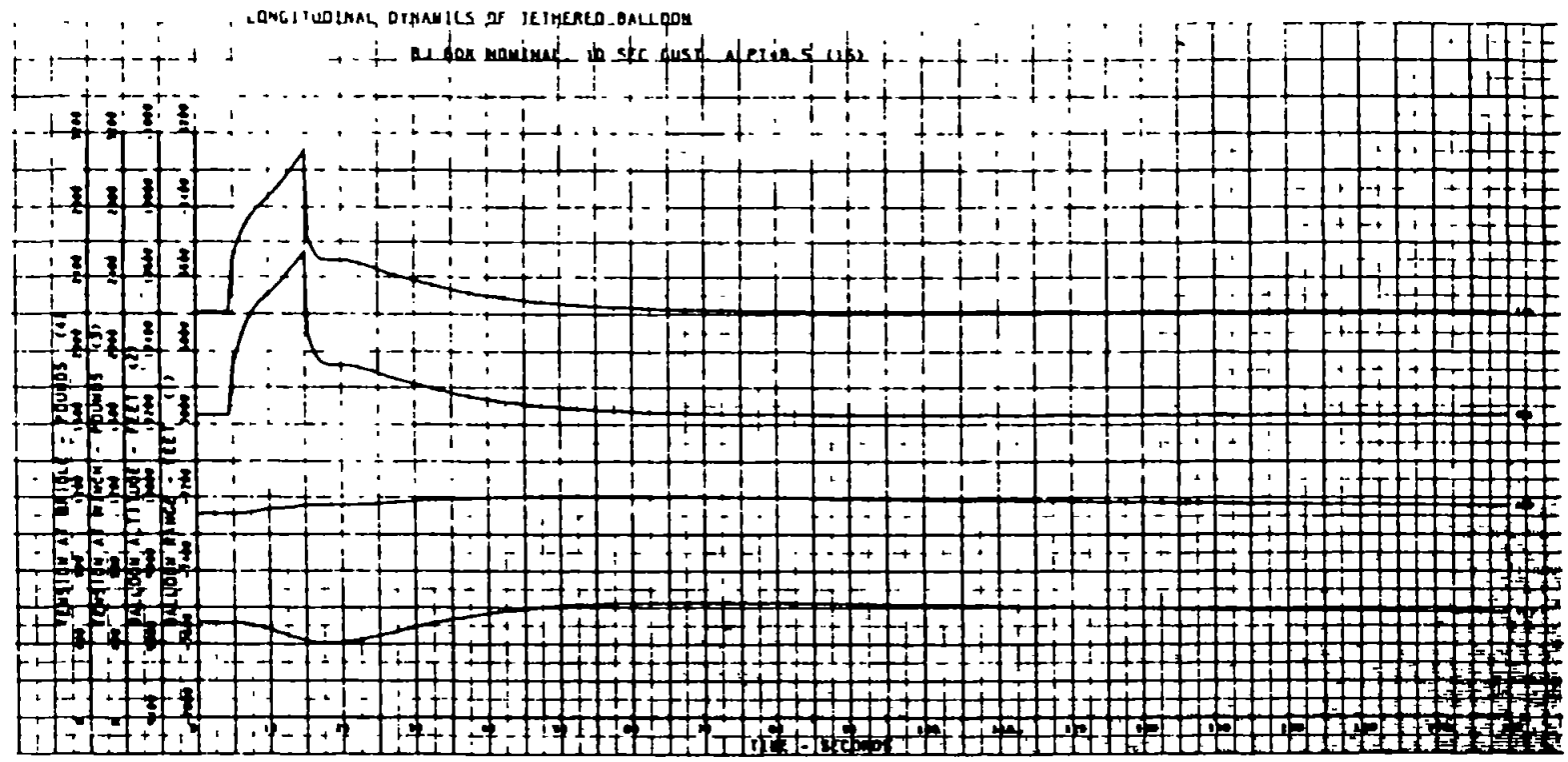
LONGITUDINAL DYNAMICS OF TETHERED BALLOON
BJ 60K NOMINAL. 10 SEC GUST. ALPT=8.5 (16)
TENSION AT BUOYL - POUNDS (4)
TENSION AT WINCH - POUNDS (3)
BALLOON ALTITUDE - FEET (2)
BALLOON RANGE - FEET (1)
TIME - SECONDS

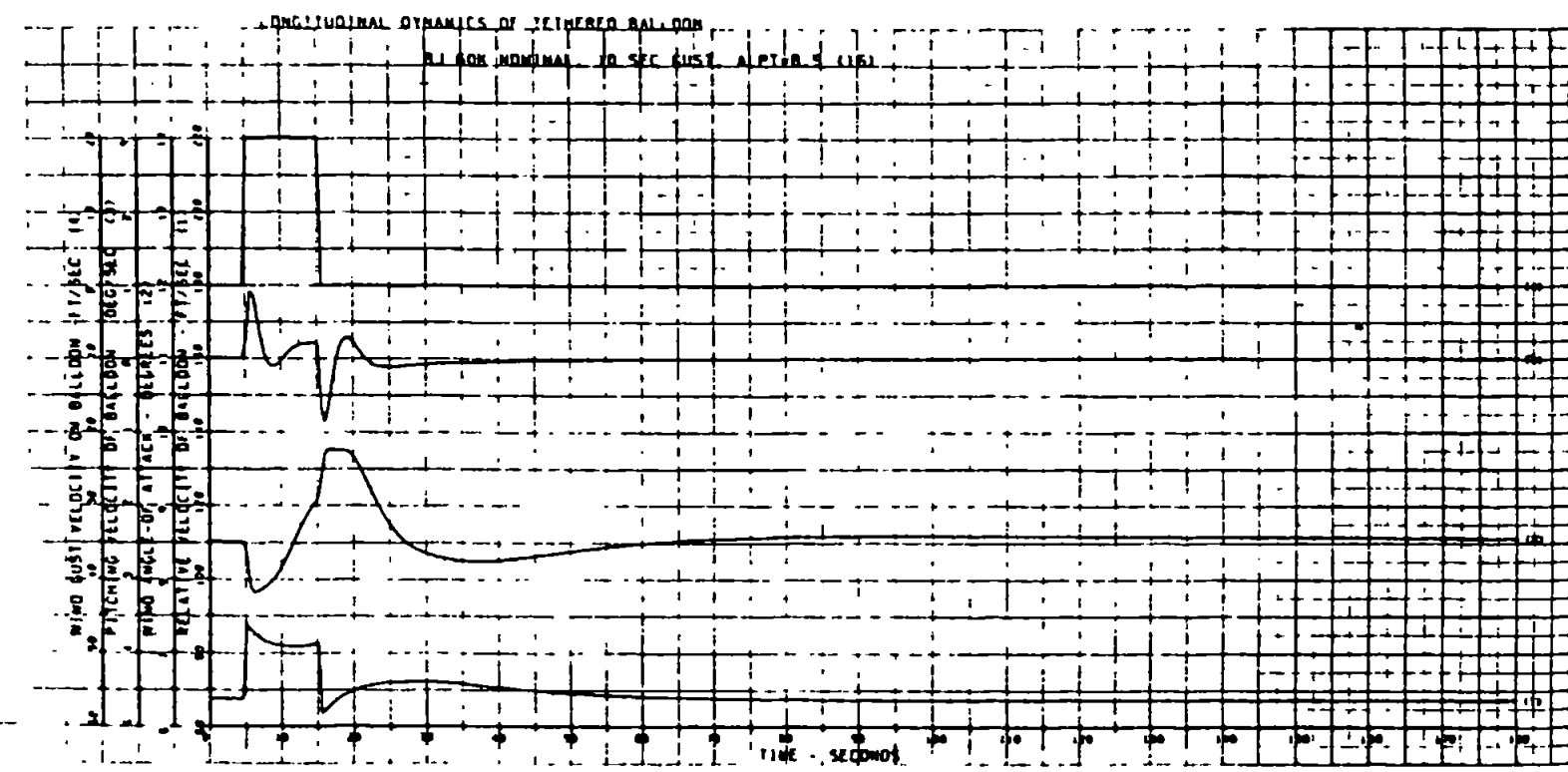
LONGITUDINAL DYNAMICS OF TETHERED BALLOON
BJ 60K NOMINAL. 10 SEC GUST. ALPT=8.5 (16)
WIND GUST VELOCITY ON BALLOON - FT/SEC (4)
PITCHING VELOCITY OF BALLOON - DEG/SEC (3)
WIND ANGLE-OF-ATTACK - DEGREES (2)
RELATIVE VELOCITY OF BALLOON - FT/SEC (1)
TIME - SECONDS

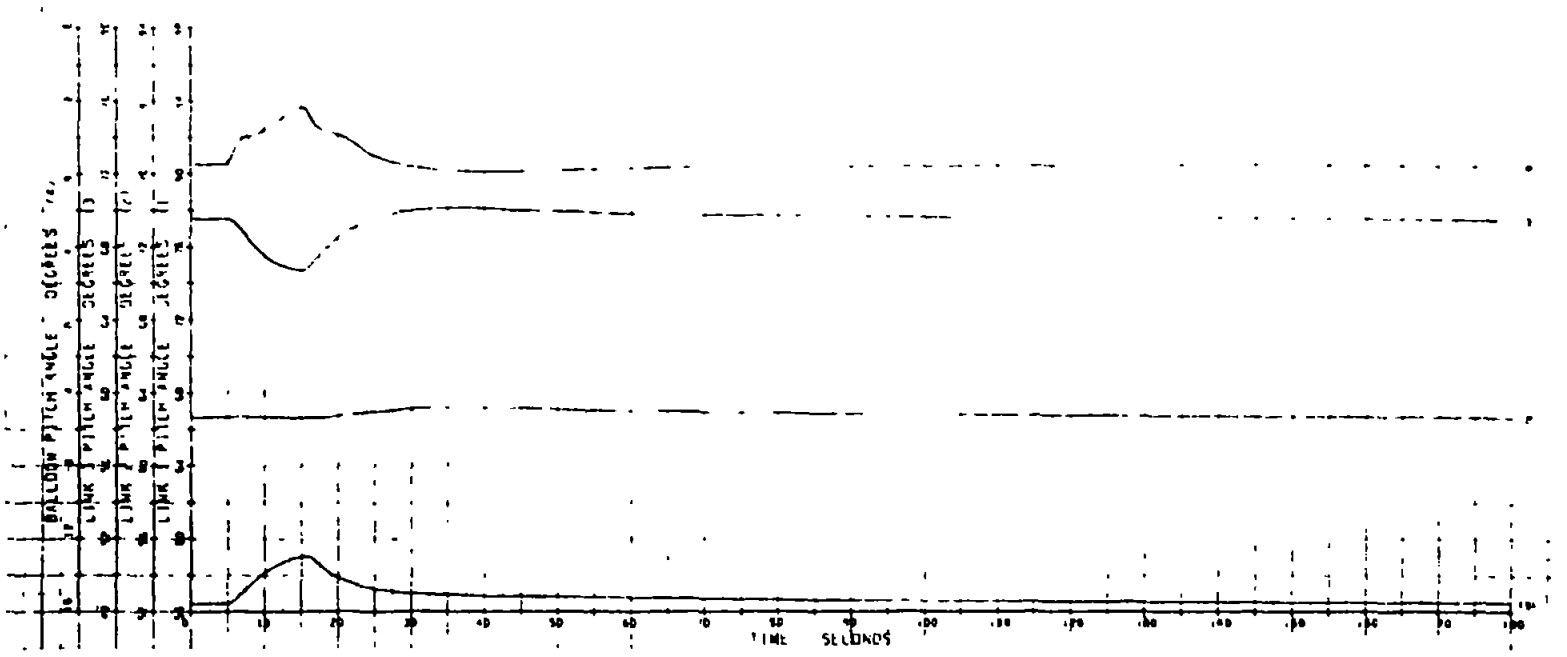

LONGITUDINAL DYNAMICS OF TETHERED BALLOON
BJ 60K WINCH AT SK , 10 SEC. GUST (17)

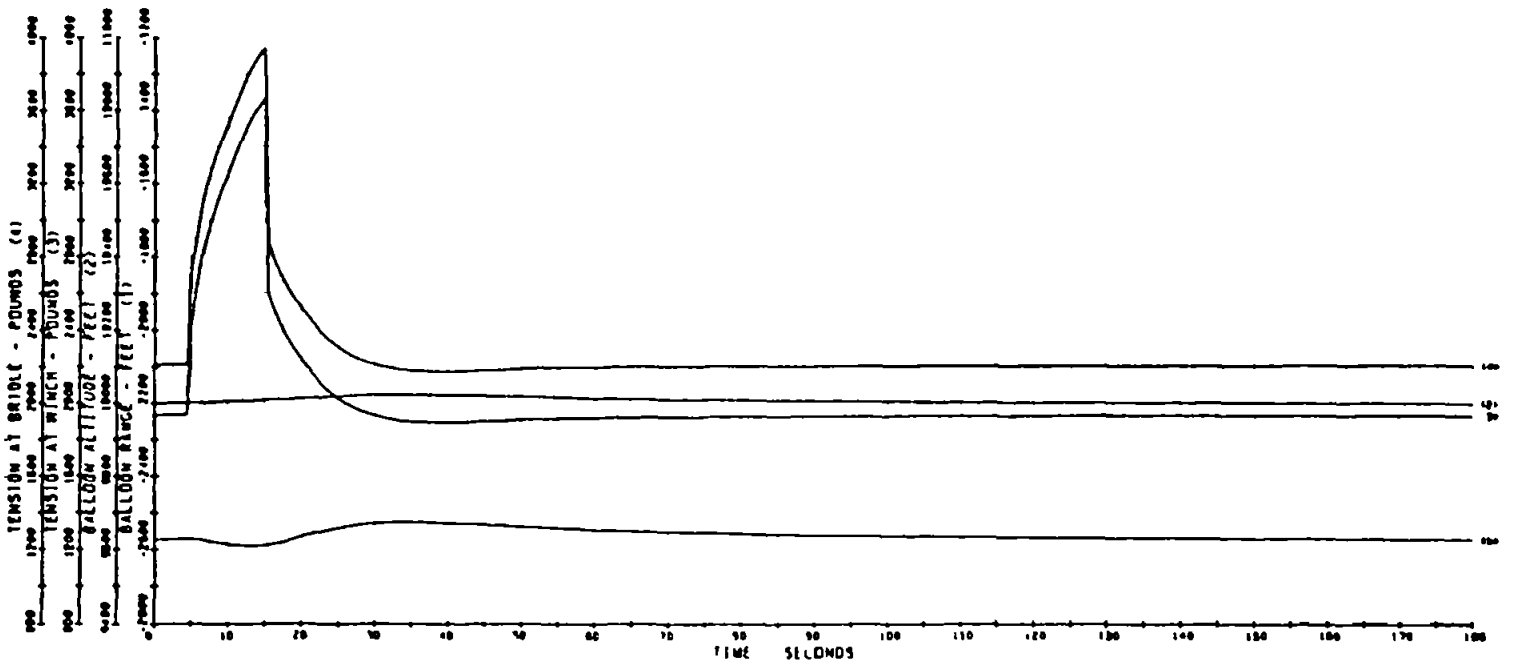

LONGITUDINAL DYNAMICS OF TETHERED BALLOON
BJ 60K WINCH AT SK , 10 SEC. GUST (17)

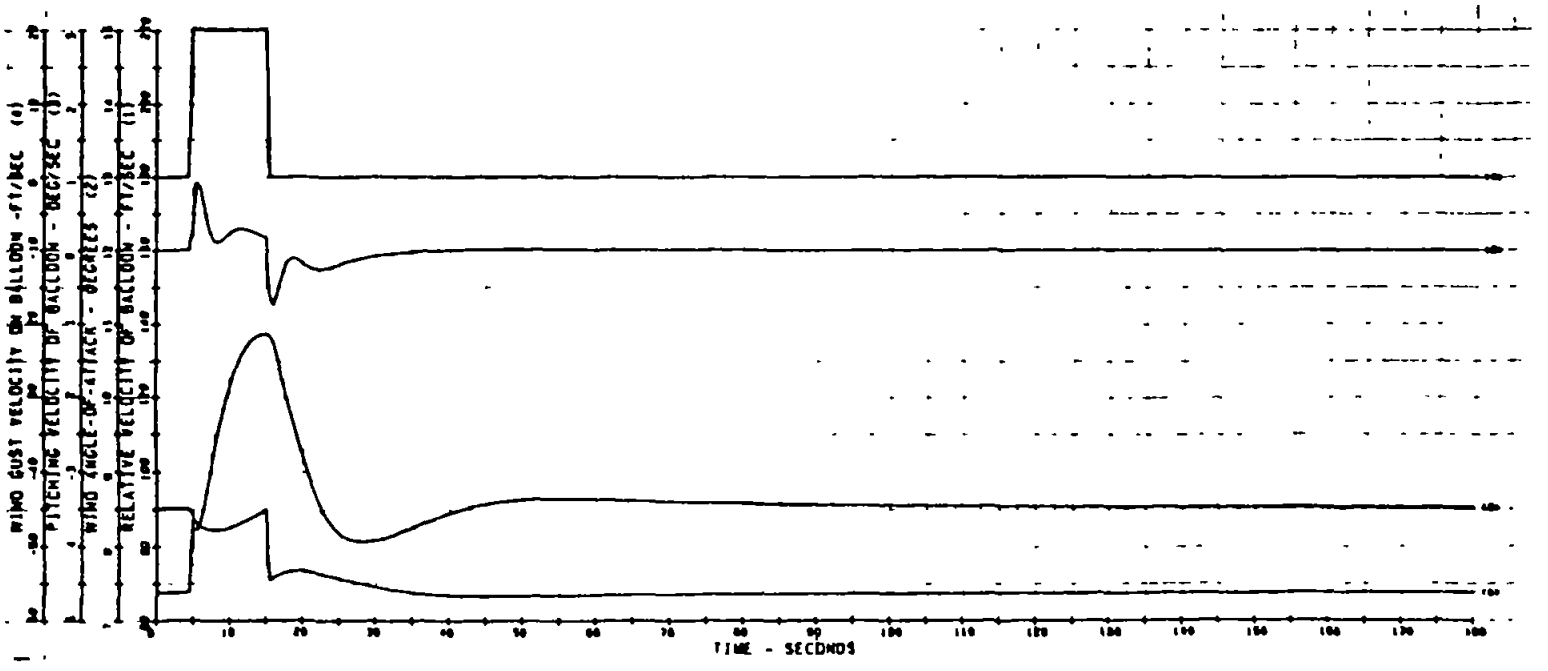

LONGITUDINAL DYNAMICS OF TETHERED BALLOON

VEE BOX. 10 SEC GUST. ALPT=7 (18)

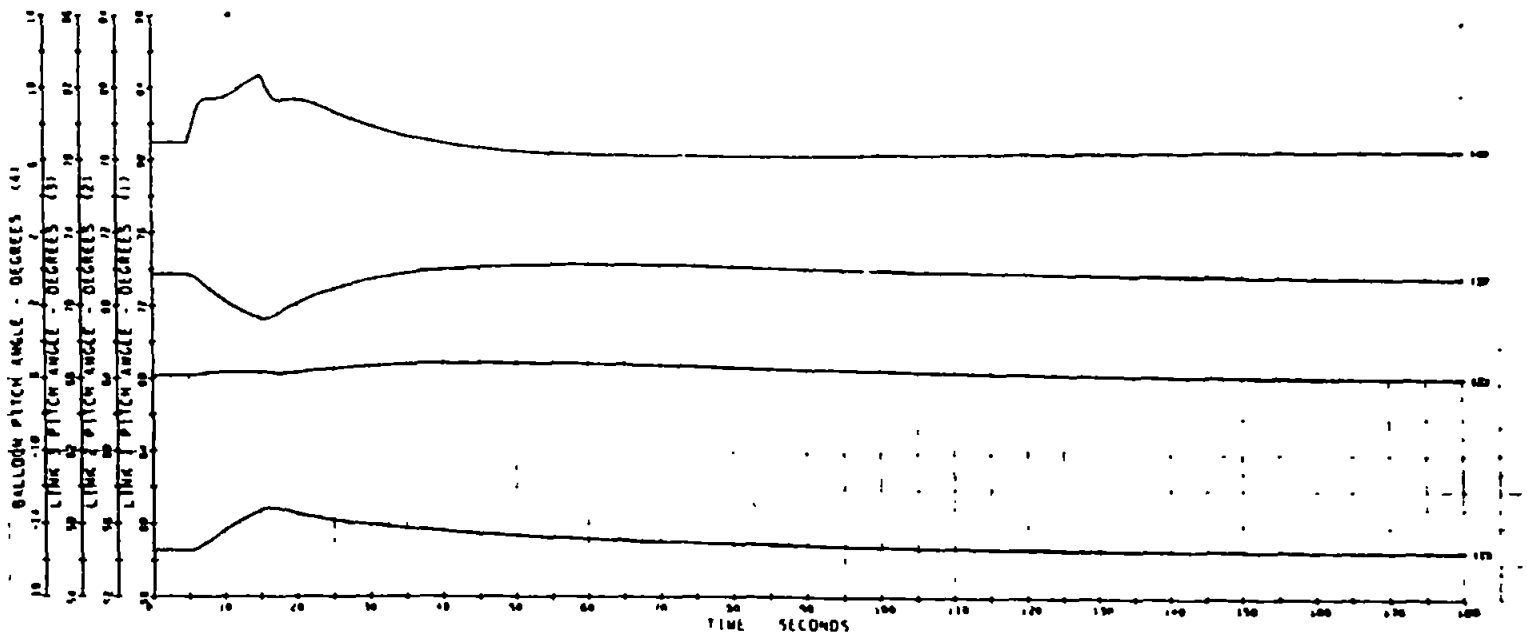

LONGITUDINAL DYNAMICS OF TETHERED BALLOON

VEE BOX. 10 SEC GUST. ALPT=7. (18)

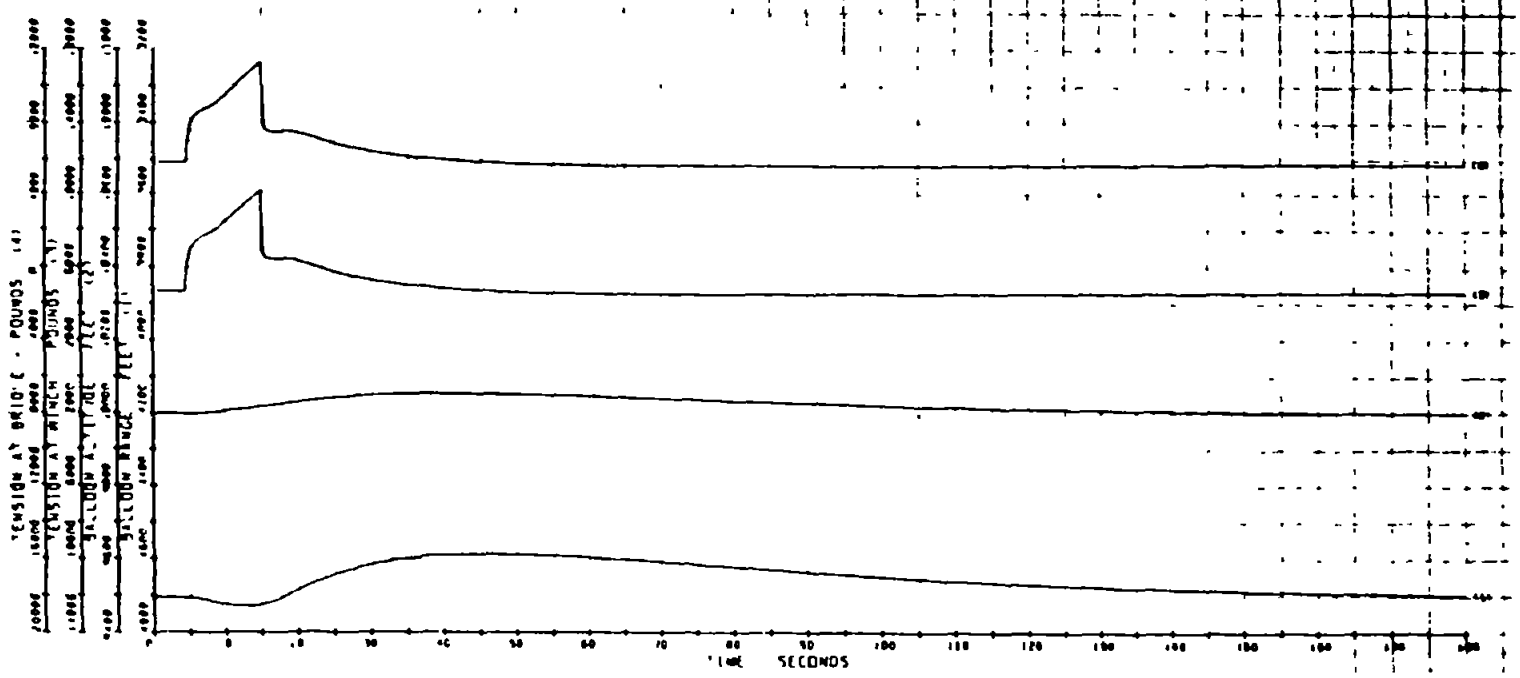

LONGITUDINAL DYNAMICS OF TETHERED BALLOON

VEE BOX. 10 SEC GUST. ALPT = 7 (18)

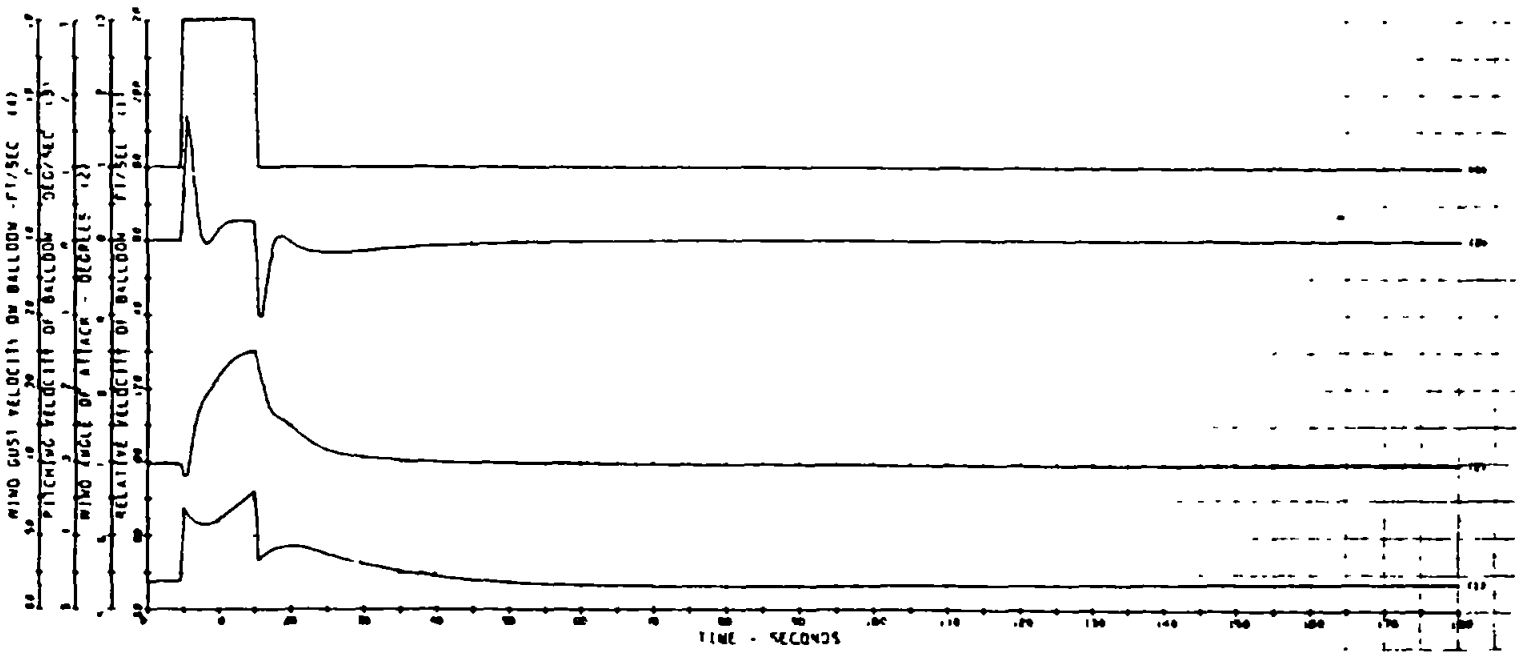

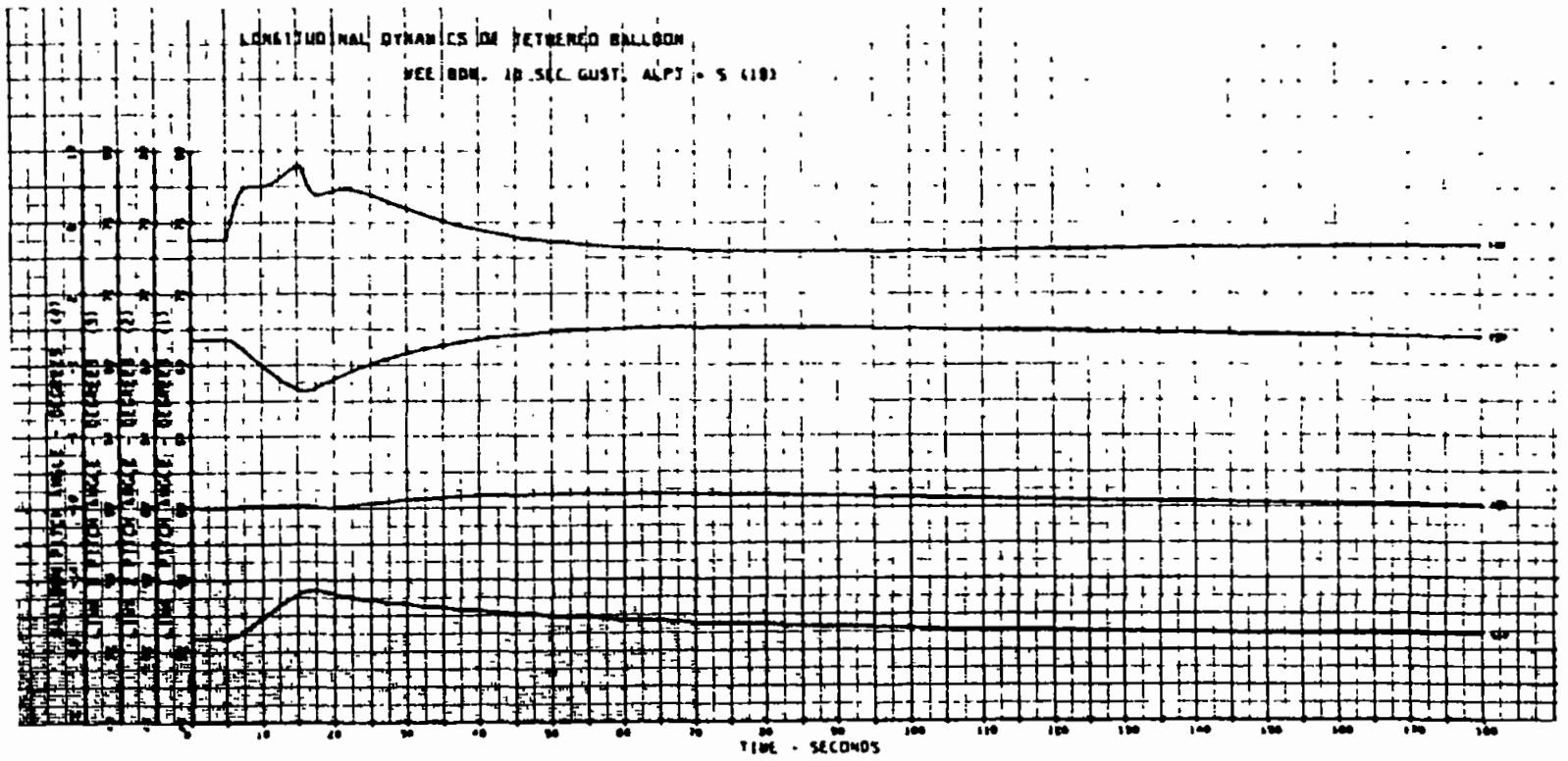
LONGITUDINAL DYNAMICS OF TETHERED BALLOON
WEE BOK. 10 SEC GUST. ALPT = 5 (10)
TIME - SECONDS

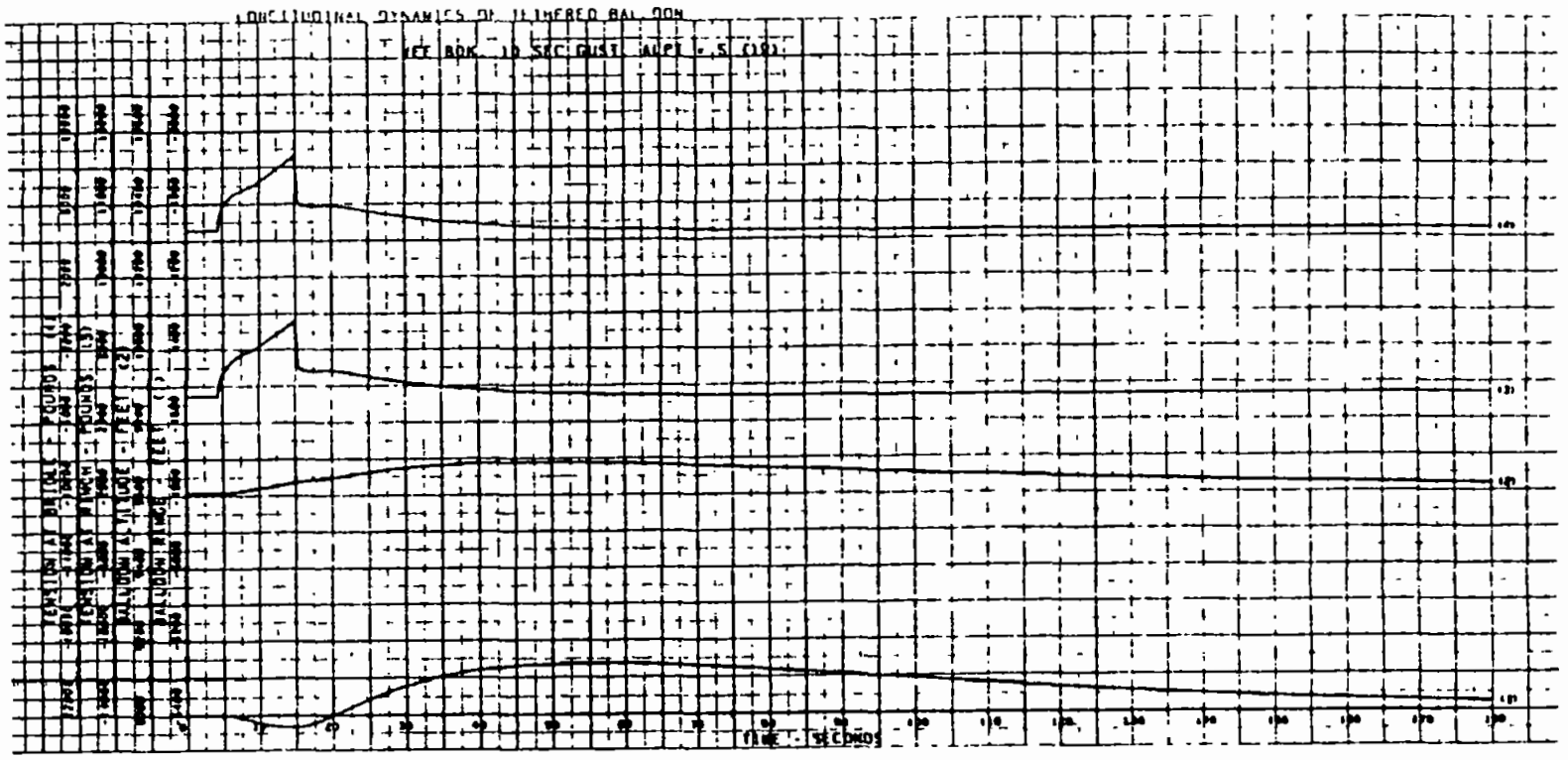
LONGITUDINAL DYNAMICS OF TETHERED BALLOON
WEE BOK. 10 SEC GUST. ALPT = 5 (10)
TIME - SECONDS

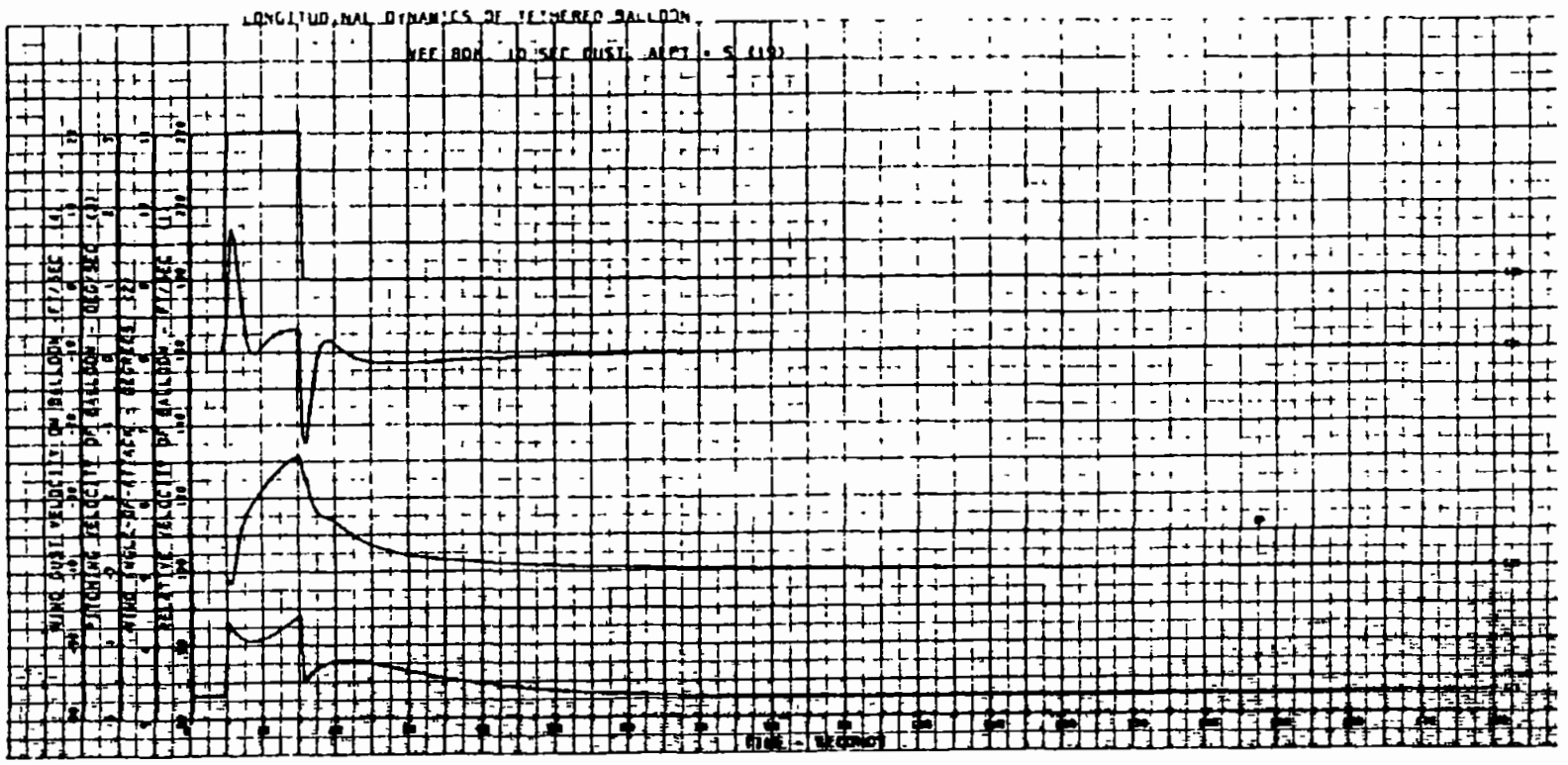
LONGITUDINAL DYNAMICS OF TETHERED BALLOON
WEE BOK. 10 SEC GUST. ALPT = 5 (10)
TIME - SECONDS

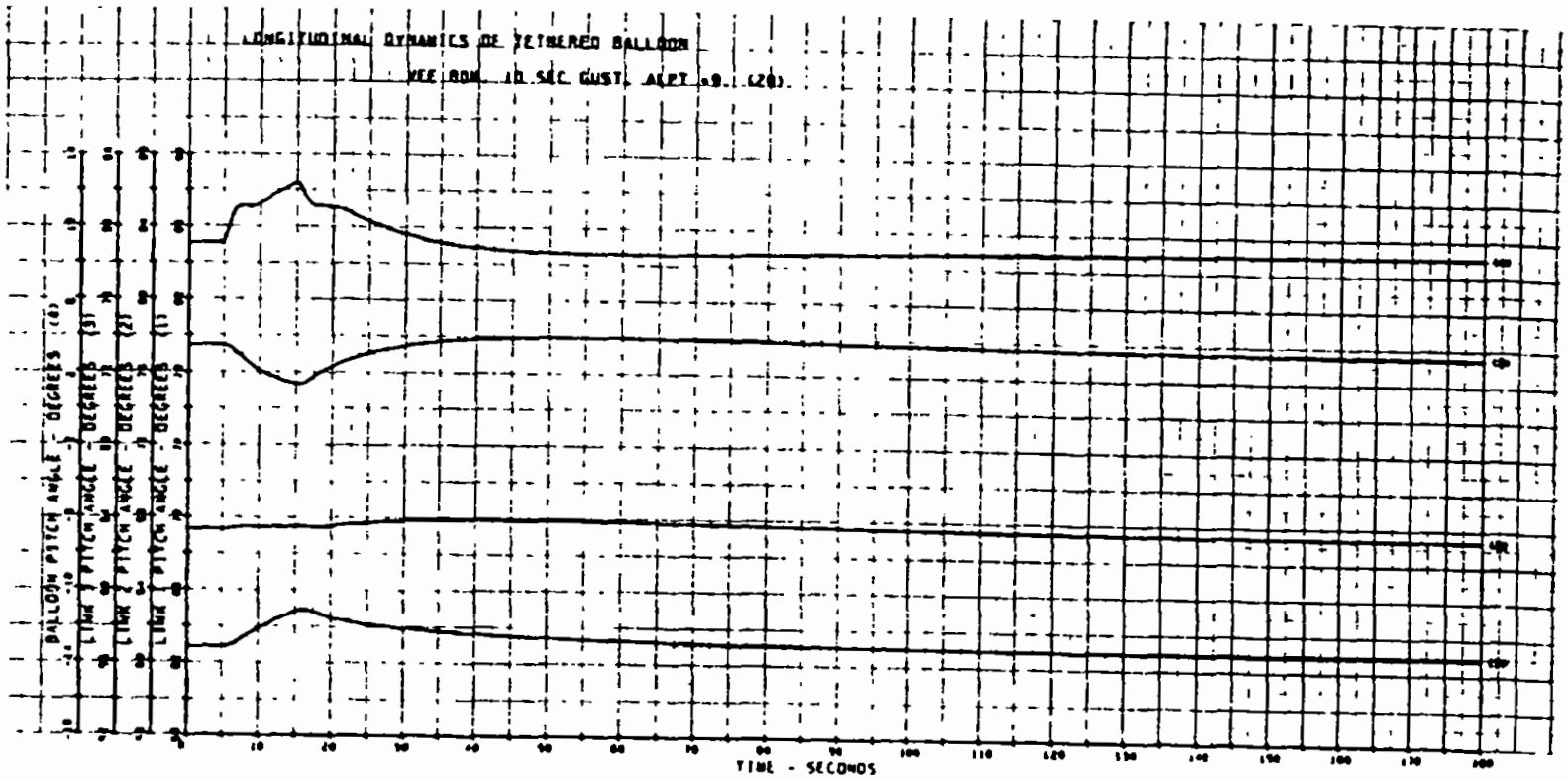
LONGITUDINAL DYNAMICS OF TETHERED BALLOON
BALLOON PITCH ANGLE - DEGREES
LINK 2 PITCH ANGLE - DEGREES
LINK 3 PITCH ANGLE - DEGREES
LINK 1 PITCH ANGLE - DEGREES
TIME - SECONDS

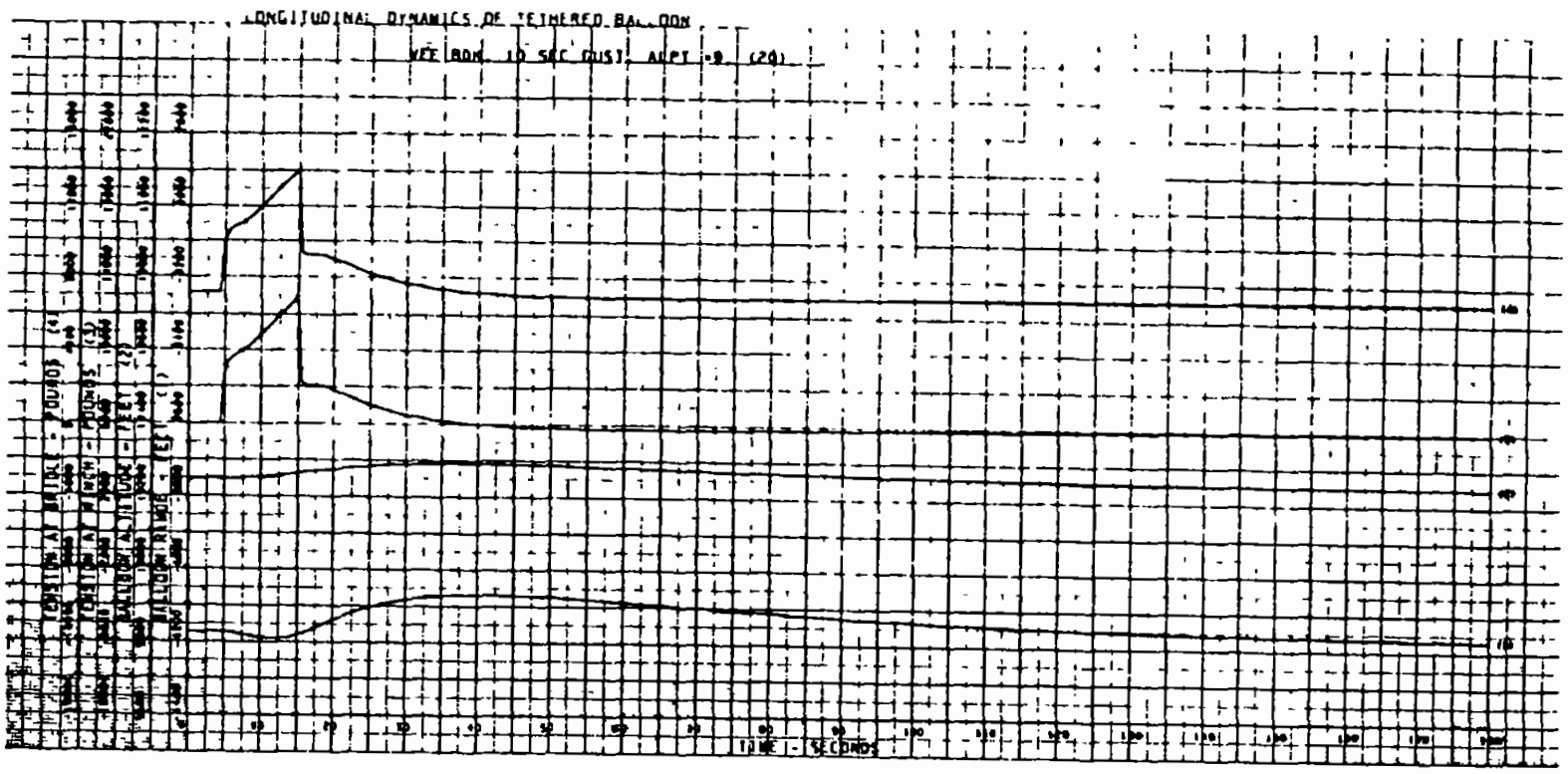
LONGITUDINAL DYNAMICS OF TETHERED BALLOON
TIME - SECONDS

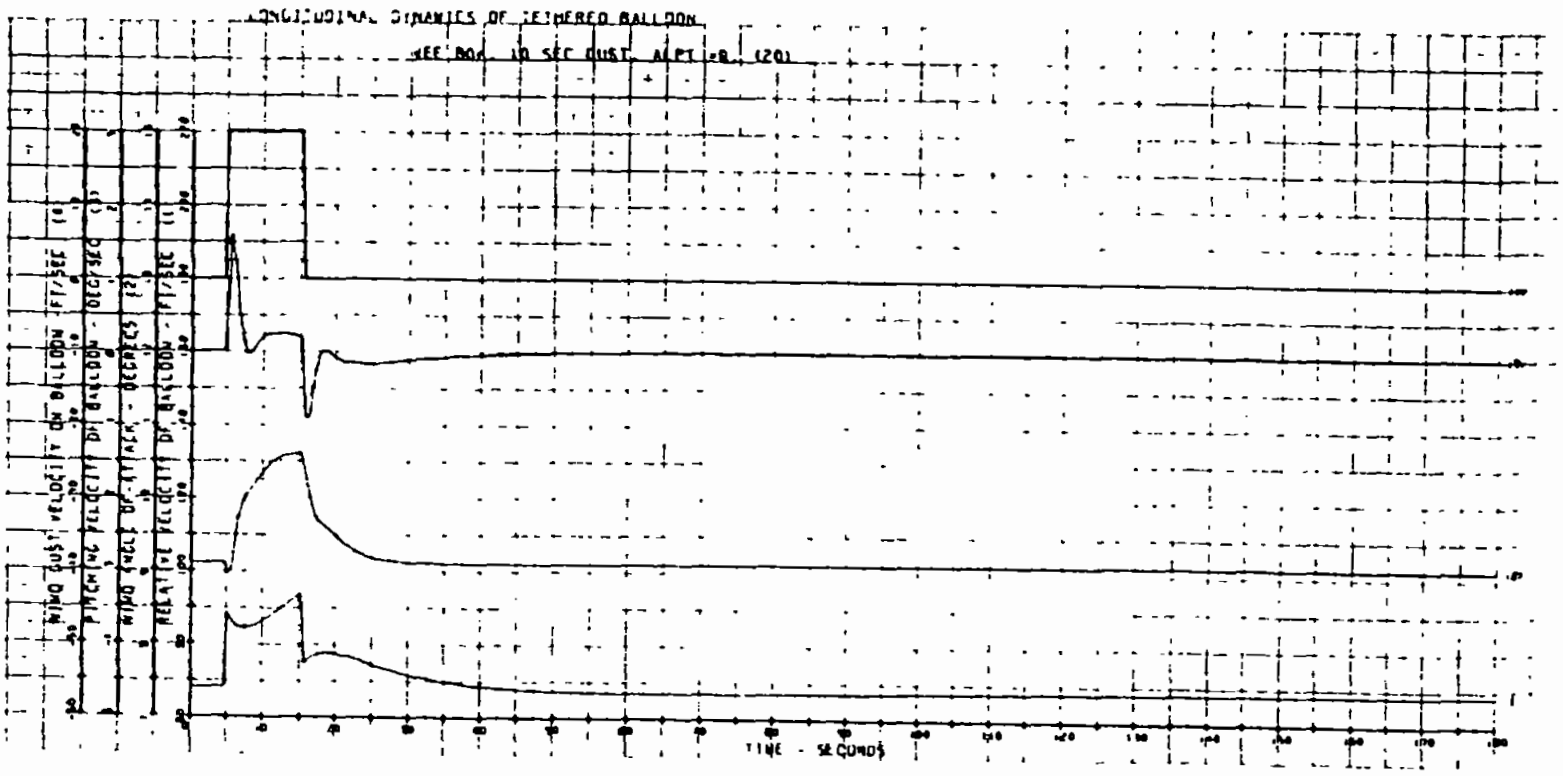
LONGITUDINAL DYNAMICS OF TETHERED BALLOON
TIME - SECONDS

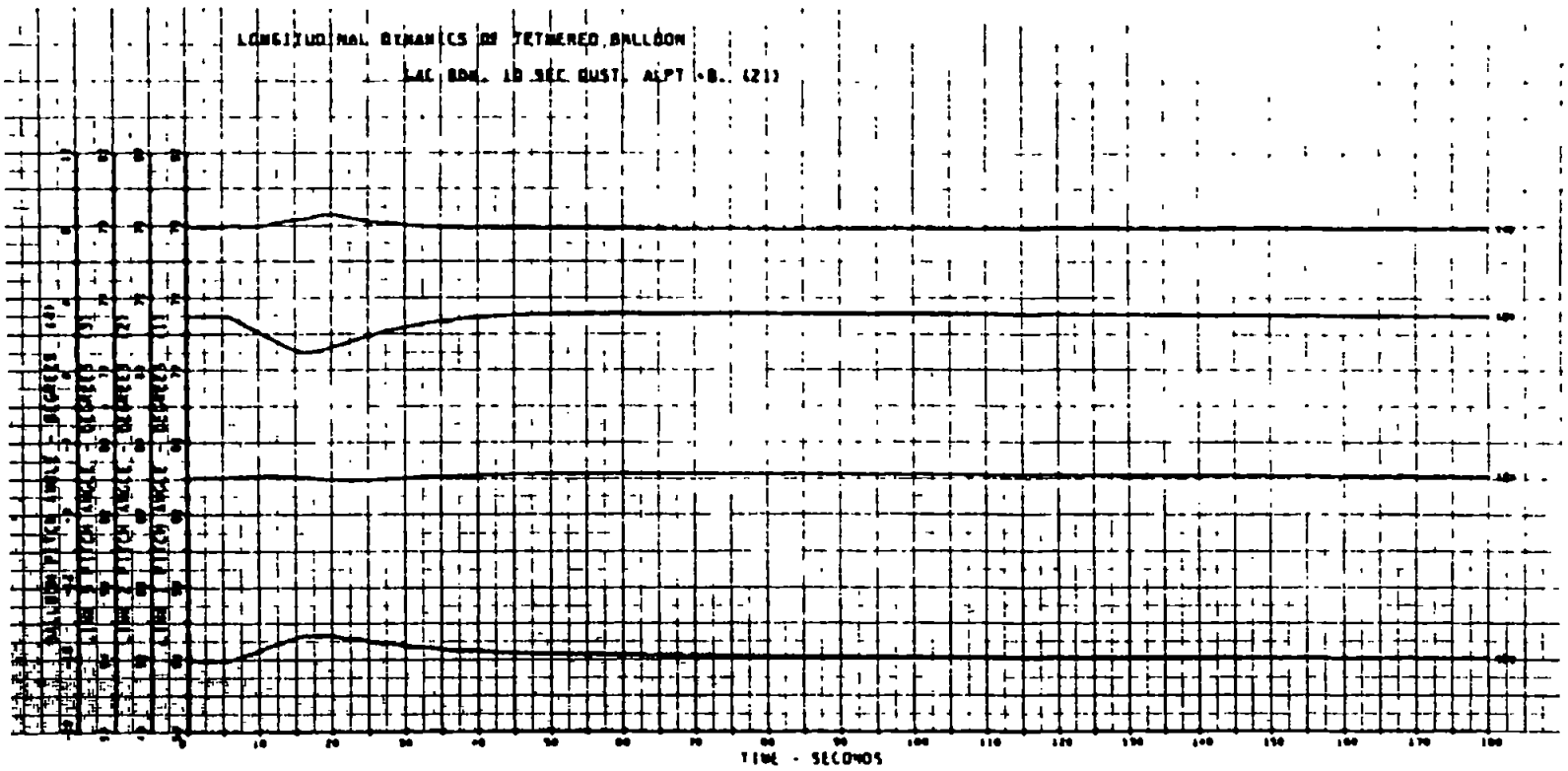
LONGITUDINAL DYNAMICS OF TETHERED BALLOON
TIME - SECONDS

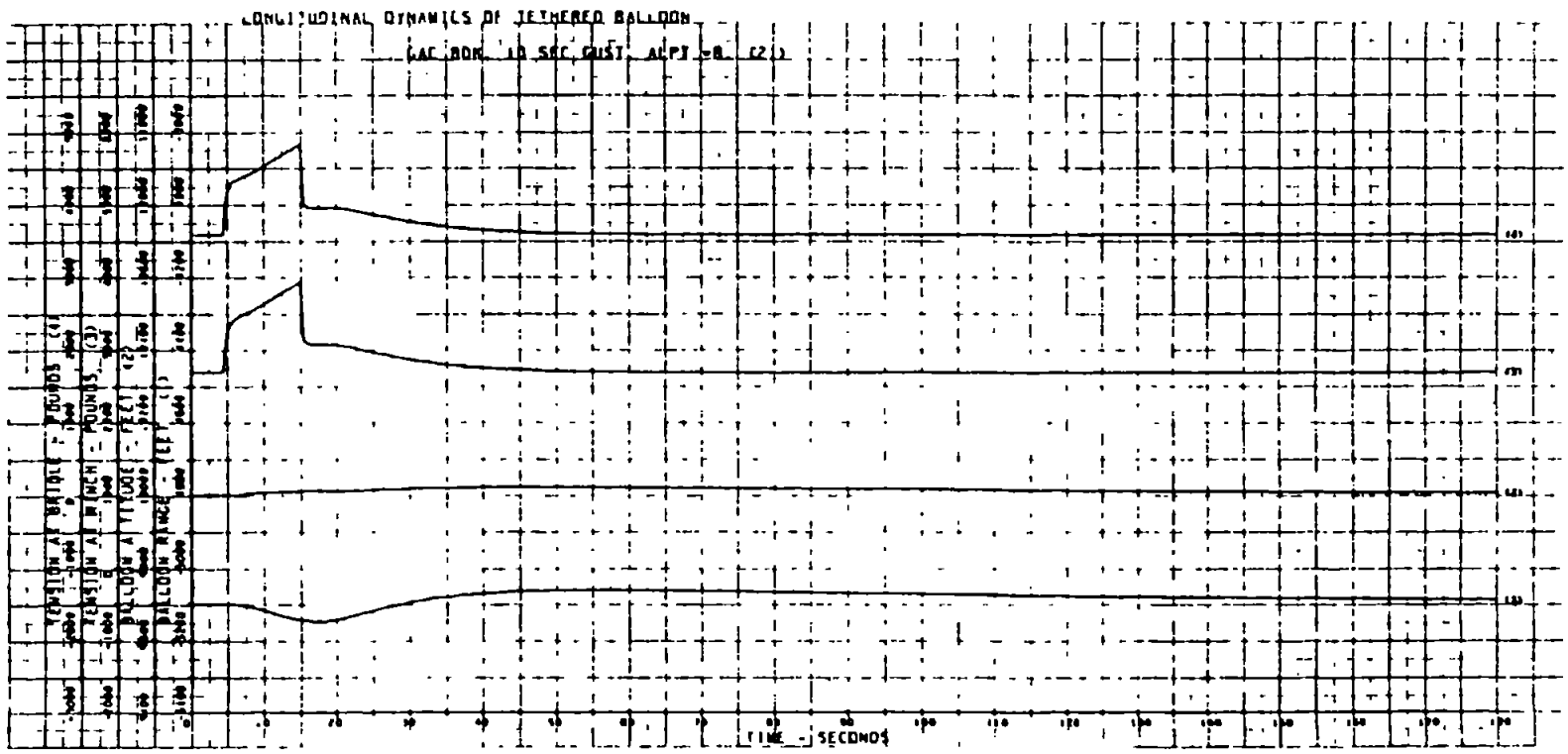
LONGITUDINAL DYNAMICS OF TETHERED BALLOON
TIME - SECONDS

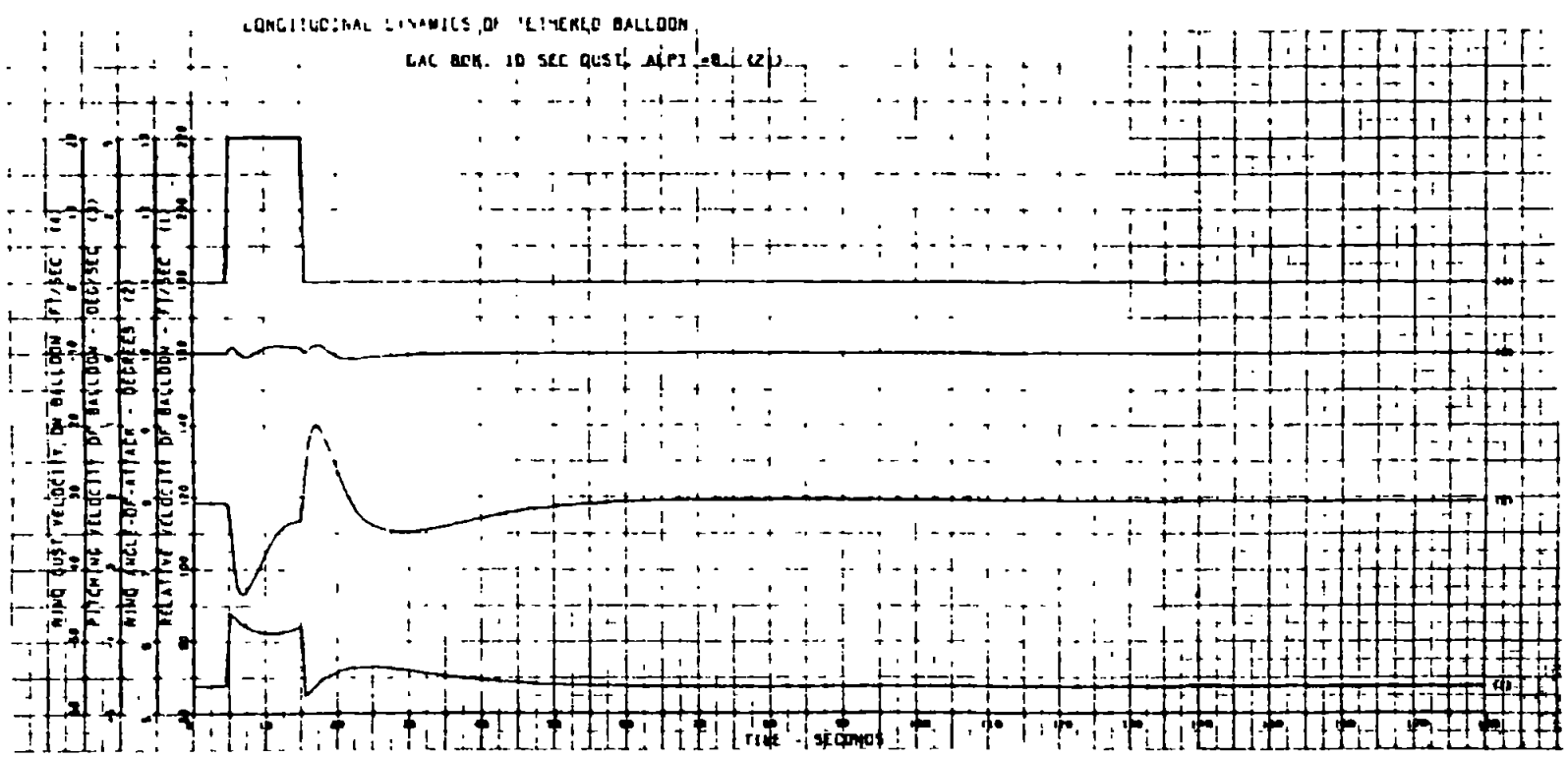
LONGITUDINAL DYNAMICS OF TETHERED BALLOON
TIME - SECONDS

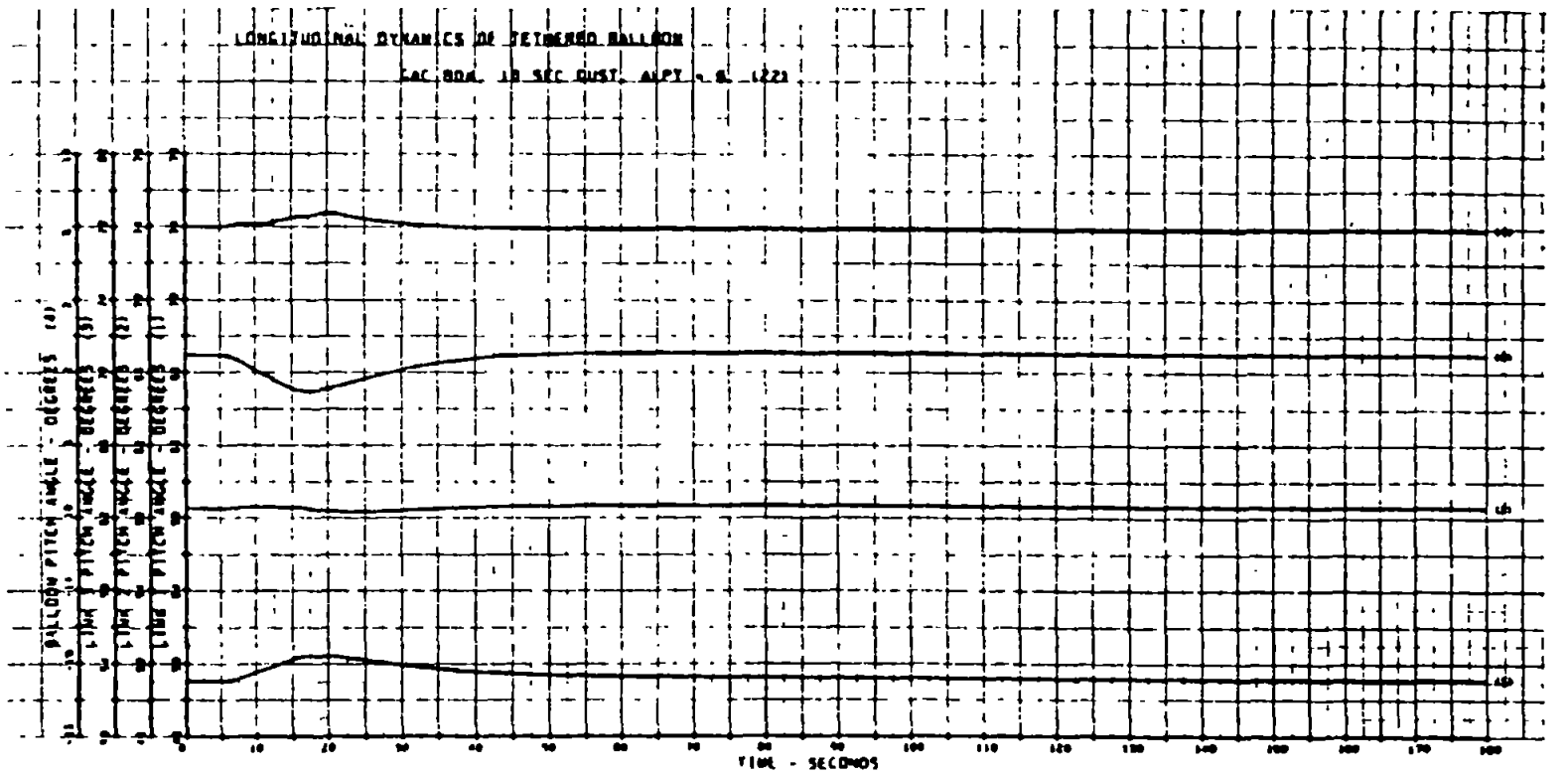
LONGITUDINAL DYNAMICS OF TETHERED BALLOON
TIME - SECONDS

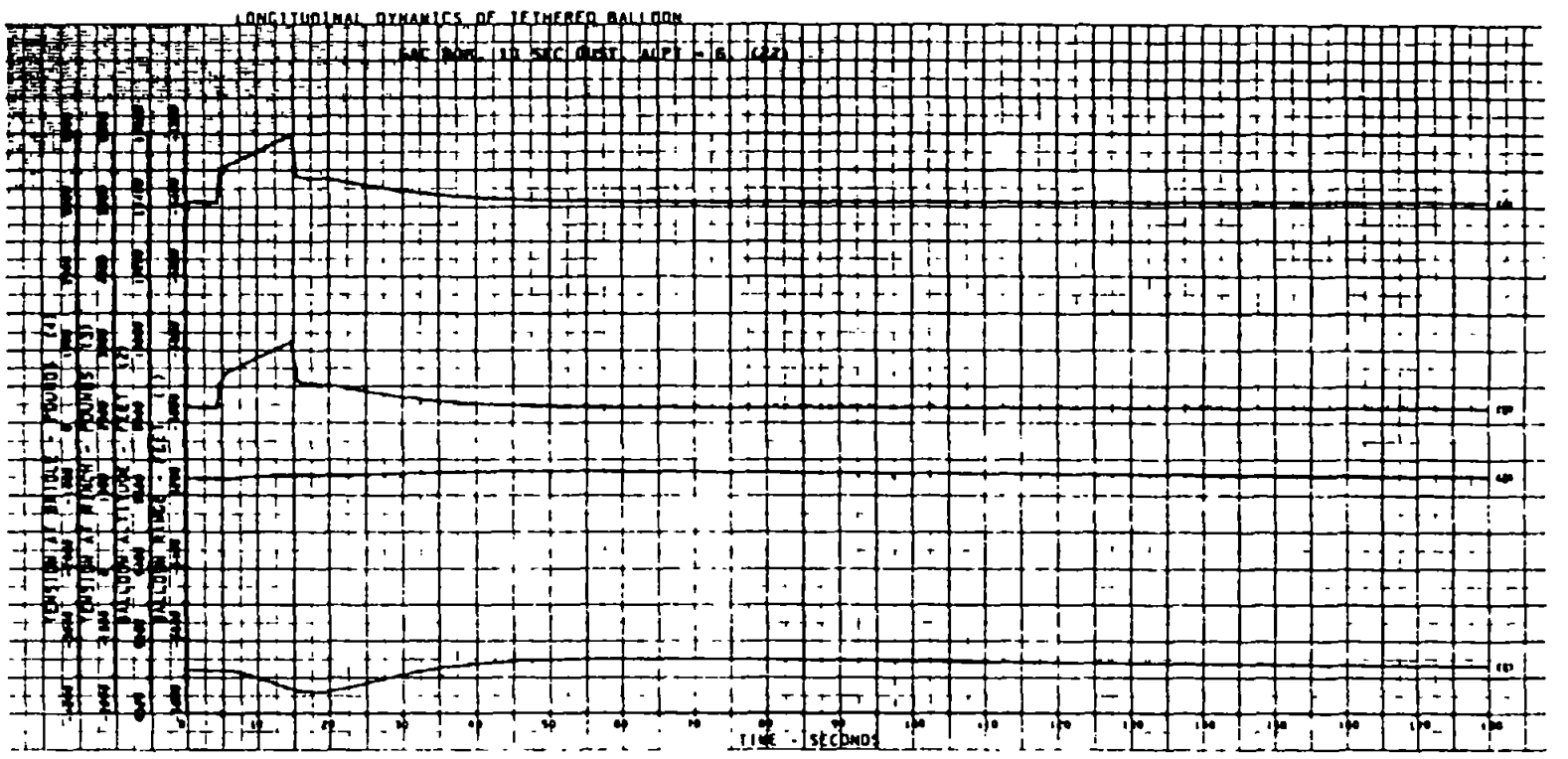
LONGITUDINAL DYNAMICS OF TETHERED BALLOON
TIME - SECONDS

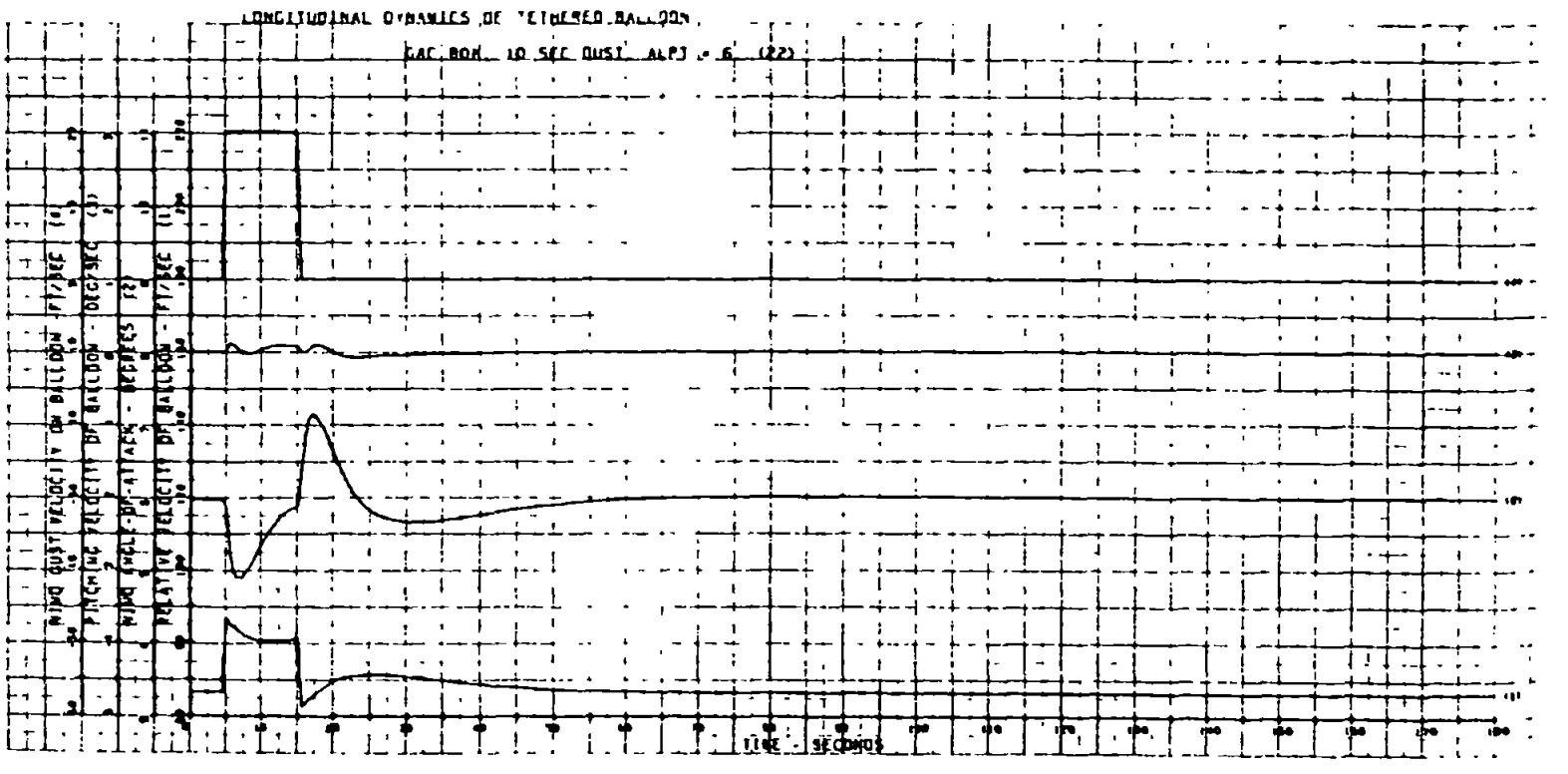
LONGITUDINAL DYNAMICS OF TETHERED BALLOON
TIME - SECONDS

LONGITUDINAL DYNAMICS OF TETHERED BALLOON

GAC BOK. 10 SEC GUST. ALPT = 10.. (23)

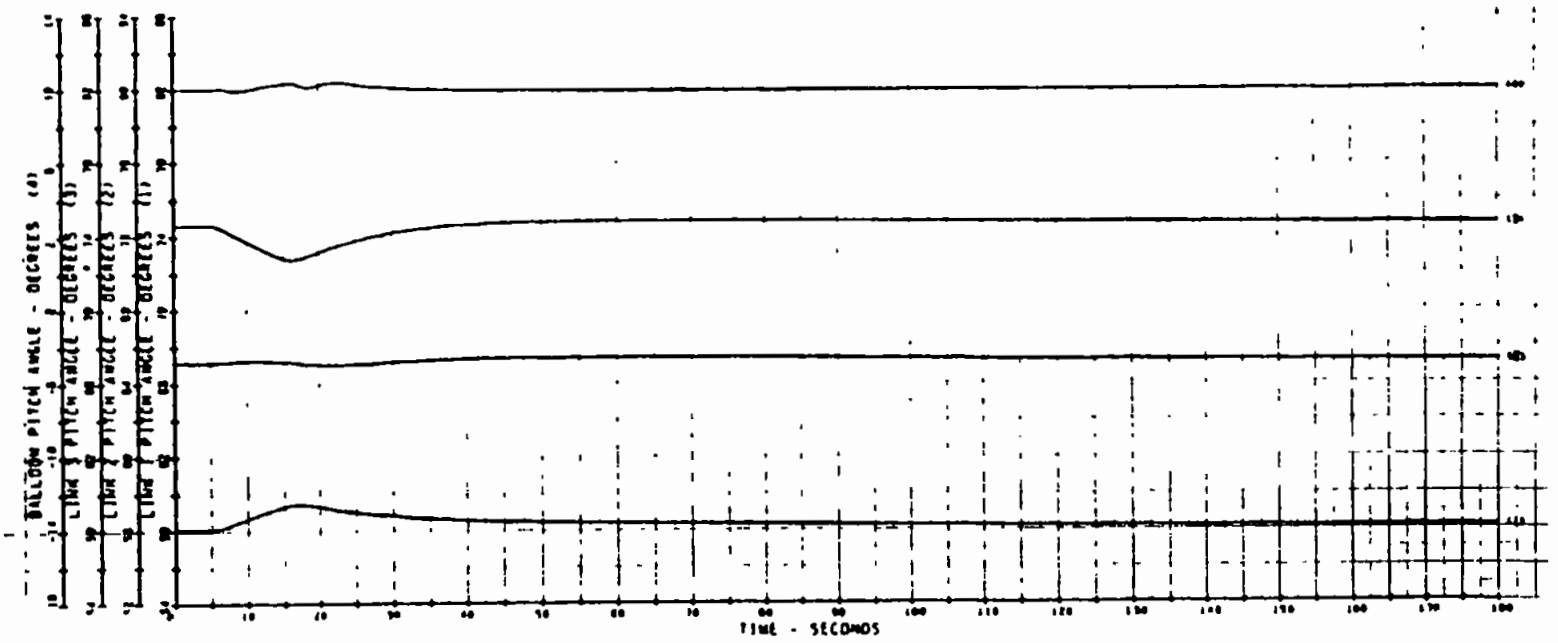

LONGITUDINAL DYNAMICS OF TETHERED BALLOON

GAC BOK. 10 SEC GUST. ALPT = 10.. (23)

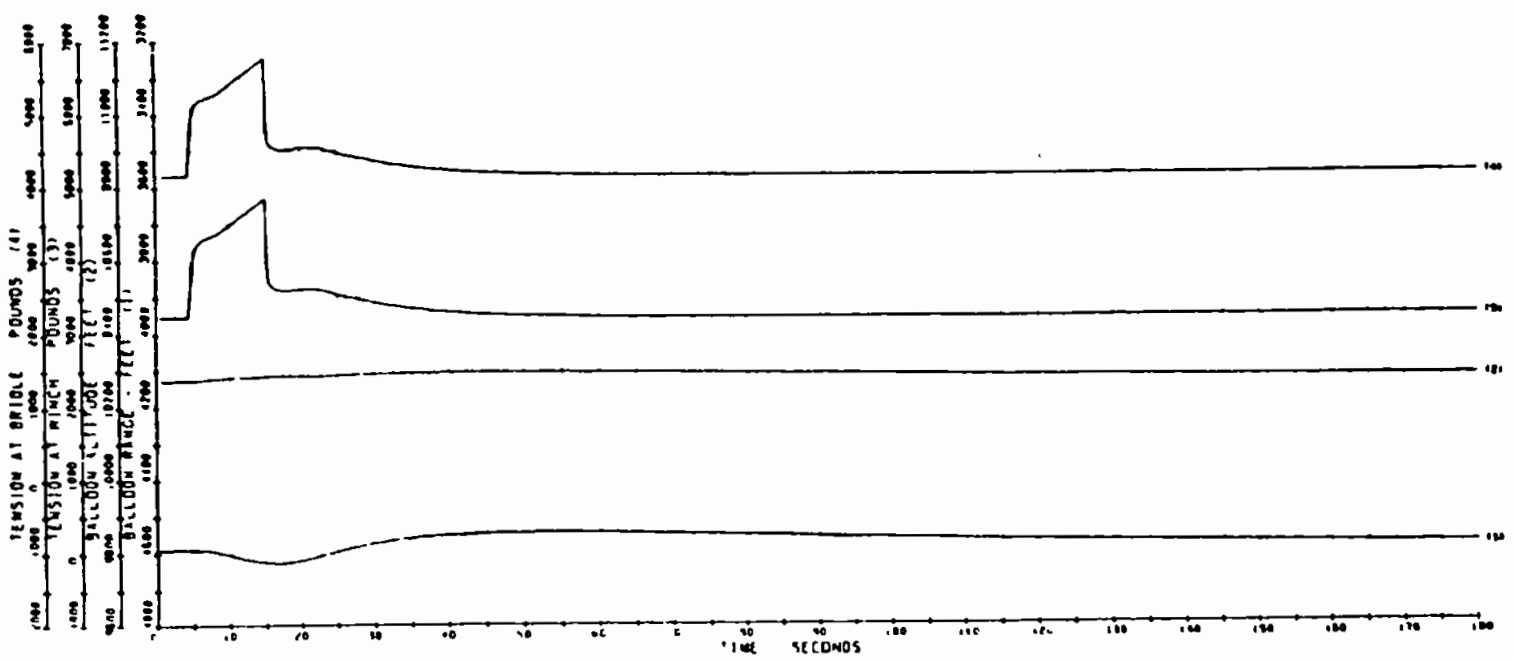

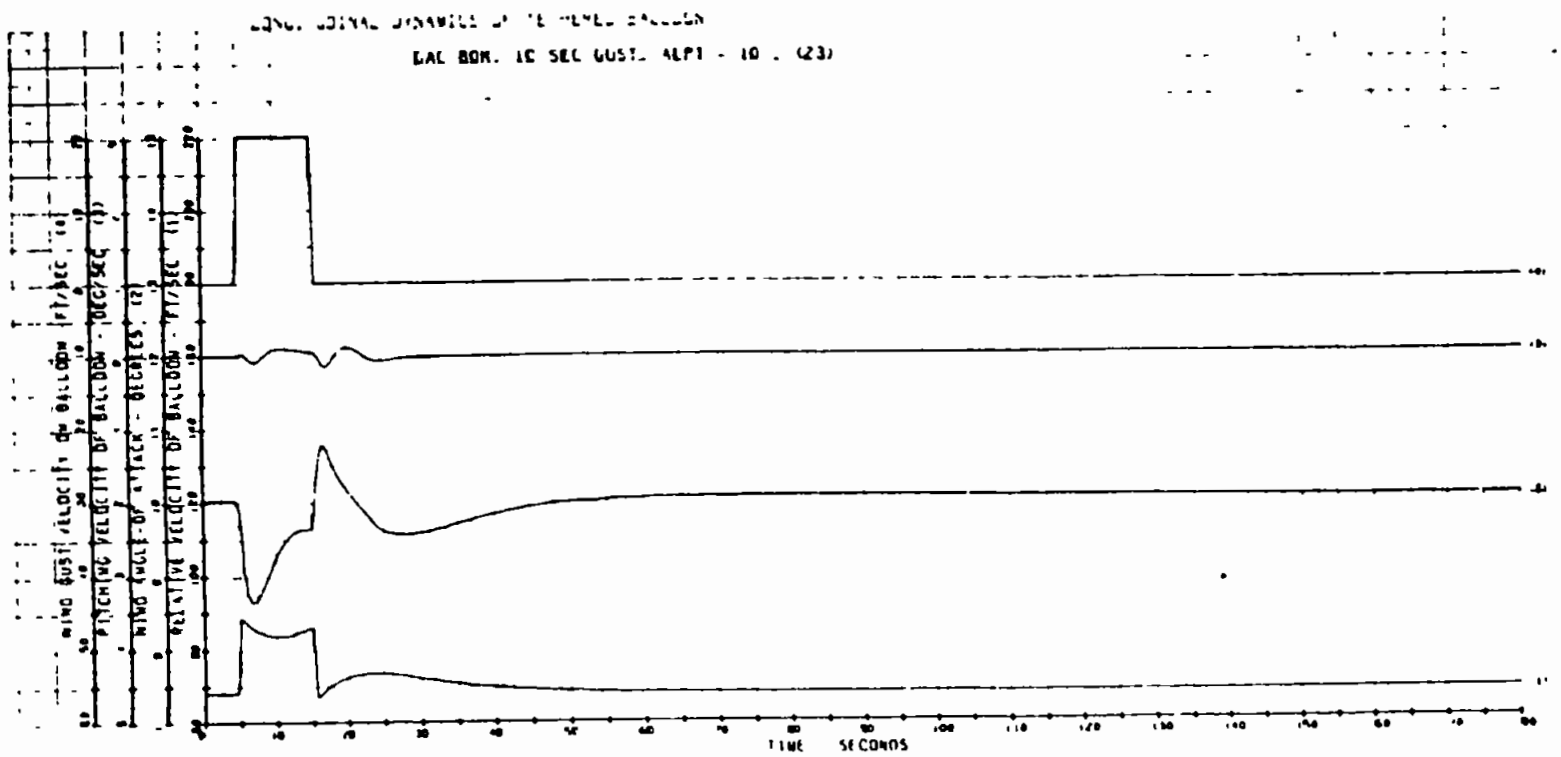

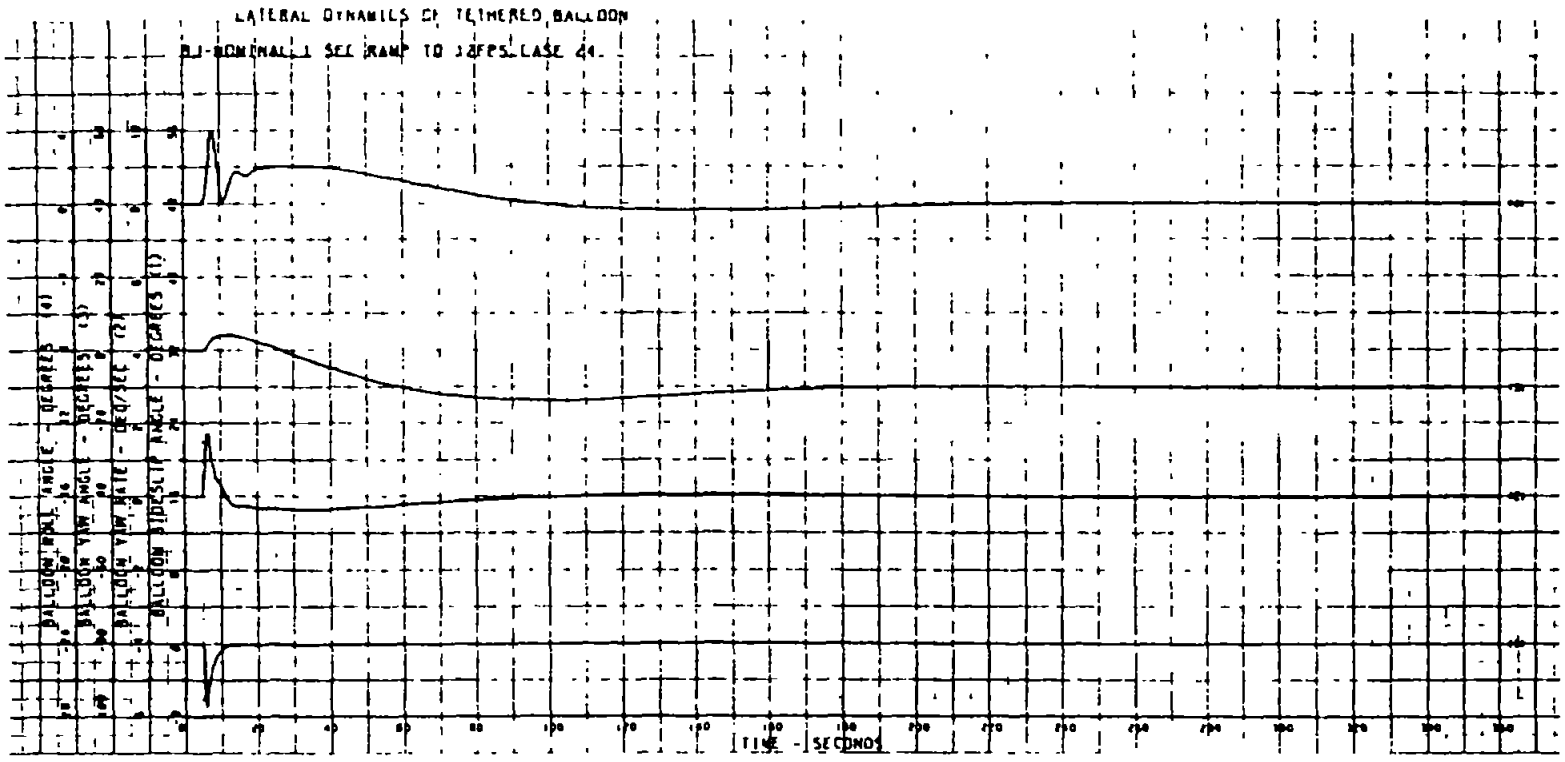
LATERAL DYNAMICS OF TETHERED BALLOON
BJ-NOMINAL, 1 SEC RAMP TO 12FPS, CASE 24
BALLOON PITCH ANGLE - DEGREES (4)
BALLOON YAW ANGLE - DEGREES (3)
BALLOON YAW RATE - DEG/SEC (2)
BALLOON SIDESLIP ANGLE - DEGREES (1)
TIME - SECONDS

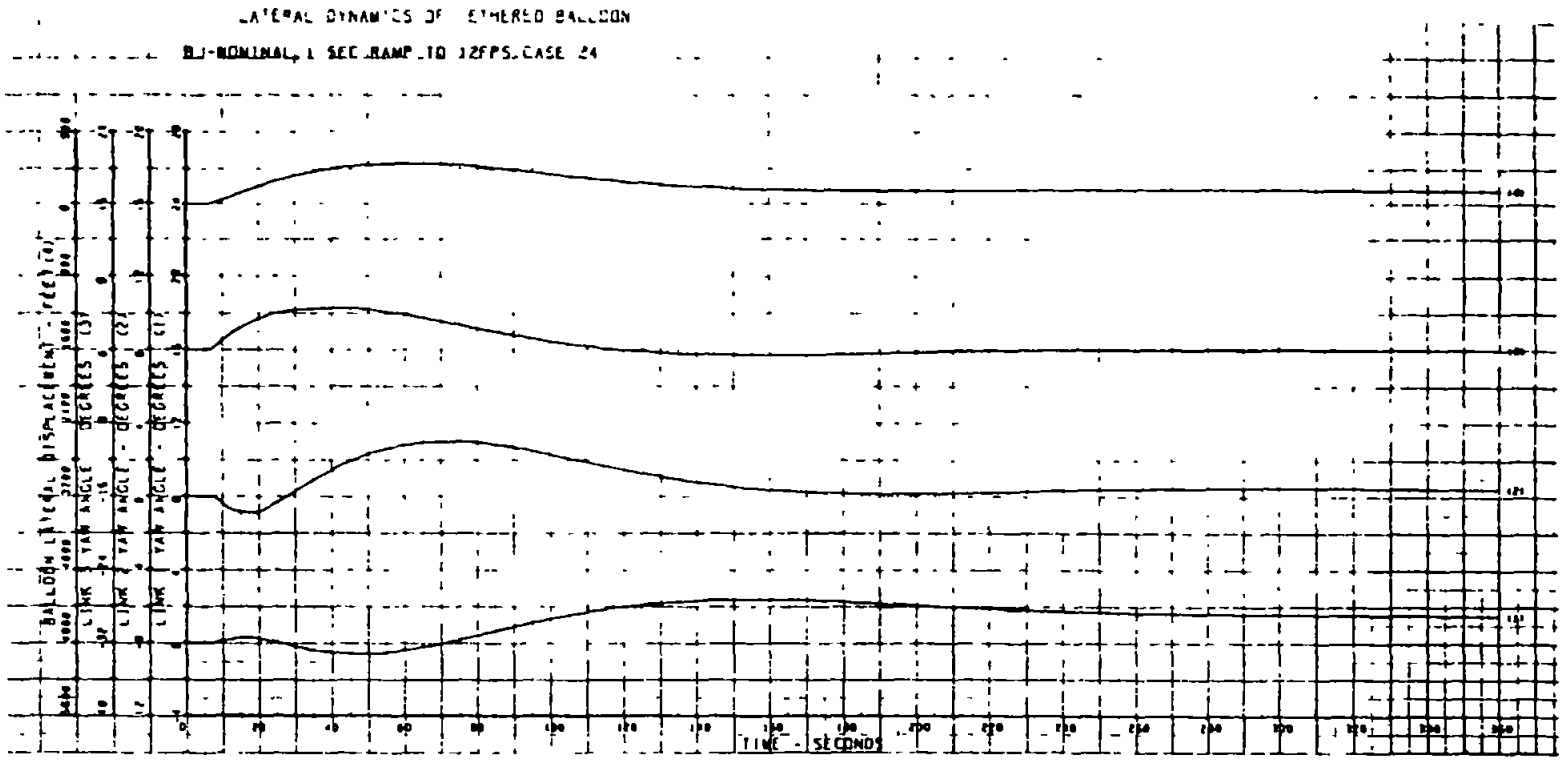
LATERAL DYNAMICS OF TETHERED BALLOON
BJ-NOMINAL, 1 SEC RAMP TO 12FPS, CASE 24
BALLOON LATERAL DISPLACEMENT - FEET (4)
LINK YAW ANGLE - DEGREES (3)
LINK YAW ANGLE - DEGREES (2)
LINK YAW ANGLE - DEGREES (1)
TIME - SECONDS

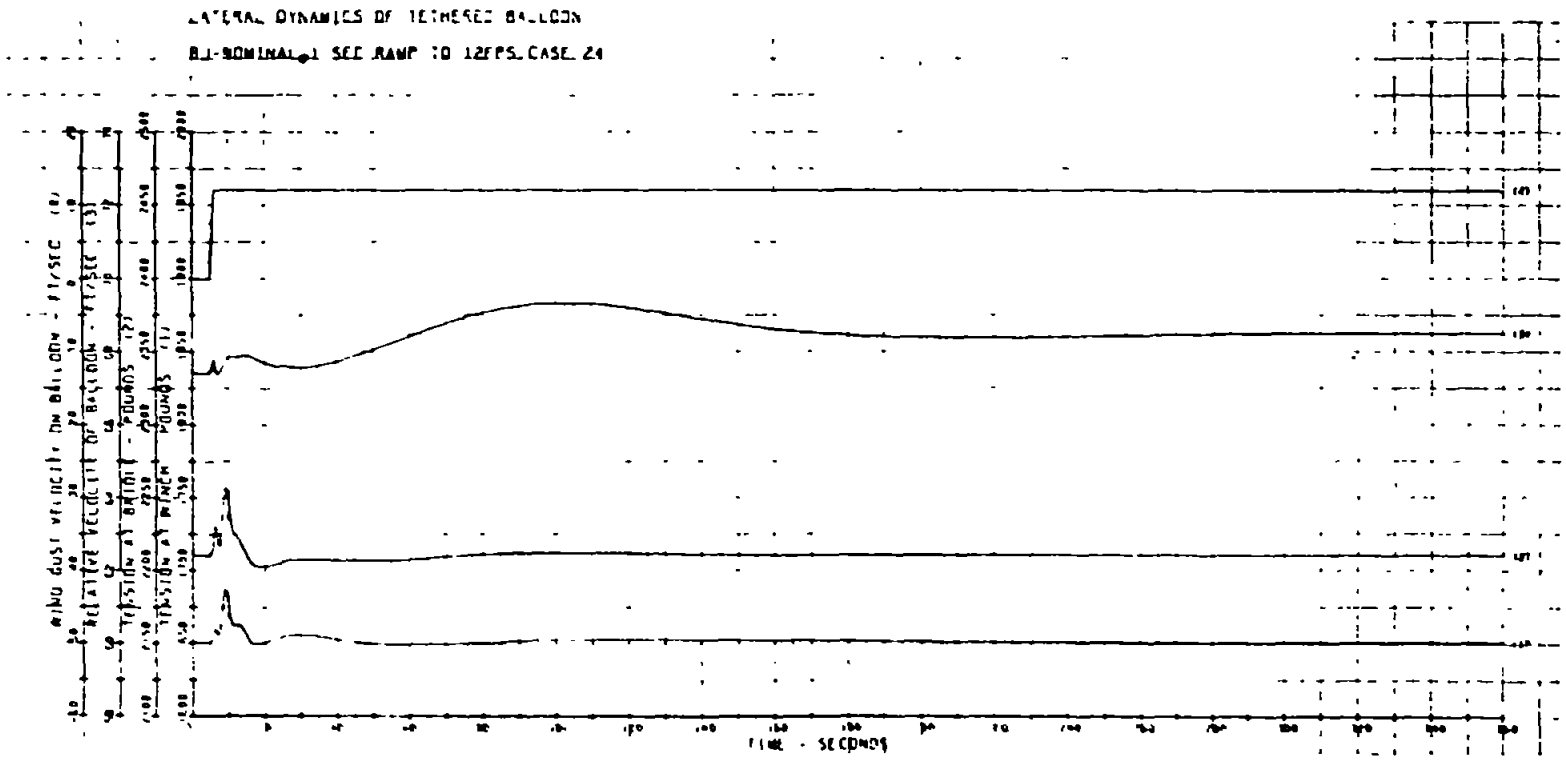
LATERAL DYNAMICS OF TETHERED BALLOON
BJ-NOMINAL, 1 SEC RAMP TO 12FPS, CASE 24
WIND GUST VELOCITY ON BALLOON - FT/SEC (4)
RELATIVE VELOCITY OF BALLOON - FT/SEC (3)
TENSION AT BRIDLE - POUNDS (2)
TENSION AT WINCH - POUNDS (1)
TIME - SECONDS

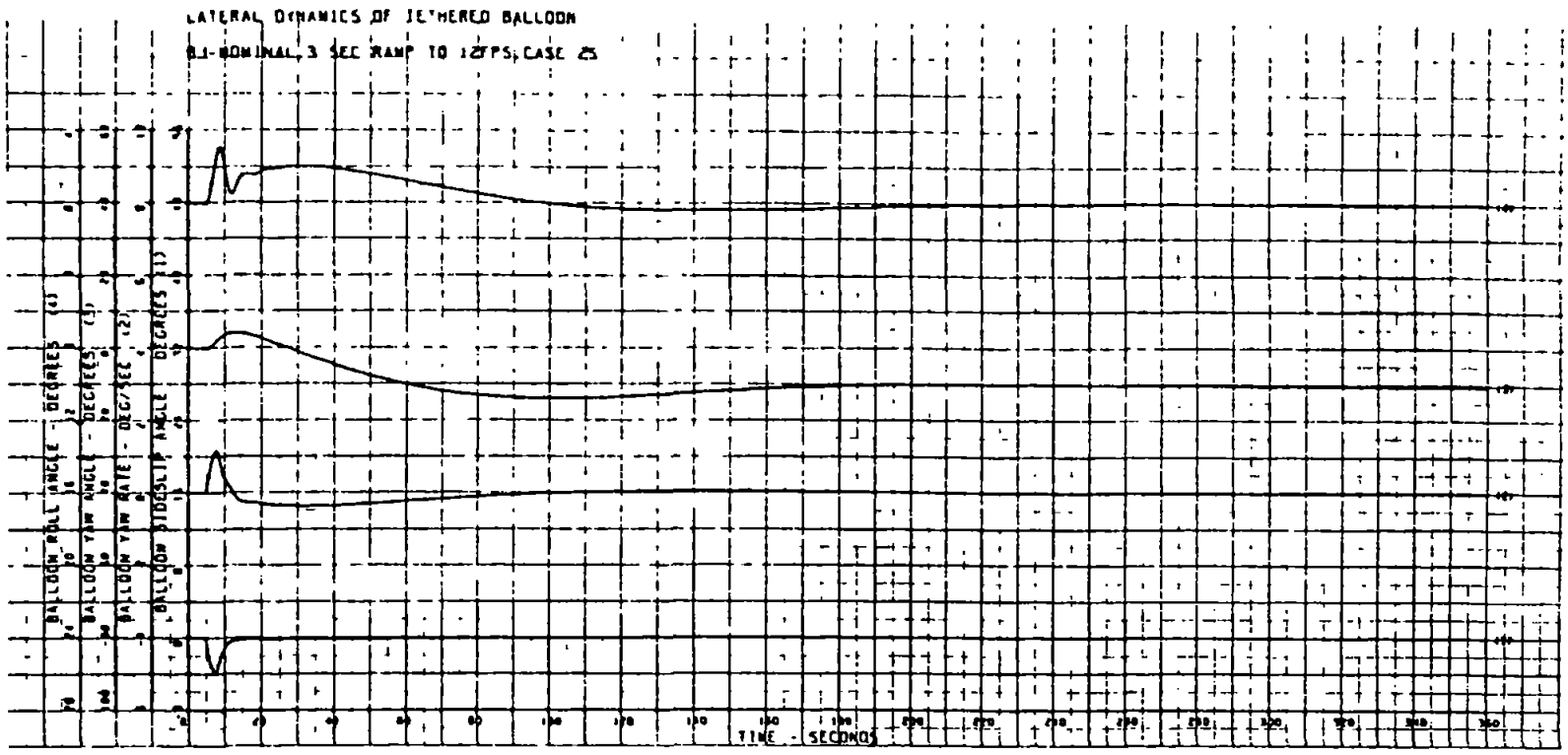
LATERAL DYNAMICS OF TETHERED BALLOON
B1-NOMINAL 3 SEC RAMP TO 12FPS CASE 25
BALLOON ROLL ANGLE - DEGREES (4)
BALLOON YAW ANGLE - DEGREES (3)
BALLOON YAW RATE - DEG/SEC (2)
BALLOON SIDESLIP ANGLE - DEGREES (1)
TIME - SECONDS

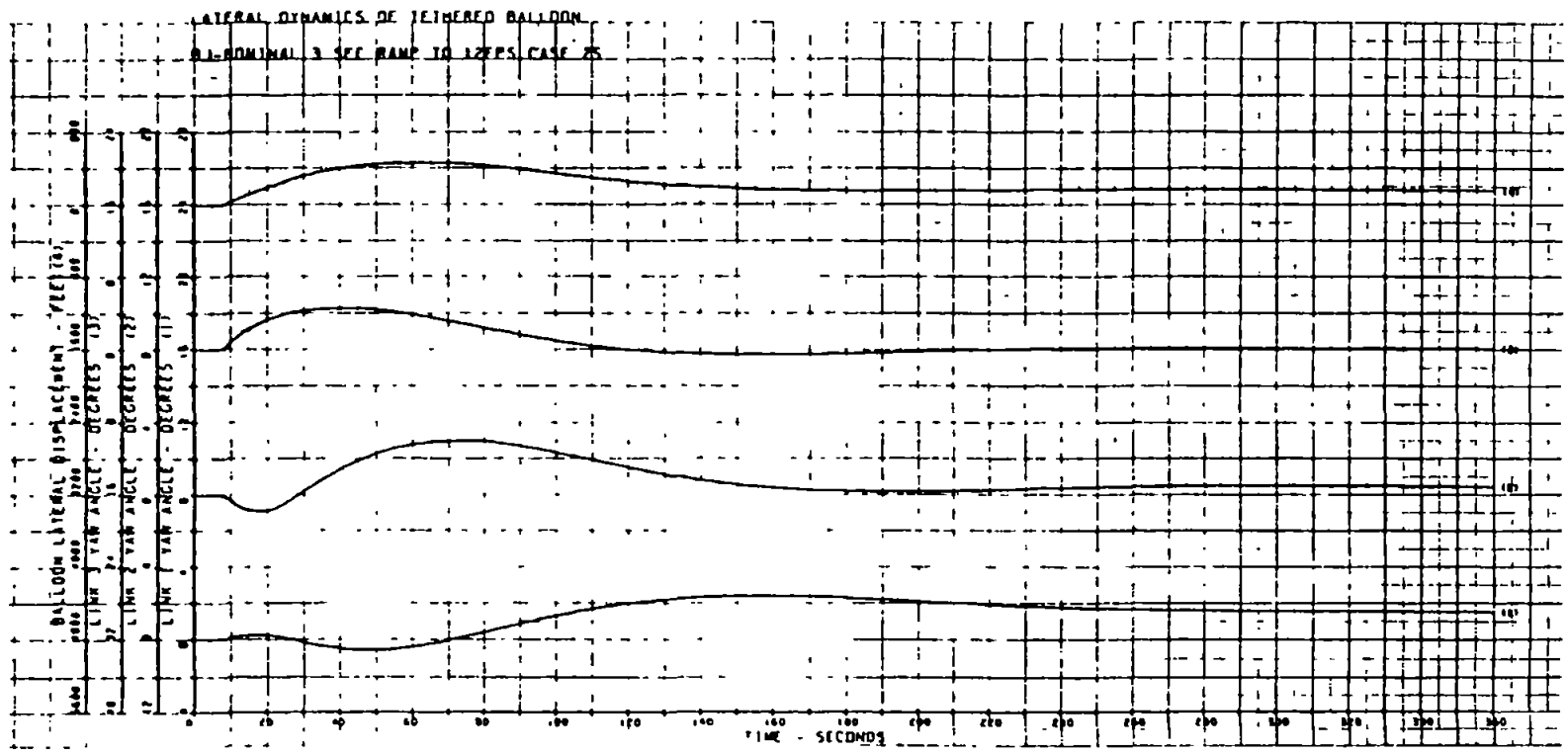
LATERAL DYNAMICS OF TETHERED BALLOON
B1-NOMINAL 3 SEC RAMP TO 12FPS CASE 25
BALLOON LATERAL DISPLACEMENT - FEET (3)
LINK 3 YAW ANGLE - DEGREES (2)
LINK 2 YAW ANGLE - DEGREES (1)
TIME - SECONDS

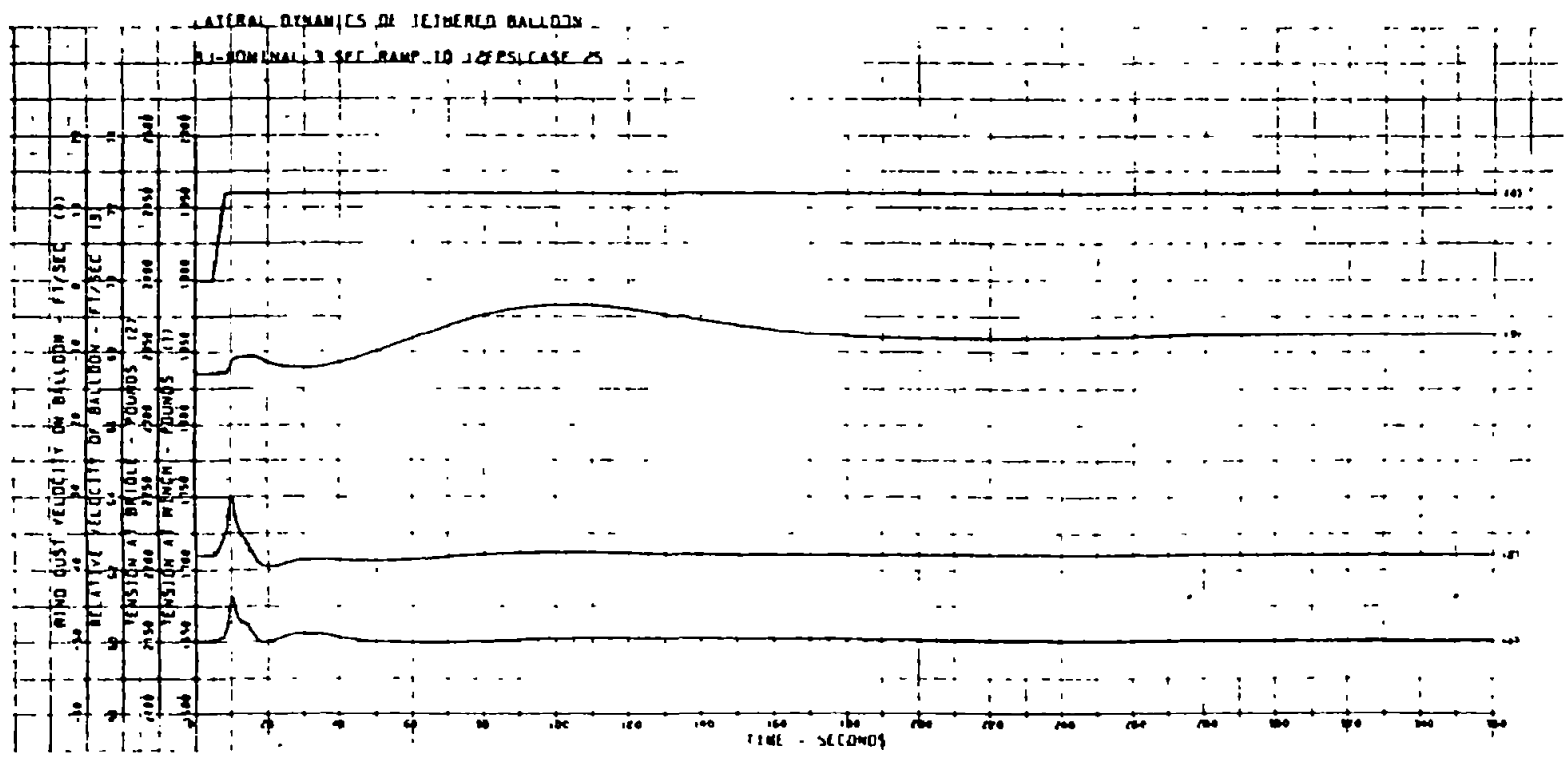
LATERAL DYNAMICS OF TETHERED BALLOON
B1-NOMINAL 3 SEC RAMP TO 12FPS CASE 25
WIND GUST VELOCITY ON BALLOON - FT/SEC (4)
RELATIVE VELOCITY OF BALLOON - FT/SEC (3)
TENSION AT BALLOON - POUNDS (2)
TENSION AT WINCH - POUNDS (1)
TIME - SECONDS

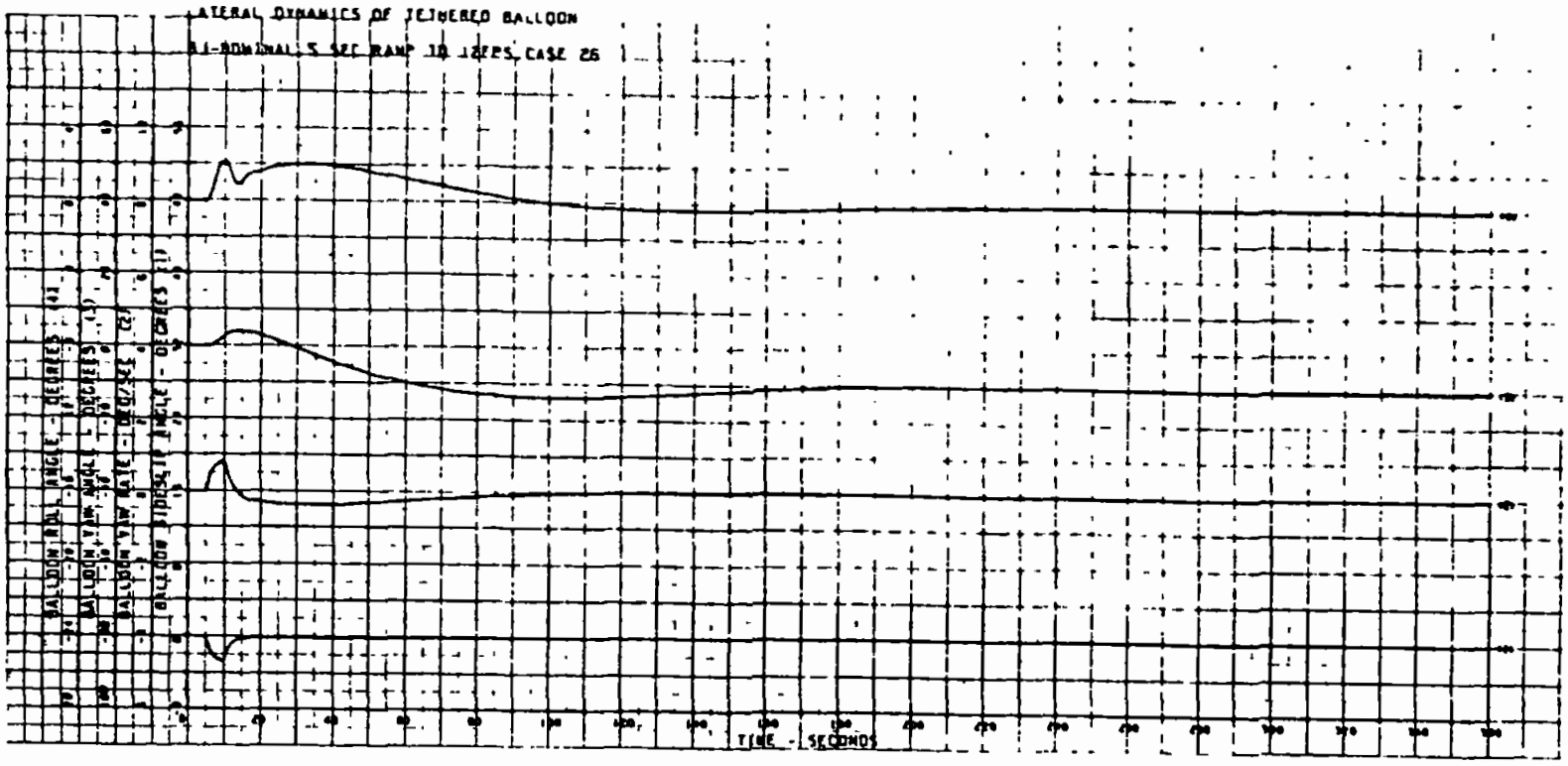
LATERAL DYNAMICS OF TETHERED BALLOON
B1-NOMINAL.5 SEC RAMP TO 12FPS.CASE 26
BALLOON ROLL ANGLE - DEGREES
BALLOON YAW ANGLE - DEGREES
BALLOON YAW RATE - DEGREES/SEC
BALLOON SIDESLIP ANGLE - DEGREES
TIME - SECONDS

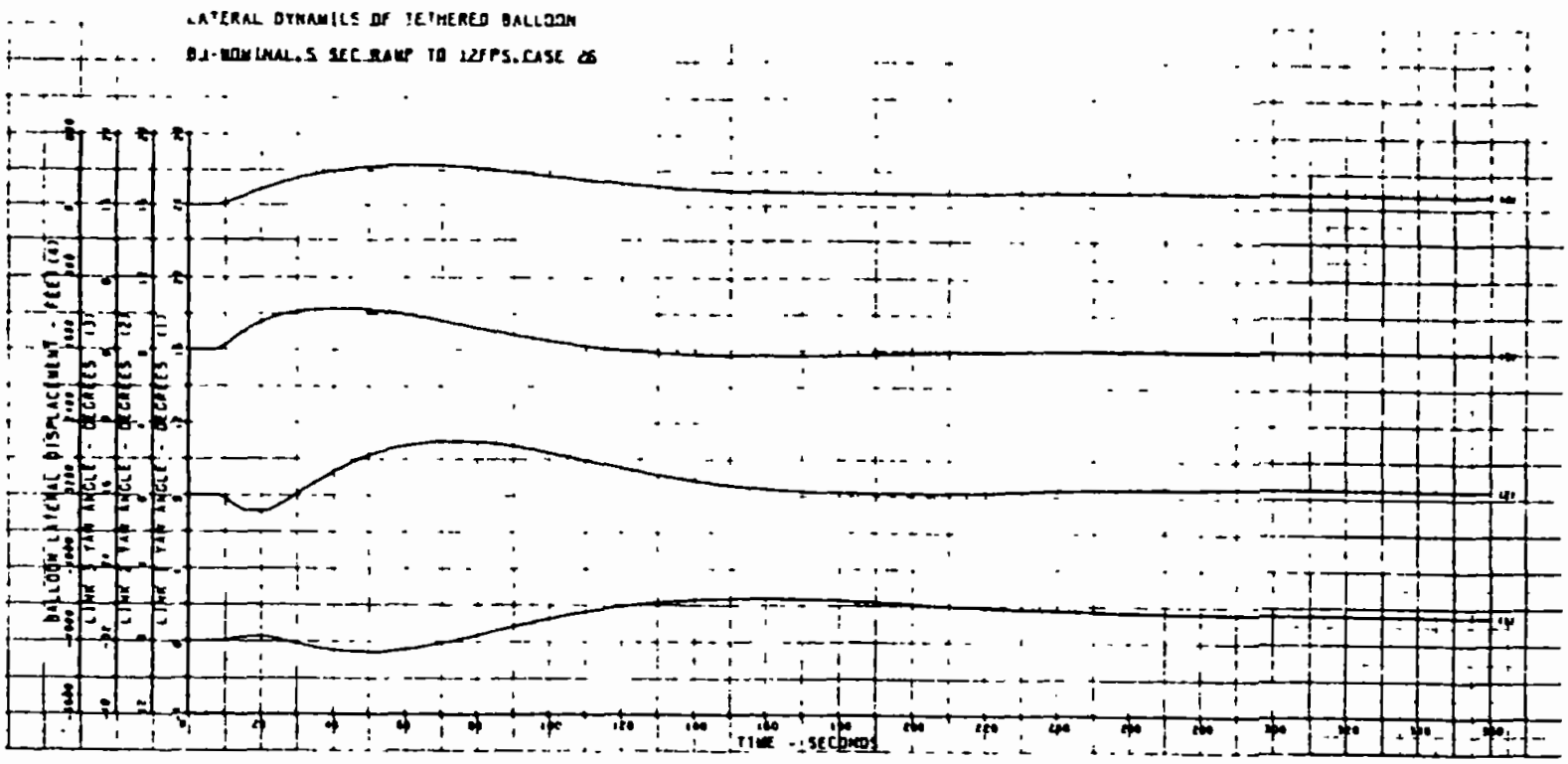
LATERAL DYNAMICS OF TETHERED BALLOON
B1-NOMINAL.5 SEC RAMP TO 12FPS.CASE 26
BALLOON LATERAL DISPLACEMENT - FEET
LINK 1 YAW ANGLE - DEGREES
LINK 2 YAW ANGLE - DEGREES
LINK 3 YAW ANGLE - DEGREES
TIME - SECONDS

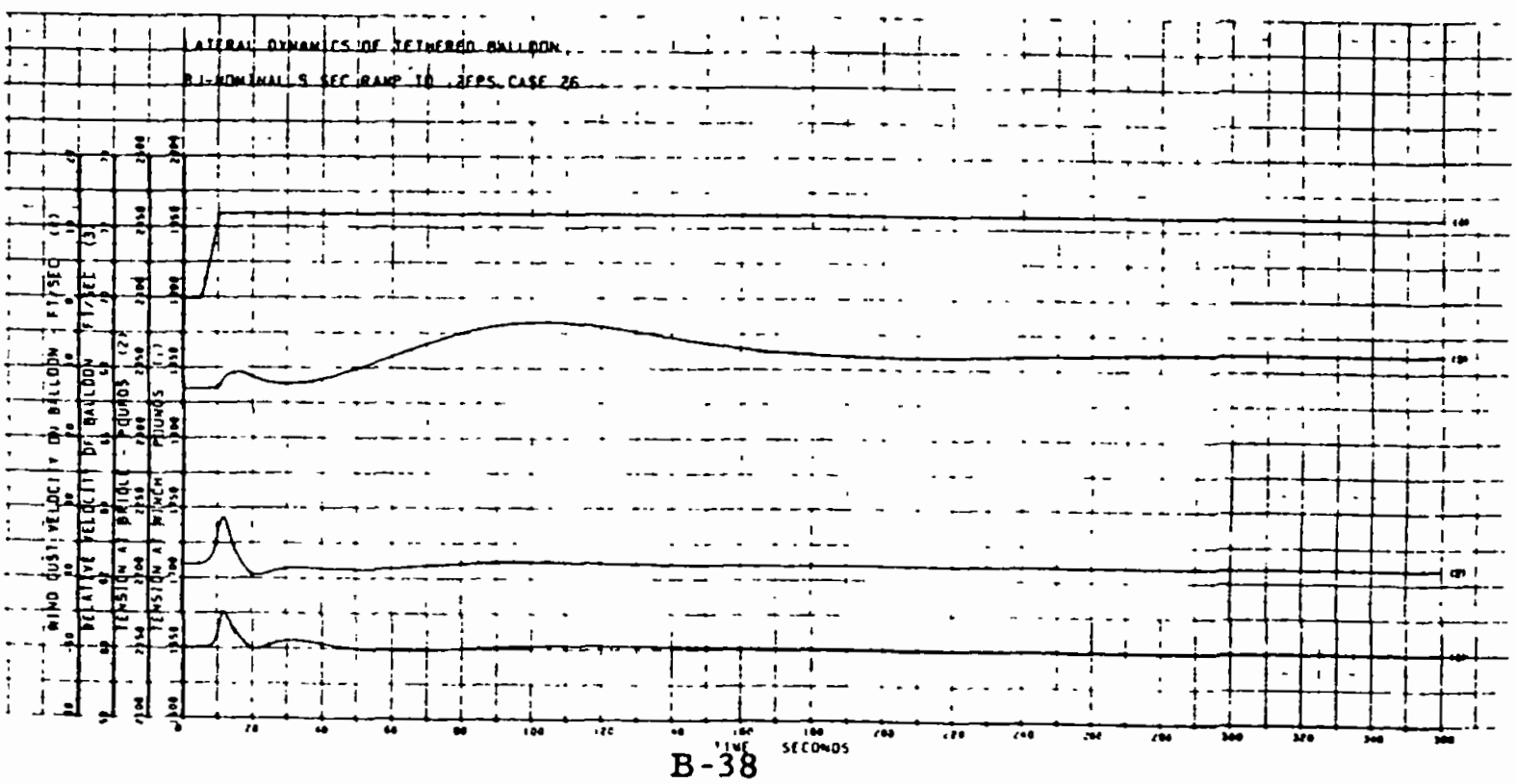
LATERAL DYNAMICS OF TETHERED BALLOON
B1-NOMINAL.5 SEC RAMP TO 12FPS.CASE 26
WIND GUST VELOCITY ON BALLOON - FT/SEC
RELATIVE VELOCITY OF BALLOON - FT/SEC
TENSION AT BRIDLE - POUNDS
TENSION AT WINCH - POUNDS
TIME - SECONDS

LATERAL DYNAMICS OF TETHERED BALLOON

BJ-NOMINAL.5 SEC RAMP TO 18FPS.CASE 27

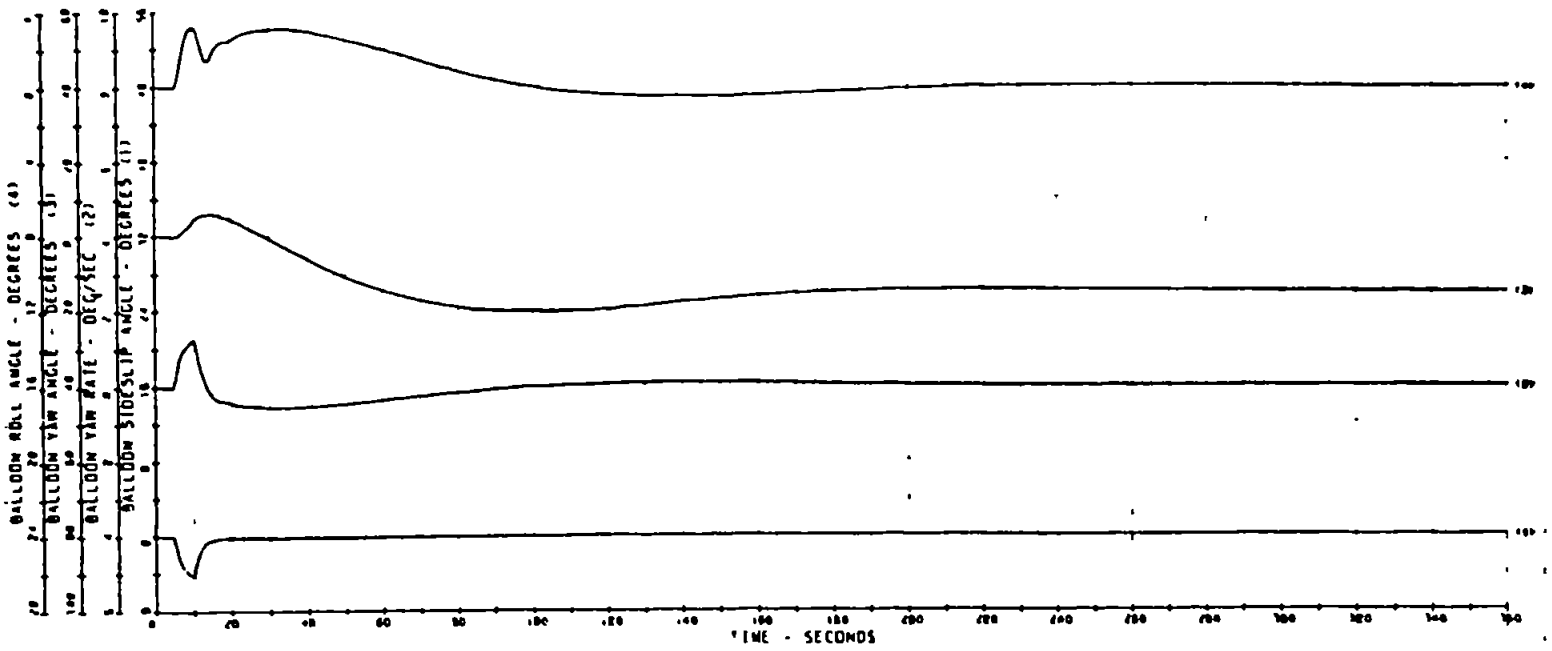

LATERAL DYNAMICS OF TETHERED BALLOON

BJ-NOMINAL.5 SEC RAMP TO 18FPS.CASE 27

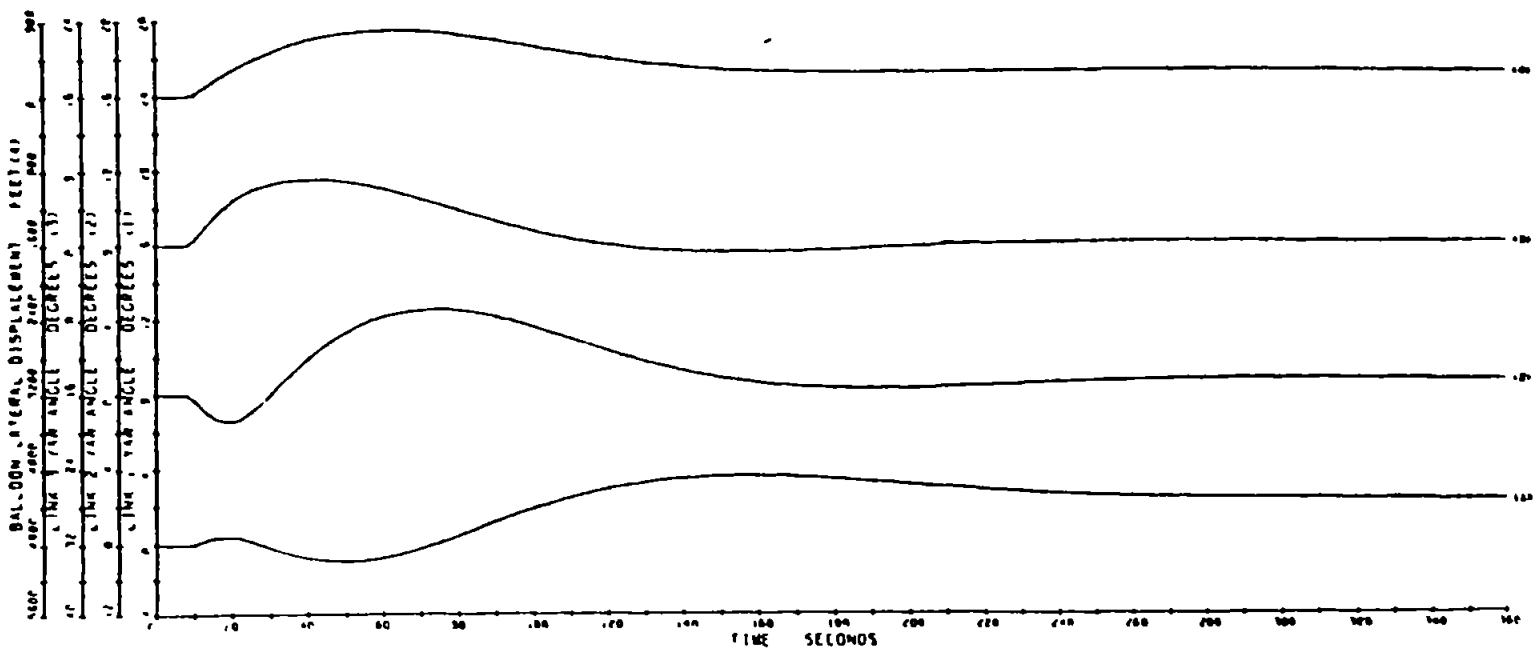

LATERAL DYNAMICS OF TETHERED BALLOON

BJ-NOMINAL.5 SEC RAMP TO 18FPS.CASE 27

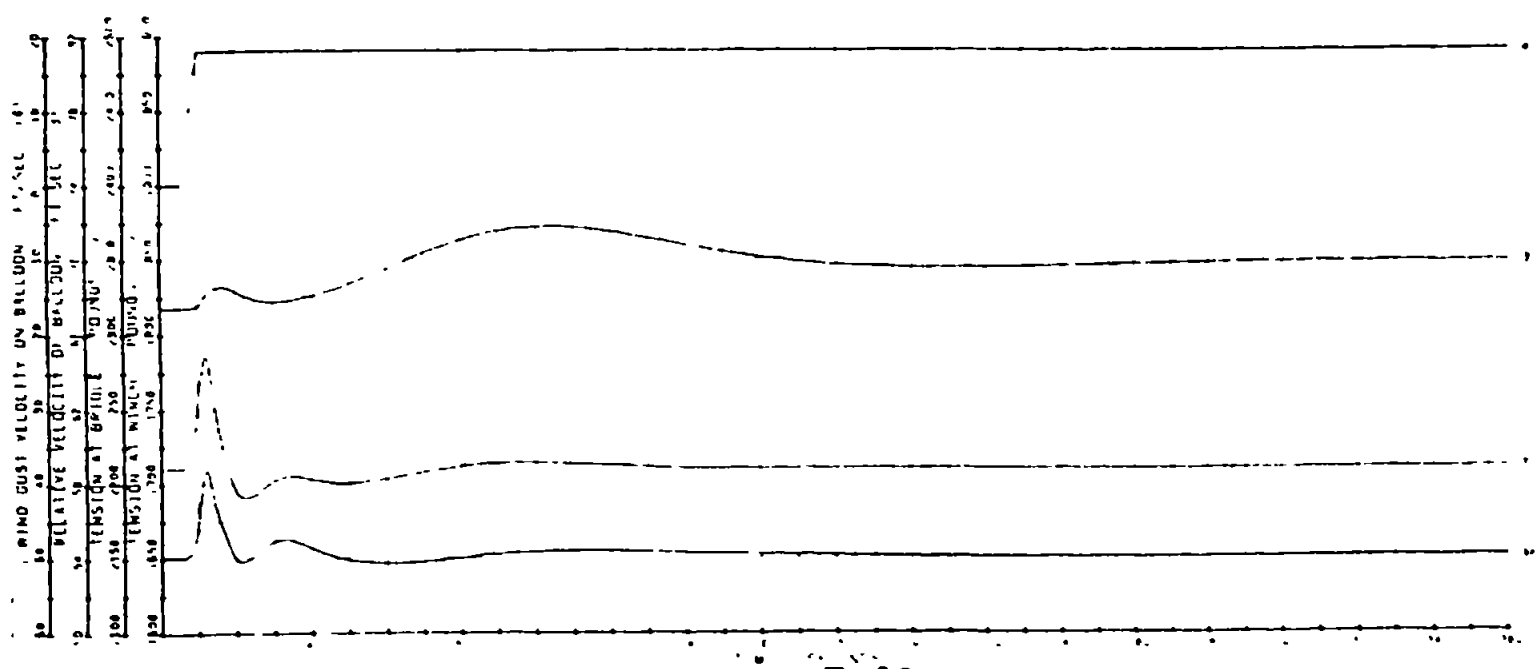

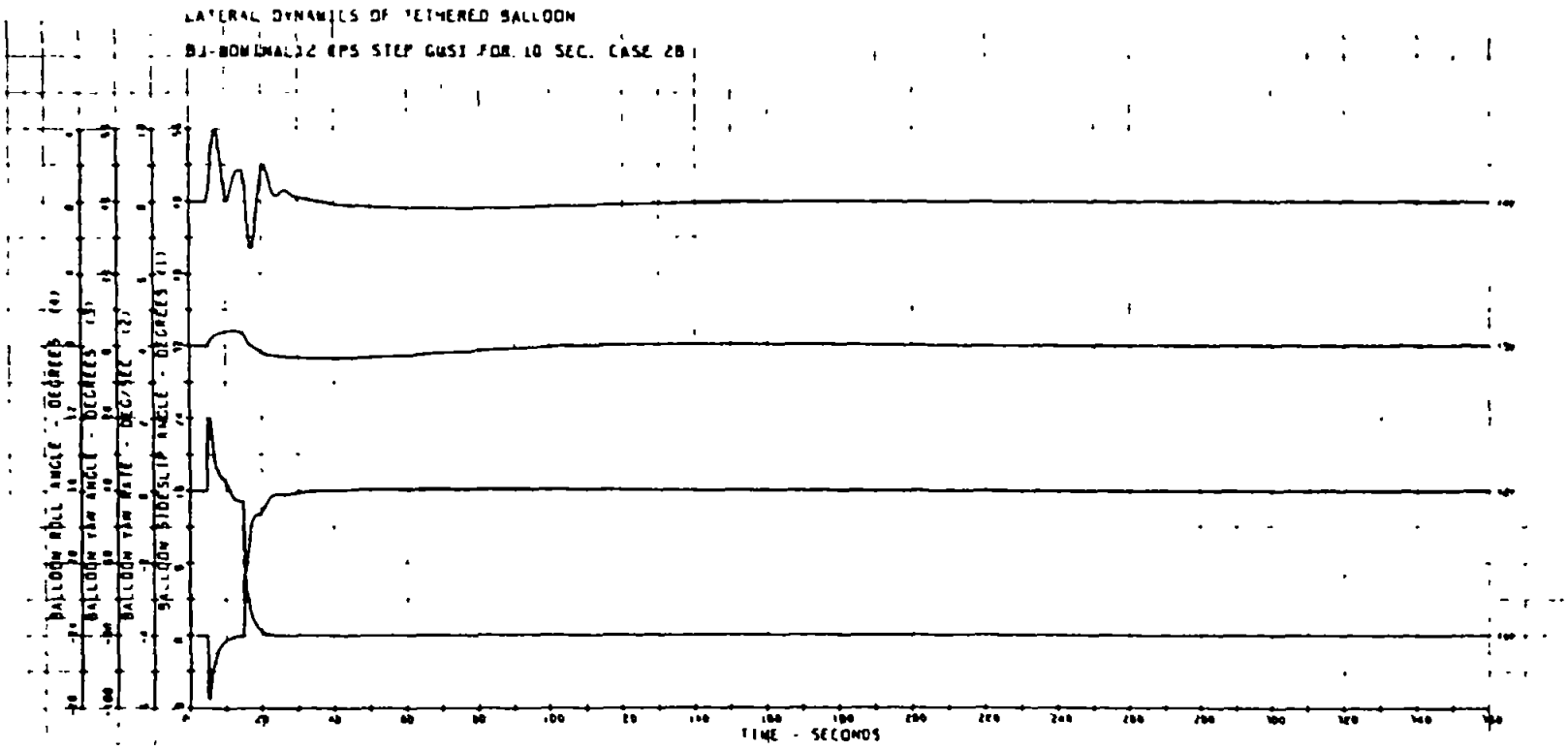
LATERAL DYNAMICS OF TETHERED BALLOON
BJ-NOMINAL12 FPS STEP GUST FOR 10 SEC. CASE 2B
BALLOON ROLL ANGLE - DEGREES
BALLOON YAW ANGLE - DEGREES
BALLOON YAW RATE - DEG/SEC
BALLOON SIDESLIP ANGLE - DEGREES
TIME - SECONDS

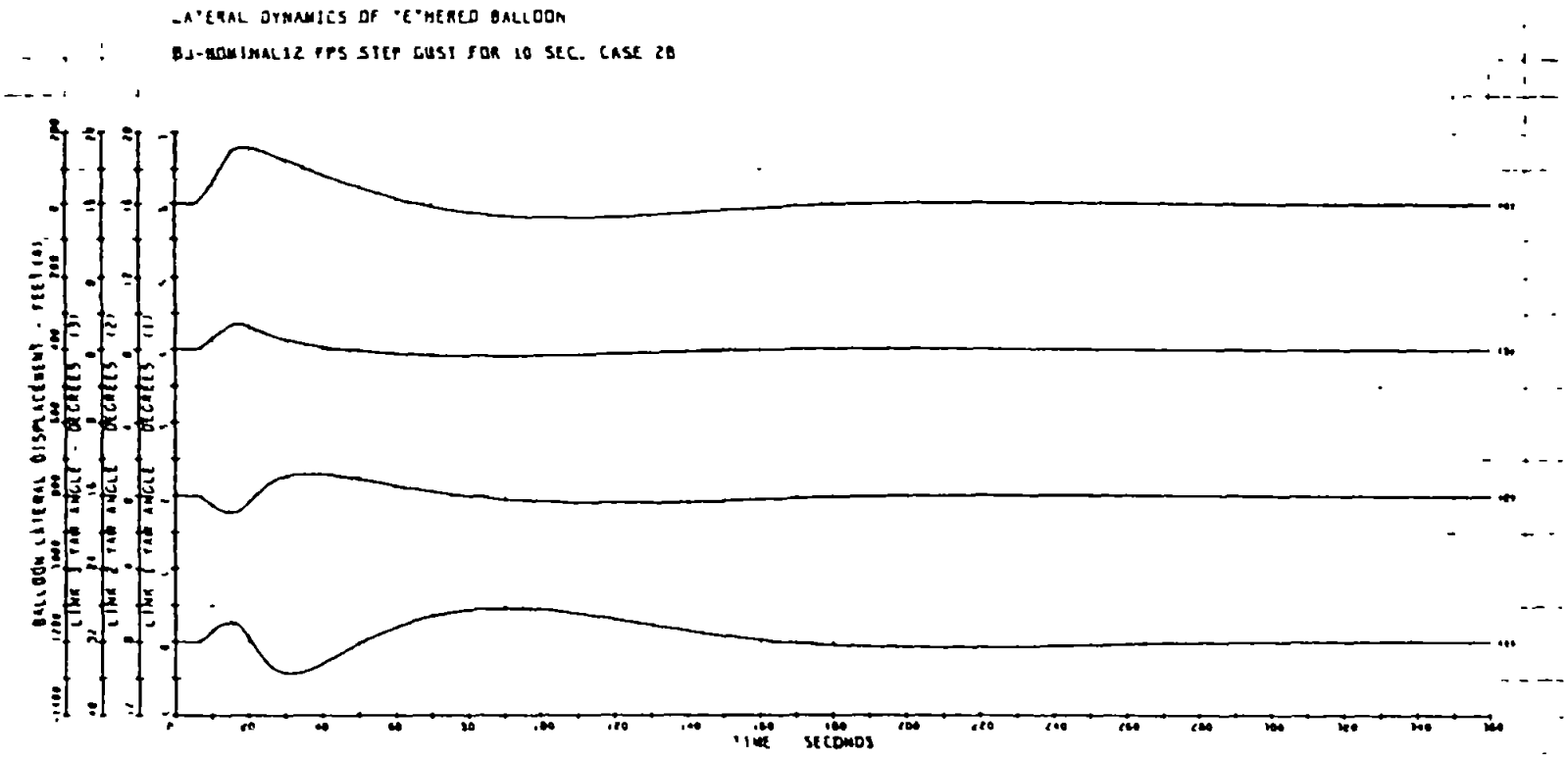
LATERAL DYNAMICS OF TETHERED BALLOON
BJ-NOMINAL12 FPS STEP GUST FOR 10 SEC. CASE 2B
BALLOON LATERAL DISPLACEMENT - FEET
LINK 1 YAW ANGLE - DEGREES
LINK 2 YAW ANGLE - DEGREES
TIME - SECONDS

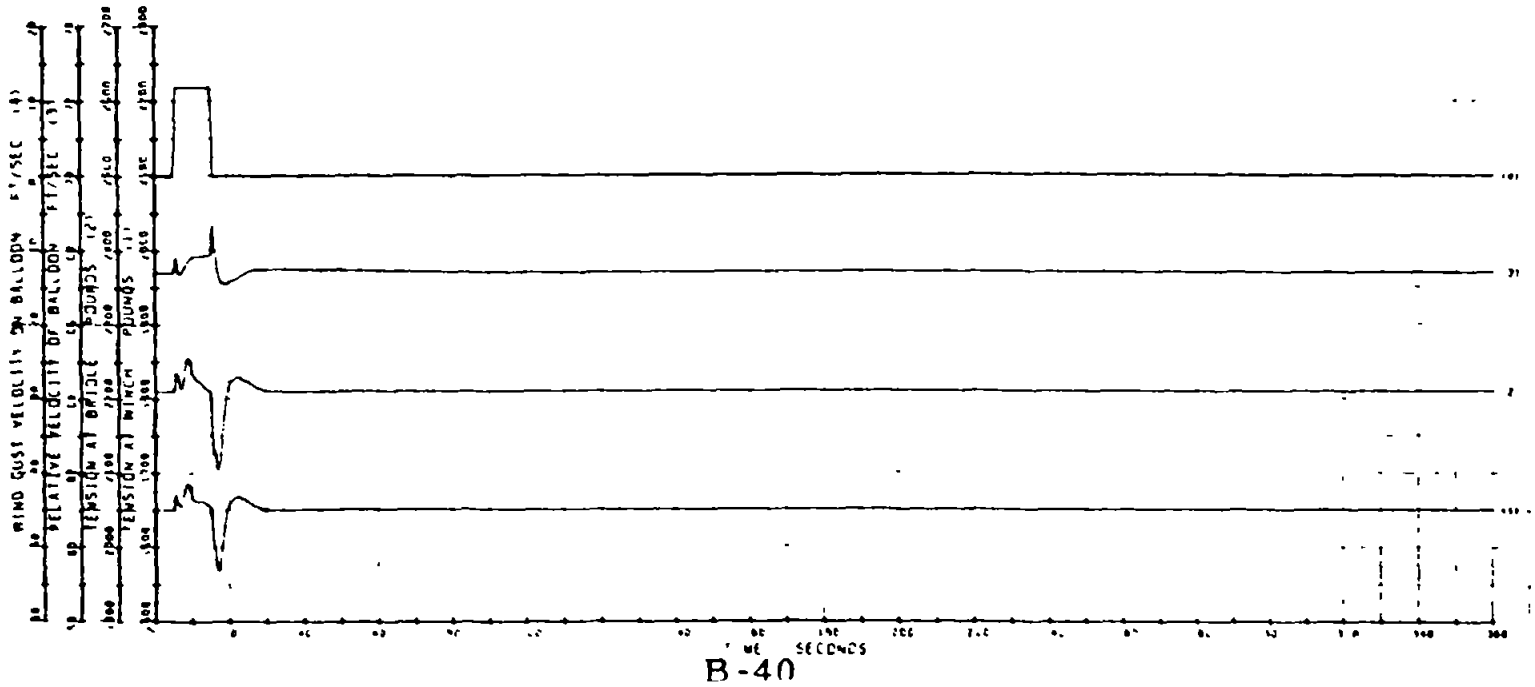
LATERAL DYNAMICS OF TETHERED BALLOON
BJ-NOMINAL12 FPS STEP GUST FOR 10 SEC. CASE 2B
WIND GUST VELOCITY ON BALLOON - FT/SEC
RELATIVE VELOCITY OF BALLOON - FT/SEC
TENSION AT BRIDLE - POUNDS
TENSION AT WINCH - POUNDS
TIME - SECONDS

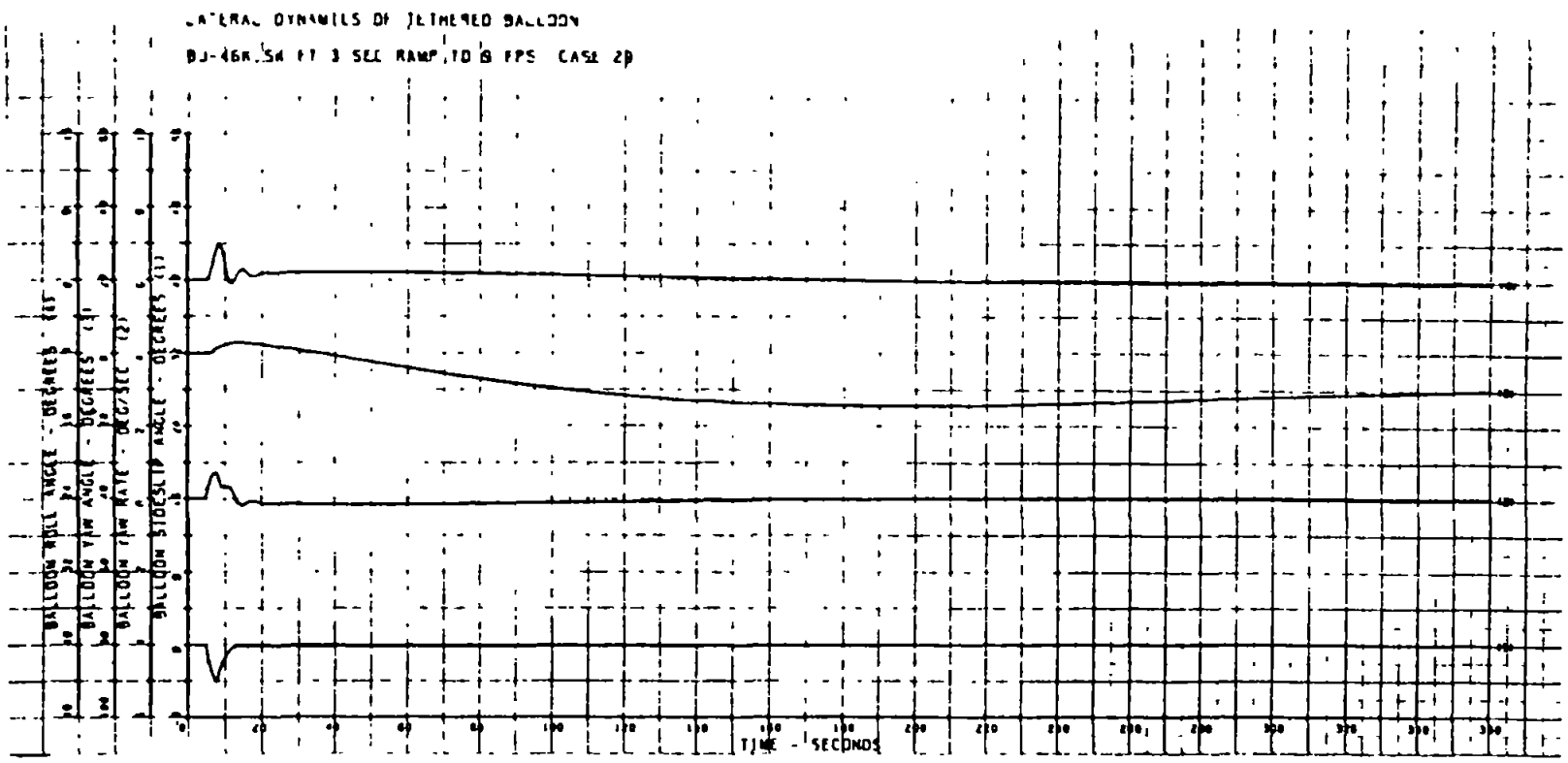
LATERAL DYNAMICS OF TETHERED BALLOON
BALLOON ROLL ANGLE - DEGREES
BALLOON YAW ANGLE - DEGREES
BALLOON YAW RATE - DEG/SEC
BALLOON SIDESLIP ANGLE - DEGREES
TIME - SECONDS

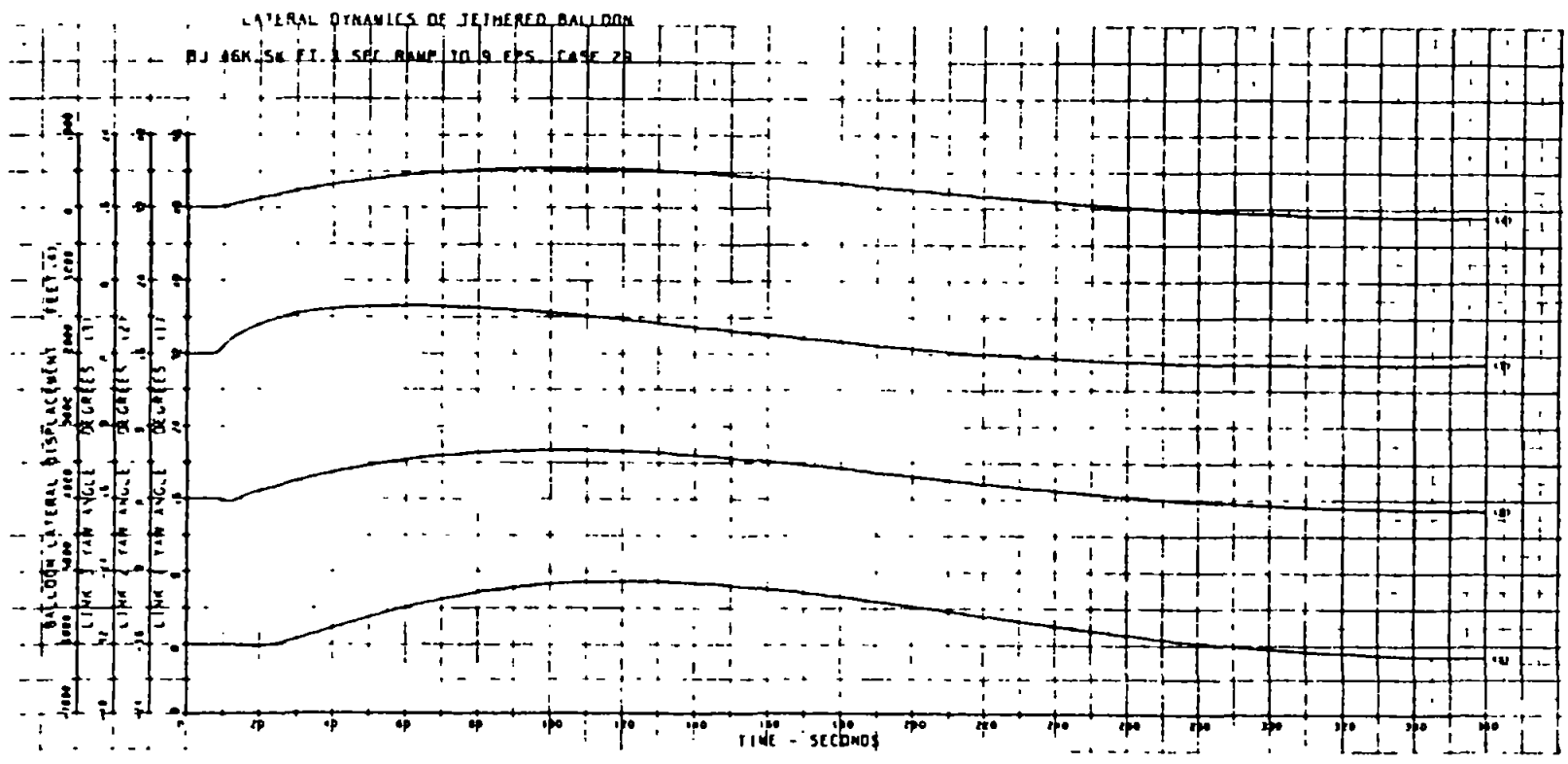
LATERAL DYNAMICS OF TETHERED BALLOON
TIME - SECONDS

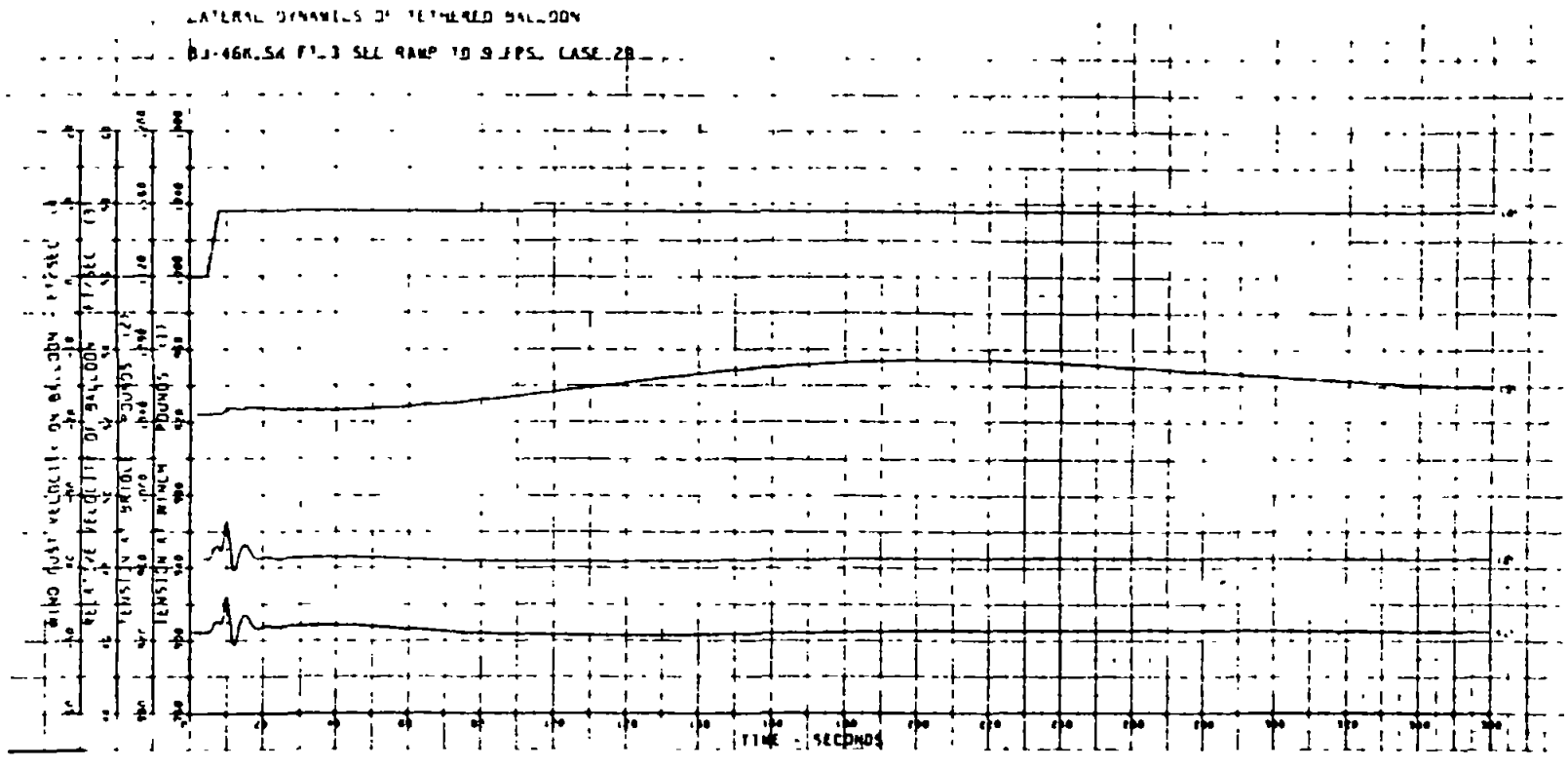
LATERAL DYNAMICS OF TETHERED BALLOON
TIME - SECONDS

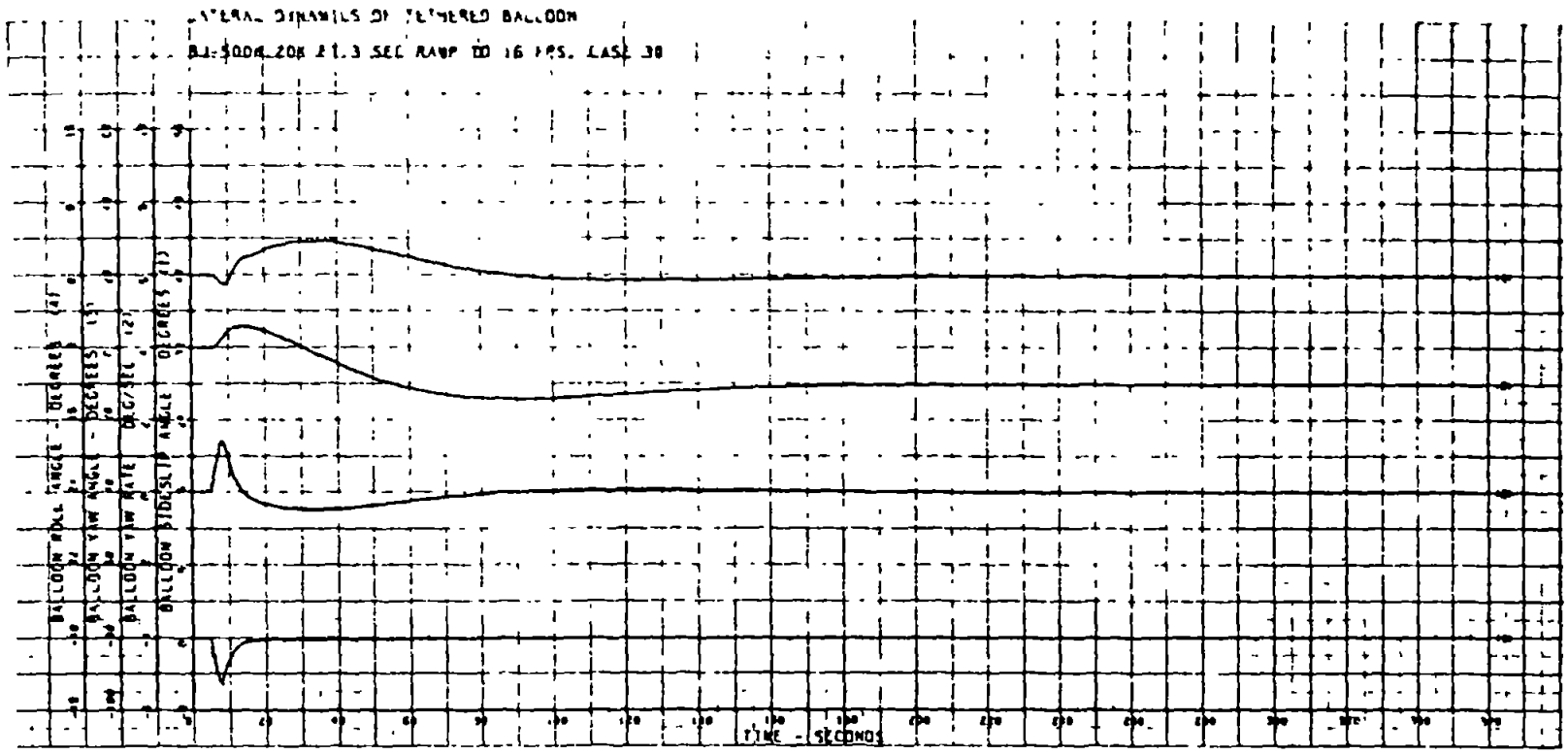
LATERAL DYNAMICS OF TETHERED BALLOON
BALLOON ROLL ANGLE - DEGREES
BALLOON YAW ANGLE - DEGREES
BALLOON YAW RATE - DEG/SEC
BALLOON SIDESLIP ANGLE - DEGREES
TIME - SECONDS

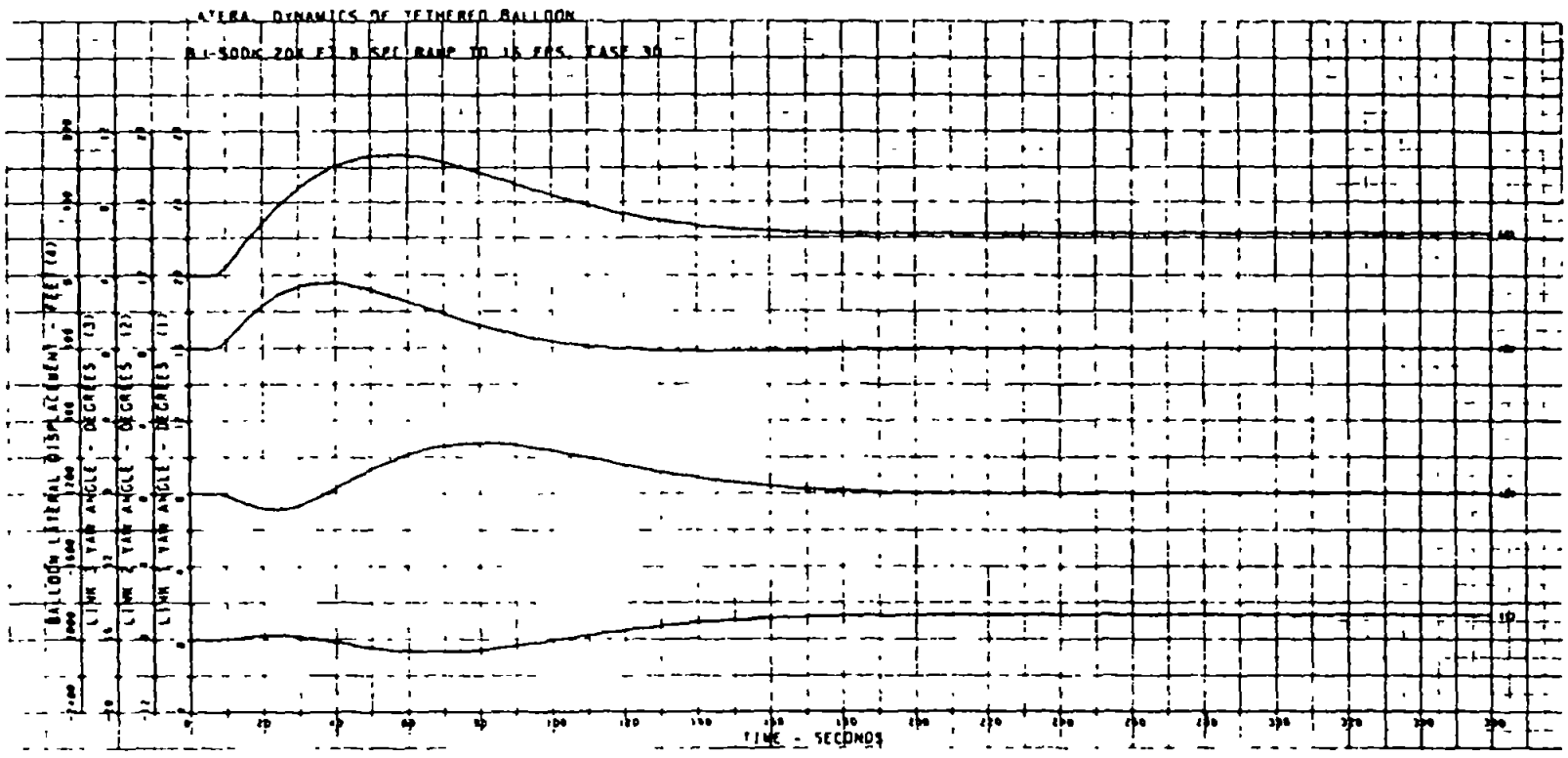
LATERAL DYNAMICS OF TETHERED BALLOON
BALLOON LATERAL DISPLACEMENT - FEET
LINK 1 YAW ANGLE - DEGREES
LINK 2 YAW ANGLE - DEGREES
LINK 3 YAW ANGLE - DEGREES
TIME - SECONDS

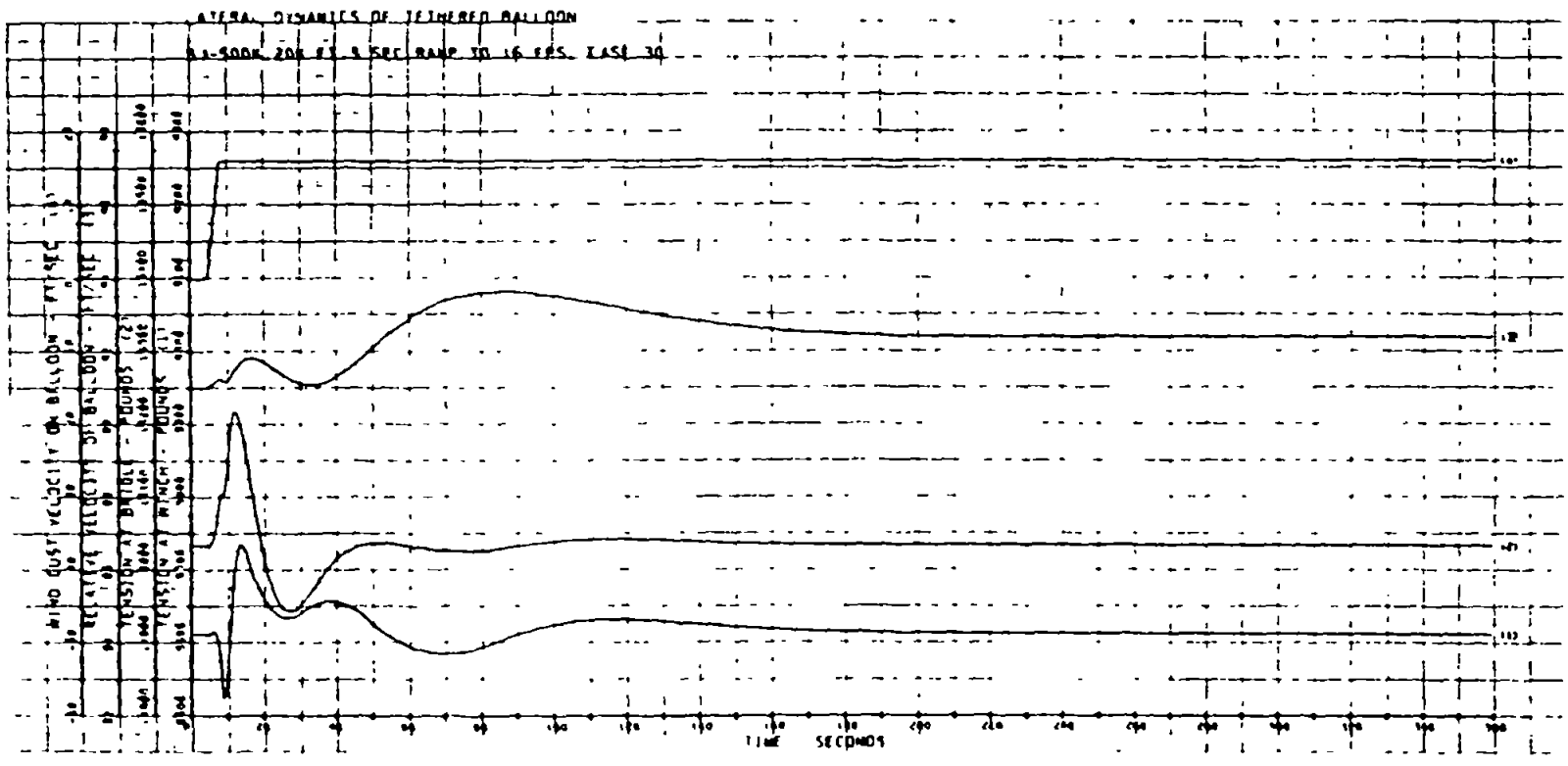
LATERAL DYNAMICS OF TETHERED BALLOON
WIND GUST VELOCITY ON BALLOON - FT/SEC
RELATIVE VELOCITY ON BALLOON - FT/SEC
TENSION AT BRIDLE - POUNDS
TENSION AT WINCH - POUNDS
TIME - SECONDS

LATERAL DYNAMICS OF TETHERED BALLOON

B1 NOMINAL.3 SEC RAMP TO 12 FPS ANGAL. CASE 31

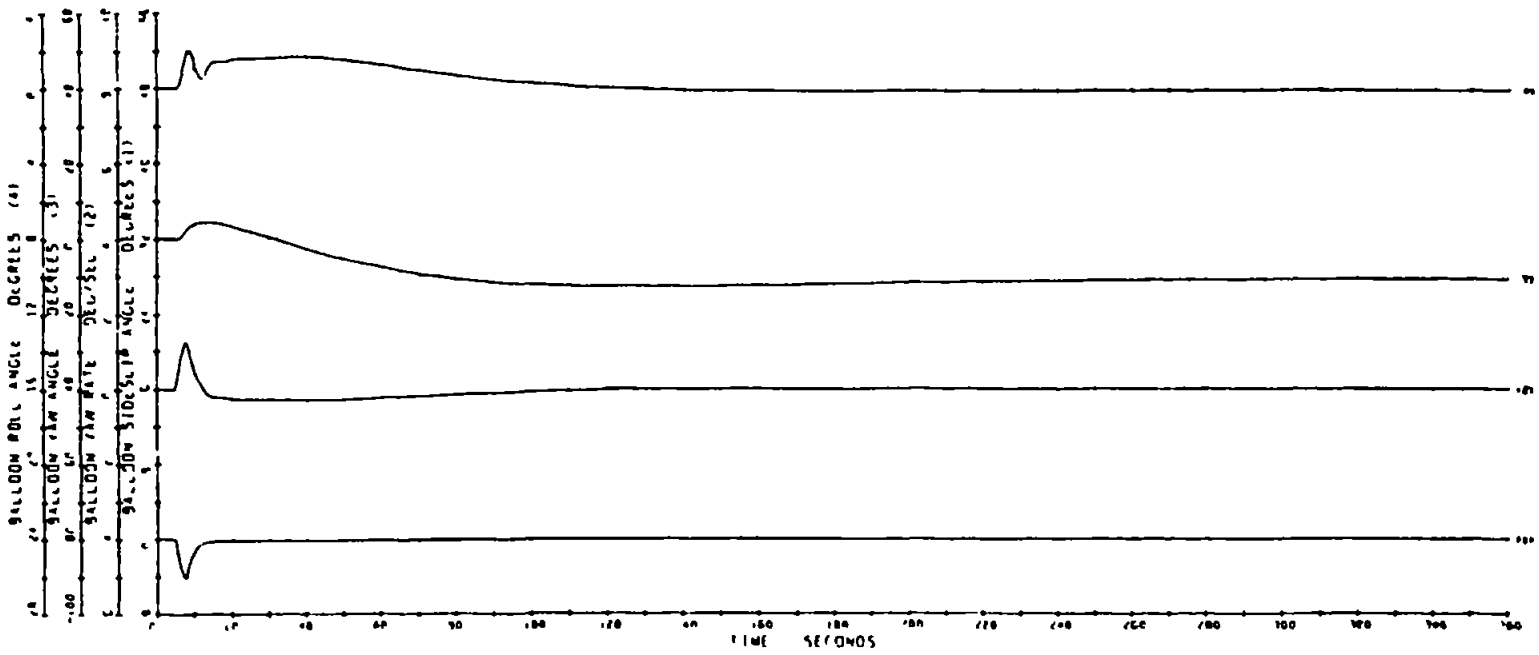

LATERAL DYNAMICS OF TETHERED BALLOON

B1 NOMINAL.3 SEC RAMP TO 12 FPS.ANGAL. CASE 31

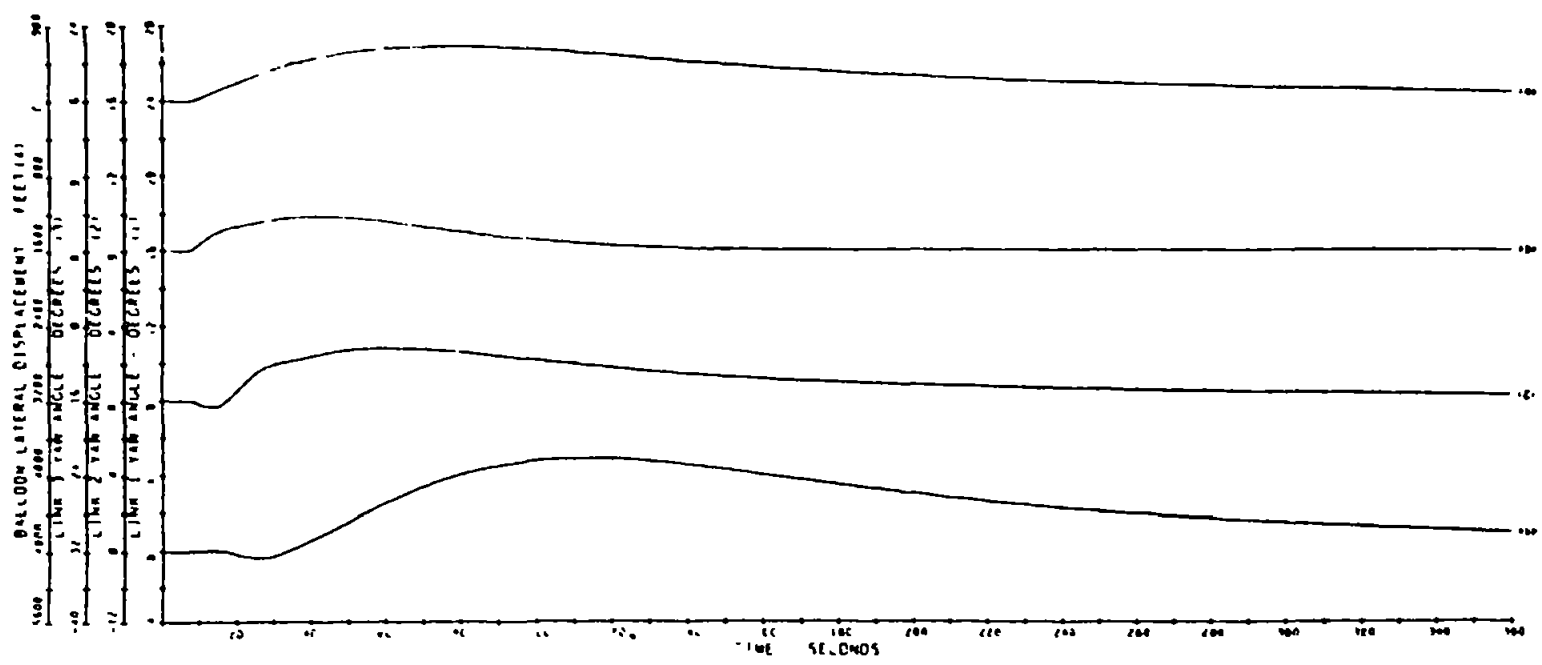

LATERAL DYNAMICS OF TETHERED BALLOON

B1-NOMINAL 3 SEC RAMP TO 12 FPS ANGAL CASE 31

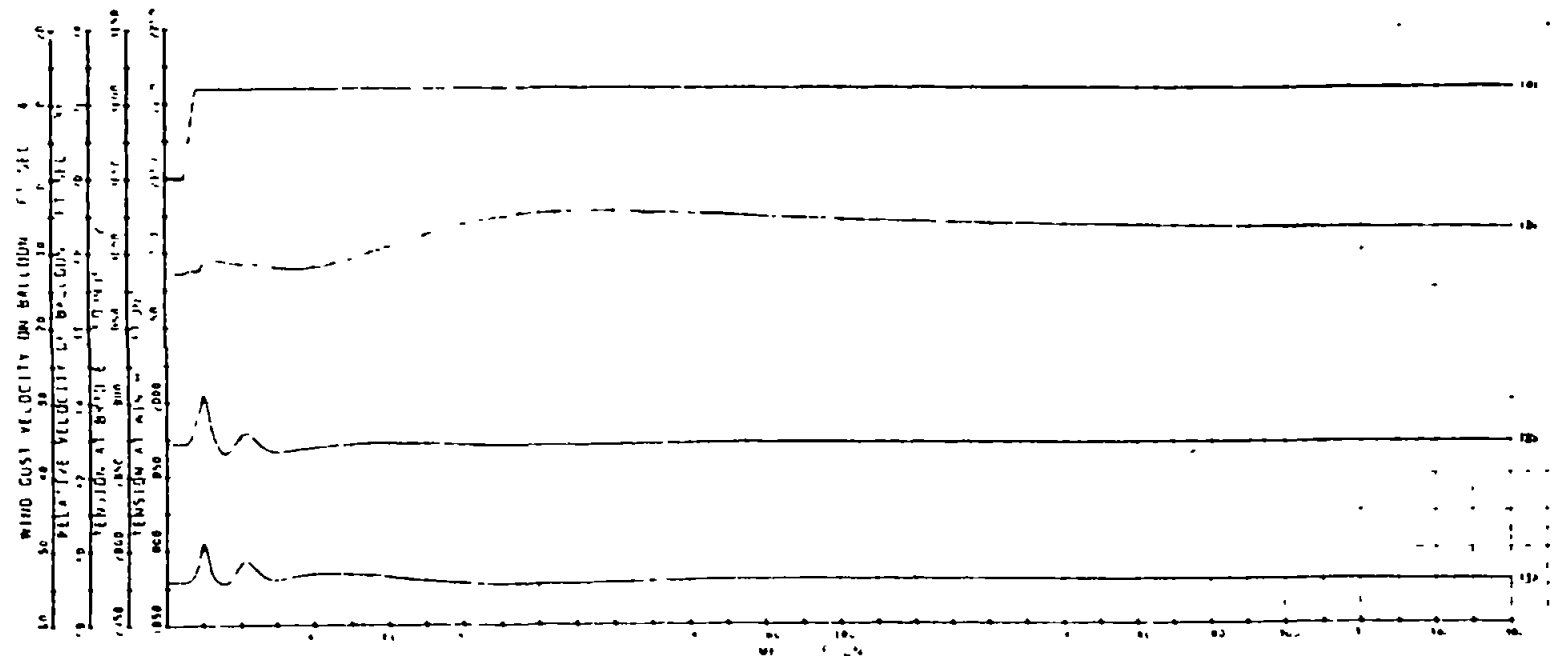

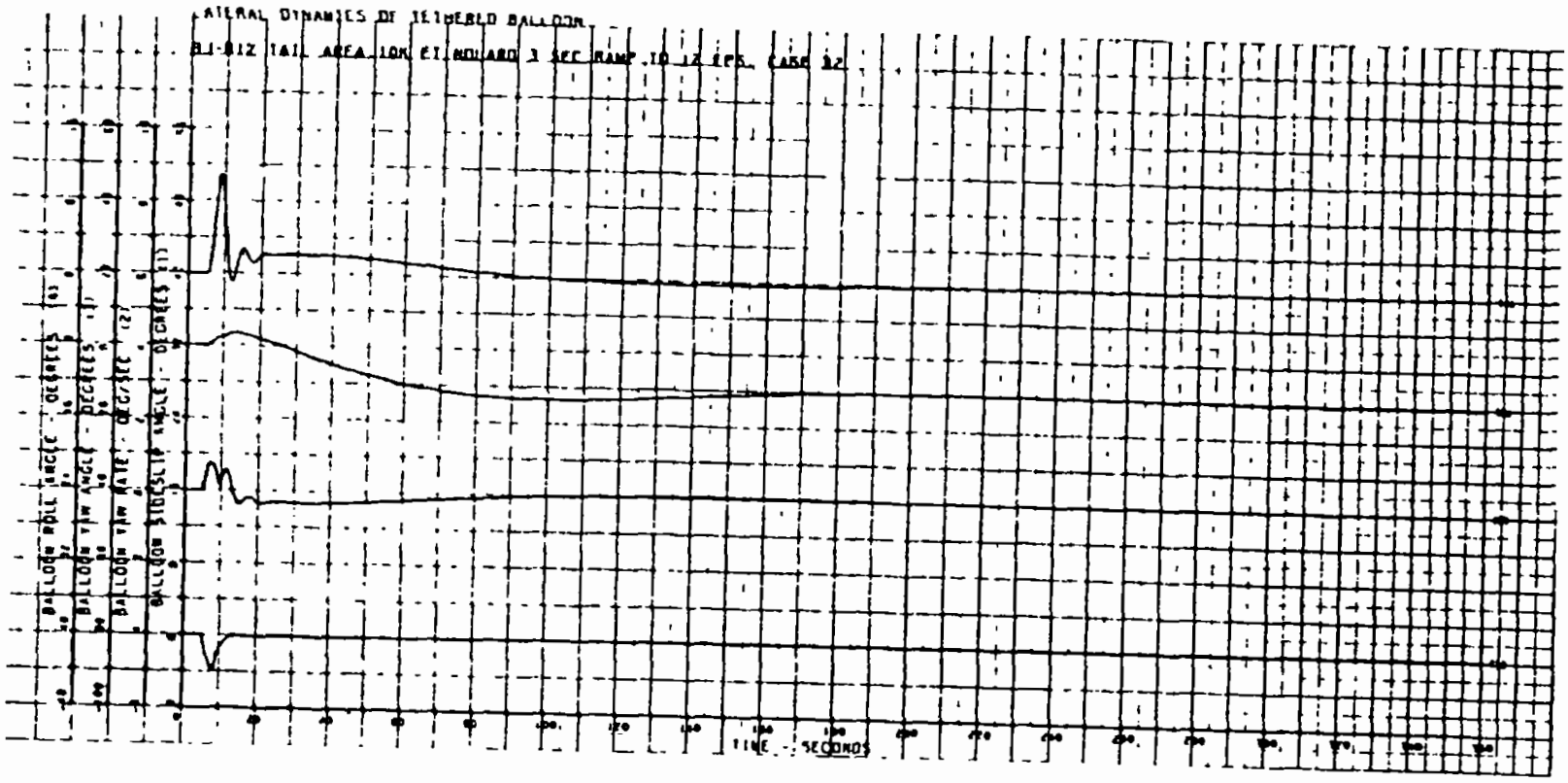
LATERAL DYNAMICS OF TETHERED BALLOON
TIME - SECONDS

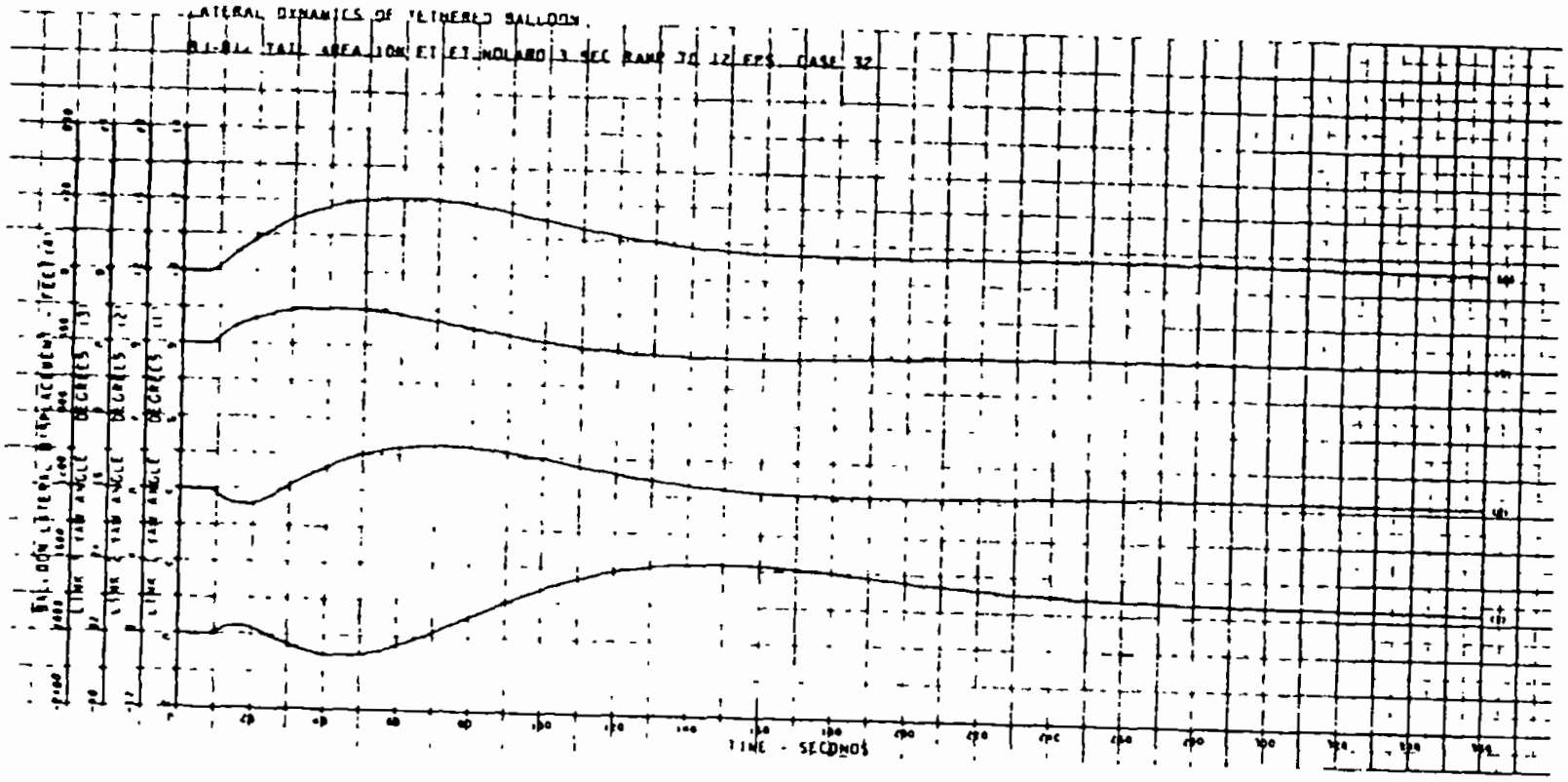
LATERAL DYNAMICS OF TETHERED BALLOON
TIME - SECONDS

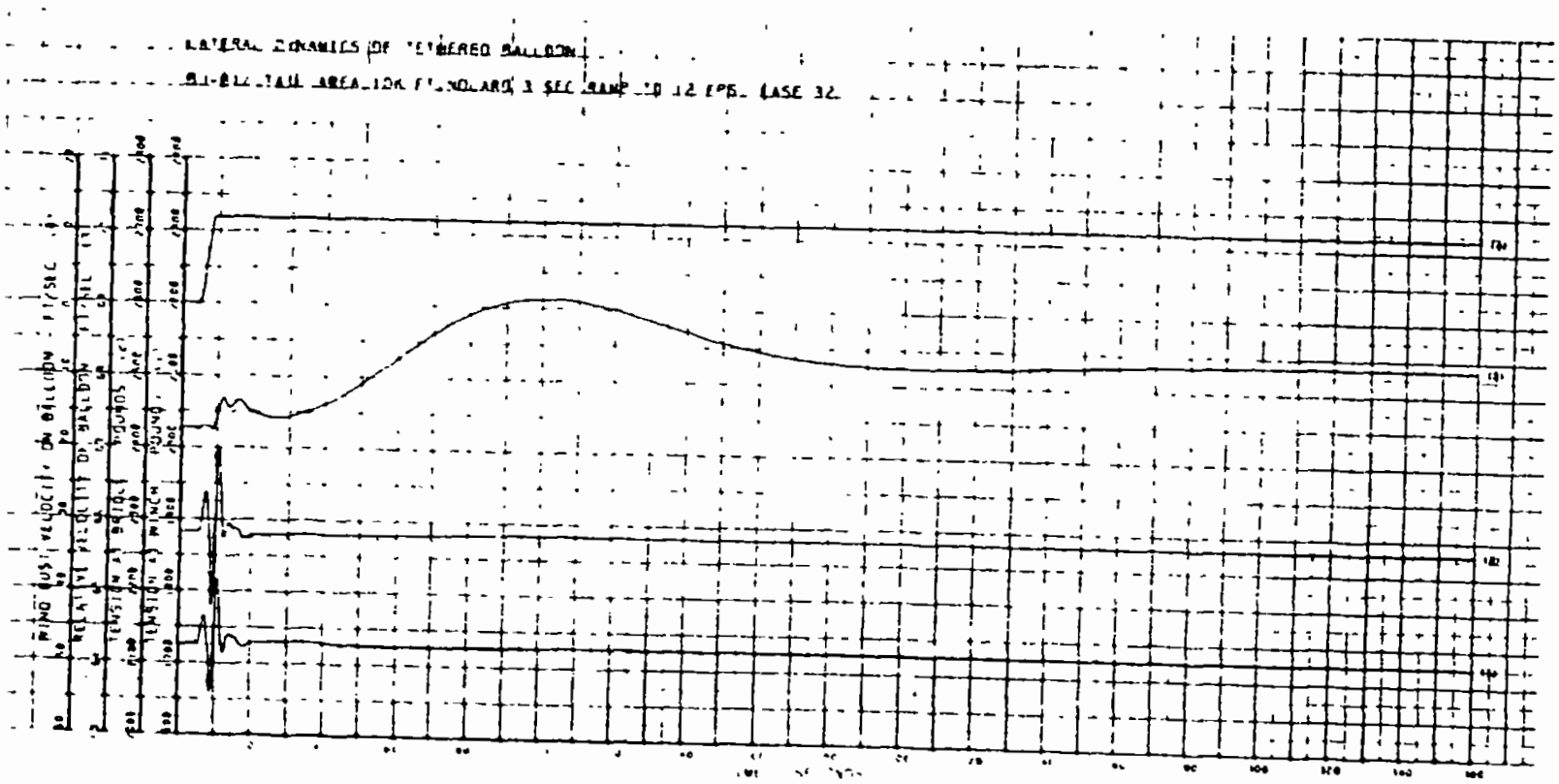
LATERAL DYNAMICS OF TETHERED BALLOON

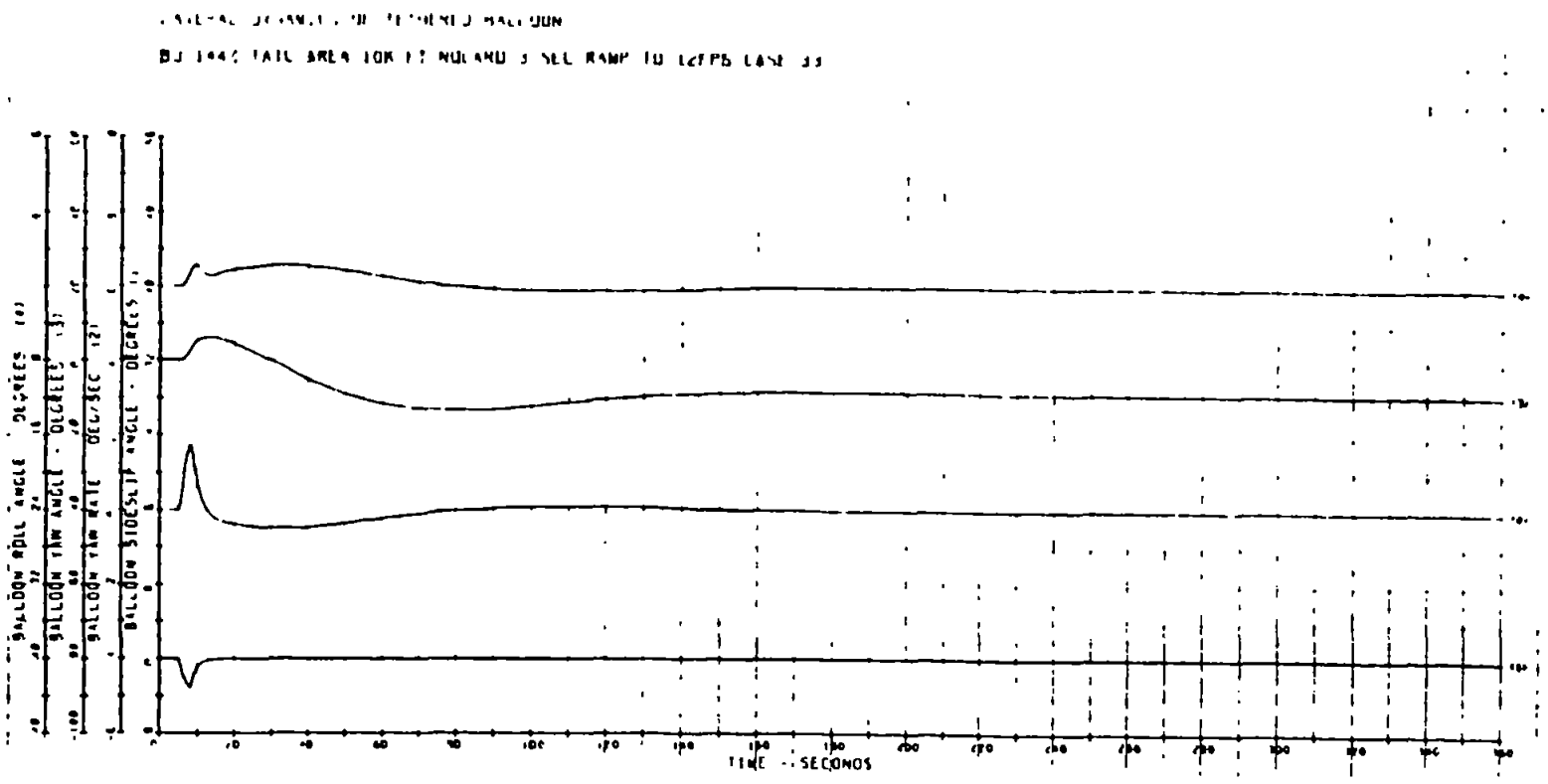
BALLOON ROLL ANGLE - DEGREES
BALLOON YAW ANGLE - DEGREES
BALLOON YAW RATE - DEG/SEC
BALLOON SIDESLIP ANGLE - DEGREES
TIME - SECONDS

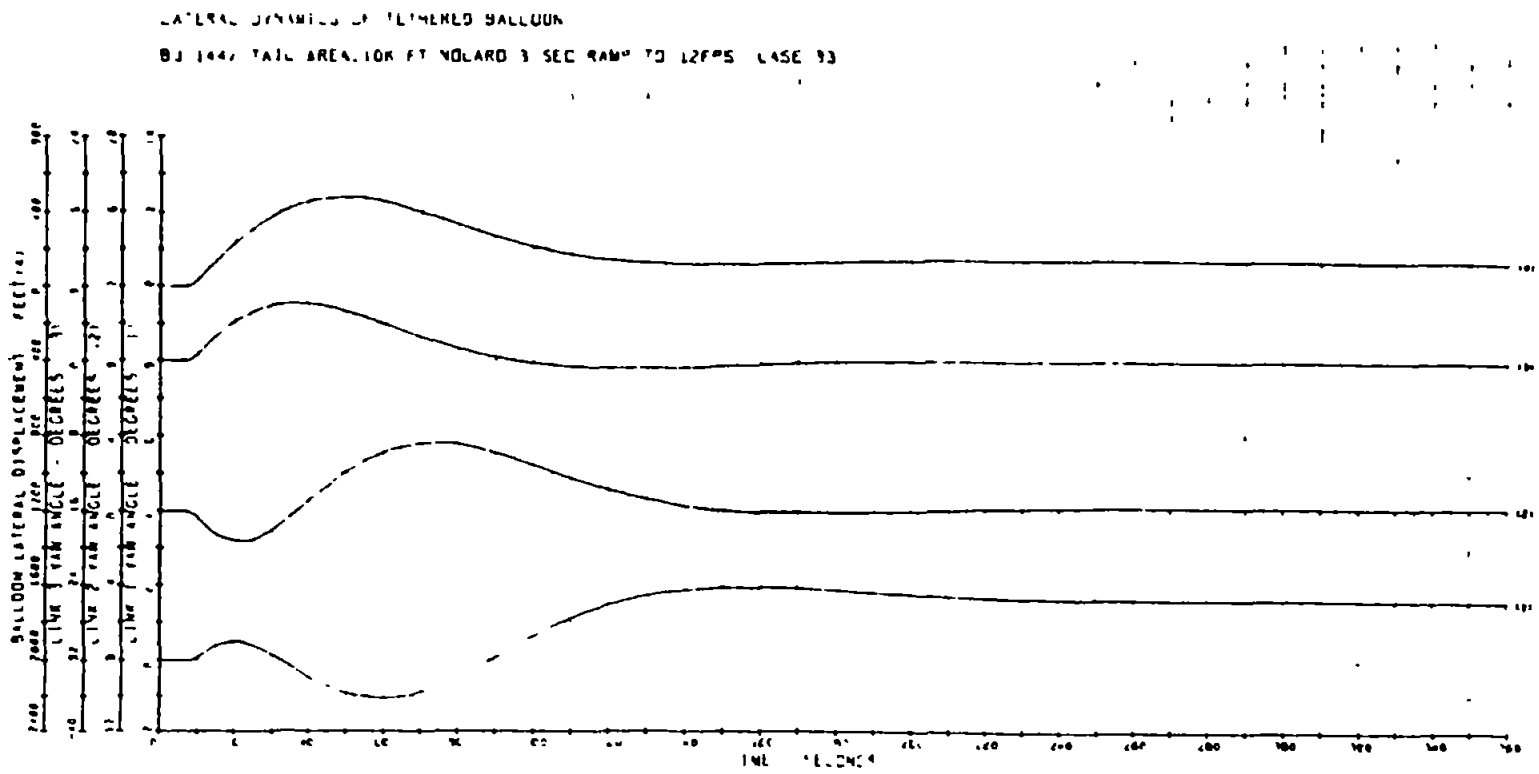
BALLOON LATERAL DISPLACEMENT - FEET
BALLOON YAW ANGLE - DEGREES
BALLOON YAW ANGLE - DEGREES
TIME - SECONDS

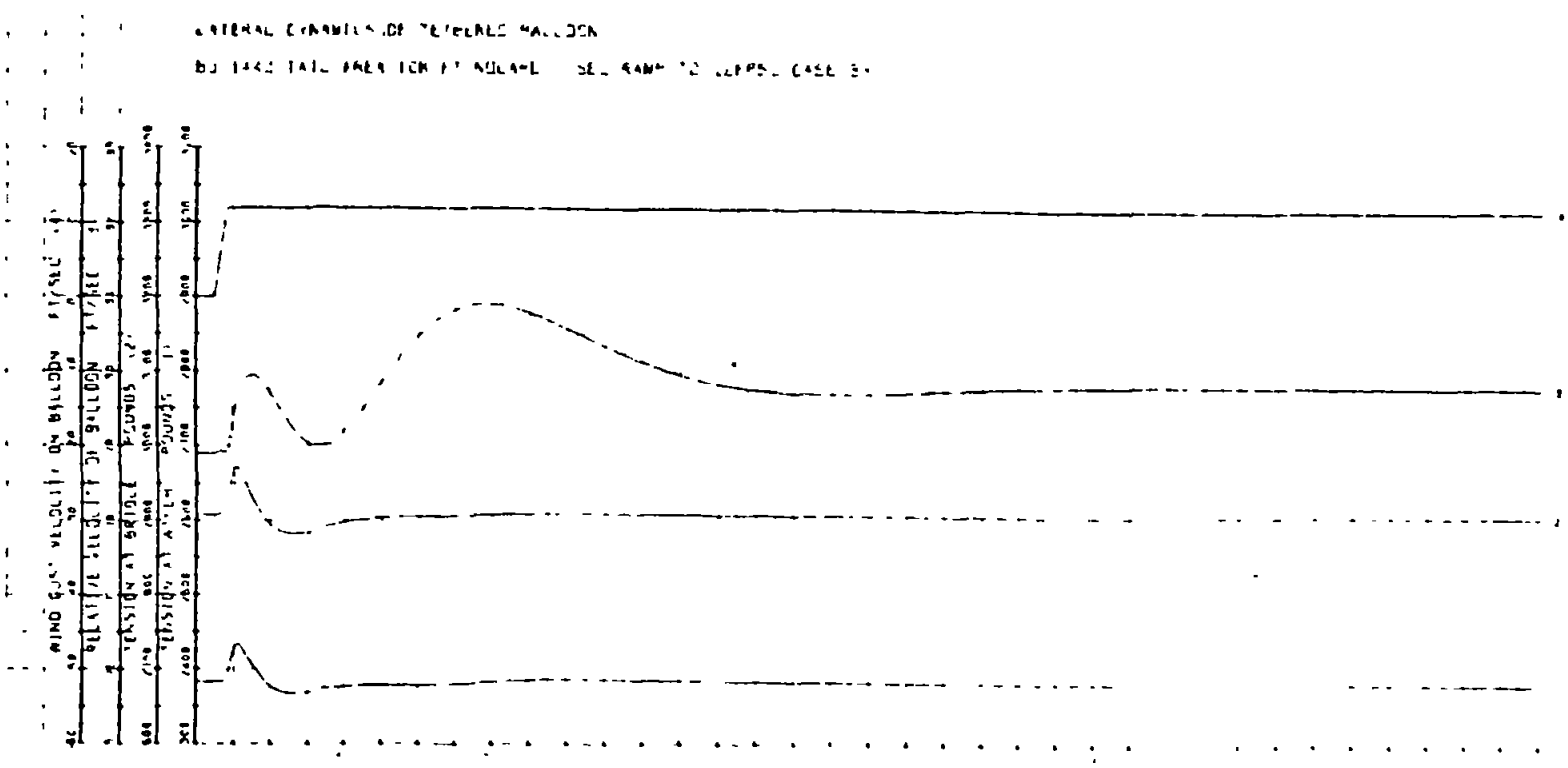
WIND GUST VELOCITY ON BALLOON - FT/SEC
RELATIVE VELOCITY ON BALLOON - FT/SEC
TENSION AT BRIDLE - POUNDS
TENSION AT MAST - POUNDS

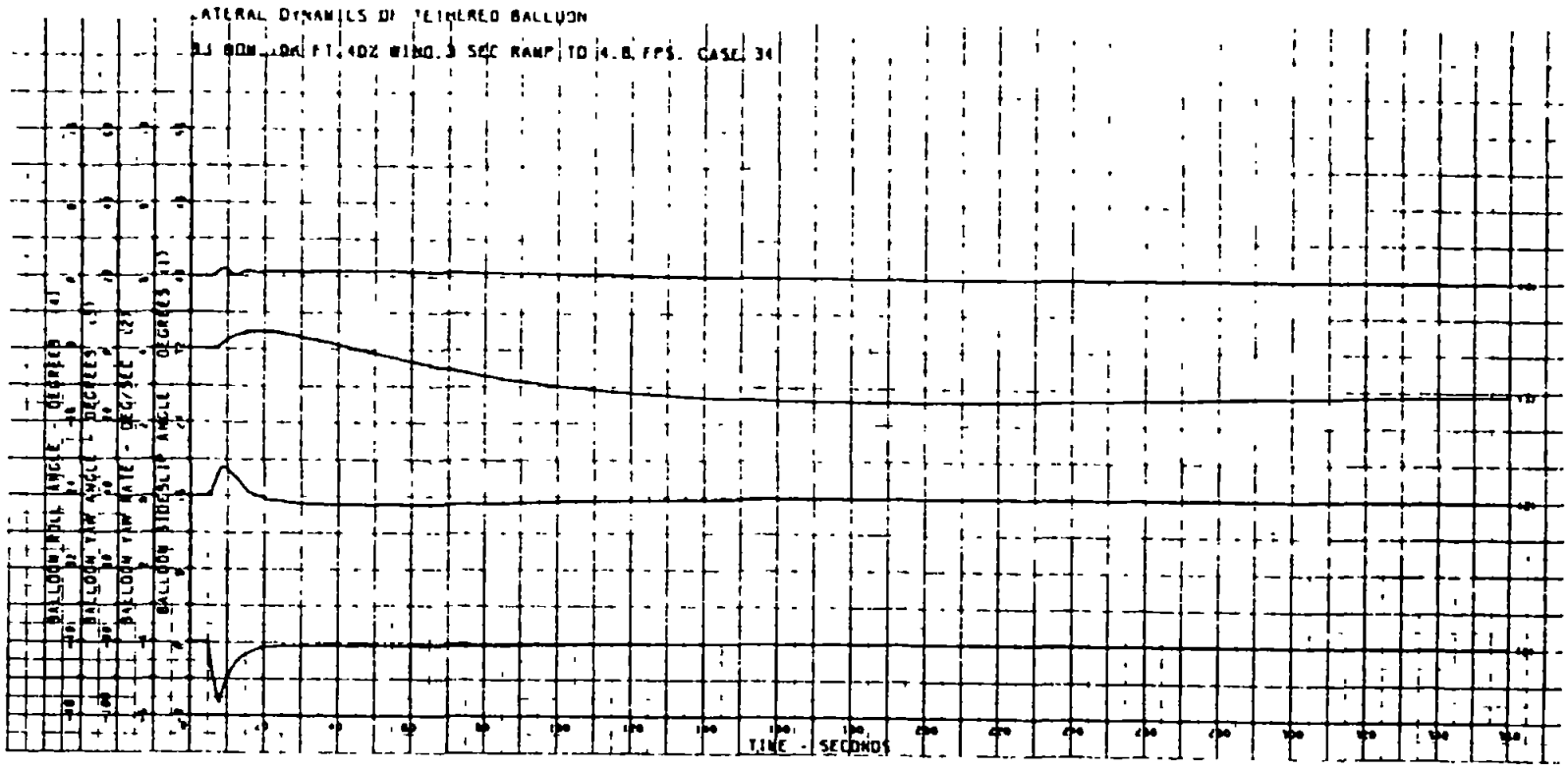
LATERAL DYNAMICS OF TETHERED BALLOON
TIME - SECONDS

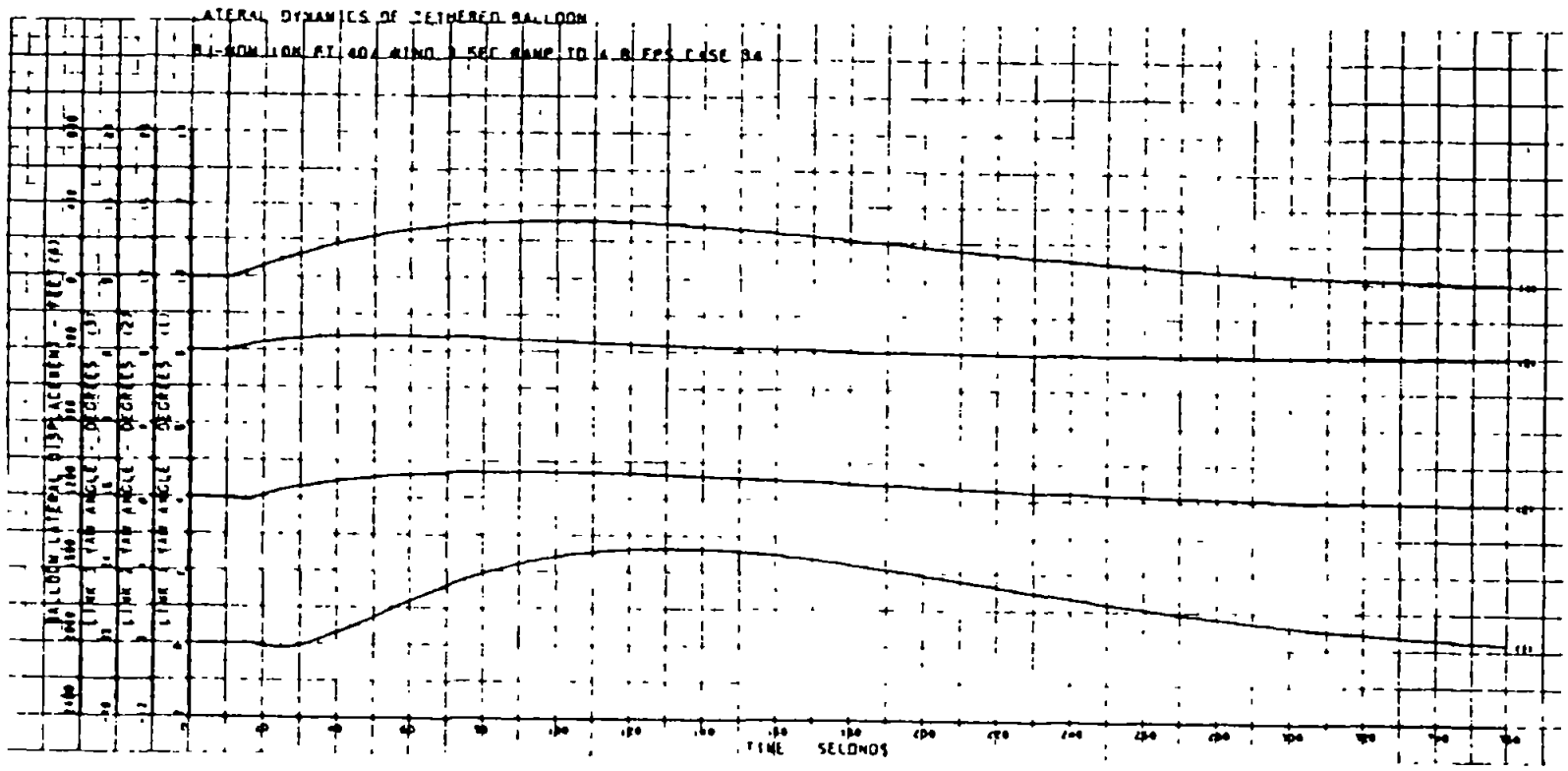
LATERAL DYNAMICS OF TETHERED BALLOON
TIME SECONDS

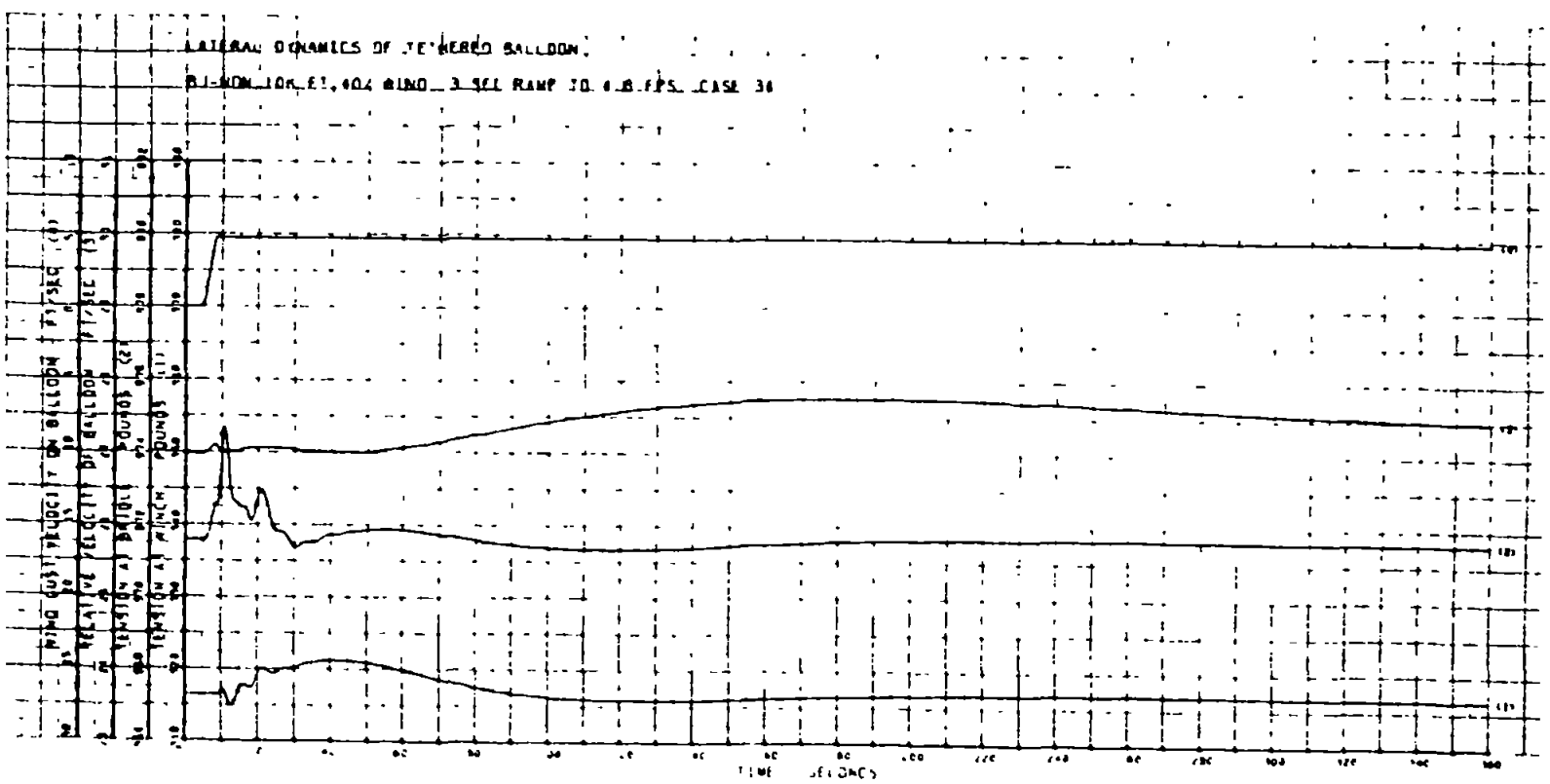
LATERAL DYNAMICS OF TETHERED BALLOON

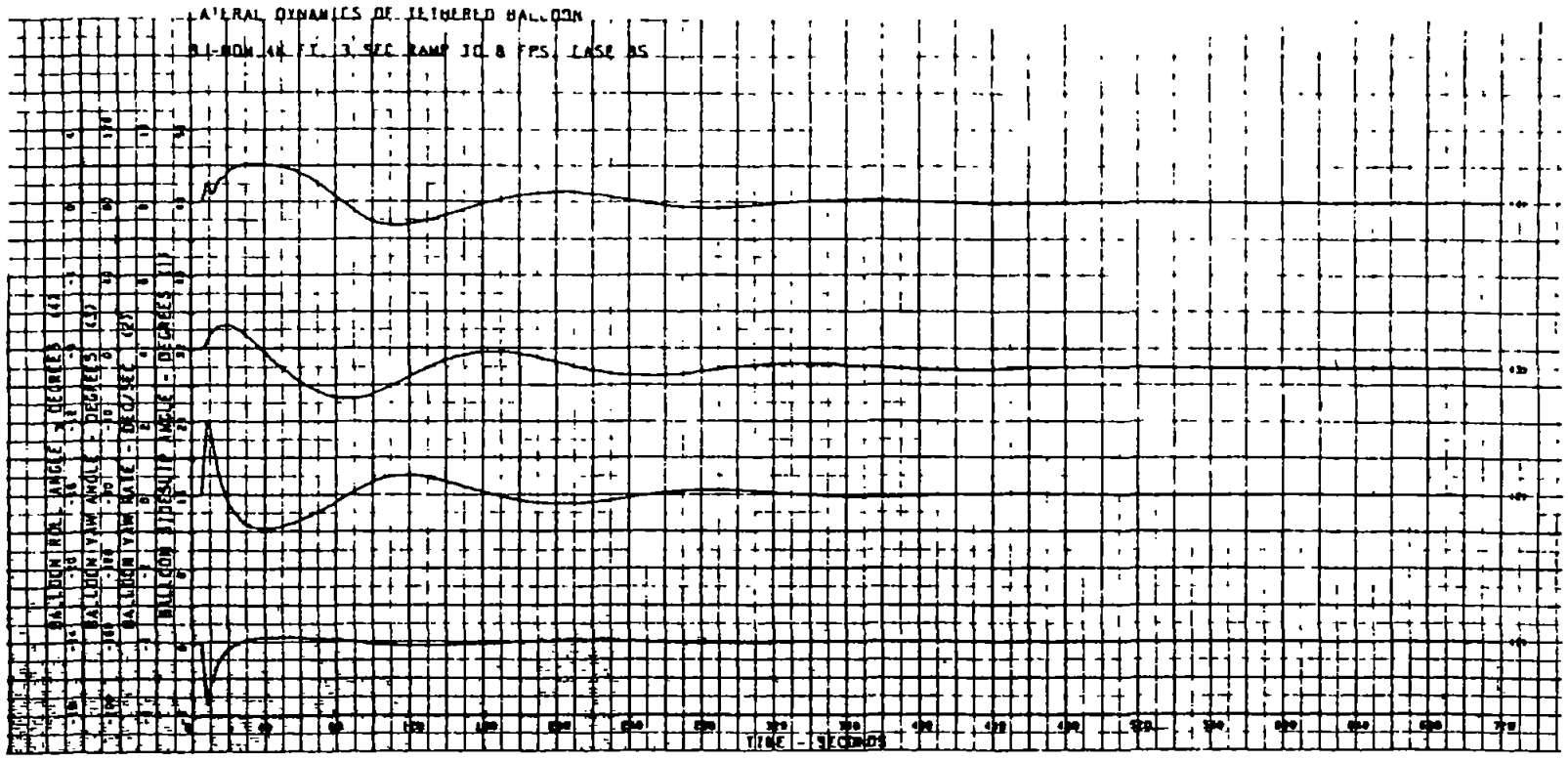
LATERAL DYNAMICS OF TETHERED BALLOON
BI-BOW 48 FT. 3 SEC RAMP TO 8 FPS, CASE 35
BALLOON ROLL ANGLE - DEGREES
BALLOON YAW ANGLE - DEGREES
BALLOON YAW RATE - DEGREES/SEC
BALLOON SIDESLIP ANGLE - DEGREES
TIME - SECONDS

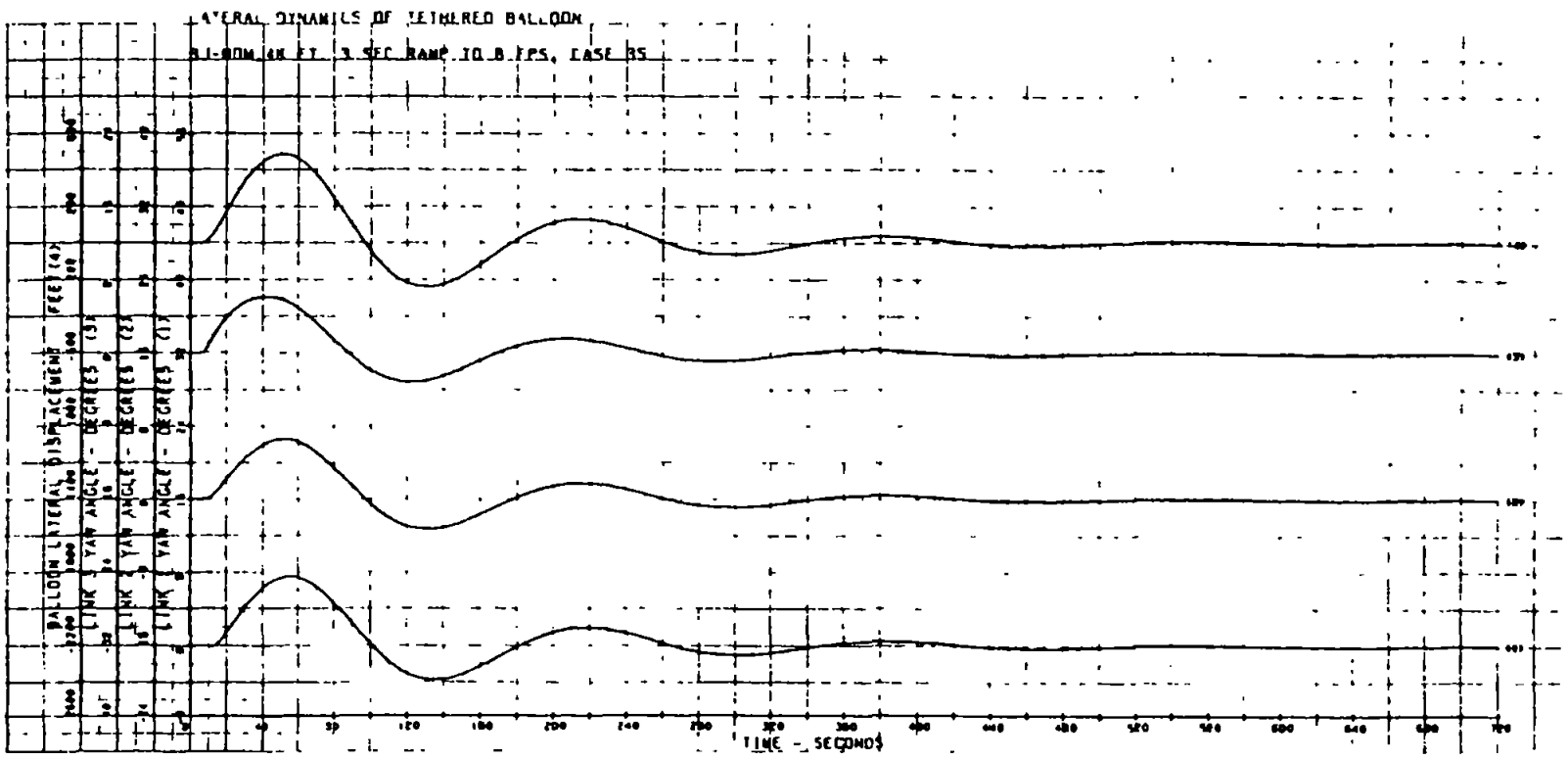
LATERAL DYNAMICS OF TETHERED BALLOON
BI-BOW 48 FT. 3 SEC RAMP TO 8 FPS, CASE 35
BALLOON LATERAL DISPLACEMENT - FEET
LINK 1 YAW ANGLE - DEGREES
LINK 2 YAW ANGLE - DEGREES
TIME - SECONDS

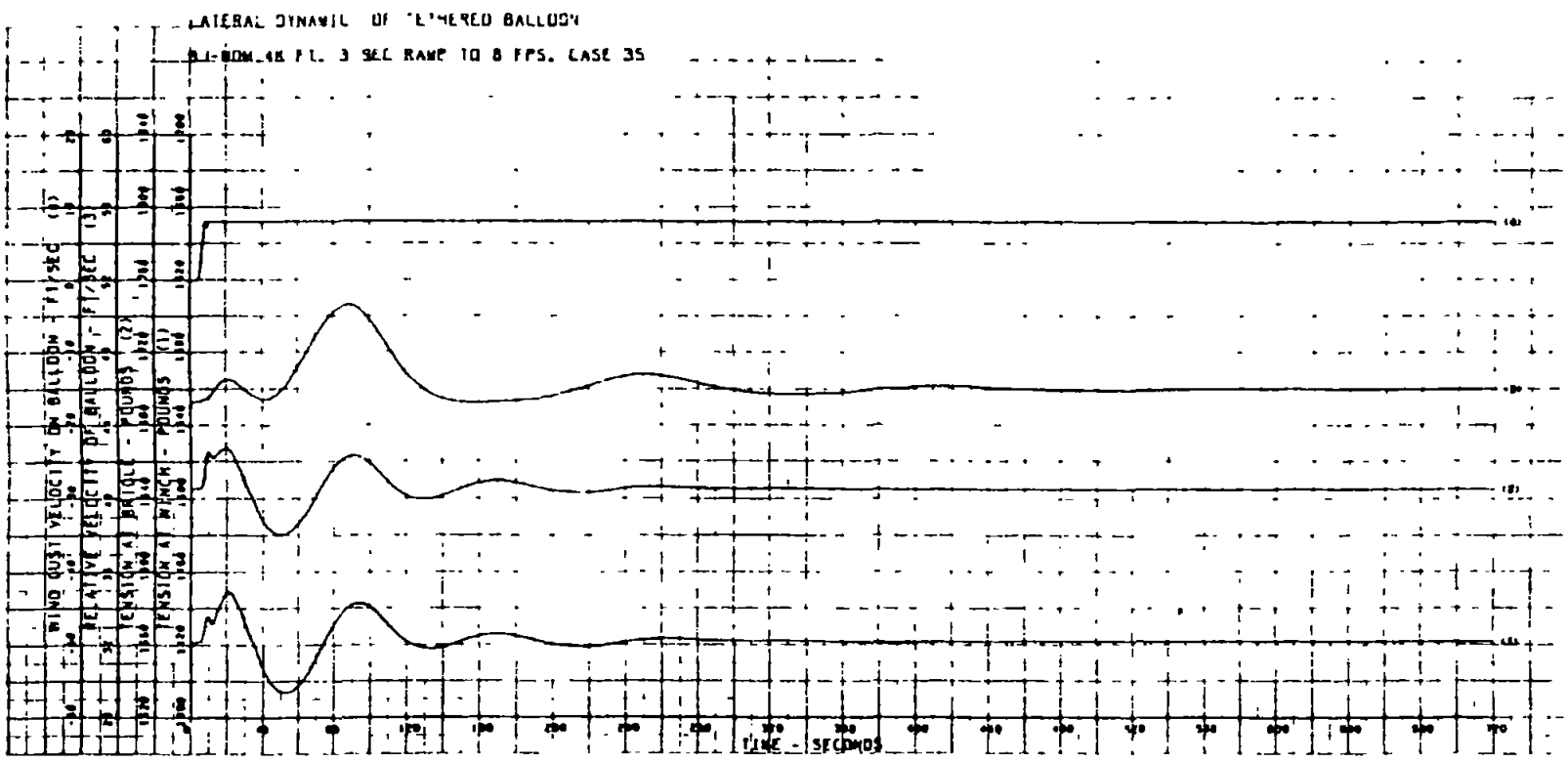
LATERAL DYNAMICS OF TETHERED BALLOON
BI-BOW 48 FT. 3 SEC RAMP TO 8 FPS, CASE 35
WIND GUST VELOCITY ON BALLOON - FT/SEC
RELATIVE VELOCITY OF BALLOON - FT/SEC
TENSION AT BRIDLE - POUNDS
TENSION AT WINCH - POUNDS
TIME - SECONDS

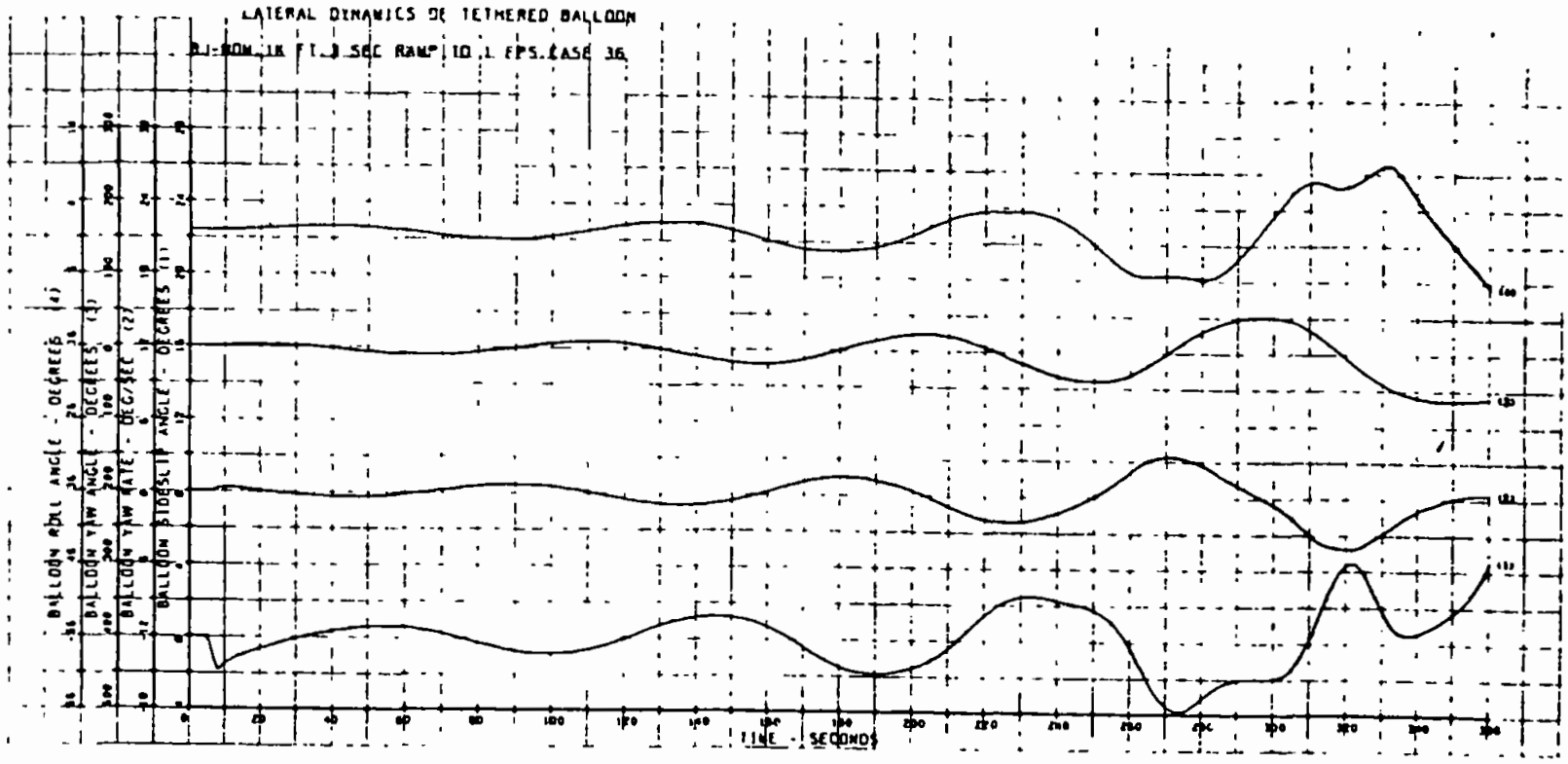
LATERAL DYNAMICS OF TETHERED BALLOON
BALLOON ROLL ANGLE - DEGREES
BALLOON YAW ANGLE - DEGREES
BALLOON YAW RATE - DEG/SEC
BALLOON SIDESLIP ANGLE - DEGREES
TIME - SECONDS

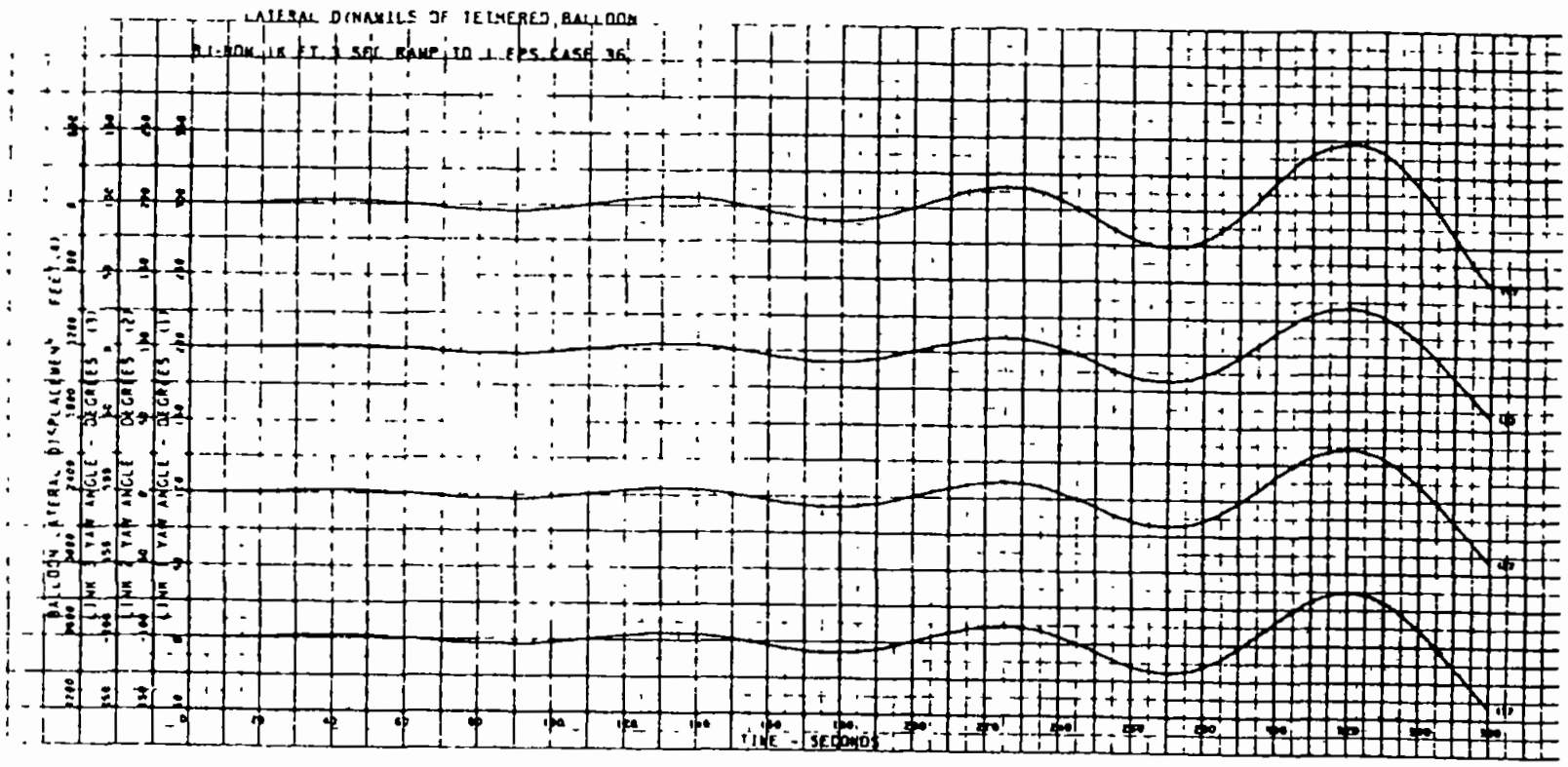
LATERAL DYNAMICS OF TETHERED BALLOON
BALLOON LATERAL DISPLACEMENT - FEET
BALLOON YAW ANGLE - DEGREES
BALLOON LINK YAW ANGLE - DEGREES
TIME - SECONDS

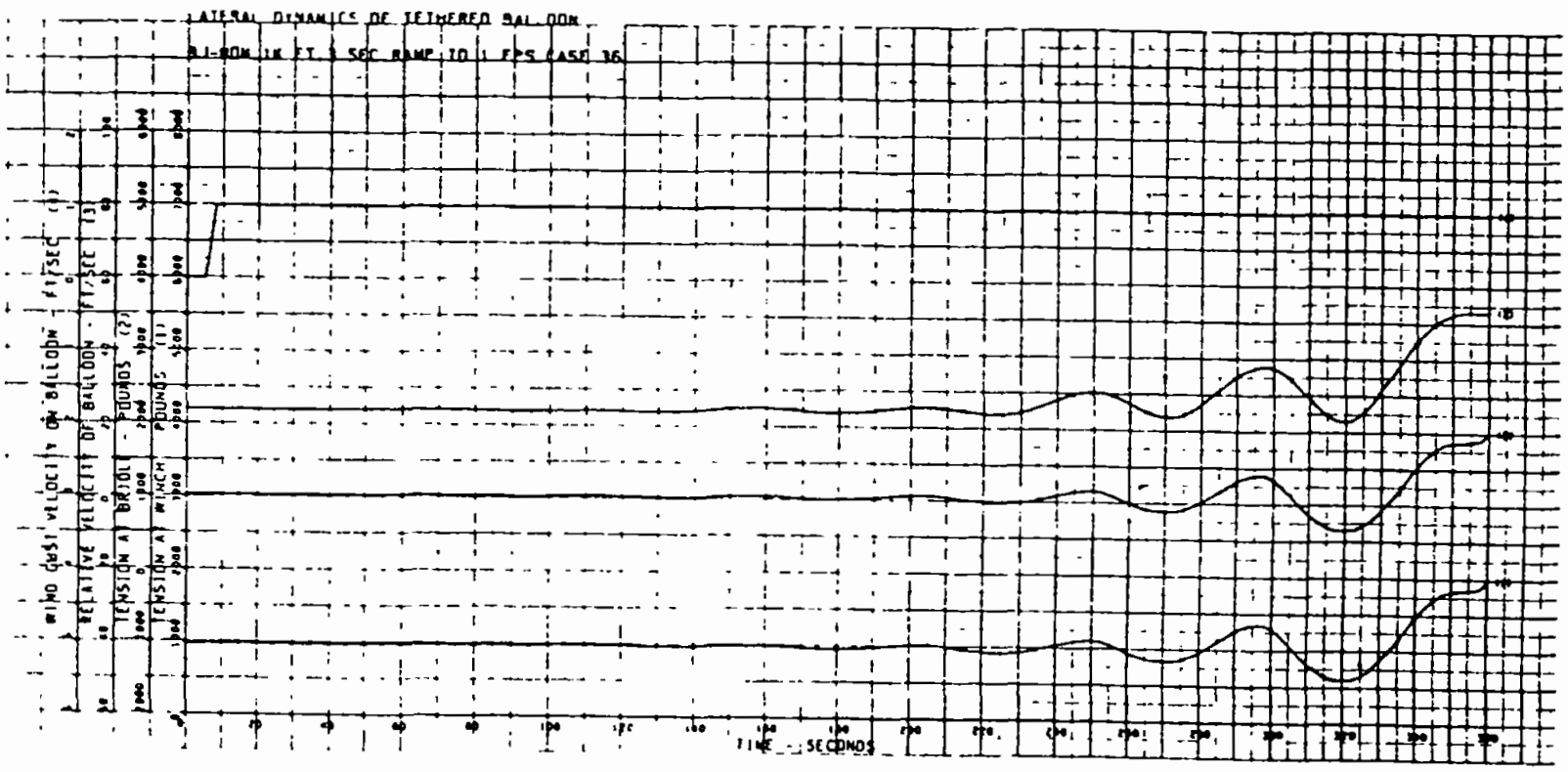
LATERAL DYNAMICS OF TETHERED BALLOON
WIND GUST VELOCITY ON BALLOON - FT/SEC
RELATIVE VELOCITY OF BALLOON - FT/SEC
TENSION AT BRIDL - POUNDS
TENSION AT WINCH - POUNDS
TIME - SECONDS

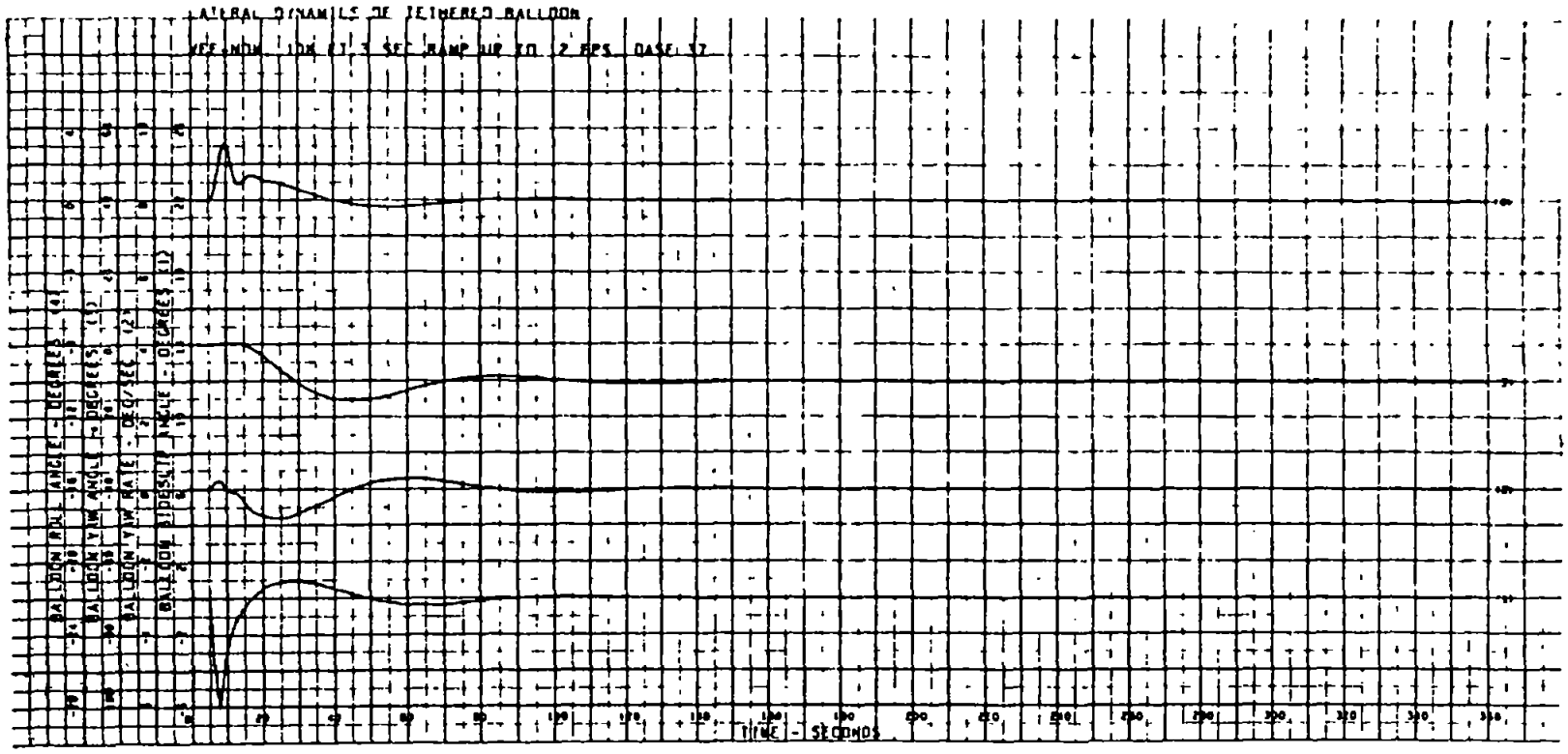
LATERAL DINAMICS OF TETHERED BALLOON
REF-NOM. 10M FT.3 SEC RAMP UP TO 12 RPS. CASE 37
BALLOON ROLL ANGLE - DEGREES
BALLOON YAW ANGLE - DEGREES
BALLOON YAW RATE - DEG/SEC
BALLOON SIDESLIP ANGLE - DEGREES
TIME - SECONDS

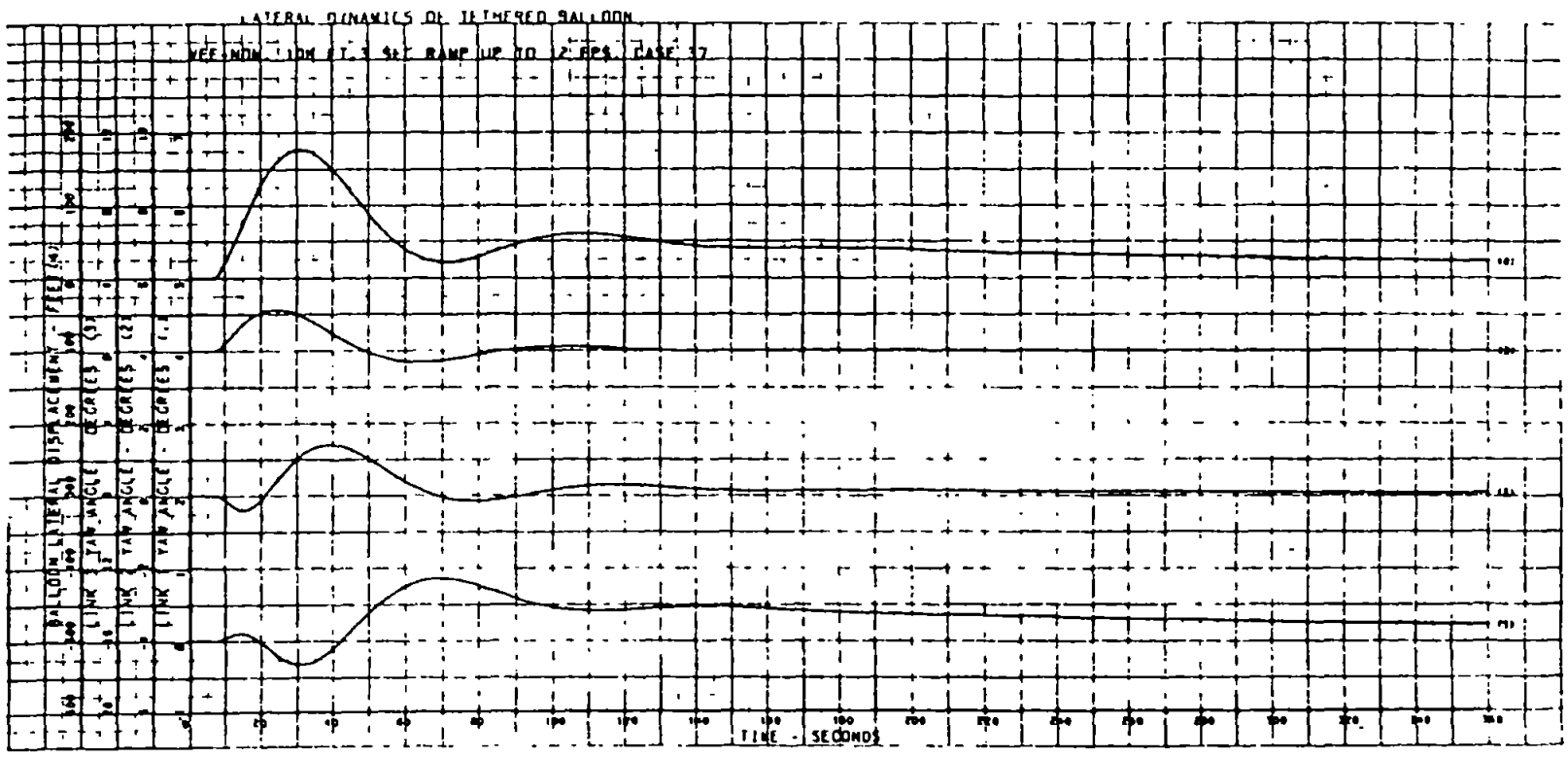
LATERAL DINAMICS OF TETHERED BALLOON
REF-NOM. 10M FT.3 SEC RAMP UP TO 12 RPS. CASE 37
BALLOON LATERAL DISPLACEMENT - FEET
LINK TAN ANGLE - DEGREES
LINK TAN ANGLE - DEGREES
TIME - SECONDS

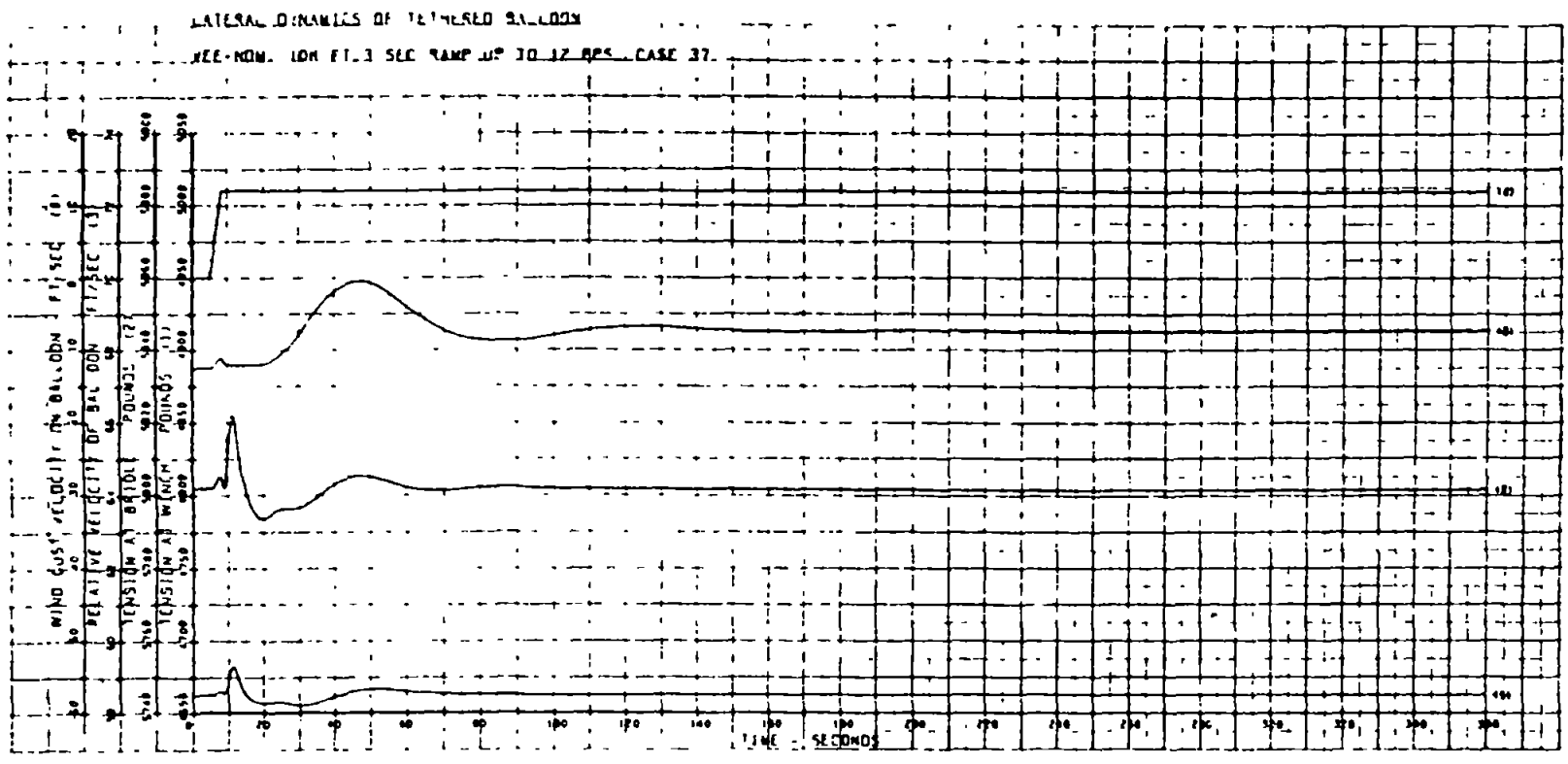
LATERAL DINAMICS OF TETHERED BALLOON
REF-NOM. 10M FT.3 SEC RAMP UP TO 12 RPS. CASE 37
WIND GUST VELOCITY ON BALLOON - FT/SEC
RELATIVE VELOCITY OF BALLOON - FT/SEC
TENSION AT BRIDLE - POUNDS
TENSION AT WINCH - POUNDS
TIME - SECONDS

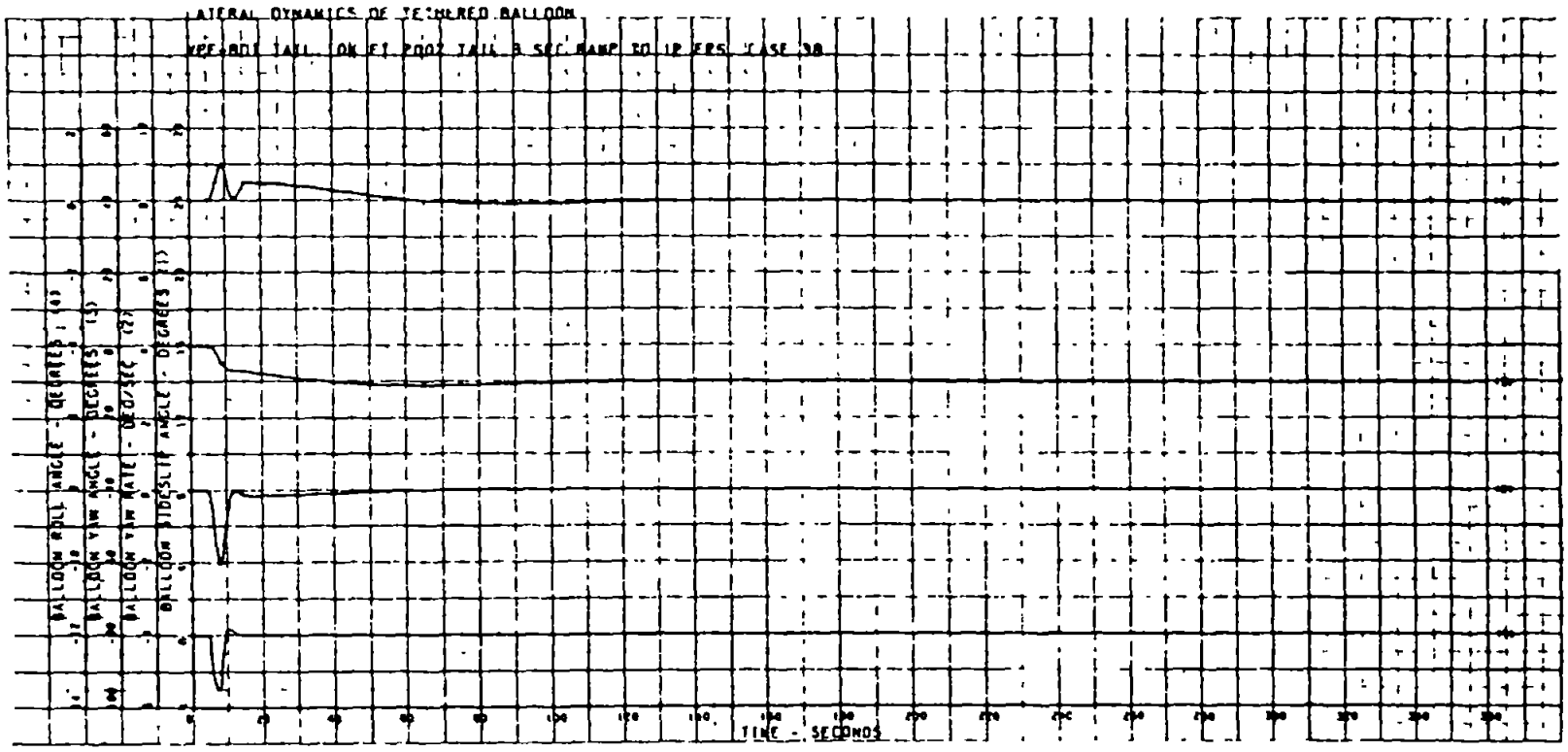
LATERAL DYNAMICS OF TETHERED BALLOON
TIME - SECONDS

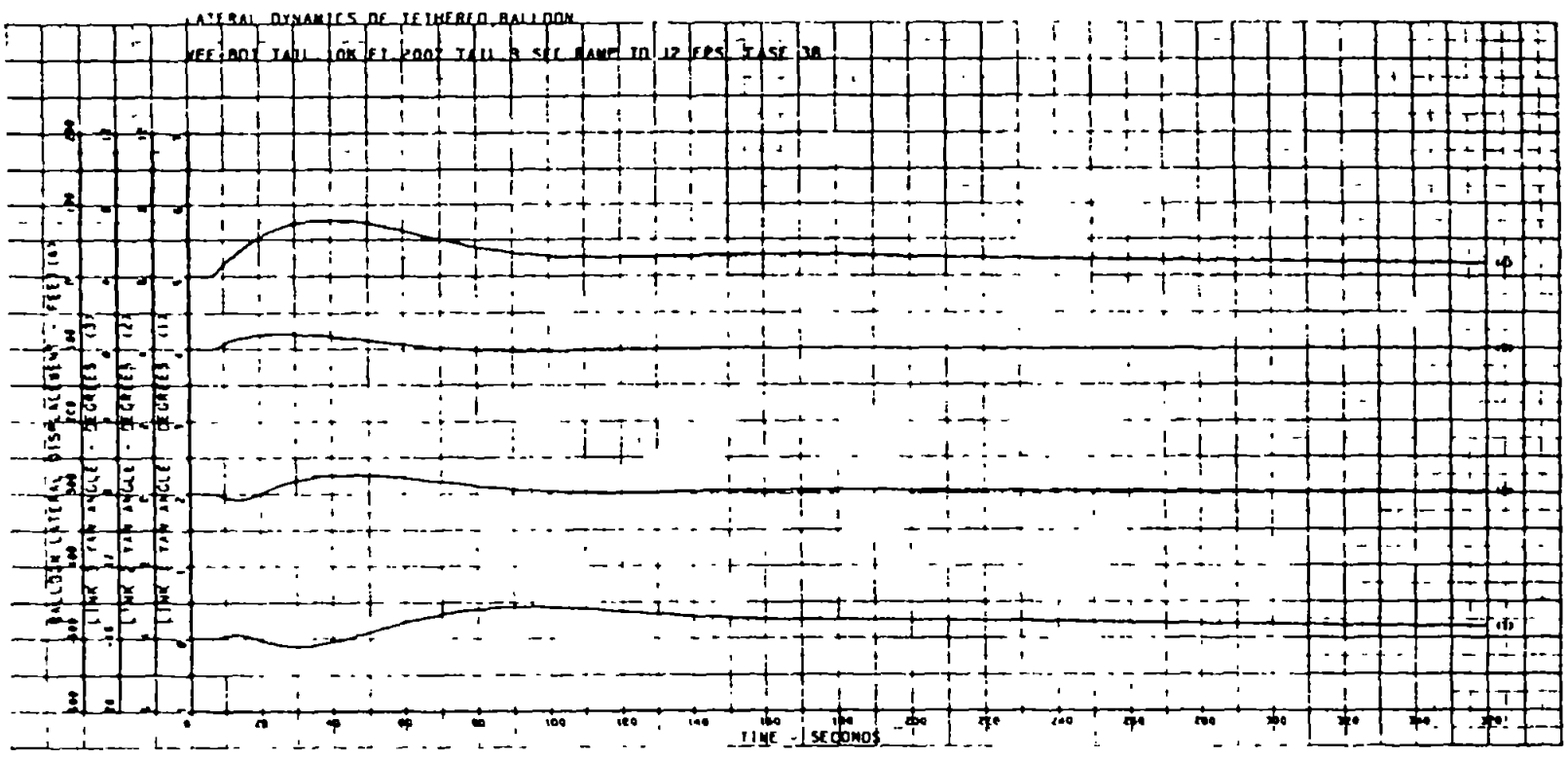
LATERAL DYNAMICS OF TETHERED BALLOON
TIME - SECONDS

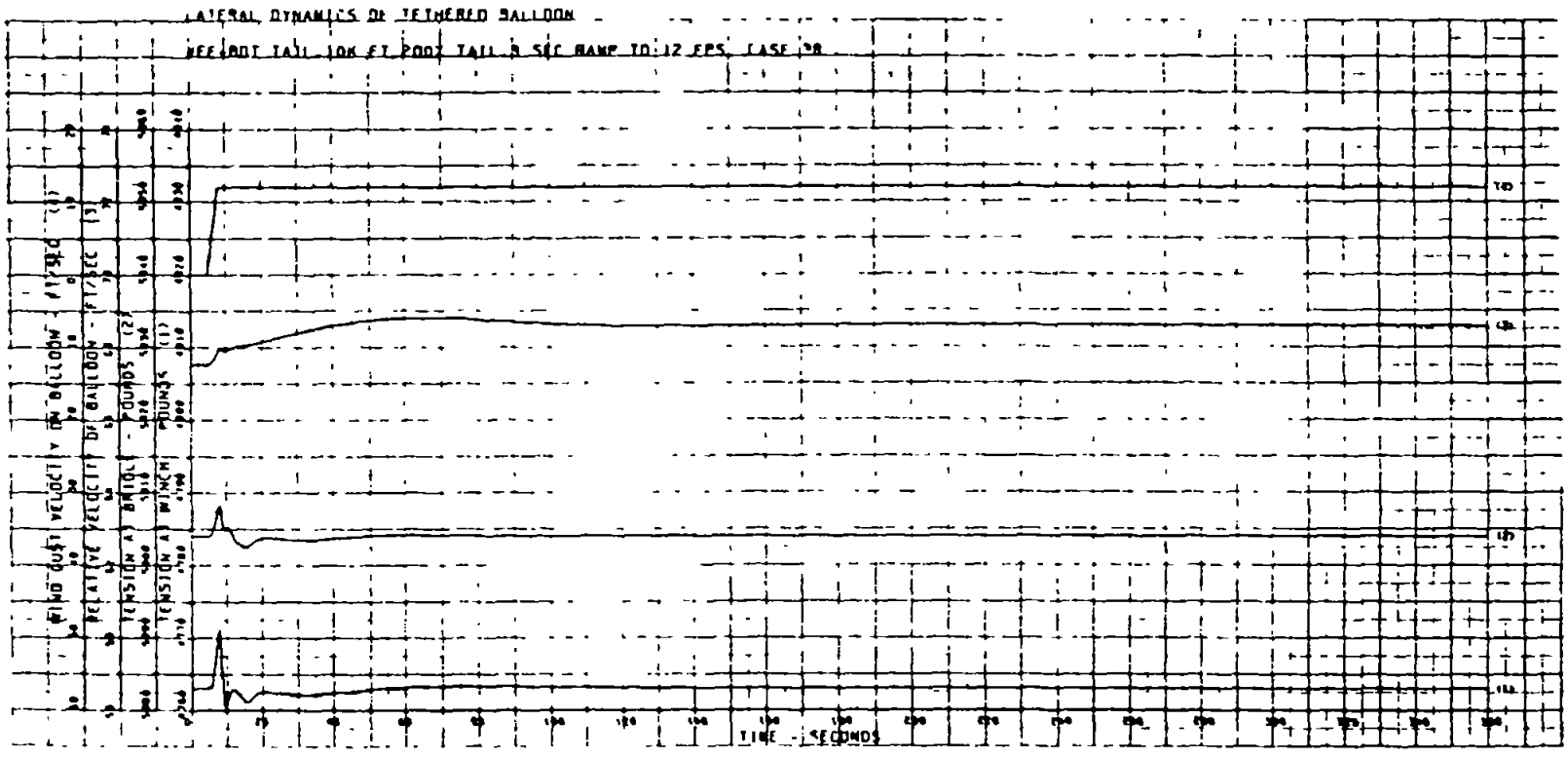
LATERAL DYNAMICS OF TETHERED BALLOON
TIME - SECONDS

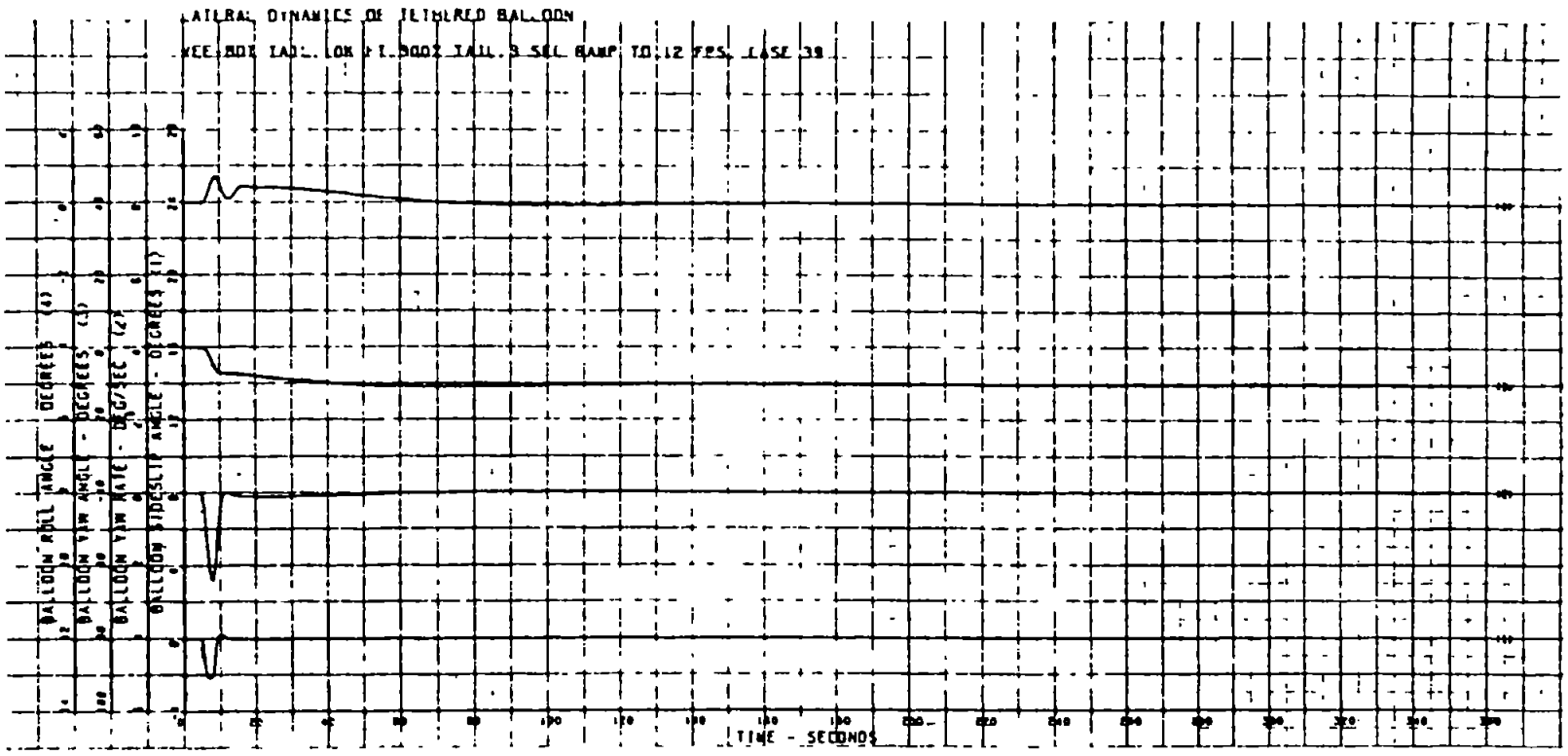
LATERAL DYNAMICS OF TETHERED BALLOON
BALLOON ROLL ANGLE - DEGREES (4)
BALLOON YAW ANGLE - DEGREES (3)
BALLOON YAW RATE - DEG/SEC (2)
BALLOON SIDESLIP ANGLE - DEGREES (1)
TIME - SECONDS

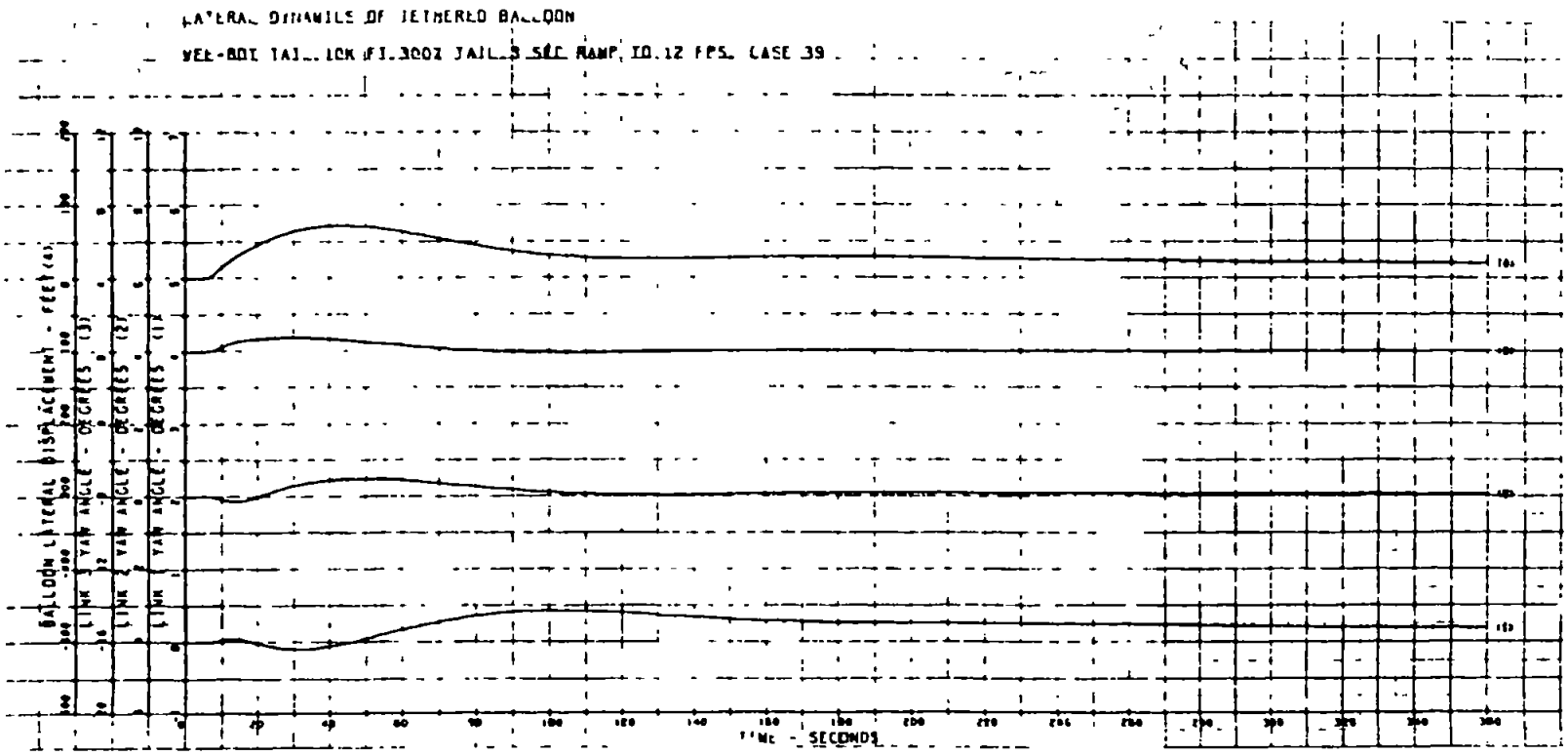
LATERAL DYNAMICS OF TETHERED BALLOON
BALLOON LATERAL DISPLACEMENT - FEET (4)
LINK 3 YAW ANGLE - DEGREES (3)
LINK 2 YAW ANGLE - DEGREES (2)
LINK 1 YAW ANGLE - DEGREES (1)
TIME - SECONDS

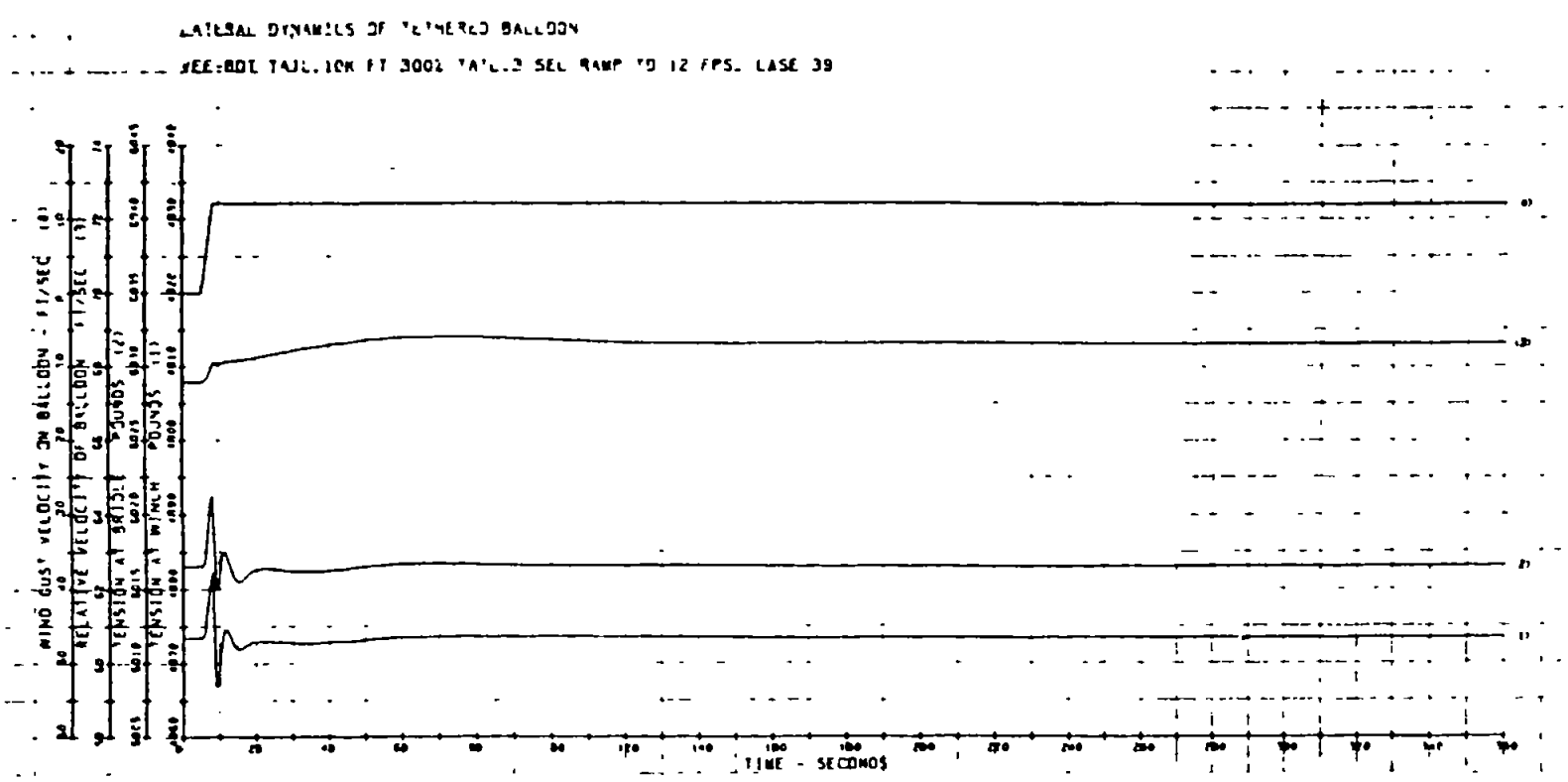
LATERAL DYNAMICS OF TETHERED BALLOON
WIND GUST VELOCITY ON BALLOON - FT/SEC (4)
RELATIVE VELOCITY OF BALLOON - FT/SEC (3)
TENSION AT SHIELD - POUNDS (2)
TENSION AT WINCH - POUNDS (1)
TIME - SECONDS

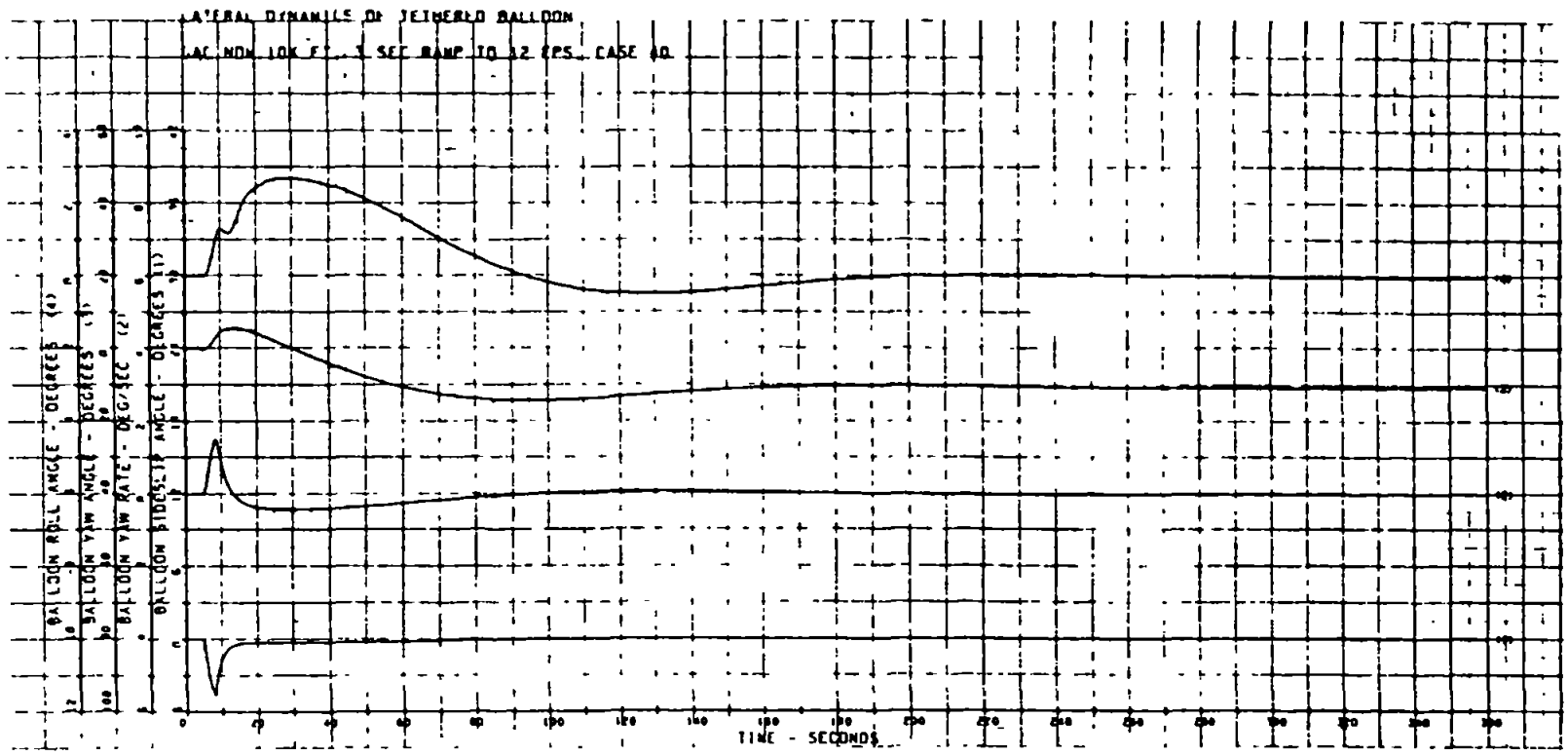
LATERAL DYNAMICS OF TETHERED BALLOON
GAC NOM. 10K FT. 3 SEC RAMP TO 12 FPS. CASE 40
BALLOON ROLL ANGLE - DEGREES
BALLOON YAW ANGLE - DEGREES
BALLOON YAW RATE - DEG/SEC
BALLOON SIDESLIP ANGLE - DEGREES
TIME - SECONDS

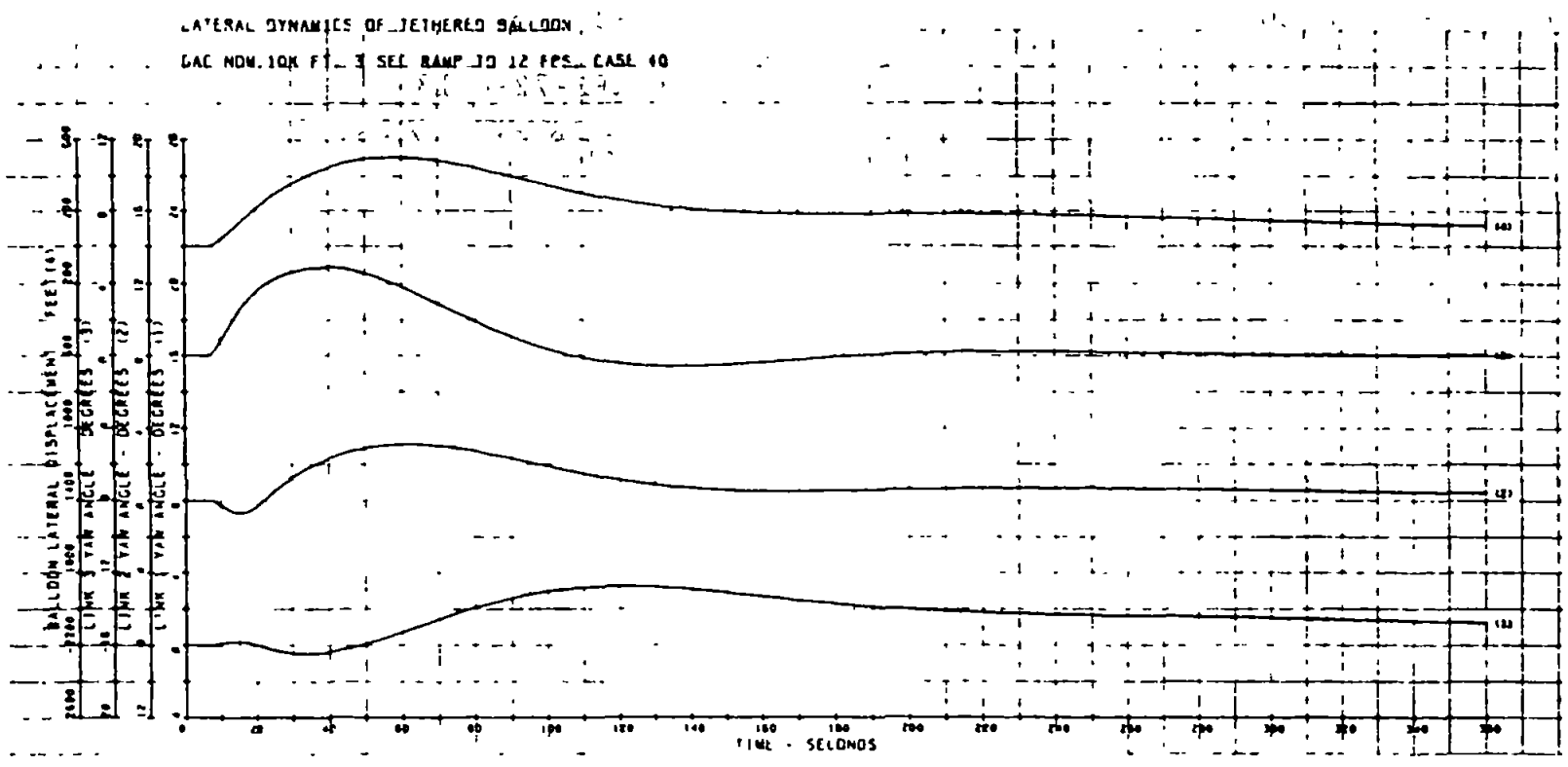
LATERAL DYNAMICS OF TETHERED BALLOON
GAC NOM. 10K FT. 3 SEC RAMP TO 12 FPS. CASE 40
BALLOON LATERAL DISPLACEMENT - FEET
LINK 3 YAW ANGLE - DEGREES
LINK 2 YAW ANGLE - DEGREES
LINK 1 YAW ANGLE - DEGREES
TIME - SECONDS

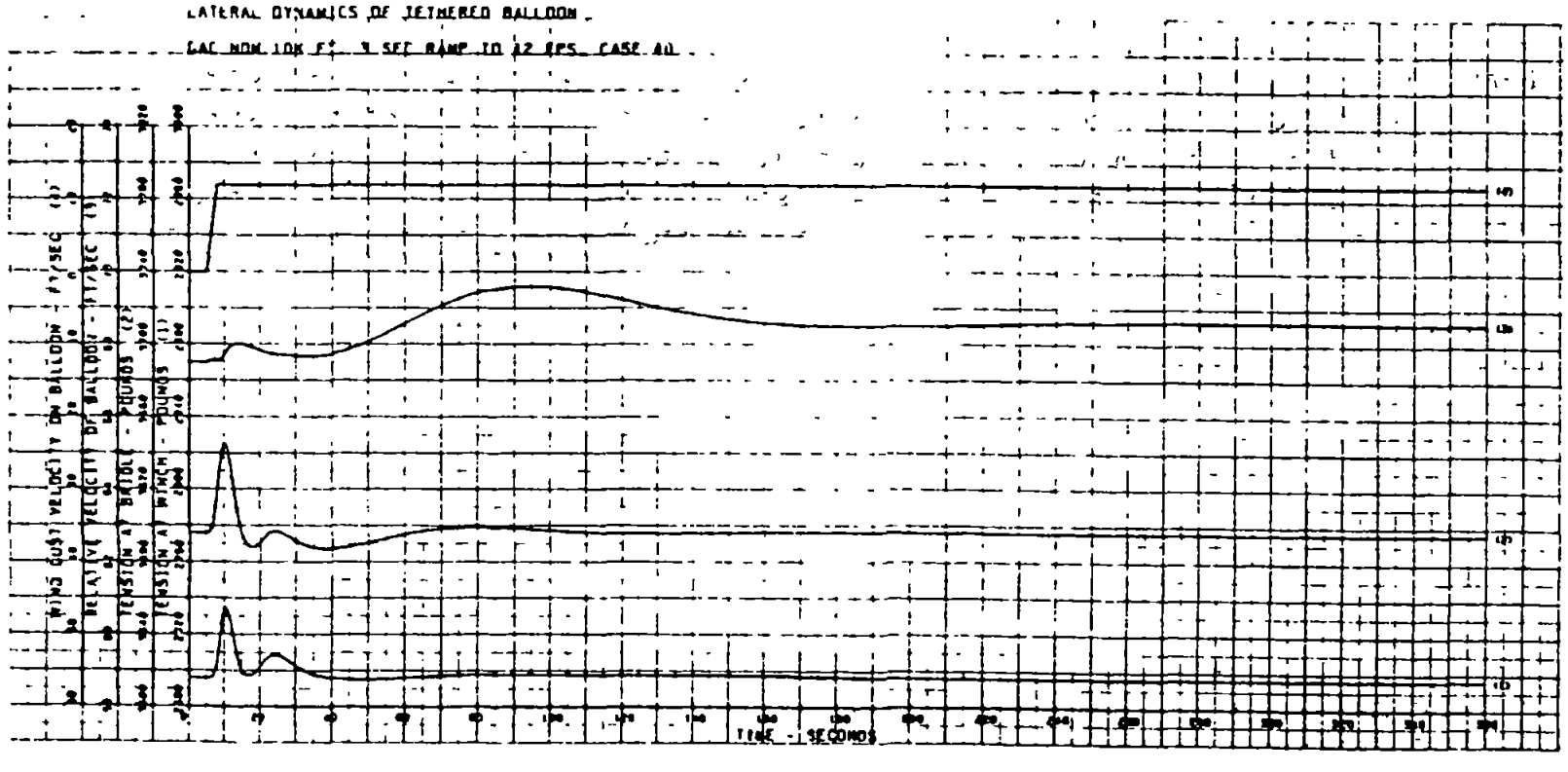
LATERAL DYNAMICS OF TETHERED BALLOON
GAC NOM. 10K FT. 3 SEC RAMP TO 12 FPS. CASE 40
WIND GUST VELOCITY ON BALLOON - FT/SEC
RELATIVE VELOCITY OF BALLOON - FT/SEC
TENSION AT BRIDLE - POUNDS
TENSION AT WINCH - POUNDS
TIME - SECONDS

Unclassified
Security Classification

DOCUMENT CONTROL DATA - R & D

(Security classification of title, body of abstract and indexing annotation must be entered when the overall report is classified)

1. ORIGINATING ACTIVITY *(Corporate author)*
Goodyear Aerospace Corporation
1210 Massillon Road
Akron, Ohio 44315

2a. REPORT SECURITY CLASSIFICATION
Unclassified

2b. GROUP

3. REPORT TITLE
INVESTIGATION OF DYNAMIC BEHAVIOR OF TETHERED BALLOON SYSTEMS

4. DESCRIPTIVE NOTES *(Type of report and inclusive dates)*
Scientific. Final. 1 January 1971 through 31 January 1972 Approved 29 Feb. 1972

5. AUTHOR(S) *(First name, middle initial, last name)*
Jerome J. Vorachek
James W. Burbick
George R. Doyle Jr.

6. REPORT DATE
31 January 1972

7a. TOTAL NO OF PAGES
164

7b. NO OF REFS
4

8a. CONTRACT OR GRANT NO
F-19268-71-C-0091

b. 7659-06-01

c. DoD Element: 62101F

d. DoD Subelement: 687659

9a. ORIGINATOR'S REPORT NUMBER(S)
GER-15325

AFCRL-72-0113

9b. OTHER REPORT NO(S) *(Any other numbers that may be assigned this report)*

10. DISTRIBUTION STATEMENT
A - Approved for public release; distribution unlimited

11. SUPPLEMENTARY NOTES
TECH OTHER

12. SPONSORING MILITARY ACTIVITY
Air Force Cambridge Reseach Laboratories(L
L. G. Hanscom Field
Bedford, Massachusetts 01730

13. ABSTRACT
An analytical investigation of the dynamic behavior of tethered balloons was conducted. This report covers definition of tethered balloon systems and a study of stability characteristics and dynamic response to wind gusts of tethered balloon systems. Balloon systems which are investigated use the British BJ Barrage Balloon, the Vee Balloon and a Goodyear Aerospace Model No. 1649 Single-Hull Balloon. The major tether construction is Columbian Rope Company's NOLARO utilizing prestretched polyester filaments. Three design altitudes, 5,000, 10,000 and 20,000 feet, are considered.

The model for the tethered balloon system consists of the streamlined balloon and a tether made up of three discrete links. The derivation of nonlinear equations of motion for this system in three dimensions is presented. The equations are linearized for stability analysis and treated as uncoupled in the longitudinal and lateral degrees of freedom. Characteristic equations which incorporate the physical, aerodynamic, and mass characteristics of the system are developed and solved for the roots which represent the frequency and damping qualities. The nonlinear equations of motion are programmed for solution on a digital computer.

An exploratory investigation to establish the trends of dynamic characteristics for various design parameters is reported. Design parameters considered include balloon shape and altitude, trim angle of attack, vertical location of the bridle confluence point, net static lift, tail size, reduced wind profiles, varying altitude as encountered in launch and retrieval, payload location, and wind location above mean sea level.

DD FORM 1 NOV 65 1473

Unclassified
Security Classification

Unclassified

Security Classification

14

KEY WORDS

Aerostats

Balloons

Balloon Aerodynamics

Balloon Dynamics

Balloon Behavior

Balloon Flying Qualities

Balloon Mass Characteristics

Balloon Stability

Balloon Systems

Cables

Cable Dynamics

Captive Balloons

Dynamic Simulation Analysis

Kite Balloons

Stability Analysis

Tethered Balloons

Tethered LTA Vehicles

Tethers